I.O.S.

A STUDY OF ERS-1 RADAR ALTIMETER DATA PROCESSING REQUIREMENTS

BY

T.H. GUYMER, P.G. CHALLENOR, M.A. SROKOSZ,
C.G. RAPLEY, P. QUEFFEULOU, D.J.T. CARTER,
H.D. GRIFFITHS, N.F. McINTYRE, R.F. SCOTT & A.R. TABOR

REPORT NO. 220

1985

NATURAL ENVIRONMENT RESEARCH COUNCIL

INSTITUTE OF OCEANOGRAPHIC SCIENCES

INSTITUTE OF OCEANOGRAPHIC SCIENCES

Wormley, Godalming, Surrey, GU8 5UB.

(042 - 879 - 4141)

(Director: Dr A.S. Laughton FRS)

Bidston Observatory,

Birkenhead, Merseyside, L43 7RA.

(051 - 653 - 8633)

(Assistant Director: Dr D.E. Cartwright FRS)

When citing this document in a bibliography the reference should be given as follows:-

GUYMER, T.H., CHALLENOR, P.G., SROKOSZ, M.A., RAPLEY, C.G., QUEFFEULOU, P., CARTER, D.J.T., GRIFFITHS, H.D., McINTYRE, N.F., SCOTT, R.F. & TABOR, A.R. 1985
A study of ERS-1 radar altimeter data processing requirements.
Institute of Oceanographic Sciences, Report, No. 220, 268pp.

INSTITUTE OF OCEANOGRAPHIC SCIENCES

WORMLEY

A study of ERS-1 radar altimeter data processing requirements

by

T.H. Guymer, P.G. Challenor, M.A. Srokosz,
C.G. Rapley[1], P. Queffeulou[2], D.J.T. Carter,
H.D. Griffiths[3], N.F. McIntyre[1], R.F. Scott[1]
& A.R. Tabor

I.O.S. Report No. 220

1985

This report was originally issued as the Final Report for European Space Agency Contract No. 5681/83/NL/BI.

Addresses of non-IOS staff:

[1]*Mullard Space Science Lab*
University College London
Holmbury St Mary
Dorking
SURREY, RH5 6NT
UK

[2]*Centre Oceanologique de Bretagne*
IFREMER
BP 377
29273 BREST
FRANCE

[3]*Dept. of Electronic & Electrical Engineering*
University College London
Torrington Place
LONDON, WC1E 7JE
UK

A STUDY OF ERS-1 RADAR ALTIMETER DATA PROCESSING REQUIREMENTS

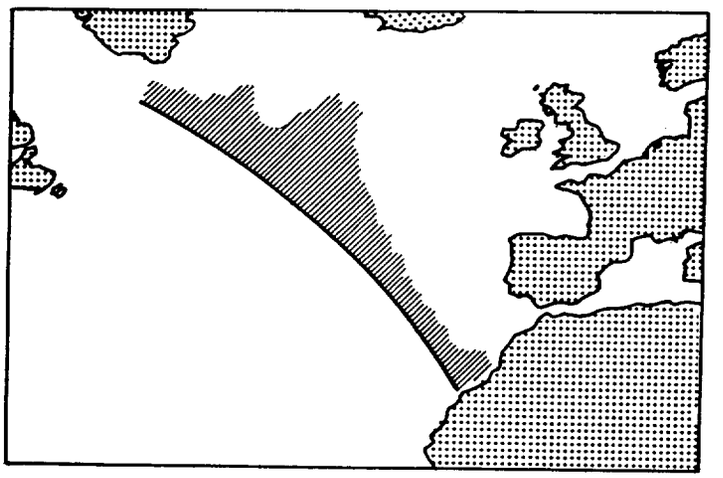

FINAL REPORT

JANUARY 1985

Natural Environment Research Council
Institute of Oceanographic Sciences

University College London
Mullard Space Science Laboratory
and the
Department of Electronic and Electrical Engineering

Centre Oceanologique de Bretagne
Centre National pour L'Exploitation des Oceans

EUROPEAN SPACE AGENCY
CONTRACT REPORT

The work described in this report was carried out under ESA contract. Responsibility for the contents resides with the authors or organizations that prepared it.

ESA Contract 5681/83/NL/BI

Abstract

ERS-1 will provide two classes of data. The first will contain a limited number of Fast Delivery Products, which will be generated in near real-time either on board the spacecraft or at the Kiruna ground station. The second involves a wide range of products, whose processing and interpretation is less straightforward, and will be produced at a separate off-line Processing and Archival Facility.

The present study discusses aspects of data processing for the ERS-1 radar altimeter over oceans and sea-ice for both these classes. After identifying useful products the report reviews the status of algorithms for extracting the relevant geophysical parameters from sensor data. Suggestions are made concerning retrievals from ERS-1 data taking into account differences between ERS-1 and Seasat. Particular problems concerning the extraction of wind speed and the effects of sea-surface non-linearities are identified and several new parameters, including a wave period, are proposed. Finally, some implications for the overall radar altimeter ground segment philosophy are outlined, including the accessibility and dissemination of products and standardization of formats.

A broader account of the scientific usefulness and applications of ERS-1 radar altimeter data is given in a parallel study report by Rapley et al. (1985) which also describes the development of an altimeter performance simulator.

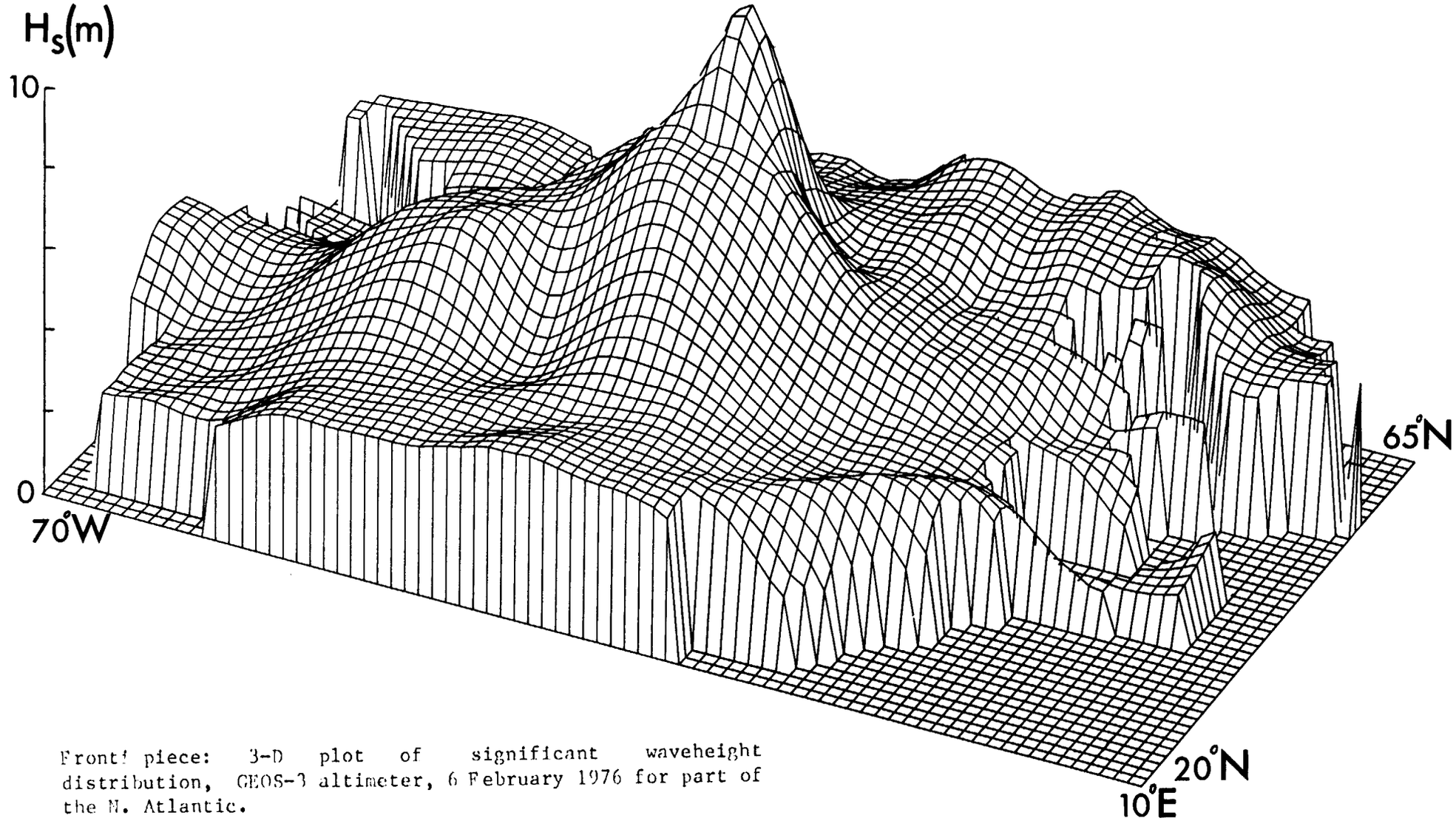

Front piece: 3-D plot of significant waveheight distribution, GEOS-3 altimeter, 6 February 1976 for part of the N. Atlantic.

Acknowledgements

We would like to thank Polly Parsons, who typed much of this report, Vivienne Kouzeleas, who typed earlier drafts, Andrew Margetts and Seymour Laxon, who assisted in the computing, and Sylvia Harvey. Vernon Squire and Andrew Cowan of the Scott Polar Research Institute contributed Section 7.5. Some of the Seasat data used in the analysis were obtained from the Pilot Ocean Data System at the Jet Propulsion Laboratory.

[Study Manager's note: My particular thanks go to Peter Challenor, Meric Srokosz and David Carter for their tremendous effort in assisting with the editing and production of this report.]

LIST OF CONTENTS

3. GENERAL REVIEW OF GEOPHYSICAL DATA RETRIEVAL ON OTHER ALTIMETER MISSIONS

1. Introduction

1.1 Scope of study

In July 1984 approval was granted for Phase C/D of Europe's Remote sensing Satellite ERS-1. One of the sensors to be carried is a radar altimeter, similar to that successfully flown on the U.S. Seasat in 1978. It is important for any spaceborne sensor not only that it should be designed and constructed to perform reliably and within specification under extreme conditions but also that the ground segment (i.e. the reception of data from the instrument, the subsequent processing to produce calibrated data and its dissemination in a convenient form to interested parties) is developed with equal care. Such a development is particularly important for ERS-1 which will be a pre-operational system. Some aspects of the ground segment have already been examined by industry in Phases A and B but consideration was mainly restricted to the requirements of so-called Fast Delivery data (to be delivered within three hours of acquisition; other data (termed off-line or precision-processed) have been treated separately both financially and conceptually by national delegates to ESA's Remote Sensing Programme Board. It is, therefore, appropriate that the subject of data processing requirements should be approached from the users' point of view. The purpose of this report is to provide a preliminary outline of these requirements for the radar altimeter. This study does not claim to be comprehensive and, in some cases, for example ocean topography, the treatment is less detailed than others. We have

concentrated rather on matters which seem to us to be in need of most attention.

The study is a natural progression from two previous studies, one on the uses of satellite altimetry in climate and oceanographic research (Foster et al., 1980) and the other on altimeter operation over ice surfaces (Rapley et al., 1983). A companion study by Rapley et al.(1985) discusses the uses of satellite altimeter data across a broad range of disciplines and describes the development of a performance simulator in which pulses characteristic of the returns from a variety of surfaces are generated and fed into the simulator to assess their effects on the tracker, etc. The calibration and validation of altimeter data over continental ice is also included in the report. Preliminary results from the present study provided a significant input to the ERS-1 Radar Altimeter Data Products Workshop held at Frascati in May 1984 and Chapters 2 & 8 incorporate material from the Workshop.

1.2 Study overview

In Chapter 2 we assess the usefulness of altimeter data in several disciplines and, for each, attempt to identify the products which are required and their associated accuracies, formats and delivery times. Some implications of the choice of orbit on data processing and special problems arising from non-standard ocean returns are discussed.

Algorithms developed for previous altimeter missions are reviewed in Chapter 3. Before outlining the details of the retrieval

schemes the physical basis of the techniques is examined. For the ocean an extended non-linear theory of the sea surface has been used to study the nature of the radar return. Problems with the Seasat wind algorithm are identified and implications for the interpretation of mean wind field intercomparisons are discussed. A brief outline of the processing stages involved in extracting ocean topography is then given, followed by an assessment of the present status of extracting sea-ice products, particularly the location of the ocean/sea-ice boundary.

Chapter 4 compares the ERS-1 altimeter (designed by Selenia) with that of Seasat, emphasising the resulting impact on data processing. A description of the Sub-optimal Maximum Likelihood Estimator algorithm for significant waveheight is included.

In Chapters 5, 6 and 7 attention is devoted to the estimation of geophysical parameters from ERS-1 data based partly on the review of published work in Chapter 3 and also on new analyses conducted by the study team. Chapter 5 discusses wave parameters for both real-time and research use, including the possibility of estimating parameters other than significant waveheight. A more rigorous approach to the problem of sea-state bias is also given. Chapter 6 details the topics which must be considered if an improved wind algorithm is to be developed for ERS-1 including the absolute accuracy of backscatter intensity determinations, an improved understanding of the relationship between the mean square slope of the sea surface and wind speed, and an outline of a possible scheme for joint calibration/validation of the ERS-1 altimeter and wind scatterometer.

Recent work on the characteristics of return pulse shape over sea-ice is reported in Chapter 7. A new 'pulse peakiness' parameter and preliminary attempts to use it as a means of identifying the sea-ice boundary and different zones within the pack ice are described. The application of altimeter data to the study of ocean swell interaction with sea-ice is also outlined.

The last major chapter, Chapter 8, covers some of the implications that the results of previous chapters have for the overall organization of the ground segment and expands some of the themes discussed at the ERS-1 Altimeter Data Products Workshop. Topics include the requirement for global data, strategy for reprocessing of data and accessibility of the data to users.

Finally, conclusions and recommendations are given in Chapter 9, with cross-references to relevant sections of the report.

2. ERS-1 radar altimeter data products over oceans and sea-ice.

2.1 Definition of a data product and product levels

It is important at the outset to recognise that there are differing views of what constitutes a data product. For those involved in the design of facilities to process, archive and disseminate data in suitable forms to users the term has a rather restricted meaning. In general it is confined to data sets (both digital forms such as computer compatible tapes or visual displays such as images, contour plots, etc.) which can be routinely generated, are reasonably well validated and understood, and are of sufficiently general interest to be considered a marketable product. A similar view is likely to be taken by that section of the user community whose chief requirements are operational e.g. ice and weather forecasting, oil pollution monitoring. Here there is a need to have data processed to a level where meaningful geophysical outputs are obtained and are disseminated in a manner and at a speed commensurate with the decisions that need to be taken. It may be helpful to call these Routine Data Products. According to NOAA (1980), which lists ocean products to be generated by NOAA from the National Oceanic Satellite System (NOSS), a product is broadly defined as any item routinely produced and available for applications within the environmental sciences. This wider definition is closer to the scientific community's concept for ERS-1.

The research community (and some sections of the applications community e.g. designers of off-shore structures) is not so concerned

with the rapid reception of highly-condensed data but is interested in exploiting the information contained in order to add to its understanding of phenomena. This often entails careful examination of the data and re-analysis to extract data products of sufficiently high precision or attempts to present the data in differing ways so as to cast new light on the problem being studied. This may involve generating new one-off data products, whose value may appear somewhat limited and which may need interpretation. These may be referred to as Scientific Data Products.

Much of the work using data from previous oceanographic satellites e.g. GEOS-3, Seasat and NIMBUS-7 has been by scientists, partly because of the novelty of the techniques and partly because of the intermittency of the coverage obtained. This has produced a wealth of papers many of which use, or have resulted in the generation of, data products of one sort or another. With regard to the altimeter specifically, the ERS-1 Radar Altimeter Data Products Workshop Report provides a good illustration of the wide range of products (Guymer, Drewry & Rapley, 1984).

In this section we shall review the usefulness of altimeter data in several disciplines and for each attempt to translate applications into products which will be described in terms of accuracy, format and delivery time requirements. Assessments will be made of the extent to which such products are operational. However, it is important to note that the division into Routine and Scientific Products is somewhat arbitrary and that between now and the launch of ERS-1 some of the latter are likely to become routine. Therefore any

processing facility which is designed now should be flexible enough to cope with an increase in the number of routine products. For example a 50% growth allowance, as included in the NOSS design, would seem to be a reasonable compromise between the extremes of an over-rigid and an under-defined system. The relationship between Routine/Scientific and Fast-Delivery/Precision Products, also needs clarification. Both the F.D. and Precision sets will contain 'Routine' products; F.D. products will be extremely useful in providing a first-look at suitable scientific data sets.

It will also aid discussion in the subsequent sections to use as a starting point the same product levels as assumed at the Data Product Workshop (see Table 2.1), though this should be regarded as a scheme which may evolve a little. These are similar to those adopted by NASA's Pilot Ocean Data System (PODS) and NOSS. Basic data sets are generated at low levels and serve as the source for all higher level products, which may require restructuring or processing of the data in such a way as to reduce the quantity of information.

2.2 Wave Data Products

2.2.1 Usefulness of R.A. data for waves

Much of the emphasis in recent studies of the scientific interest in altimetry has centred on the ability to monitor the topography of the sea surface and of ice sheets (e.g. Foster et al.,1980; NERC/SERC 1983; TOPEX 1982). This has a particular relevance to climate. The ability of the altimeter to measure waves

Table 2.1 Product Levels for Wind, Waves and Sea-Ice

Level	
1	Instrument-corrected, earth located, engineering units (including the full waveform) + instrument corrections that have been applied, mode and blunder point information, coast/land/ice flags. Data stored at 20 per second. Archive period: 2-5 years depending on confidence in Level 1.5.
1.5	All Level 1 data, corrected for atmospheric effects, tides, etc. + list of corrections applied. Data stored at 20 per second. Archive period: Permanent.
2	Geophysical data (similar to Seasat GDR) corrected for atmospheric effects, etc., including separate list of corrections. 1 per second. Archive period: Permanent.
3	Geographically-ordered and/or gridded products. Archive period: Permanent.
4	Temporal/spatial summaries. Archive period: Permanent.

Note

This table is based upon Table 1.1 in Guymer (1984) but differs from it in that geophysical corrections are included at Level 2 as well as 1.5. The reason is that Level 2 data will probably be transferred to specialist data centres. Users who require instrument corrections would still have to access the Processing and Archival Facility.

has been regarded as more of an operational tool and as such significant waveheight (H_s) has been incorporated into the fast delivery products from ERS-1. However, there is also considerable interest in the scientific benefits of altimeter wave data (see Guymer, 1984), and the Sub-optimal Maximum Likelihood Estimator (SMLE) algorithm on ERS-1 is expected to improve the accuracy of the onboard values of H_s.

Carter and Challenor (1984) have assessed the impact of satellite altimeter data on wave research in two main areas. The first is the short-term statistical description of the sea-surface. Many important properties can be shown to depend only on the low order spectral moments corresponding to the variances of the surface elevation (m_0), vertical velocity (m_2) and vertical acceleration (m_4). This model is also very useful for understanding the nature of the altimeter return. The altimeter has provided estimates of m_0 (related to H_s) which are probably as accurate as the best measurements from in-situ platforms. The requirement to interpret R.A. returns in terms of sea-state parameters has proved an incentive to further research, mainly but not entirely in the spatial domain. This research is leading to the realisation that parameters of interest which are not measurable by conventional instruments might be extracted from the altimeter return. Among these are m_4 from which a wave period may also be derivable.

A realistic description of the sea surface has to account for a non-Gaussian sea-surface in which skewness is an important parameter. The altimeter can be used to measure the skewness of the distribution

of specular points but not of the sea surface directly. To obtain one from the other it is necessary to assume a specific non-Gaussian model. Nevertheless since surface-following buoys cannot measure the non-linearities (Srokosz, 1984a) even with these problems skewness is likely to prove to be one of the more useful outputs of the altimeter and should stimulate further research on non-linear aspects of the sea surface. This is explored further in 5.1. A particular problem with spatial analysis (which is what altimeter data require) is that results depend upon the "long-crestedness" of the waves i.e. the directional spreading of the waves between the two extremes of isotropy and uni-directionality. Since the altimeter can make no measurements of the directional properties it will be necessary to make some assumptions if some parameters are to be estimated from the return.

The second area (long-term statistics) is concerned with much larger space and time scales in which a wave climatology of certain parameters is built up which is useful as a basis for a statistical estimation of extreme values. A particularly important parameter in the design of off-shore structures is the value that is exceeded, on average, once every 50 (or 100 years). Consequently, a considerable part of the research in long-term statistics is concerned with deriving the upper tail of the distribution of H_s from which the value of H_{50} can be extrapolated (Carter & Challenor, 1981). Unfortunately there are very few data (for most sites less than 2 years, Fig. 2.1) and there is no physical model on which to base interpolation between points so that the confidence limits are large.

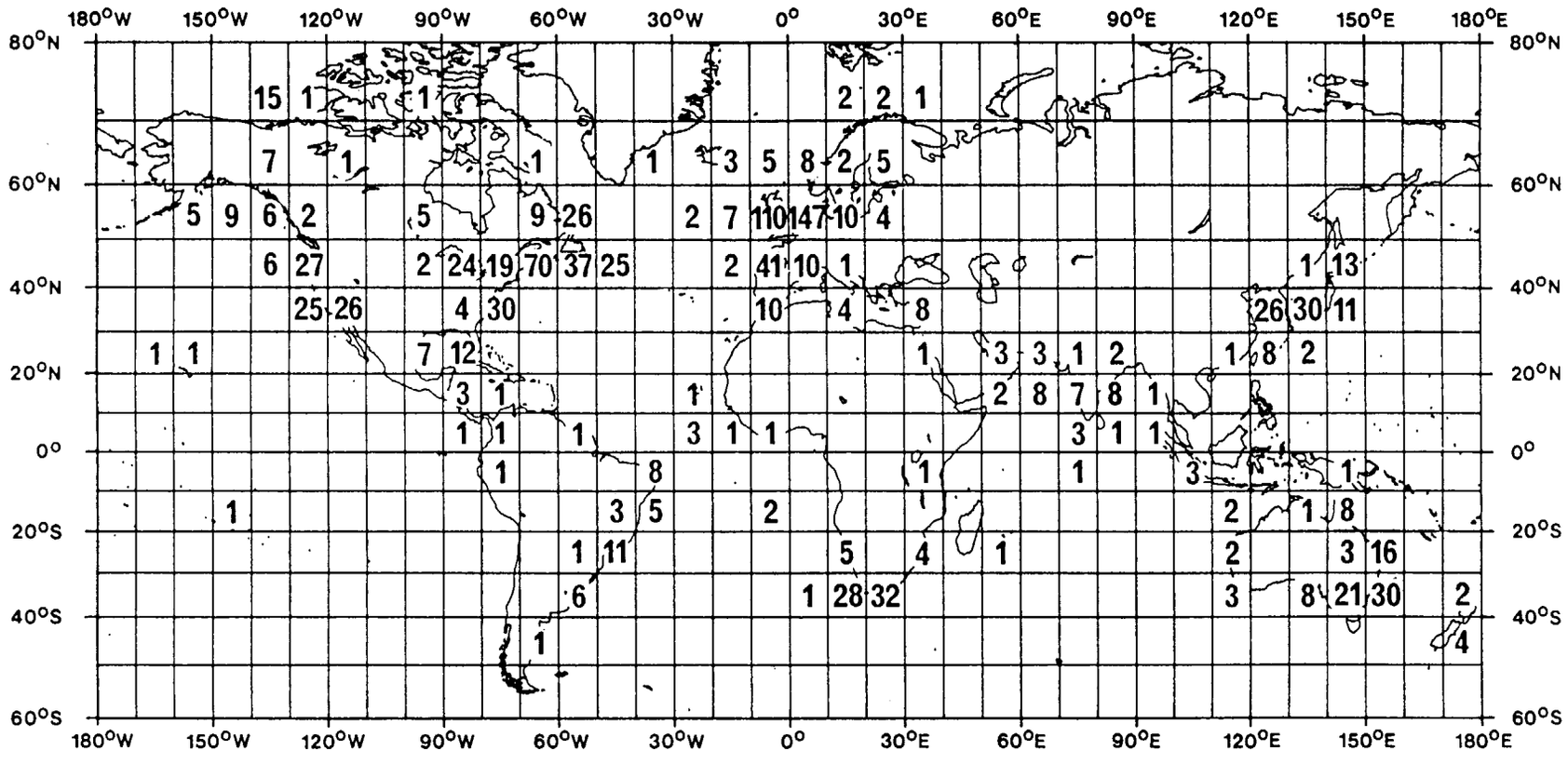

Fig. 2.1 Number of instrumental wave recording sites per 10° degree square.

The altimeter will provide a completely different kind of data. Each day it will produce twice the number of estimates of H_s that have been measured by the Seven Stones Light Vessel during the last twenty years. However, the sampling rate at a specific location will be a lot poorer. Depending upon the satellite orbit one or two observations might be obtained at a particular site every 3 days (see 2.6). This means that our methods of analysis must be modified to include the additional spatial information which will cover areas at present devoid of any instruments. One need is to find out the spatial correlation scale and the distance over which the wave field is homogeneous so that we know how many points along the track can be incorporated to produce extended time series. Unfortunately most commercial interest in the long-term statistics is concentrated in coastal waters where these horizontal scales are smallest and where a satellite altimeter suffers most problems due to land interference (Frassetto et al., 1984). Improvements in hardware design and in the ground processing which improve the quality of data in the footprints adjacent to coasts will therefore be of benefit. Long-term statistics of wave period and of a skewness parameter will also be of great value.

A third area of wave research mentioned by Carter & Challenor, and also discussed in relation to altimetry by Guillaume (1984), Bouws et al.(1984), and Kjelaas & Guddal (1984) is wave modelling. Ewing (1983) gives an account of the present state of wave modelling and Draper (1983) catalogues the models. One of the largest sources of error in these models is in the initial wind field (this applies

not only to forecast winds but also to observed winds when the model is being used in a hindcast mode to derive wave statistics). At first sight it might appear that the incorporation of a line of H_s data across the model domain would be of considerable value but Carter & Challenor (1984) and Guillaume (1984) point out that models are not designed to accept H_s as input, and it is difficult to see how the numerical spectral information at the grid point might be adjusted to give the correct integrated spectrum. They suggest a more realistic role for the altimeter may be in the verification of the models. Kjelaas & Guddal (1984) describe such use of GEOS-3 waveheights, with satisfactory agreement. Guillaume believes that ERS-1 H_s will provide an important global reference data set for the comparison of the many wave models.

Bouws et al (1984) are of the opinion that ERS-1 wave data in the Norwegian Sea will improve wave forecasts in the southern North Sea where the present wave model at the Royal Netherlands Meteorological Institute has difficulty in estimating the swell from the north. It is possible to obtain some information on swell from altimeter measurements by using wind speed estimates to partition H_s into a wind-wave component and a swell component (Hognard, 1981, 1984; Parsons 1979). Hognard derives a minimum swell height and examines the evolution of such swell maps for consecutive periods of 3 days inferring the propagation of swell systems across ocean basins. Such products would be very ueful but great care is required in interpreting the data in this way. A review of the technique is given in 3.1.3.

2.2.2 Real-time use - some further comments

From the foregoing it will be seen that R.A. wave data in themselves will be of extremely limited use in forecasting wave conditions by their incorporation into wave models e.g. as initialisation data. However, this is not to deny the value of real-time dissemination of waveheight products. These could be used to modify analyses of H_s based on conventional data, similar to the use of cloud imagery in positioning features in synoptic weather analyses, capturing small-scale features lost in the analysis, or they could be produced as a stand-alone product combining, say, data from 3 consecutive passes covering the N. Atlantic. For ships or coastal regions lying reasonably close to satellite tracks in space and time (100 km, 3 hr) the altimeter may provide a more accurate very short-term forecast (by extrapolation) than a wave model especially in regions where the latter is based upon unreliable wind fields. The R.A. could then be regarded in a similar way to the role of land-based radars in nowcasting precipitation for selected areas. With the addition of two or three more altimeters measuring H_s the space-time coverage would be improved significantly.

Another possible use of real-time waveheights would be to identify high sea-state areas for inclusion in storm warnings.

2.2.3 Data products required

In the previous section we have described a number of wave parameters which it may be possible to extract from altimeters similar to that planned for ERS-1 and have outlined some

applications. The problem then is to convert these into data products. The extent to which these ought to be regarded as routine and therefore included in the sizing of the processing and archiving facility depends on how broad the interest is and how well validated such products are. The interface with specialist data centres (8.3.4) will be important here. Often several products will be based upon the same parameter (e.g. H_s) but organised in different ways (e.g. along-track, time series at a point, mean plus variance in an extended geographical region. The important point is to ensure that a basic product is available from which the others can be generated.

The wave parameters of relevance in altimetry are:- H_s, s (variance of sea surface slopes), period, skewness, cross-skewness (possibly related to long-crestedness), and minimum swell. For each of these, requirements need to be expressed in terms of accuracy and, depending on the actual product, the spatial sampling update period, delay time and source information required. Table 2.2 is an attempt to categorise what is a desirable accuracy. There are various ways of doing this. We regard an altimeter estimate as useful if (i) it duplicates a conventional measurement but to a greater accuracy (ii) its accuracy is similar to or slightly inferior to in-situ data but is in a data-sparse location, (iii) regardless of accuracy it cannot be obtained at all from surface-based instruments. It is also important to know over what range of a parameter the accuracy is required.

Algorithms for deriving the above parameters are detailed in 3.1 and 5.1. H_s will be calculated in real-time using on-board estimates

Table 2.2 Desired accuracies for 1s means of altimeter wave parameters

Parameter	Achievable accuracy	Desirable accuracy	Not useful	Rank	Comments
Significant waveheight	$\pm$ 10cm (0-5m)	$<\pm$ 10% (0-20m)	$>\pm$ 20%	1A	Less accuracy may be acceptable in data sparse regions.
Period	?	$<\pm$ 1s (1-15s)	$>\pm$ 3s	3	
Skewness	?	$<\pm$ 0.05 (0.05-0.2)	$>\pm$ 0.2	3	Longer averaging period may be necessary.
Skewness coefficient	?	?	?	3	Longer averaging period may be necessary.
Mean square slope	?	$<\pm$ 0.01 (0-0.08)	$>\pm$ 0.03	3	
Min. swell	~1m if $U < 10ms^{-1}$	$<\pm$ 1m for $U < 20ms^{-1}$	$>\pm$ 3m	2	For Seasat min. swell is seriously over-estimated at high wind speeds.

Key to rank

1A Well established and validated

1B Well established - not validated

2 Possible (more processing needed)

3 Research

Numbers in brackets denote ranges.

of the leading edge of the altimeter pulse. It will also be generated at the PAF together with the other wave parameters. The basic source information is the tracker-loop parameters contained in the $20s^{-1}$ sensor records, but for skewness access to the raw waveforms is needed.

2.2.4 Product descriptions

Off-line products, based on the above parameters, are required at a number of levels as discussed in 2.1. The levels most commonly accessed by the wave data user community will be levels 3 and 4 because this avoids the need to sort through large amounts of global data. However, in order to generate these and to meet the needs of researchers studying global wave data, level 2 is the primary product which needs to be routinely generated; it is the basic level of geophysical data record. Possible contents of this product are listed in Table 2.3.

(In addition a Fast Delivery Product will be generated in near real-time from tracker loop parameters. This will consist of H_s but it is suggested in this report (Section 5.2) that it could also include a wave period parameter.)

Although geographical reordering of the wave data is very desirable it is questionable whether gridding should be carried out at the same time. This is because of the coarse cross-track sampling in relation to typical horizontal scales of the wave field. Examples of products at each level are listed in Table 2.4 but this is only meant to be illustrative. Higher level products should be defined

Table 2.3

Possible Contents of Basic Geophysical (Level 2) Product required for waves

Tape header: Algorithm IDs, start/end times of tape, start/end pass numbers, list of variables, units, formats.

1st File header: Satellite pass number, equator crossing time, equator crossing longitude, number of data cycles to follow, number of gaps.

1st data file: 1 sec. means of the following variables (number of bytes in brackets):

1.	t	Time since start of pass	(4)
2.	La	Latitude	(4)
3.	Lo	Longitude	(4)
4.	H_s	Significant waveheight	(2)
5.	σ_{H_s}	Variance of 20/s H_s	(2)
6.	T_A	wave 'period'	(2)
7.	σ_{T_A}	Variance of 'period'	(2)
8.	λ	Skewness	(2)
9.	σ_λ	Variance of skewness	(2)
10.	δ	Cross-skewness	(2)
11.	$\sigma\delta$	Variance of cross-skewness	(2)
12.	S^2	Mean square slope of surface	(2)
13.	$\sigma_s 2$	Variance of S^2	(2)
14.	u	Wind speed at 19.5m	(2)
15.	σ_u	Variance of u	(2)
16.	H_m	Minimum swell height	(2)
17.	σH_m	Variance of Hm	(2)
18.		Data quality flags	(1)
19.		Land/water/ice flags	(1)
20.		Rain, atmospheric attenuation flags	(1)

2nd File header

2nd data file

etc.

Note Each one-second data cycle consists of 43 bytes (= 344 bits)

Table 2.4 Description of possible wave data procducts

Product level	Type	Source level	Data quantity	Production frequency	Delivery time	Parameters	Usefulness Ranking
Fast Delivery	1 s chronological within 50km of land 5 s chronological outside 50km of land	TM	10^5 bits/pass	1/pass	3hr	H_s, U_z, position time	1
2	1 s along-track, chronological	1.5	6×10^8 bits	1 month	3 months	Full set as in Table 2.3	1
3	1 s geographically-ordered, chronological within each area	2	7×10^5 bits/ 10° square	1 month	3 months	As Table 2.3 less skewness	1
4	(i) Box means + statistics (?10° boxes)	2	10^3 bits/ 10° box	1 month	3 months	As for level 3	1
	(ii) Mean along-track profiles for repeats (+ variance) within each geographical zone	3	7×10^4 bits/ 10° box	1 month	3 months	As for level 3	2
	(iii) Time series of parameters at cross-over points, etc.	3	10^3 bits/ 10° box	1 month	3 months	As for level 3	2
5	Combined wave statistics from ALT and other sensors	4	?	1 month	3-6 months	TBD with AMI Team	?

Notes: TM = Telemetered data.

U_z - Z is height to which winds are referred
Same height should be chosen for R.A. and scat.

Usefulness Ranking: 1 = Very useful
2 = Useful

with end users, and the extent to which these should be produced routinely or in response to specific requests will depend on the interest displayed.

Some of the products, particularly at level 4, can be produced in hard-copy form which will also serve as a useful means of disseminating information on data availability and quality and to interest potential users. Figs 2.2-2.7 show some examples of products that could be generated. Fig. 2.2 is a plot of the along-track variation of H_s obtained from GEOS-3 using the ground track as the abscissa. On this occasion (6 February 1976) waveheights exceeding 10 m were associated with a very intense low pressure area near $50^{o}N$, $30^{o}W$. Such a product could be generated as part of the Fast Delivery Data Set and is amenable to dissemination via radio-facsimile as used for meteorological charts. If desired similar plots combining three successive passes could be disseminated every 6 hours or so. The latter could also be represented as contour maps (Fig. 2.3) or as 3-D H_s topography distribution (Fig. 2.4). The problem is that interpolation across quite large space and time gaps is necessary. However, Parsons (1979) suggests that even with such uncertainties the interpolated waveheights are more accurate than visual estimates from ships - but high waves are underestimated by some 20%.

Fig. 2.5 illustrates how the coverage for a particular month can be represented (February 1976). The relationship between H_s and wind speed Fig. 2.6 can be used to summarise the range of conditions sampled and how these measurements compare with those expected in a

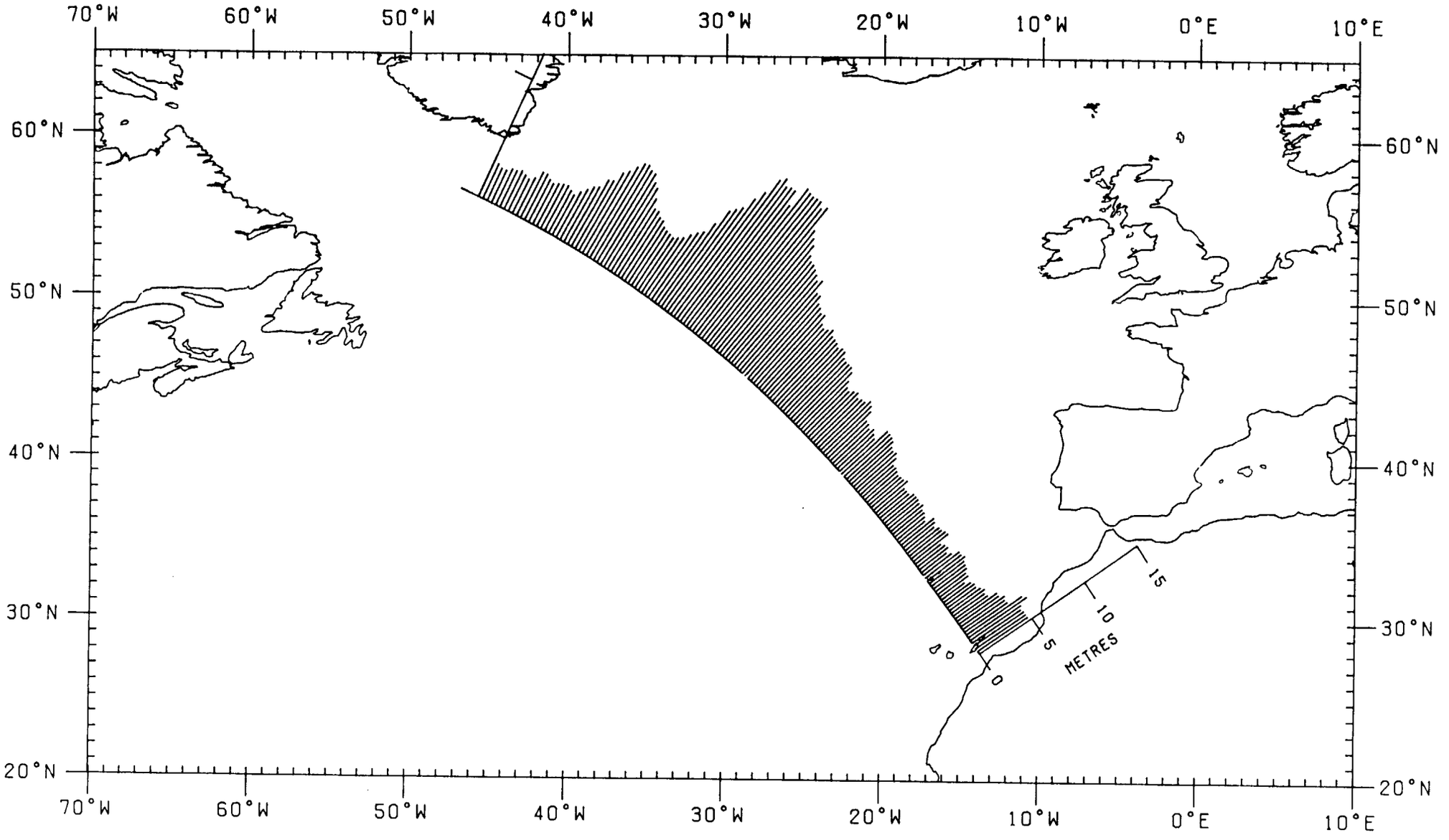

MIAS

Fig. 2.2 Along-track variation of significant waveheight on 6 February, 1976, GEOS-3, N. Atlantic.

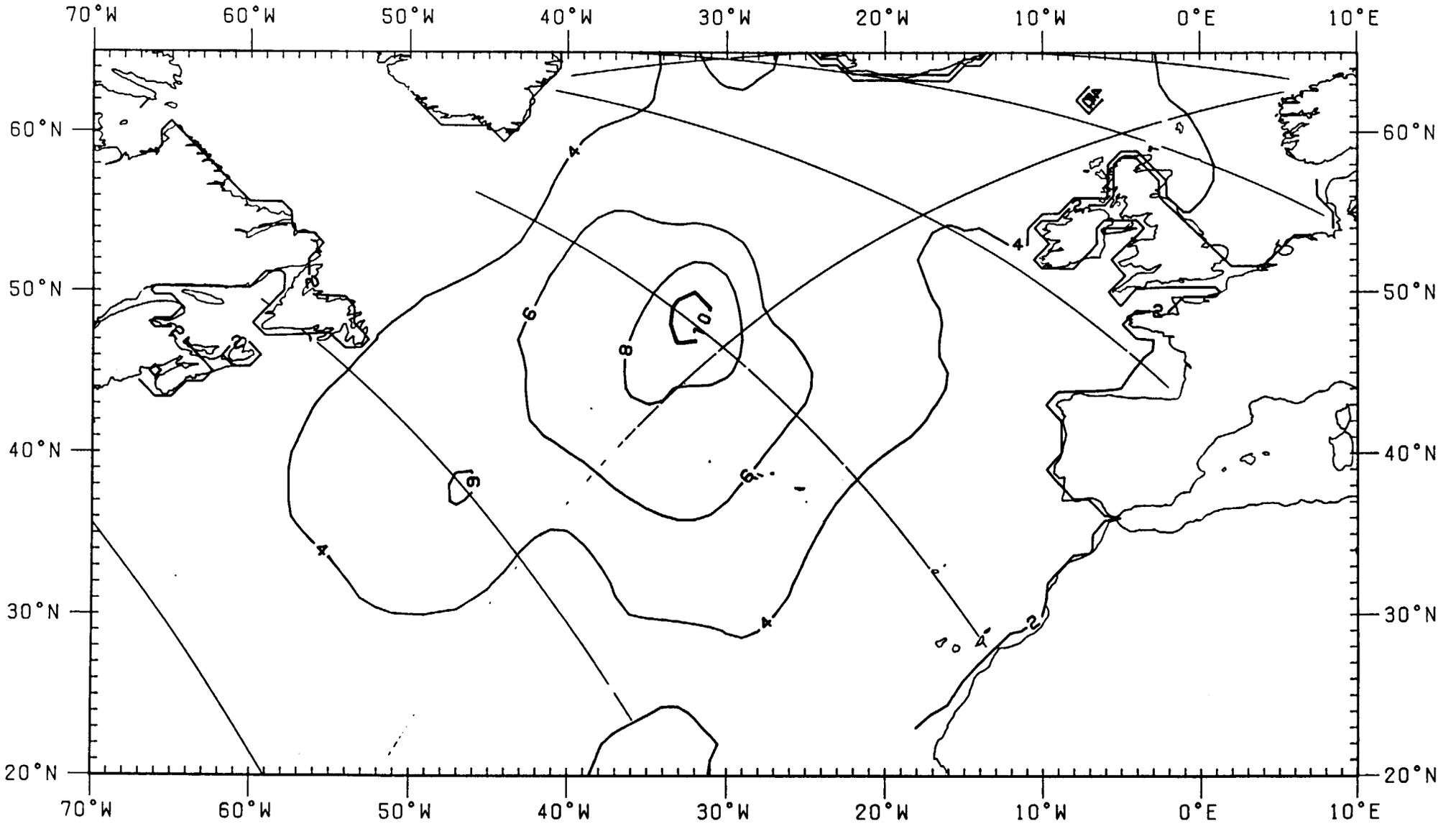

MIAS

Fig. 2.3 Contours of significant waveheight (m) derived from GEOS-3 data, 6 February 1976. Altimeter tracks are also plotted.

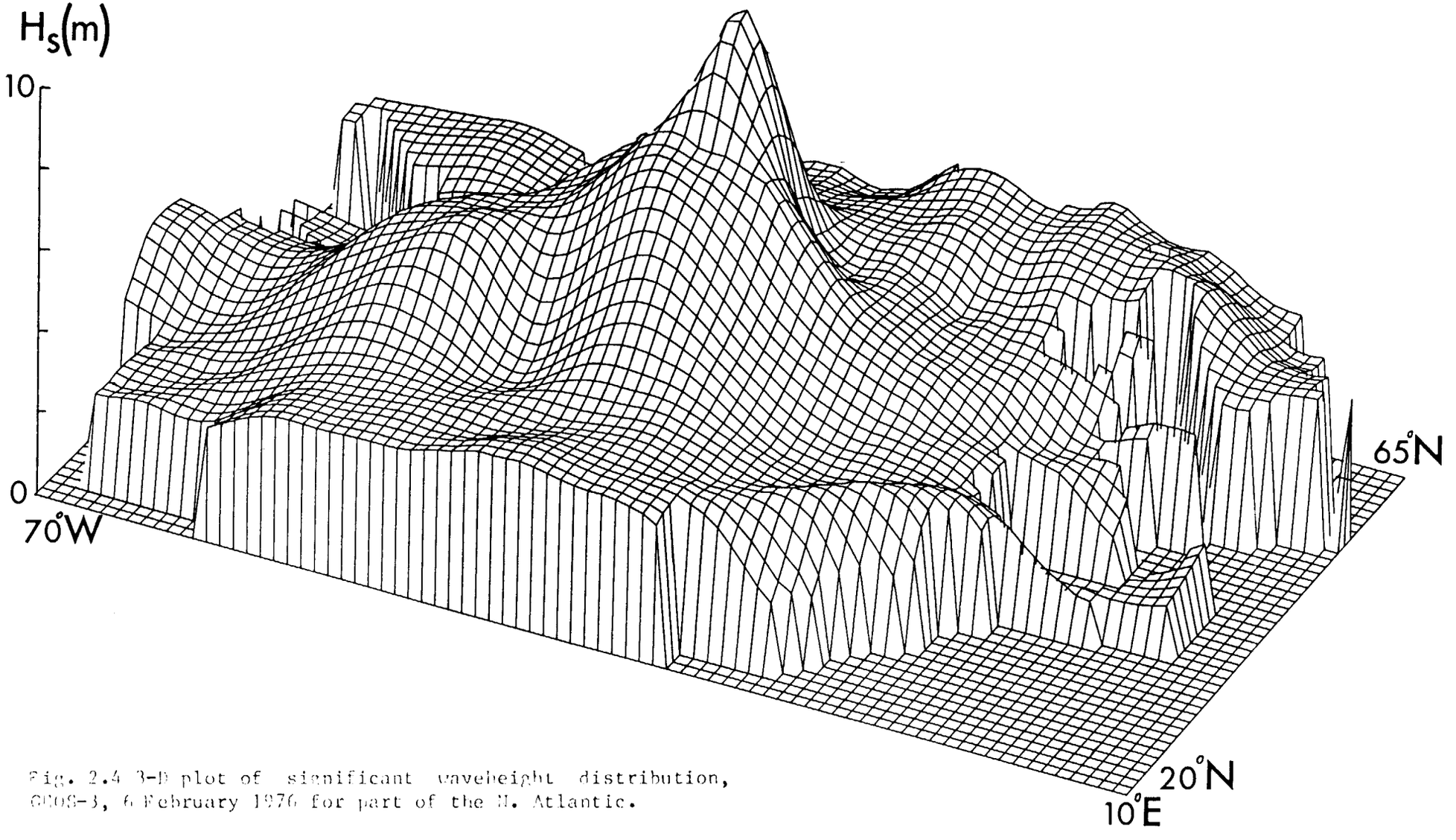

Fig. 2.4 3-D plot of significant waveheight distribution, GEOS-3, 6 February 1976 for part of the N. Atlantic.

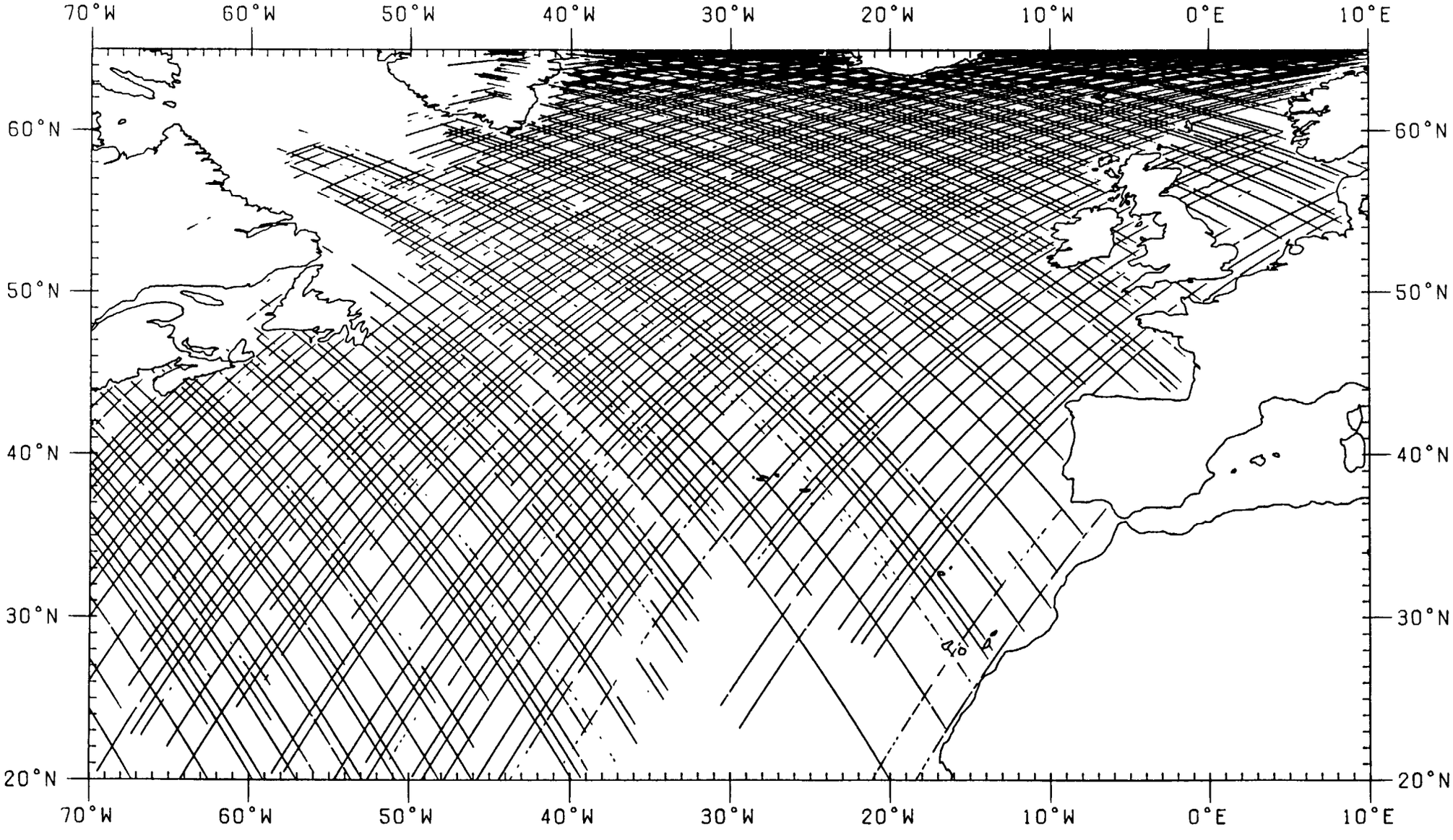

MIAS

Fig. 2.5 GEOS-3 altimeter tracks for February 1976. Lines show where data was obtained.

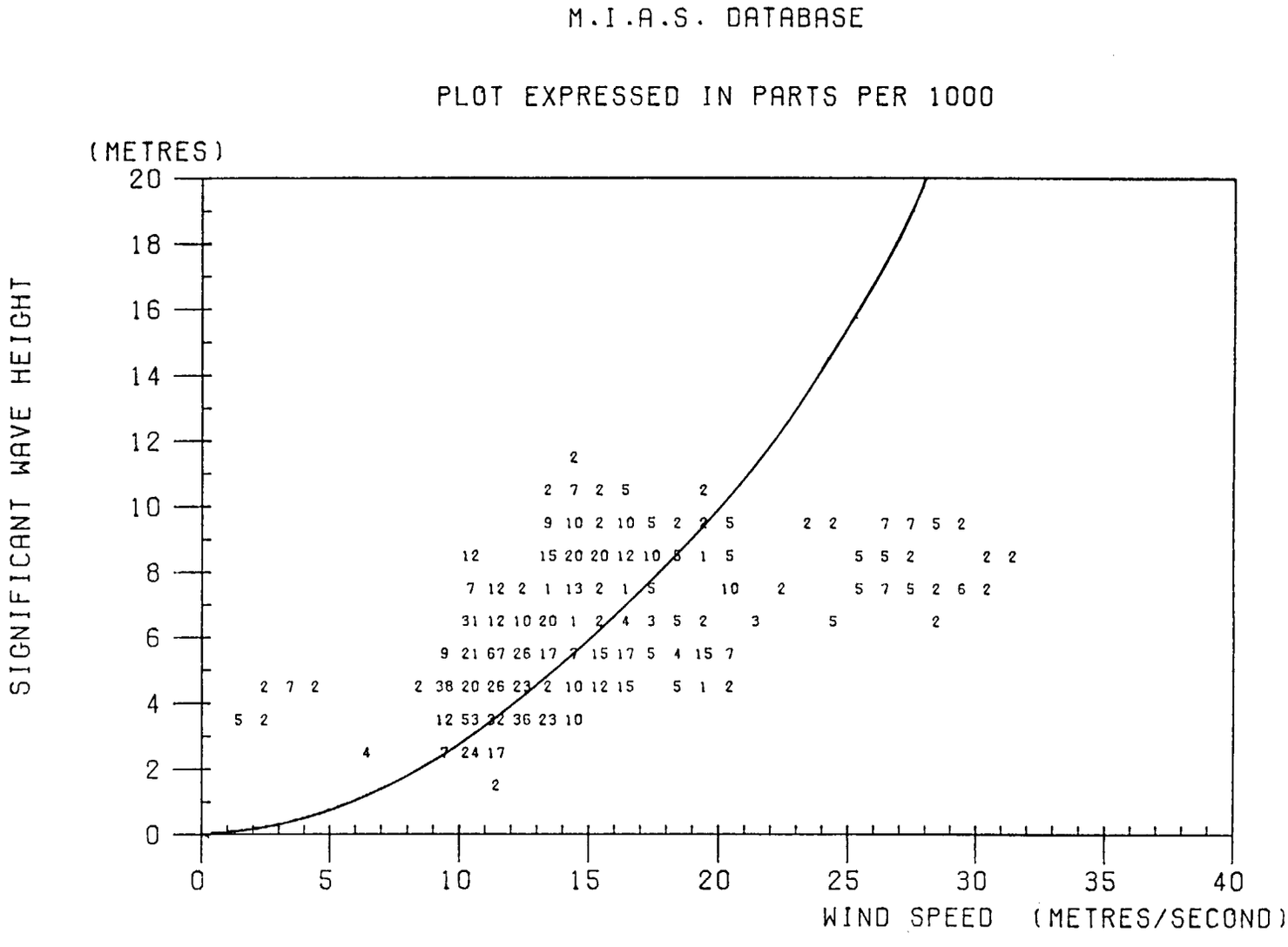

Fig. 2.6 Plot of significant waveheight (m) against wind speed (m/s) derived from GEOS-3 data in February 1976; area covered is 54.5-59.5°N and 17.5-22.5°W. The curve shows the relationship for a fully-developed sea.

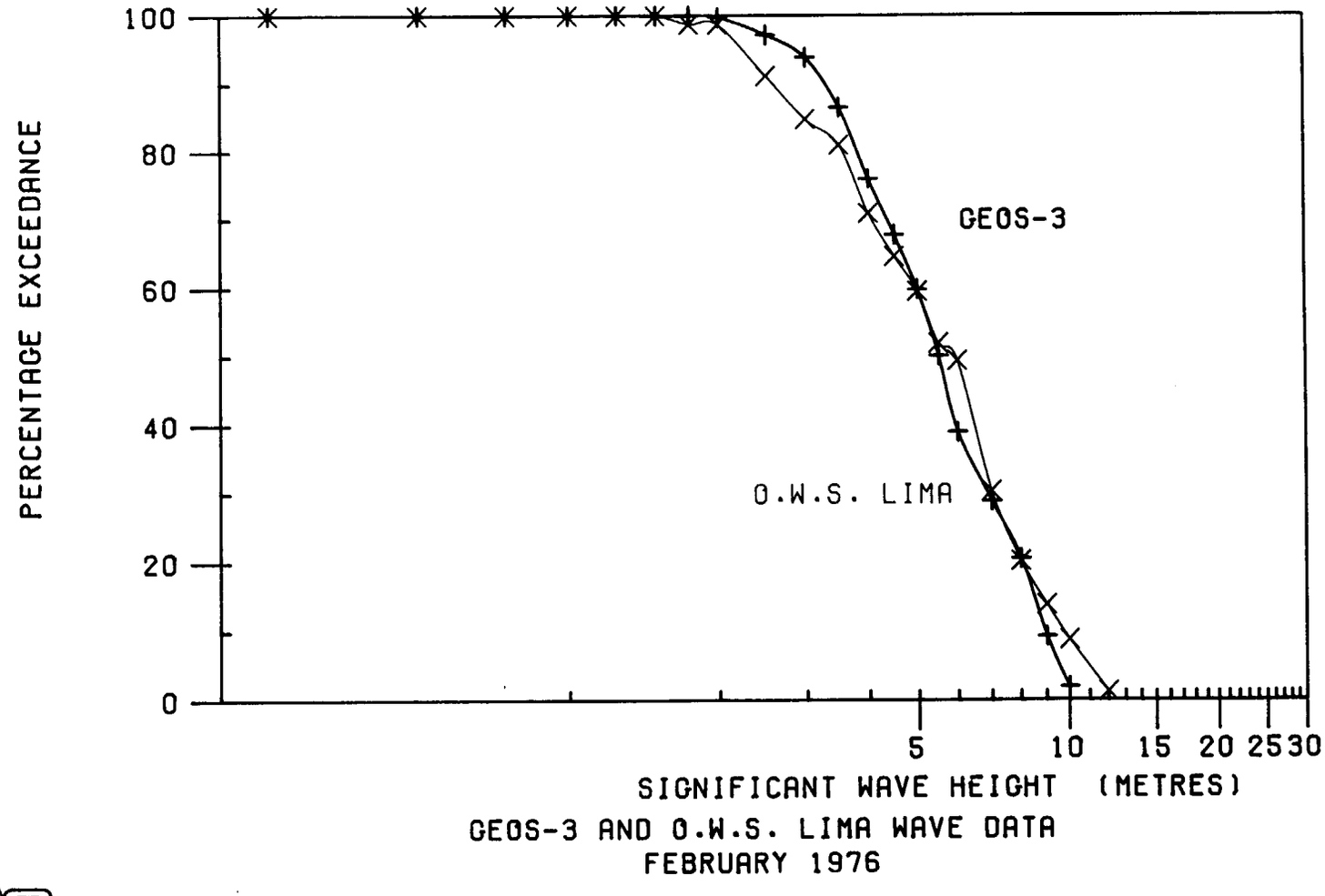

Fig. 2.7 Exceedance diagram for significant waveheight derived from GEOS-3 and O.W.S. Lima data in February 1976. Geographical area same as in Fig. 2.6.

fully-developed sea. In Fig. 2.7 an exceedance diagram is displayed based on GEOS-3 and in-situ data. The agreement is encouraging, suggesting that monthly statistics from a 5^{o} square have some validity. In this example the satellite estimates indicate that H_s exceeded 5 m for 60% of the time and 8 m for 20% of the time.

2.3 Wind Products

2.3.1 Usefulness of R.A. data for winds

Surface winds are required as an input to numerical weather forecasting models, to wind-wave models and, in the form of wind stress, to ocean circulation models. It is generally assumed that altimeter winds are not as useful as those from a scatterometer because they give no directional information and the coverage is limited to a few kilometres either side of the sub-satellite track compared with several hundred kilometres. However, the altimeter on ERS-1 has the potential to produce useful wind products in several areas. These are:

(i) to provide estimates of wind speed at the same points as waveheight measurements

(ii) to extend coverage of ERS-1 for wind speed

(iii) to examine small-scale variations in wind speed

(iv) to obtain wind information closer to land and ice than is possible with the scatterometer

(v) to provide wind speed for the Along-Track Scanning Radiometer/Microwave (ATSR/M) so that the accuracy of water vapour retrievals can be improved

(vi) to correct cloud-motion vectors derived from geostationary VIS/IR images to the ocean surface.

(i) Coincidence with waveheight measurements

On ERS-1 the radar altimeter will be the only instrument capable of giving wind speeds at nadir. The wind scatterometer, unlike that carried by Seasat, has no footprints near nadir and the microwave part of the ATSR, although sampling at nadir, does not have the appropriate frequencies to retrieve wind speed. On Seasat the Scanning Multichannel Microwave Radiometer (SMMR) swath extended from 50 km to the left of nadir to 600 km to the right. Such overlaps have proved important in the evaluation of the sensors which in turn has begun to shed light on the different physical processes associated with wind determination by the three sensors (see 3.2). For many purposes winds are required in the interpretation of wave records and so as to minimise problems caused by spatial variability both parameters should be measured as close together as possible. The altimeter samples the same footprint for wind and waves. This allows some information on swell component to be extracted from the significant waveheight estimated by the altimeter (Mognard, 1983; Parsons, 1979).

(ii) Extend wind speed coverage of ERS-1

As implied in (i) using Seasat it is possible by combining SMMR and Seasat-A Satellite Scatterometer (SASS) data to map wind speed in a swath extending from 50 km to the left to 700 km to the right of

the satellite track and in some modes a swath on the left-hand side from 200-700 km. The lack of a scanning microwave radiometer on ERS-1 and the reduced swath of the scatterometer (400 km wide, near edge 250 km off nadir, single-sided mode only) means that the altimeter winds help to fill in a significant gap in the coverage for both real-time and precision products.

(iii) Small-scale variability of winds

The size of the altimeter footprint over the ocean is a few kilometres compared with ~50 km for the ERS-1 scatterometer. Although the AGC tracker loop (from which altimeter wind speed is derived) has a time constant of 3 s, implying that independent wind estimates are obtained every 21 km, (footprint velocity ~7 kms^{-1}) this is only a constraint for fast delivery data. Reprocessing of the waveform data will allow a spatial resolution of a few km to be realised. Such sampling will be useful in studying the detailed variation of winds across atmospheric fronts and in relation to mesoscale convective systems.

(iv) Winds close to land/ice

Related to (iii) is the problem of obtaining good wind data close to land and ice. The small footprint of the altimeter gives it an advantage over other sensors but with Seasat there were difficulties when loss-of-lock occurred as the footprint moved from land to open water(Rapley et al., 1985 Appendix I(d)). Methods are currently being explored to minimise this problem. Coastal winds are

important in studying pollution and sediment transport, for harbour control and a variety of leisure activities. Near sea ice a knowledge of surface winds is useful for studying break-up of the ice and predicting drift of ice-floes.

(v) Input to ATSR/M water vapour retrieval

In order to extract atmospheric water content from passive microwave data it is necessary to remove the effects of surface wind on the emissivity of the sea surface and hence on the brightness temperatures of the channels being used. On Seasat there were sufficient channels on the SMMR to estimate wind speed but for ERS-1, where the two channels chosen are those most sensitive to atmospheric water, wind speeds will have to be derived from an external source. The altimeter is the obvious choice because of coincidental coverage. It should also be remembered that the main reason for deriving atmospheric water vapour estimates is to provide the wet tropospheric range correction for topography products from the altimeter.

(vi) Correction of cloud-motion wind vectors to the surface

It has been suggested (WCP, 1984) that altimeter winds could be used to correct wind speeds derived from geostationary satellite cloud-motion data (representative of a height of 1-2 km) to the sea surface. This relationship may well hold for some distance either side of the satellite track and, since wind direction may also be derived from the cloud motion such a technique would offer possibilities of obtaining the wind vector over a swath perhaps 200

km wide, centred on the sub-satellite track. Such data would also comp lement the wind scatterometer coverage.

2.3.2 Wind data products required

Some wind products have already been discussed in 2.2.4 because of the requirement of wave data users to have access to relevant wind information. There is a class of users who will not need to have a combined wave/wind data set. Therefore a separate wind product should be considered consisting of $\sigma^o(0^o)$, $U_{19.5}$ (the 19.5m wind speed), and τ the surface wind stress. Accuracy requirements are given in Table 2.5. A reason for retaining σ^o in the geophysical product is that, given the uncertainty in the relationship between radar backscatter and wind speed discussed in 3.2, users may wish to have the option of developing their own algorithm. Surface stress is included because it is the parameter used in representing wind forcing in ocean models. It seems most likely that for ERS-1 the stress will have to be obtained from the wind via the bulk parametrization formulae (e.g. Large & Pond,1981). Uncertainties in the parametrization schemes will contribute an additional error to the stress determination. There is some hope that a more direct relationship between σ^o and stress can be obtained but the lack of high quality direct measurements of the latter has prevented much progress in that direction. It is generally believed that to relate σ^o to stress rather than wind has a sounder physical basis (Woiceshyn et al., 1984) though Donelan & Pierson (1984) provide an alternative view-point.

Table 2.5 Desired accuracies for 1s means of altimeter wind parameters

Parameter	Achievable accuracy	Desirable accuracy	Not useful	Rank	Comments
Sigma nought	$\pm$ 1.0dB (8-20dB)	$<\pm$0.5dB at 8dB $<\pm$1.0dB at 20dB	$>\pm$1.5dB at 8dB $>\pm$2dB at 20dB	1A	Doubt over absolute accuracy of 0^{o}
Wind speed (at reference height)	$\pm$2m/s (0-10ms^{-1})	$<\pm$2m/s (0-24ms^{-1}	$>\pm$20%	1A	1B for speeds exceeding ~10ms^{-1}
Surface stress	?	$<\pm$25% (0-0.8Nm^{-2})	$>\pm$45%	3	Includes errors in drag coefficient

Key to rank

1A Well established and validated

1B Well established

2 Possible (more processing needed)

3 Research

Notes

1. Reference height for winds should be same for altimeter and scatterometer.

2. The oceanographic components of WCRP require monthly averages of wind stress and wind speed for 10^{o} lat. x 10^{o} long. boxes (2^{o} x 5^{o} in tropics). Accuracy of analysed fields should be 20% of signal for wind speed and 10% for wind stress (WCP, 1984).

Sections 3.2 and 6.2 discuss the processing stages involved in extracting wind parameters from the raw altimeter data. Surface wind speed will be produced as a fast delivery product using on-board estimates of Automatic Gain Control (AGC). Together with stress it will also be generated at the PAF from level 1.5 data (sensor records at $20s^{-1}$ sampling).

As with waves it is expected that most end users will access the data at levels 3 and 4. One example is the requirements of the World Ocean Circulation Experiment (WOCE) and Tropical Ocean Global Atmosphere (TOGA), two of the oceanographic components of the World Climate Research Programme (WCRP, 1983). In order to meet their objectives winds and stress are needed in areas a few degrees square and meaned over one month. Accuracies have been expressed in terms of these averaged quantities since it is on these scales that surface forcing is considered to be important. These accuracies are stringent but attainable if there are sufficient independent samples over the specified area per month to reduce the random errors and if systematic errors can be minimised. It is the latter constraint which is the more serious since, given the empirical nature of the algorithms, biases due to geographical location and sea-state conditions may enter. Atmospheric attenuation may also prove to be a serious problem at this level of accuracy.

It should be noted that WCRP will use a combination of winds from different sources, particularly scatterometers. It is therefore of paramount importance that the calibration/validation of wind products from these sensors should be standardised as far as possible

(6.4). Possible contents of the level 2 wind product which will serve as the basic geophysical product and which must be routinely available on a global-coverage basis, are listed in Table 2.6. Examples of higher level products are given in Table 2.7. Some of these could be made available in a useful hard-copy form using Figs 2.2-2.7 as a basis but plotting wind speed for waveheight.

2.4 Sea-ice data products

2.4.1 Usefulness of R.A. data

The relevance of satellite radar altimetry to sea-ice studies has been discussed by Rapley et al. (1983), Squire et al. (1984), and Rapley et al. (1984). Several areas have been identified in which it is believed that ERS-1 altimeter data will be useful and in one or two cases this has been demonstrated from previous spaceborne and airborne altimeter missions. These are:-

(i) determining the position of the ice-edge/ ocean boundary

(ii) sea-ice characteristics

(iii) iceberg detection

(iv) penetration of ocean waves into the ice field.

(i) Ice-edge/ocean boundary

This is a very important parameter for weather prediction, monitoring climate, and commercial activities such as shipping and off-shore drilling in high latitudes. The extent of sea-ice varies considerably especially on a seasonal time-scale, occupying on

Table 2.6

Possible contents of Basic Geophysical (Level 2) Product for Winds

Tape header: Algorithm IDs, start/end times of tape, start/end pass numbers, list of variables, units, formats.

1st File header: Satellite pass number, equator crossing time, equator crossing longitude, number of data cycles to follow, number of gaps.

1st data file: 1 sec. means of the following variables (number of bytes in brackets):

1. t	Time since start of pass	(4)
2. La	Latitude	(4)
3. Lo	Longitude	(4)
4. U_z	Wind speed at reference height	(2)
5. σ_{u_z}	Variance of 20/s values of U_z	(2)
6. τ	Magnitude of surface stress	(2)
7. σ_τ	Variance of τ	(2)
8. $\sigma^o(0^o)$	Normalised radar cross-section at nadir	(2)
9. σ_{σ^o}	Variance of σ^o	(2)
10.	Data quality flags	(1)
11.	Land/water/ice flags	(1)
12.	Rain, atmospheric attenuation flags	(1)

2nd File header

2nd data file

etc.

Note Each one-second data cycle consists of 27 bytes (= 216 bits)

Table 2.7 Description of possible wind data products

Product level	Type	Source level	Data quantity	Production frequency	Delivery time	Parameters	Usefulness ranking
Fast delivery	1 s chronological within 50km of land 5 s chronological outside 50km of land	TM	10^5 bits/pass	1/pass	3 hr	U_z, $\sigma°(0°)$, position, time	1
2	1 s along-track, chronological	1.5	$4x10^8$ bits	1 month	3 months	Full set as in Table 2.6	1
3	1 s geographically ordered, chronological within each area	2	$4x10^5$ bits/ 10° box	1 month	3 months	Full set as in Table 2.6	1
4	Box means + statistics	2	10^3 bits/ 10° box	1 month	3 months	Full set as in Table 2.6	1
5	Combined mean wind and stress data from ALT and Wind Scatterometer	4	?	1 month	3-6 months	TBD	?

Notes: TM = telemetered data

Usefulness ranking: 1 = Very useful
2 = Useful

average about 2.4 x 10^7 km^2 or 7% of the ocean surface. Knowledge of the boundary position is required in atmospheric and ocean circulation models so that its effects on momentum, heat and water vapour transfer, through surface roughness, albedo and mechanical barrier effects can be taken into account.

In practical terms, sea ice acts as an impediment and hazard for all ship-borne activities at high latitudes. Accurate and timely ice data are essential for the optimum routing of commercial shipping and for the exploration and exploitation of the polar resources of fish, gas, oil and minerals.

It has been well established that the presence of new or first year ice may be detected by the altimeter, using changes in the echo waveform shape and strength (e.g. Dwyer & Godin, 1980; Rapley, 1984a). For GEOS-3 and Seasat, these changes affected the on-board computed parameters, allowing ice boundary locations to be defined using the 1 s^{-1} data in the Geophysical Data Records (GDRs) (i.e. without having to analyse the waveform data).

Limitations, as for wave parameters, are chiefly associated with the sampling characteristics of a single space-borne instrument. Even though the separation of altimeter tracks becomes less with increasing latitude they are still likely to be separated by gaps many times larger than the sensor footprint and to eliminate these would imply increasing the orbit repeat to the point where the rapid variability of ice-edge position could not be meaningfully monitored (see 2.6). Other problems arise from the definition of what constitutes the ice-edge and the presence of eddying and banding in

the ice fields which may cause multiple ice-edge indicators along a single track or ambiguities in the interpretation of data from consecutive repeat tracks.

In order to distinguish between such features, and so identify relatively stationary eddy features that may be bathymetrically or oceanographically induced, repeated altimeter crossover passes will be needed. Additionally, such information on ice edge morphology will allow calculations to be made of ice transport beyond the mean ice edge. This will be of value in estimating the total heat flux budget in the ice edge region. Seasat data studied so far suggests that the altimeter may be particularly good at identifying regions where freezing is occurring. The ice-edge deduced from the altimeter can be used to update the map of ocean/ice boundaries required for flagging data from other sensors.

(ii) Sea-ice characteristics

Required sea-ice characteristics include: concentration, floe size distribution, surface roughness and ice thickness. Concentration is undoubtedly one of the most influential factors of the Marginal Ice Zone (MIZ) regions. Its variation provides the spatial inhomogeneity of the pack; its value indicates how much ice is present relative to open water. It is often observed that the concentration does not increase monotonically with penetration into the ice field as might be expected and as predicted by numerical models. The existence of low ice-concentration regions and any quantitative measurements made of their distribution, persistence,

etc. would be a stimulus to further research aimed at improving the models. Related to this is the detection of leads and polynyas where the varying mixtures of open water and ice will affect consecutive waveforms. Floe size distribution, which appears to be exponential above a minimum size of 7.5 m, is of interest because its variation with distance into the ice cover reflects the controlling scenario for that location, particularly ocean waves, currents and winds. Although a mapping instrument may be more effective in this task the fact that a single parameter is able to represent the floe size distribution suggests that with adequate modelling it may be possible to extract this parameter from altimeter waveforms.

The roughness of the upper ice surface will affect the shape of the return pulse. This may be related to the age and type of the ice. Not only will the reflection coefficient, height and slope distributions control the intensity of the backscatter but the presence of meltpools will lead to additional interpretive problems. It may be possible to relate ice thickness to waveform type, classified according to ice type, e.g. multi-year, or fresh ice.

The techniques for extracting these parameters almost certainly require analysis of the waveform data and are as yet at an early stage of development. Indeed, this is now an active area of research, using altimeter data from Seasat and from the Marginal Ice Zone Experiment (MIZEX) aircraft campaigns (Powell et al.,1984).

(iii) Iceberg detection

A knowledge of iceberg positions and movement is essential for work involving ships and off-shore platforms in polar regions. Another application would be to obtain an estimate of iceberg occurrence density along the satellite path. By combining this with known statistical distributions of iceberg sizes it has been suggested (Squire et al., 1984) that this could then be used to estimate the mass balance of the Antarctic ice sheet. The calving of icebergs at the margin is by far the most important ablation mechanism for the Antarctic ice sheet. The problems are that single icebergs cannot be tracked because they cannot be unambiguously reidentified given the space-time sampling, and that the altimeter may grossly overestimate the size of large bergs because of the gaps due to loss of lock and execution of the subsequent reacquisition sequence.

(iv) Penetration of ocean waves

Some work has been carried out using conventional techniques on this aspect, but all the data suffer from limited temporal and spatial extent. It would be useful, with the advent of petroleum engineering in the MIZ, to be able to provide industry with the equivalent long-term statistics to those we have for waves in the North Sea for example. Rapley (1984) has examined the potential for measuring the attenuation of waves by the ice from Seasat altimeter data. Although the ocean model (and hence the H_s algorithm) is strictly invalid for water containing ice he finds that the computed

values of H_s gradually decrease with increasing distance into the pack and relates this to the proximity of high swell regions in the open ocean.

2.4.2 Sea-ice data products required

One of the major difficulties in defining sea-ice products is that many of the uses outlined above have not been developed to the point where the relevant parameters can be extracted with confidence, much less validated. The greater latitudinal coverage and/or technical improvements of the ERS-1 altimeter over previous missions (Skylab, GEOS-3, Seasat) plus the understanding gained in recent years in interpreting altimeter returns over ice (satellite and airborne) provides encouragement that products will be produced routinely. The basic product for sea-ice studies should be at level 1.5 where, along with housekeeping and position/time, raw waveforms would be available at 20 s^{-1}. Unlike winds and waves, because the modelling of altimeter interaction with the complicated ice surface is poorly understood, most effort will have to be spent on developing the extraction algorithms. For the ocean, a 1 s mean waveform would be sufficient but sea-ice is so spatially inhomogeneous that waveforms averaged over shorter times are required. The 20 s^{-1} rate is a compromise between this and the need to average a number of pulses (in this case ~50) to reduce the effects of noise on the pulse shape.

From the 20 s^{-1} data Guymer (1984) recommended that a Level 3 data product should be generated for ice edge position and iceberg

flags. Geographical ordering obviously makes sense for ice products since large portions of the ocean are not affected by ice at all. In view of the interest in relating ice break-up to wave activity, ice products should contain wave parameters (and probably also wind) to facilitate such work. Rather than attempting to have a product in which the position of the ocean/ice boundary is identified (i.e. one data cycle per pass through the area) it may be better to generalise the parameter to a sea-ice indicator. This would leave the interpretation of where the main boundary was located (in complex conditions which gave multiple ice/ocean transitions) to experienced analysts. Possible contents of the Level 3 sea-ice product are shown in Table 2.8. Different levels of products are described in Table 2.9.

Other ERS-1 sensors are capable of providing sea-ice information. The Synthetic Aperture Radar (SAR) if operating should clearly indicate where sea-ice exists but not at the same location as the altimeter. Nevertheless the information can be used to interpolate the sea-ice boundary between tracks. Because of its high spatial resolution the SAR is well-suited to identifying polynyas and small-scale structures in the ice. The ATSR/M should also be capable of identifying the ocean/ice boundary and possibly yield information on ice-type. The SAR and ATSR/M data will therefore be of importance in developing methods of retrieving ice parameters from the AGC, and for suitably validated parameters it can be envisaged that products obtained from a combination of the sensors will be generated.

Table 2.8

Possible contents of Basic Geophysical (Level 3) Product for Sea-Ice

Tape header: Algorithm IDs, start/end times of tape, start/end pass numbers, list of variables, units, formats.

1st File header: Geographical zone ID, satellite pass number, equator crossing time, equator crossing longitude, number of data cycles to follow, number of gaps.

1st data file: 1 per second samples of the following variables (Number of bytes in brackets):

1.	t	Time	(4)
2.	La	Latitude	(4)
3.	Lo	Longitude	(4)
4.	I	Sea-ice index	(1)
5.	σ^o	Normalised radar cross-section	(2)
6.	H_s	Significant waveheight	(2)
7.		Iceberg flag	(1)
8.		Data quality flags	(1)
9.		Precipitation, atmospheric attenuation flags	(1)

2nd File header

2nd data file

etc.

Each 1s data cycle contains 20 bytes (= 160 bits)

Notes

1. Data product will be generated from retracked waveform data.
2. This product will only be produced poleward of 50^o latitude.
3. From sea-ice index ice boundary can be obtained (rated 1B) and possibly surface characteristic (rated 3). Iceberg flag is rated 2.

Table 2.9 Description of possible sea-ice data products

Product level	Type	Source level	Data quantity	Production frequency	Delivery time	Parameters	Usefulness ranking
Fast delivery	(i) Coordinates of ice/ocean transitions on each pass from 1 s^{-1} on-board data	TM	60 lat/long pairs per day	1/pass	3 hr	Time, position, ice/ocean flag	1
	(ii) Possibly 1 s values of ice index	TM	10^3 bits/pass	1/pass	3 hr	Time, position, ice index	?
1.5	20 s^{-1} chronological, only for 'ice regions'	1.0	10^9-10^{10} bits	1 month	3 months	Raw waveform, instrument and geophysical corrections	1
3	1 s^{-1} geographically ordered, chronological	1.5	$4x10^5$ bits/10° box	1 month	3 months	All parameters, as in Table 2.8	1
4	Statistics for defined areas	3	10^3 bits/ $10^\bullet$ box	1 month	3 months		2
5	Combined ice indices, surface characteristics from ALT and other ERS-1 sensors (e.g. ATSR/M, SAR	3	?	1 month	6-9 months		?

2.5 Ocean topography data products

2.5.1 Usefulness of radar altimetry for ocean topography

The shape of the sea surface is of great importance to oceanographers and geodesists. Its largest variations (when compared with the reference ellipsoid) are of order 100m and reflect the inhomogeneity of the Earth's gravity field, partly due to differences in the composition of the underlying mantle and partly due to the bottom bathymetry. The equipotential surface known as the geoid corresponds, over the oceans, to the mean position of the free surface in the absence of fluid motion. Until a few years ago the best estimates of the geoid on global scales were from the observed perturbations in the orbital motion of artificial satellites using ground-based tracking stations. However, altimeters on board Skylab and GEOS-3 measured the range between the satellite and the ocean surface to a precision (1m and 50cm respectively) that revealed significant geoidal variations on space scales shorter than could possibly be studied using previous techniques. Deep ocean trenches were associated with marked features in height profiles. Subsequent work with Seasat data has shown with remarkable detail the effect that geophysical features can have on the surface elevation.

Superimposed on the geoidal variations are those associated with tides and ocean currents. These are much smaller (typically by two orders of magnitude, except in the case of coastal tides). Just as surface pressure charts can be used in meteorology to infer the near-

surface wind through the geostrophic relationship so surface elevation can be used to yield surface currents. In practice, this has not proved viable because of the lack of a reference surface against which to measure the small slopes. The traditional approach has been to assume a level of no-motion in the deep ocean and, using horizontal density gradient measurements and the "thermal wind" relationship to calculate vertical shear, to integrate upwards so that the surface geostrophic current is obtained. Both the assumption of a level of no-motion and the paucity of synoptic data lead to large uncertainties in the flow obtained. Satellite altimeter measurements offer great possibilities for the synoptic mapping of ocean topography particularly as the measurement precision increases. Seasat had a precision of slightly less than 10 cm similar to that expected of ERS-1 and future satellites are likely to achieve ~2 cm.

GEOS-3 was capable of detecting the Gulf Stream but the present generation of altimeters is capable of providing improved estimates of tides and weaker currents. However, as the instrument precision is improved in order to study these weaker ocean signals it becomes increasingly important to make accurate corrections for propagation errors in the pulse travel time from which height information is derived and for errors in orbit determination. These are outlined in 3.3. Once these have been applied there still remains the problem of analysing the data according to the phenomenon to be studied. The geodesist can, for example, average all the data to produce a mean sea surface which will be the best estimate of the geoid for large

areas. The oceanographer may subtract out such a mean surface so that he can examine the residual effects due to tides and currents but in so doing he removes the part of the geostrophic circulation that is time-invariant during the averaging period. An independent knowledge of the geoid is required. There are also other oceanic effects which may lead to a false interpretation of the data - the wave-bias (5.1.3) and inverse barometer effects (3.3.2).

It is expected that ERS-1 topography products will contribute significantly to tidal studies (though its sun-synchronous orbit means that some constituents will not be retrievable) and to mapping of mesoscale variability of the sea surface which can be related to velocity fields in eddies and rings. Particular interest has been shown in ERS-1 data by planners of WOCE and TOGA.

2.5.2 Ocean topography data products required

It is clear that the basic parameter common to all of the applications outlined in 2.5.1 is the height of the sea surface above a reference level, h, and that the required products differ mainly in the space and time scales on which h is analysed so as to isolate the feature being studied from other contributing factors. However, the altimeter does not measure h but rather a time delay which is converted to h by applying a number of propagation and orbit corrections. These are detailed in Foster et al. (1980) and Allan et al. (1984). Since some of these corrections are uncertain it is advantageous to include all the corrections in the basic data records so that if necessary they can be removed and new corrections made.

The problems of discussing topography products differ from those of waves, wind and sea-ice in that a single, easily understood and more or less directly measured parameter (range) is common to all the applications but its correction to the desired precision, and its subsequent partition into that part of the spectrum which is of interest, requires the synthesis of a number of highly disparate data streams.

The required accuracy of h depends on the purpose that is intended. Table 2.10 lists accuracy requirements which are based on those documented in Foster et al. (1980), Drewry et al. (1984) and Allan et al. (1984). Descriptions of products and their delivery time requirements are detailed in Table 2.11. One of the biggest constraints on delivery time is likely to be the time taken to determine precisely the orbit.

At present the incorporation of height data into the Fast Delivery Product is being considered. However, range data uncorrected for propagation or orbit errors could prove very useful in some circumstances if available in near real-time. Western boundary currents are associated with large changes of surface elevation (>1 m) over a short distance which would be identifiable on raw data provided they could be distinguished from any similar gradient in the geoid. In some regions, for example off the eastern seaboard of North America, the geoid is known rather well. These geoidal data could be held at Kiruna and subtracted from the height signal before dissemination. Alternatively, users could compare successive profiles along repeat tracks, applying suitable offsets to

2.10 Accuracy requirements for absolute height measurements

Feature	Achievable accuracy (cm)	Desirable accuracy (cm)	Not useful (cm)	L* (km)	Rank
Mesoscale eddies	5	3	30	100	1A
Boundary current variability	5	3	30	300	1A
Equatorial variability	5	1	10	300	3
Seasonal circulation	?	3	30	1000	3
Tides	10?	3	30	3000	1A

*Height accuracy is residual after application of a highpass filter of cutoff wavenumber L^{-1}

Based on Allan (1984)

Key to rank

1A Well established and validated

1B Well established

2 Possible (more processing needed)

3 Research

Table 2.11 Description of possible ocean topography data products

Product level	Type	Source level	Data quantity	Production frequency	Delivery time	Parameters	Usefulness ranking
Fast delivery	1 s chronological, absolute accuracy few m, rel. accuracy 30 cm	TM	5×10^4 bits/pass	1/pass	3 hr	Time, position, range (rel. to best geoid)	2
2	1 s chronological (all corrections applied)	1.5	10^8-10^9 bits	1 month	3-6 months	Time, position, ht above ellipsoid, height above geoid, variance, skewness, geophys. corrections, orbit height	1
3	Geographically ordered, 1 s values	2	10^5-10^6 bits/ 10°	1 month	3-6 months	As level 2 but without corrections	1
4	(i) Mesoscale variability	2	10^3 bits/10° box	1 month	6 months	On for cross-overs or along repeat tracks	1
	(ii) Cotidal maps, etc.,	2	10^3 bits/10° box	3 months	6 months	Amplitude, phase of tidal constituents at cross-overs.	1
5	Products from minimising cross-over differences with other altimeter data	4	?	1 month	6-9 months	As for level 4	1 ?

correct for orbit errors, to identify regions of larger variability associated with the lateral displacement of major current systems. Such information may prove useful for operational purposes (e.g. shipping, fisheries) and for real-time planning of oceanographic experiments during the ERS-1 mission. Similarly, sudden changes in range as the altimeter footprint crosses large icebergs or ice shelves may yield useful information for operational planning. These data are not strictly required within three hours, a delay of a day or two would probably be tolerable. This raises the question as to whether an intermediate category (between Fast Delivery and Off-line Precision Products) is required. Such a 'Semi-fast Delivery Product' category would also be useful for data evaluation and as a backup to the Fast Delivery Product.

2.6 Effect of orbit repeat on products

There are conflicting requirements for the type of orbit ERS-1 should be placed in depending on sensor and application. For example, users of SAR images for mapping land features may like a non-repeating orbit such that contiguous swaths are obtained over periods of days of weeks with minimum overlaps so that as large an area could be covered within the area for which real-time acquisition is possible. By contrast, for an altimeter the oceanographic and glaciological communities have emphasised the need for repeating orbits (with a tolerance of 1 km) so that unknown geoidal errors and spatial variations can be eliminated. Even so, there is no agreement on what repeat is ideal. Wave data users would prefer 3 days while

for iceberg detection 40 days has been suggested (Guymer,1984). No decision has to be reached in the near future on the choice of orbit and ERS-1 will carry enough fuel to allow several different orbits to be used during the mission. Nevertheless it is wise to assess the impact which the different choices might have on data processing requirements:

- The quantity of data to be processed and archived is not dependent on the type of orbit since data rates and the operating times of the sensors will remain the same. (For some purposes the adoption of a non-repeat orbit would render the data virtually useless so that some high level products, such as along-track temporal averages, may not need to be generated during such a period).
- The size of the geographical area chosen at Levels 3 and 4 should be related to the distribution of tracks. In some cases, e.g. short repeat periods (large spacing between tracks) it would be possible to choose boxes in which there were no data points. To avoid this the minimum E-W length of the box should be approximately equal to the separation at the equator of the shortest repeat period likely to be used which is probably 3 days (the repeat period chosen for the commissioning phase of ERS-1). This gives a figure of 10^{o} and on average there will be 10 passes through the box per month. Longer repeats will increase the number of different tracks in the box but the number of passes per month will remain constant. Generally there will be x passes per month through

a box x^{o} longitude wide, provided $x>27/n$ (where n is the repeat period in days).

- Assuming that the orbit repeat period (and therefore the position of the tracks) will be changed several times during the mission it would appear sensible to organise the data at Levels 3 and above so that all data from one set of repeats are archived together, rather than strict observance of calendar months.
- Another consequence of the orbit repeat choice is the position of the R.A. tracks in relation to interesting ocean regions and to land. It is particularly desirable that coverage is optimised over European waters. For example an ascending pass selected so that the sub-satellite track lay in the middle of the North Sea would also give R.A. data off the W. coast of Italy. A repeat orbit could be chosen so that the next ascending pass westwards was in the SW approaches and across Biscay. The choice of orbit parameters would also affect the positions of the descending tracks. Ideally these should provide long tracks over the North Sea and to NW of Scotland but in practice this may not be possible. It would also be an advantage if the positioning of the passes allowed a direct overflight of a reliable in-situ measurement platform.
- Calibration/Validation implications are discussed separately in 6.4.
- Altimeter studies of sea ice are compromised by the limited temporal and spatial sampling of a single satellite-

borne instrument. The rapid motions and temporal changes of the ice cover, combined with the altimeter's relatively small footprint and widely separate, infrequently revisited ground tracks result in the ice data being incompletely sampled.

Fig. 2.8 shows the Seasat ground track pattern in the vicinity of Antarctica at a time when the orbit was adjusted to repeat on a three day cycle. Also shown are the Antarctic coastline and the approximate location of the sea ice boundary at maximum winter extent. For a section of sea ice boundary lying approximately along a circle of latitude (as occurs in the Antarctic) the average spatial sampling interval, l, is given by:

$$\Delta l = 2\pi R\cos\theta/\alpha n$$

where θ is the latitude, n is the number of revolutions in the orbit repeat cycle, R is the Earth's polar radius (~6360 km), and $1 \leq \alpha \leq 2$ depending on the exact disposition of the boundary with respect to the ground track pattern. Typically, altimeter satellites execute ~14 full rotations per day. Thus for an N day repeat cycle at the time of maximum winter extent ($\theta \simeq 55$) we have $800 \leq \Delta l \leq 1600$ km for 1 days data, and values 1/N times less for the full cycle.

Any increase in the density of spatial coverage necessitates increasing the period of the repeat cycle. Experience with the Seasat 3-day repeat data shows that smoothing of the data to ~70 km resolution is necessary to obtain reasonable self-

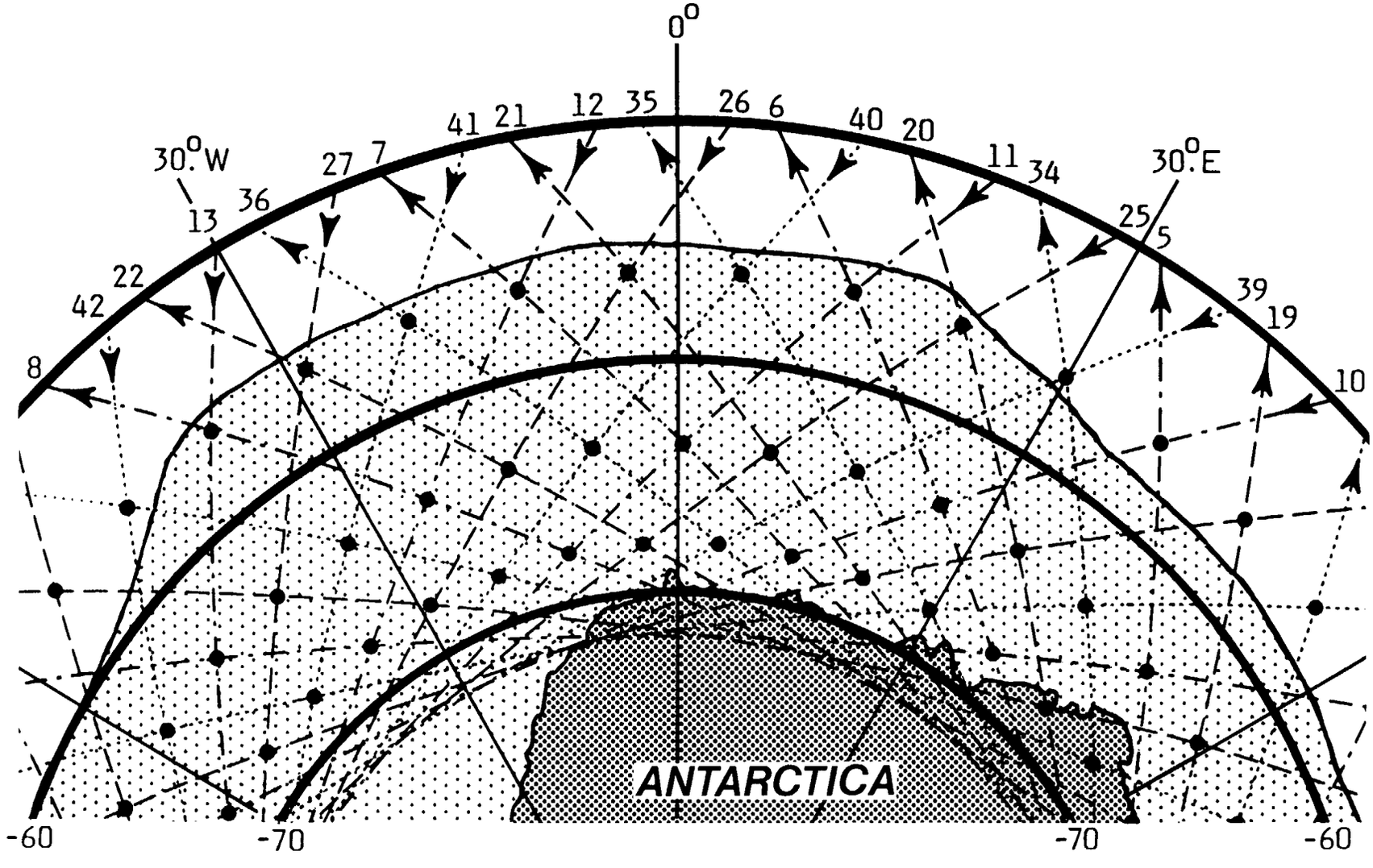

Figure 2. 8 Seasat '3-day' groundtracks in the vicinity of Antarctica. The Antarctic-continent and region covered by sea ice at the time of maximum winter extent are shown with dark dots and light dots respectively (from Rapley (1984(b)).

consistency over a full cycle. Even then localised inconsistencies occur, as might be expected given that local ice velocities as high as 50 km per day can occur. At the winter ice boundary a 3-day repeat cycle achieves $250 \leq \Delta l \leq 500$ km sampling. A factor of two or so increase in repeat cycle duration would therefore result in an approximate matching of the sampling interval and the smoothing interval required to achieve self-consistency, both being ~150 km in the vicinity of the ice edge. A six to seven day repeat cycle thus represents a near optimum compromise for sea ice observations. Global maps at this resolution would be useful for scientific purposes, particularly those related to climate research. Detailed observation of selected local areas could be carried out with much higher spatial resolution (~km) but with rather poor (7 day) repetition.

2.7 Special problems

The ERS-1 altimeter, like that of Seasat, is a pulse-limited radar designed for use over the open ocean. An on-board signal processor estimates values of height (h), significant waveheight (H_s) and backscatter coefficient (σ^o) at a rate of 20 s^{-1} for rapid dissemination on the ground. The instrument design assumes that it is pointed vertically at a flat, horizontal, isotropic sea with reflective properties as defined by Brown (1977). For echo waveforms with shapes corresponding to the Brown model, the altimeter maintains its height tracking point at the 50% power level of the leading edge ramp, and this is taken as the mean surface height.

The existence of non-linear wave effects introduces a systematic offset in the height estimate, as discussed in section 5.1. More major distortions of the waveform shape introduce proportionally larger systematic height errors (see Figs 2.9(a) and 2.9(b)), which couple into the parameter estimates output by the other on-board processing loops. Such distortions may arise in a number of ways, as follows:

(i) Instrument mispointing displaces the point of maximum antenna gain away from the nadir, attenuating the leading part of the return echo. The effect results in return echo shapes similar to that shown in Fig. 2.9(a).

(ii) The presence of clouds or intense rain cells can strongly attenuate the return from localised regions of the footprint, introducing an absorption feature in the corresponding part of the echo waveform.

(iii) The presence of slicks or patches of floating weed may alter the reflective properties of the ocean surface.

(iv) In the vicinity of islands, coastlines or over inland seas strong, off-nadir returns from elevated land surfaces can introduce features within the altimeter range window.

(v) Over sea ice, echo waveforms are generally strongly peaked and fluctuate rapidly in shape and strength as the altimeter traverses localised features.

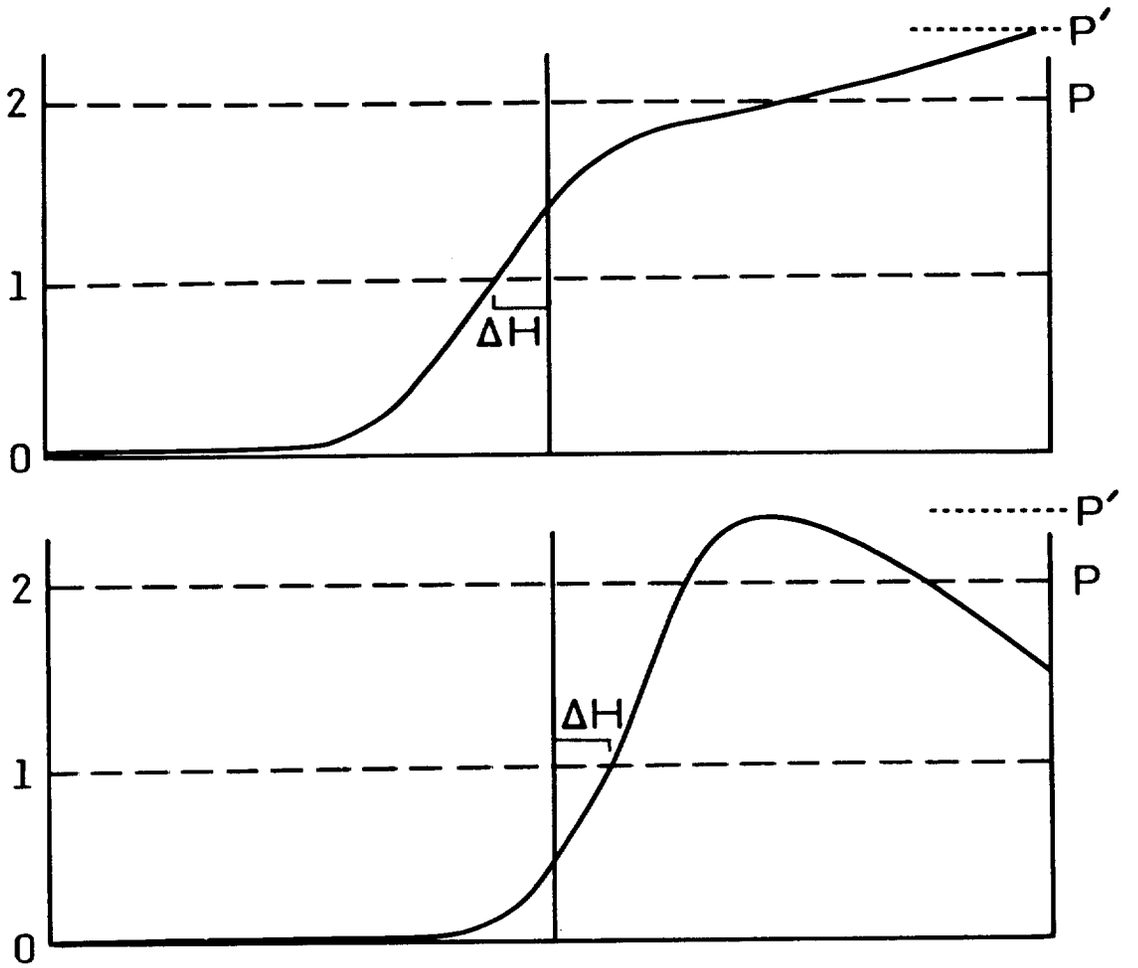

Pulse shape distortions introduce:-

- H offset
- AGC error
- 'SWH' error

Height tracker error signal is given by:-

- $\varepsilon' = \alpha\,\varepsilon$

where : $\alpha \propto \frac{P'}{P}$ and ε is the correct value

Figure 2. 9 Seasat processing algorithm pulse shape-induced errors.

The effect of non-standard, varying pulse shapes on the on-board estimates of h, H_s and σ^o can be very severe. For example Monaldo, Goldhirsh & Walsh (1984) show that passage over an intense rain cell (5 km height, rain rate = 10 mm per hour) can introduce temporary instantaneous errors of up to 1 m in the on-board estimated height value. The problem, in this case, results from the intense absorption feature associated with the rain as it affects surface returns initially passing closer to and then further from the nadir. The feature migrates from the tail of the echo waveform (greater range) passes through a point where it is at, or closest to, the leading edge and then migrates back out of the tail.

Bright quasi-specular features from land or from sea ice behave similarly. However, very peaked pulses not only introduce tracker point offsets but can introduce a tracker loop oscillation (Rapley et al,. 1983). Furthermore the backward migration of very bright features in the range window may be followed by the height tracker, resulting in large height excursions or, in cases, loss of lock. This effect, referred to as "snagging", can occur under any circumstances where a bright reflector passes out of the beam. Over sea ice it appears to occur most often over regions in which substantial areas of open water occur within the ice pack, implying an association with ice-water transitions (Fig. 2.10; also refer to Rapley, 1984).

Given that measures may be taken in the tracker design to reduce the likelihood of loss of lock (see Section 4.4), data processing methods must be devised to eliminate or correct data affected in

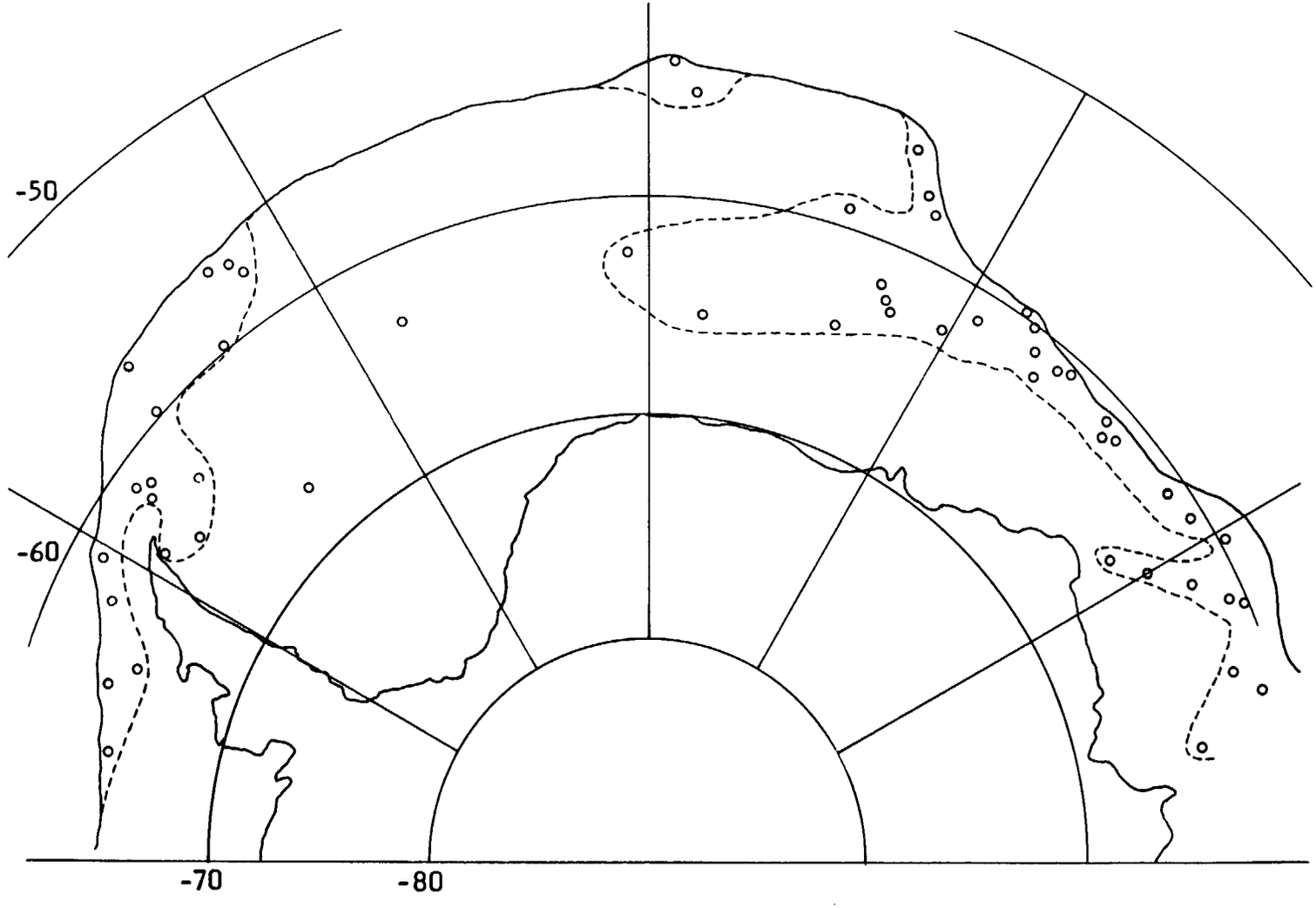

Figure 2.10 Locations of loss of tracker lock during a 1 month period of Seasat coverage. The points tend to cluster near the ice edge (approximate average location shown) and in the area where the Weddell Sea polynya forms, implying an association with regions in which areas of open water may exist (Rapley, unpublished).

these ways. For Seasat the elimination of incorrect values was achieved using a sequential fitting technique applied to the three on-board computed parameters. This permitted identification of extreme out-of-bound data (Hancock, Forsythe & Lorell, 1980). The standard deviations of the parameters were also computed, using a running average, to identify regions of poor quality data. In each case the corrupted data were eliminated. However, it is clear that processing of the waveforms on the ground could reduce the amount of data lost in this way. As yet the techniques involved have not been properly explored or developed.

3. General review of geophysical data retrieval on other altimeter missions.

3.1 Significant waveheight

3.1.1 Physical basis

Before reviewing the various extant algorithms for estimating the significant waveheight H_s from the radar return, a brief description of the physics of radar reflection from the sea surface will be given.

3.1.1.1 Factors affecting the form of the return pulse.

The three main factors affecting the radar return from the sea surface are:

(a) the radar characteristics (antenna gain, pulse shape, etc.)

(b) the satellite motion (for example, the pointing angle of the antenna)

(c) the characteristics of the ocean surface (in particular, its statistics).

Brown (1977) has combined these effects to obtain a theoretical description of the radar return from a rough surface, such as that of the sea, under the assumption of Gaussian statistics for the surface. He initially calculates the flat surface impulse response of the radar, which he then convolves with the "specular point height probability density function" and the system point target response to obtain the rough surface response.

In terms of the statistics of the sea surface the "specular point height probability density function" is perhaps best understood as the probability of obtaining a flat surface impulse response at a given surface elevation ζ, that is $p(\zeta, \zeta_x=0, \zeta_y=0)$; where $p(\zeta, \zeta_x, \zeta_y)$ is the joint distribution of surface elevation ζ and slopes (taken in two mutually orthogonal directions) ζ_x, ζ_y. Strictly use should be made of $p(\zeta, \zeta_{xspec}, \zeta_{yspec})$ where ζ_{xspec} and ζ_{yspec} vary with the angle of incidence of the radar pulse. Here this is approximated by $p(\zeta, \zeta_x=0, \zeta_y=0)$, or in normalised form $q(\zeta)$, as the angle varies little over the radar footprint. For a Gaussian surface

$$q(\zeta) = \frac{1}{\sqrt{2\pi\mu_{200}}} \exp\{-\frac{\zeta^2}{2\mu_{200}}\}$$

where μ_{200} is the variance of the sea surface elevation elevation ζ (the significant waveheight $H_s = 4\mu_{200}^{1/2}$).

This is identical to the distribution of the surface elevation $p(\zeta)$ (see Longuet-Higgins, 1957). For a non-Gaussian surface $q(\zeta)$ will differ from $p(\zeta)$, in general. The identity of the two distributions has led to some confusion as to what aspect of the sea surface the radar senses. From the above it is clear that it senses the distribution of the elevations of points with zero slope rather than the distribution of sea surface elevation. For the special case of a Gaussian surface the two are identical, but for a non-Gaussian surface they differ. This needs to be borne in mind when analysing the latter situation.

Returning to Brown's (1977) results for a Gaussian surface; it

is found that the return pulse $P_r(t)$ is given by

$$P_r(t) = \int_{-\infty}^{\infty} \left[\int_{0}^{\infty} \frac{c}{2} q\left(\frac{c\tau}{2} - \frac{c\hat{\tau}}{2} \right) d\hat{\tau} \right] P(t-\tau)\, d\tau$$

$$\times \begin{cases} P_{FS}(0) & t<0 \\ P_{FS}(t) & t \geq 0 \end{cases} \qquad (3.1)$$

where c is the speed of light in vacuo and P is the system point target response. (The change from elevation ξ to time t is made by setting $\xi = -ct/2$.) Here t = 0 corresponds to the mean of $q(\xi)$, that is, the mean level of the points on the surface with zero slope.

$P_{FS}(t)$ is the flat surface impulse response and is given by

$$P_{FS}(t) = \frac{G_o^2 \lambda^2 c\, \sigma^o(\psi_o)}{4(4\pi)^2 L_p h^3} \times \exp\left\{ -\frac{4}{\gamma} \sin^2 \xi - \frac{4c}{\gamma h} t \cos 2\xi \right\} \times I_o\left(\frac{4}{\gamma} \sqrt{\frac{ct}{h}} \sin 2\xi \right)$$

where λ is the radar wavelength

L_p is the two-way propagation loss

h is the height of the satellite above the mean level

ξ is the pointing angle (measured from nadir)

G_o and γ are antenna gain parameters

$\sigma^o(\psi_o)$ is the backscattering coefficient

and ψ_o is given by

$$\tan \psi_o = (ct/h)^{1/2}$$

The point target response is assumed to be Gaussian and given by

$$P(t) = \eta P_T \exp(-t^2/(2\sigma_p^2))$$

where η is the pulse compression ratio

P_T is the peak transmitted power

and σ_p is a measure of the pulse width

If the double integral in eq. (3.1) is denoted by I(t) it may be evaluated to obtain

$$I(t) = \eta P^T (2\pi)^{1/2} \sigma_p [1+\mathrm{erf}(t/(\sqrt{2}\,\sigma_c)]/2$$

where

$$\sigma_c^2 = \sigma_p^2 + 4\mu_{200}/c^2$$

and

$$\mathrm{erf}(x) = \frac{2}{\sqrt{\pi}} \int_0^x \exp(-t^2)dt$$

(See Brown, 1977, for more details.)

Examples of the (normalised) return waveform obtained from the above analysis are given in Figs 3.1 and 3.2. From these it can be seen that with increasing surface roughness (that is, increasing significant waveheight) the return signal becomes more smeared out, while variations in the pointing angle primarily affect the fall off of the return at large times.

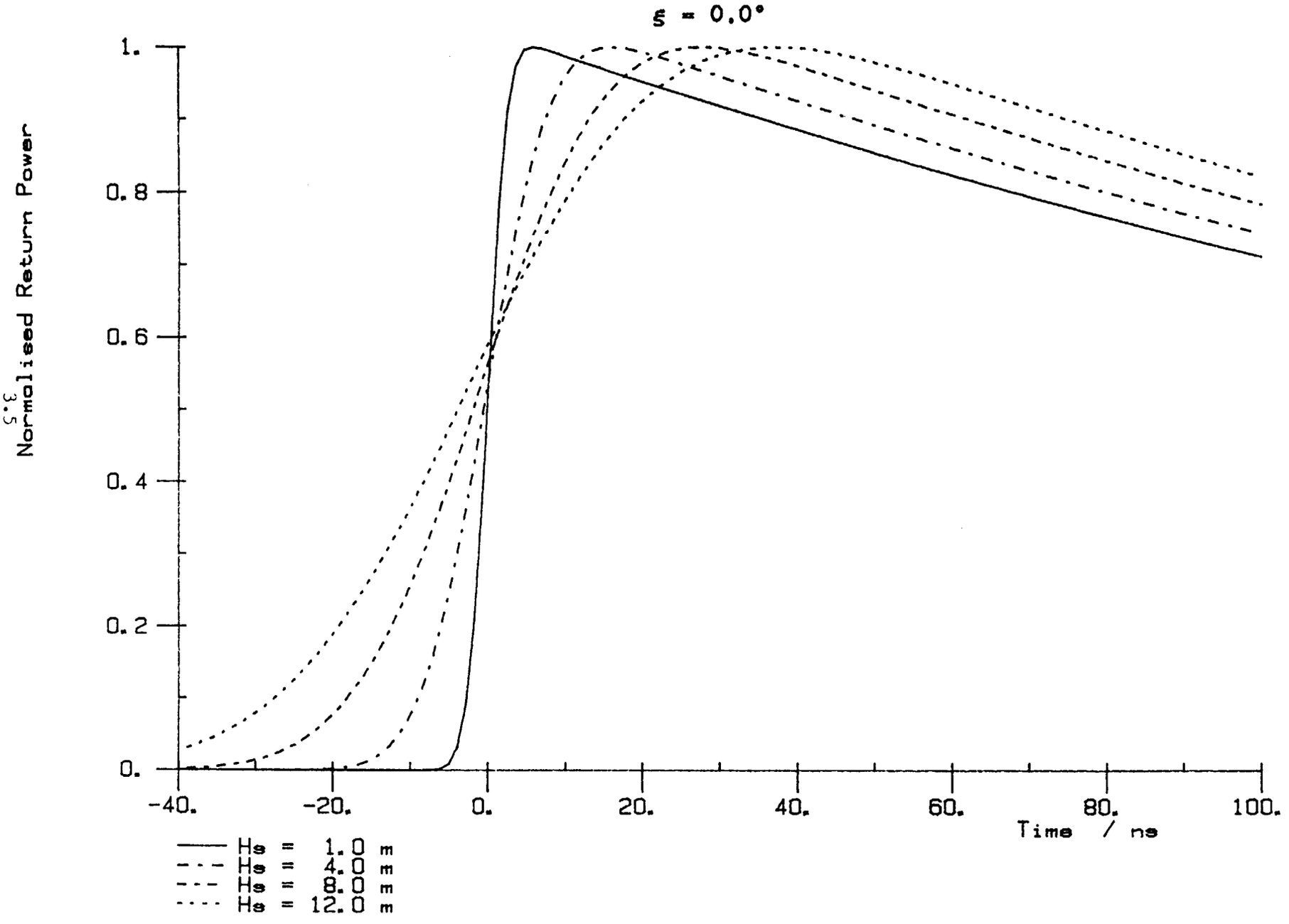

Fig. 3.1 Normalised return power $P_r(t)$ for zero pointing angle, $\xi = 0^o$, and H_s=1,4,8,16 m.

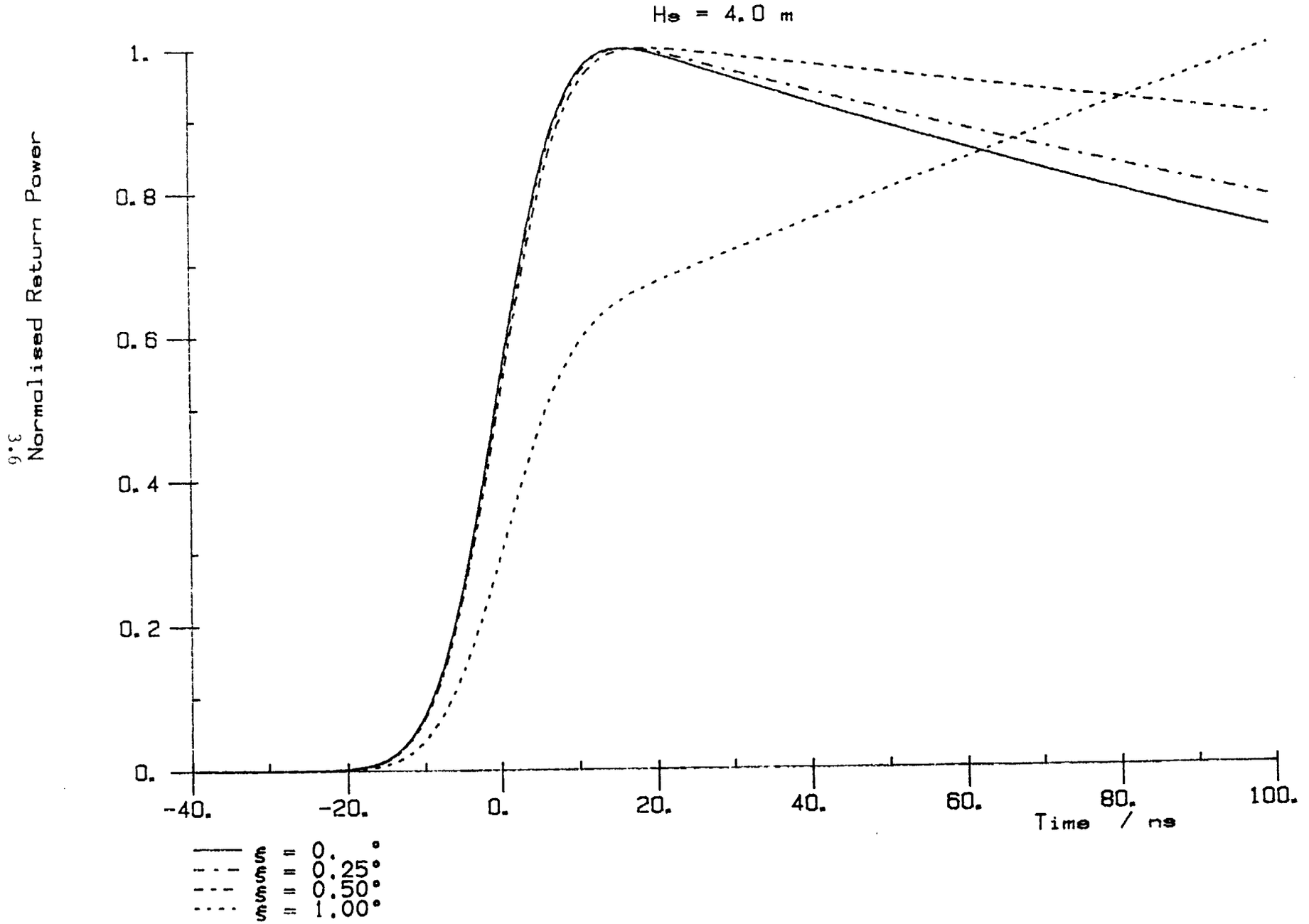

Fig. 3.2 Normalised return power $P_r(t)$ for H_s=4 m and ξ =0,0.25,0.5,1°.

3.1.1.2 Modelling the statistics of the sea surface.

From the previous section it can be seen that in order to obtain the theoretical form of the radar return some assumption has to be made as to the statistics of the sea surface. If the waves on the sea surface can be described by linear wave theory then the statistics of the sea surface may be shown to be Gaussian (Longuet-Higgins, 1957). Thus the simplest (and most common) assumption used about the sea surface is that its statistics are Gaussian.

If, however, nonlinear wave effects are important then Gaussian statistics are no longer adequate and a different statistical model is necessary. Longuet-Higgins (1963) obtained a non-Gaussian theory for the sea surface on the basis of a weakly nonlinear dynamical model for the wavefield. Jackson (1979) used this theory to obtain the joint distribution of the surface elevation and slope (in one direction only) $p(\zeta, \zeta_x)$. He then used this to study the radar return from the sea surface. Srokosz (1984b) has further extended the theory to obtain the joint distribution of surface elevation and slopes (in two mutually orthogonal directions) $p(\zeta, \zeta_x, \zeta_y)$, which allows a fuller description of the sea surface. The relevant results are

$$p(\zeta, \zeta_x, \zeta_y) = \frac{1}{(2\pi)^{3/2}} \frac{1}{(\Delta_2 \mu_{200})^{1/2}} \cdot \exp\left\{ -\frac{\zeta^2}{2\mu_{200}} - \frac{1}{2}\left[\mu_{002}\zeta_x^2 - 2\mu_{011}\zeta_x\zeta_y + \mu_{020}\zeta_y^2 \right] / \Delta_2 \right\}$$

$$\times \left[1 + \frac{1}{6}\left(\lambda_{300} H_{300} + 3\left(\lambda_{120} H_{120} + \lambda_{102} H_{102} + 2\lambda_{111} H_{111} \right) \right) \right]$$

where $\Delta_2 = \mu_{020}\mu_{002} - \mu_{011}^2$

and H_{mnp} are generalised Hermite polynomials - see below.

$$p(\xi) = \frac{1}{\sqrt{2\pi\mu_{200}}} \exp\left\{-\frac{\xi^2}{2\mu_{200}}\right\} \cdot \left[1 + \frac{1}{6}\lambda_{300} H_{300}\right]$$

and

$$q(\xi) = \frac{1}{\sqrt{2\pi\mu_{200}}} \exp\left\{-\frac{\xi^2}{2\mu_{200}}\right\} \cdot \left[1 + \frac{1}{6}\lambda_{300} H_{300} - \frac{1}{2}\delta \frac{\xi}{\mu_{200}^{1/2}}\right]$$

If

$$\eta = \frac{\xi}{\mu_{200}^{1/2}} \quad , \quad \eta_x = \frac{\xi_x}{\mu_{020}^{1/2}} \quad , \quad \eta_y = \frac{\xi_y}{\mu_{002}^{1/2}}$$

then

$$H_{300} = \eta^3 - 3\eta$$

$$H_{120} = \frac{\eta}{1-\lambda_{011}^2}\left[\frac{(\eta_x - \lambda_{011}\eta_y)^2}{1-\lambda_{011}^2} - 1\right]$$

$$H_{102} = \frac{\eta}{1-\lambda_{011}^2}\left[\frac{(\eta_y - \lambda_{011}\eta_x)^2}{1-\lambda_{011}^2} - 1\right]$$

$$H_{111} = \frac{\eta}{1-\lambda_{011}^2}\left[\frac{(\eta_x - \lambda_{011}\eta_y)(\eta_y - \lambda_{011}\eta_x)}{1-\lambda_{011}^2} - \lambda_{011}\right]$$

where

$$\lambda_{mnp} = \mu_{mnp} \Big/ \mu_{200}^{m/2} \cdot \mu_{020}^{n/2} \cdot \mu_{002}^{p/2} \qquad m+n+p \leq 3$$

and

$$\mu_{mnp} = \langle \xi^m \xi_x^n \xi_y^p \rangle$$

(Here $\langle\ \rangle$ denotes an ensemble average.) Finally, δ is given by

$$\delta = \left(\lambda_{120} + \lambda_{102} - 2\lambda_{011}\lambda_{111}\right) \Big/ \left(1 - \lambda_{011}^2\right).$$

The various terms in the above expressions have the following interpretations:

μ_{200}	- the variance of the sea surface elevation
μ_{020}, μ_{002}	- the variance of the slopes
μ_{011}	- the correlation between the slopes
λ_{300}	- the skewness of the sea surface elevation
λ_{120}, λ_{102}, λ_{111}	- coefficients of skewness with no clear physical meaning

In the linear limit the skewness coefficients go to zero (λ_{300}, λ_{120}, λ_{102}, $\lambda_{111} \rightarrow 0$) and the Gaussian results are recovered. Jackson's (1979) results may be recovered by integrating out the dependence on ξ_y. Finally we note that $p(\xi)$ and $q(\xi)$ differ for this non-Gaussian case, as expected. The non-zero values of the coefficients λ_{300}, λ_{120}, λ_{102}, λ_{111} are due to the nonlinear effects. In particular λ_{300}, the skewness of the sea surface elevation, is a measure of the nonlinearity of the waves, resulting from their having peakier crests and flatter troughs.

The above results will be used in section 5.1 to extend the theory given in section 3.1.1.1 to nonlinear waves and to produce extensions to the algorithms reviewed below.

3.1.2 Algorithms for significant waveheight

3.1.2.1 General Principles

The form of the altimeter return from the sea surface is explained in section 3.1.1. If Fig. 3.1 is studied it can be seen that the return waveform can be split into two sections. The first section consists of a sharply rising S-shaped curve. This is followed by a plateau that slowly decays. Significant waveheight is estimated from the first section. The basic technique is common to virtually all the algorithms described here. The actual return waveform, averaged over a large number of pulses, is compared to a theoretical return. This theoretical waveform is expressed in terms of the parameters we are trying to estimate, usually altitude of the satellite and significant waveheight, and possibly other, nuisance, parameters. By varying these parameters the theoretical waveform is fitted to the received waveform. The algorithms differ both in the assumed theoretical form of the returned pulse and in the method used to obtain a fit. The theoretical waveforms used in the algorithms in many ways constitute the greatest differences between them. Most of the methods of fitting are variations on the theme of least squares and will be described below.

Because of the large number of assumed return waveforms in use it is not proposed to go into any detail here but merely to give a general description. The simplest form of the return that can be assumed is a straight line and this form is used in the on-board algorithms where computational speed is the overriding concern. The

next simplest form is to use a Gaussian cumulative distribution function. More complex are algorithms that utilise the complete Brown model described above or some variation on it.

As stated above least squares is the most popular criterion for fitting. This is due in part to the fact that maximum likelihood turns out, in this case, to be simply weighted least squares. For large samples it can be shown that maximum likelihood is statistically optimal. It is quite instructive to derive the likelihood equations. The derivation here follows Peckham (1982).

The power output at each gate or range bin from a single pulse will have a negative exponential distribution. If the pulses are far enough apart, so that the antenna has moved at least its radius between pulses, then the returns are statistically independent and the average power over a number of pulses will have a normal distribution by the central limit theorem. To produce the likelihood of the return we need to assume that the outputs from individual gates are also statistically independent. For this to be the case the gates must be separated by at least the width of the original pulse. If these two conditions hold then the equations for the maximum likelihood estimations of the parameters of the return (α_j) are

$$\sum_i \frac{1}{\hat{g}_i^2} \left(g_i - \hat{g}_i \right) \frac{\partial \hat{g}_i}{\partial \alpha_j} = 0$$

where $\hat{g}_i = \hat{g}_i(\alpha_j)$ is the theoretical output of the i^{th} gate and g_i is the actual output.

These equations are, of course, the equations for a weighted least squares solution with weights equal to $\hat{g}_i^2$ (the variance of the return at the i^{th} gate).

These equations, both weighted and unweighted least squares, need to be solved numerically. Walsh (1979) reports convergence problems with the maximum likelihood solution and as a consequence prefers to use the unweighted least squares. He states that Gower (1979) gets around these problems by only using the weights in the maximum likelihood solution when they are greater than a certain value. We have not been able to find this in Gower (1979). Gower does find an improvement using maximum likelihood on model data, but in practice the situation is complicated because errors in the positioning of the gates of GEOS-3 violate the assumptions given above. Obviously great care must be taken to remove such errors before applying any algorithm.

The above discussion has assumed that the analysis has been done using output from each gate. Some algorithms, in particular the on-board ones, aggregate the gates and work with means. This speeds up computation at the cost of some loss of accuracy. Two algorithms are somewhat different. Rather than attempt to fit a Gaussian distribution function, a Gaussian p.d.f. is fitted to a differentiated waveform. This makes the fitting easier but adds the complication of numerically differentiating the waveform.

3.1.2.2 Description of Algorithms

Since most of the algorithms are very similar the details will be given in the form of a table, Table 3.1. One does not fit into the scheme described above and will be briefly outlined after the table. Some entries in the table are incomplete, this is because it has not been possible to discover the relevant details. This lack of information has proved to be a serious problem. Many details of the algorithms seem never to have been published and no references are given even to internal documents, etc. This makes comparisons and choosing the best method difficult. For instance, Walsh (1979) estimates skewness in addition to H_s, but it has proved impossible to find the form of return that he used, and hence assess this work.

Certain abbreviations are used in the table.

These are LS - unweighted least squares

MLE - maximum likelihood

References in the table are numbered as follows:

[1] Fedor et al.(1979)

[2] Fedor & Barrick (1978)

[3] Gower (1979)

[4] Rufenach & Alpers (1978)

[5] Mognard & Lago (1979)

[6] Walsh (1979)

[7] Walsh et al.(1978)

Table 3.1 Summary of H_s algorithms

Name of algorithm	refs.	Fits pdf ?	Method of fitting	Group gates	Theoretical Return Used	Notes
FEDOR	[1],[2]	yes	LS		Barrick(1972)	
GODBEY	[1]					Does not fit into the pattern above -described in text.
GOWER	[1],[3]		modified MLE		(1)	
RUFENACH & ALPERS	[1],[4]		LS		(1)	
MOGNARD & LAGO	[5]	yes	LS(?)		(2)	No details
WALSH	[1],[6] [7]		LS		No details given	Estimates skewness
GEOS-3	[1]		LS	?	No details	same as Seasat?
SEASAT			LS	Gates grouped into 6 triples	(3)	The middle of the leading edge is found using the first & last sets of gates. The triple corresponding to the leading edge is found and H_s taken from look-up table.

Several theoretical returns are also numbered. These are:

(1) Gower and Rufenach & Alpers use the theoretical return

$$\hat{g}_i = (\hat{g}_{\infty} - \hat{g}_{-\infty})[1 + \mathrm{erf}((t-t_0)/\sqrt{2}\,\sigma_c)]/2$$

(Rufenach and Alpers subtract an additional $\hat{g}_{-\infty}$)

where $\hat{g}_{\infty}$ is the height of the plateau

and $\hat{g}_{-\infty}$ is the noise gate output.

H_s is then calculated from:

$$H_s = 0.6(\sigma_c^2 - \sigma_\tau^2 - \sigma_j^2)^{1/2}$$

where σ_τ = Gaussian pulse width of the signal

and σ_j = r.m.s. jitter in the signal.

(2) Mognard and Lago fit a Gaussian p.d.f. to the differentiated return, one assumes by least squares, and then calculate H_s as in (1).

(3) The return form used to generate the Seasat look-up table is

$$g(t) = A(t)\{1 + \mathrm{erf}(t/\sqrt{2}\sigma_p[1+(2\sigma_s/\sigma_p)^2]^{1/2})\}/2$$

where $A(t) = \exp[-4ct/\gamma h]$, $t \geq 0$

$= 1$ $\quad t<0$.

Godbey's algorithm does not fit into the pattern outlined above. The method is described in Fedor et al.(1979) and the description given here is taken from that paper. The return is split into four sections. The first corresponds to the noise region before the leading edge. The next two are halves of the leading edge and the final portion is the plateau. Each gate in the middle sections is normalised such that

$$s_i = \frac{g_i - \text{average(section 1)}}{\text{average(section 4)} - \text{average(section 1)}}$$

The following factor is then computed

$$F_s = 2.4 + \sum_{\text{Sect.2}} s_i - \sum_{\text{Sect.3}} s_i$$

Significant waveheight is then calculated from

$$H_s = 5F_s - 3(F_s - 1.25)^3 + 3/(0.5+25F_s^2)$$

The constants in these expressions were calculated in part from the altimeter design and in part empirically.

A brief description will now be given of the comparisons of algorithms that have been given in the literature. We have been able to find two papers concerned with this topic. One Fedor et al (1979) is concerned with GEOS-3 and the other, Fedor and Brown (1982), with Seasat. Fedor et al (1979) compare five algorithms. These are given in Table 3.1 as FEDOR, GODBEY, GOWER, GEOS-3, RUFENACH & ALPERS and WALSH. The comparison is done both with simulated and real data. Very good agreement is produced although GOWER's estimates have a bias of 0.72m against a buoy. FEDOR's algorithm appears to be the best. The second paper, Fedor and Brown (1982), compares only two algorithms, FEDOR and SEASAT. They find that the Seasat algorithm produces a bias of 0.5m on all measurements greater than 2m whereas the FEDOR algorithm does not.

3.1.3 Swell retrieval

3.1.3.1 General Principles

The sea state is often categorised into 'sea' and 'swell'. The waves generated by the local wind form the 'sea', whilst waves generated elsewhere and propagated into the area form the 'swell'.

Since the sea and swell are independent and have the same mean value, the variance of surface elevation is given by the sum of their

variances. So the relationship between the significant wave height H_s ($=4\sqrt{(\text{total variance})}$) and the sea and swell components of H_s is given by

$$H_s^2 = H_{s,sea}^2 + H_{s,swell}^2 \qquad (3.2)$$

Given a constant wind blowing over the ocean, the sea state grows with $H_{s,sea}$ increasing and the dominant wave period increasing, until the rate of energy transfer from wind to wave is balanced by dissipation within the sea; the sea is then said to be fully developed. In coastal regions with an offshore wind, the limited fetch can prevent the sea from reaching its fully developed state for the given wind speed.

Based on spectral analysis by Moskowitz(1964) of 54 records from Shipborne Wave Recorders in UK weather ships on Ocean Weather Stations in the NE Atlantic (A,I,J,and K) during 1955-1960, and on Kitaigorodskii's (1961) dimensional analysis results, Pierson and Moskowitz (1964) propose the following form for the frequency spectrum of a fully developed sea:

$$S(\omega) = \alpha g^2 \omega^{-5} \exp\{-\beta(\omega_0/\omega)^4\}$$

where $\alpha = 8.10 \times 10^{-3}$

$\beta = 0.74$

and $\omega_0 = g/U_{19.5}$

with $U_{19.5}$ the wind speed measured at 19.5 m above sea level.

Note that the 54 records judged by Moskowitz to represent fully developed conditions was about 10% of all the records examined by him. The value of $U_{19.5}$ for these 54 records varied from about 10 ms^{-1} to 20 ms^{-1}.

$S(\omega)$ can be integrated to obtain the sea surface variance, m_0, and hence the corresponding significant wave height, $H_{s,PM}$ $(=4\sqrt{m_0})$. The result is

$$H_{s,PM} = 0.02133(U_{19.5})^2 \tag{3.3}$$

with units of m and ms^{-1}.

The Seasat altimeter wind speed algorithm is designed to give U_{10}, the value at 10m above sea level. The relationship between U_{10} and $U_{19.5}$ depends upon the atmospheric stability, but using the value given by Pierson (1977):

$$U_{10} \simeq 0.93\ U_{19.5} \tag{3.4}$$

leads to

$$H_{s,PM} \simeq 0.0247\ U_{10}^2 \tag{3.5}$$

This broadband spectrum, theoretically having energy from $\omega = 0$ to ∞, has a peak with corresponding period given by

$$T_p \simeq 5.00\ (H_{s,PM})^{1/2}$$

where units are s and m.

The speed with which this wave energy is propagated from the generating area is, in deep water, half the phase speed $c = \omega/k$ where k is the wave number $(=2\pi/\text{wave length})$. Thus from the dispersion relationship $(\omega^2 = gk)$, the energy is propagated with speed inversely proportional to ω. So the wave energy is 'sorted out' as the swell propagates and the swell becomes increasingly narrow-banded (and long crested) with distance from the generating area; the lower frequency, longer wavelength components arriving first. The swell waves contain less energy when they arrive than in the generating

area - partly because of this sorting out of the frequency components, also because the energy spreads laterally. Nevertheless, swell can have a marked effect for example on large ships, semi-submersibles and structures such as tension-legged platforms which might be generally little affected by shorter waves. The arrival of long swell in shallow coastal water where the waves steepen and break can also generate considerable forces on structures such as breakwaters - see for example Draper & Bowness (1983). The penetration of swell into ice fields is discussed elsewhere in this report (3.4.3).

3.1.3.2 Remote sensing of swell

Swell might be detected, if little sea were present, if either wave period or long-crestedness could be ascertained from the altimeter returns, but neither can easily be obtained at the moment (see section 5.1 and 5.3).

Parsons (1979) and Mognard et al (1981) - also Mognard (1984) - have proposed methods for estimating swell based upon altimeter measurements of H_s and wind speed. From equations (3.2) and (3.5), since $H_{s,PM}$ is the maximum value of $H_{s,sea}$ for a given wind speed U_{10},

$$H_{s,swell}^2 \geq H_s^2 - H_{s,PM}^2$$

i.e.

$$H_{s,swell}^2 \geq H_s^2 - 6.20.10^{-4}\, U_{10}^4 \qquad (3.6)$$

Mognard (1984) uses (3.6) to obtain a minimum value for $H_{s,swell}$ (except she has a constant of 6.25 following from slightly different

constants in equations corresponding to (3.3) and (3.4)). It is important to stress that the ensuing estimate of swell is a minimum. In practice considerable errors can arise in this estimate because of the possibility of large errors in U_{10}^4, particularly at high wind speeds - there is evidence that values of U_{10} greater than about 10 ms^{-1} are significantly underestimated by the Seasat radar altimeter algorithm (3.2.4). At lower wind speeds the algorithm is more accurate - also the difference between minimum and actual swell is then less (see section 3.1.3.3).

Parsons (1977) considers the ratio $R = H_s/H_{s,sea}$, arguing that large R indicates predominantly swell conditions, and using $H_{s,sea} \leq H_{s,PM}$, i.e.

$$R \geq H_s/H_{s,PM} \propto H_s/U_{10}^2$$

Parsons essentially makes the assumption that the sea state is swell-dominated if $H_{s,swell} \geq 0.8\, H_s$ to derive the constant of proportionality. In practice the inequality in (3.6) imposes a limitation upon the method - although Parsons finds good agreement between the swell-dominated region of the N. Atlantic on 24 February 1976 from his analysis of GEOS-3 data and from US National Weather Service hindcast values. (In fact, Parsons uses a more complex function of R describing the age of the sea using wave steepness from expressions for a growing sea state in the absence of swell given by Hasselmann et al. (1976). He appears to assume the altimeter gives $U_{19.5}$.) It must be concluded at present that the radar altimeter cannot measure swell, except in conditions of low winds when the energy of the sea component of the surface waves is small.

3.1.3.3 Effect of wind speed errors on swell retrieval

As discussed in section 3.2.3, Seasat altimeter winds appear to be ~6ms^{-1} low at 20 ms^{-1} when compared with both in-situ and SMMR nadir winds. This implies that for a fully developed sea $H_{s,PM}$ would be incorrectly estimated as 4.2 m instead of 8.5 m (using Eq. 3.3) which would produce a significant difference in the minimum swell height that was calculated from Eq. 3.6.

Figs 3.3-3.5 show the along-track variation of minimum swell height using SMMR and altimeter winds on 3 passes in the NE Atlantic on 28/29 September 1978. Altimeter estimates of H_s are also plotted for reference. The SMMR winds imply that large areas of sea were not fully-developed on these occasions (shown as $H_{swell} = 0$). Differences between the two minimum swell estimates (ALT-SMMR) vary from -0.5m to +4m. Fig. 3.6 expresses this difference as a function of wind speed for those occasions on which a fully developed sea was indicated. A roughly linear dependence is found but further work using other occasions is necessary to verify this.

It would be interesting to correct the winds on the basis of the comparisons with in-situ observations and SMMR and to recompute monthly mean minimum swell maps, particularly for the stormy Southern Ocean, to see what differences result. Because of the averaging involved it is not possible to apply a simple correction to the maps of swell height.

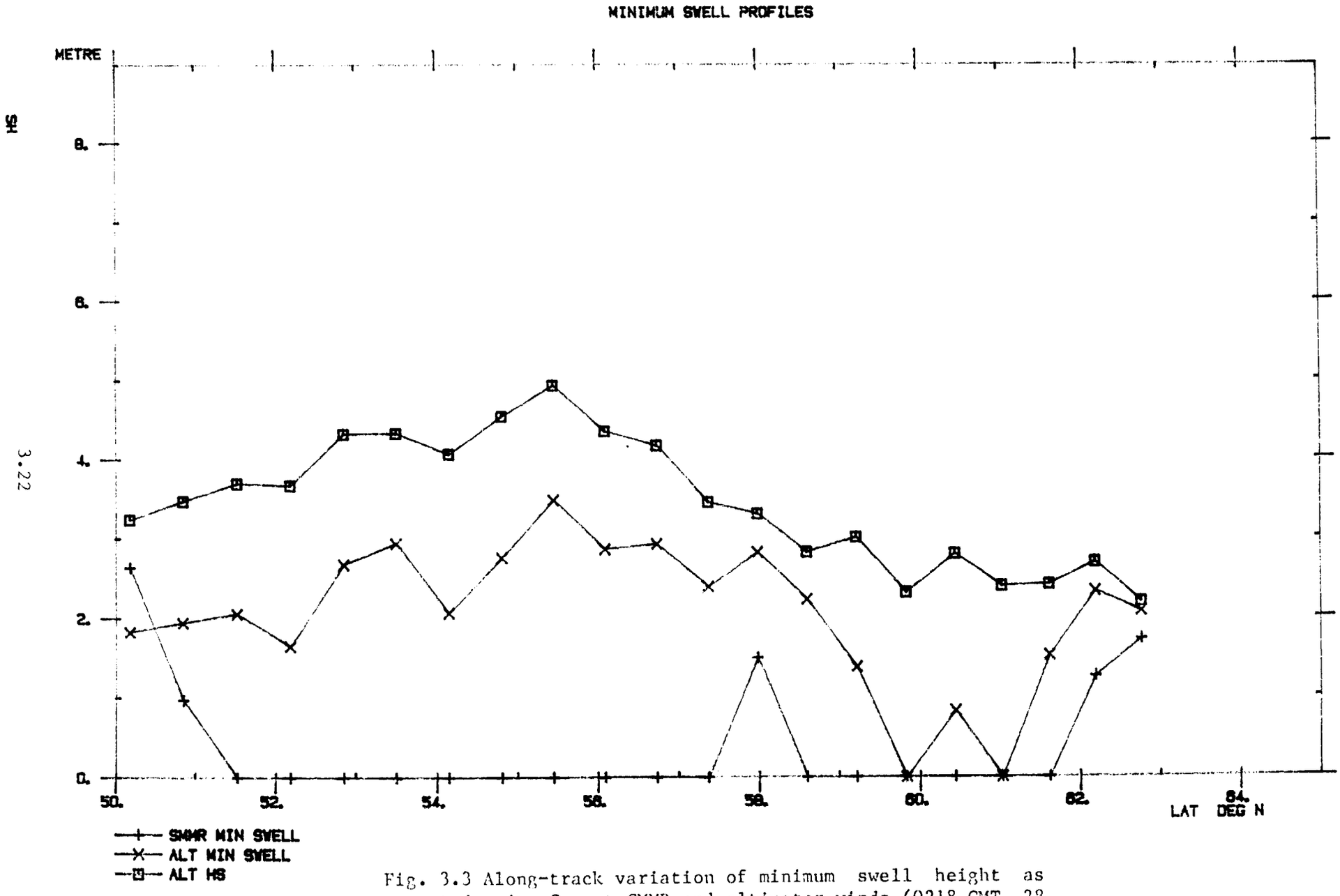

Fig. 3.3 Along-track variation of minimum swell height as computed using Seasat SMMR and altimeter winds (0218 GMT, 28 September 1978). Also shown for reference is the significant waveheight measured by the altimeter.

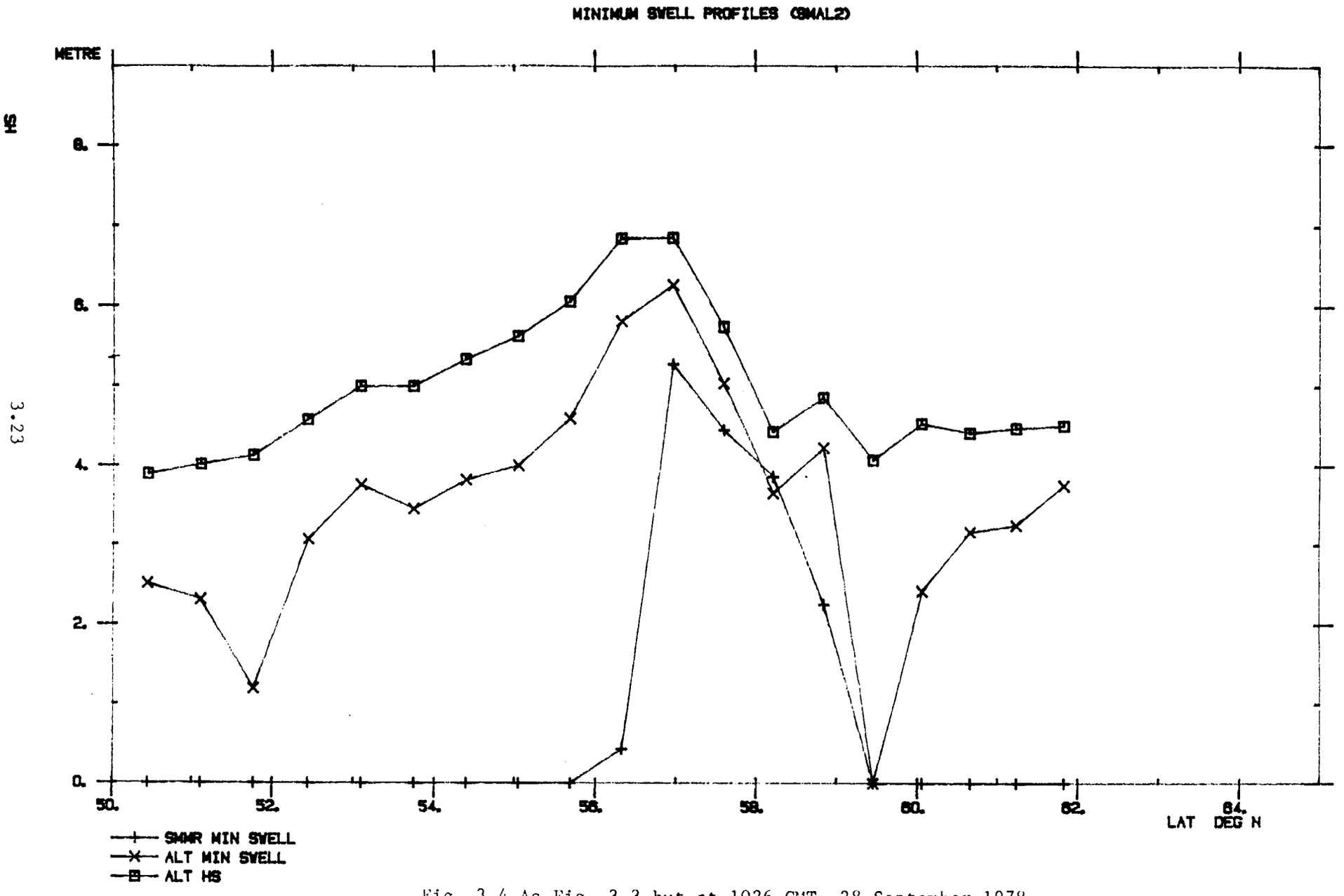

Fig. 3.4 As Fig. 3.3 but at 1026 GMT, 28 September 1978.

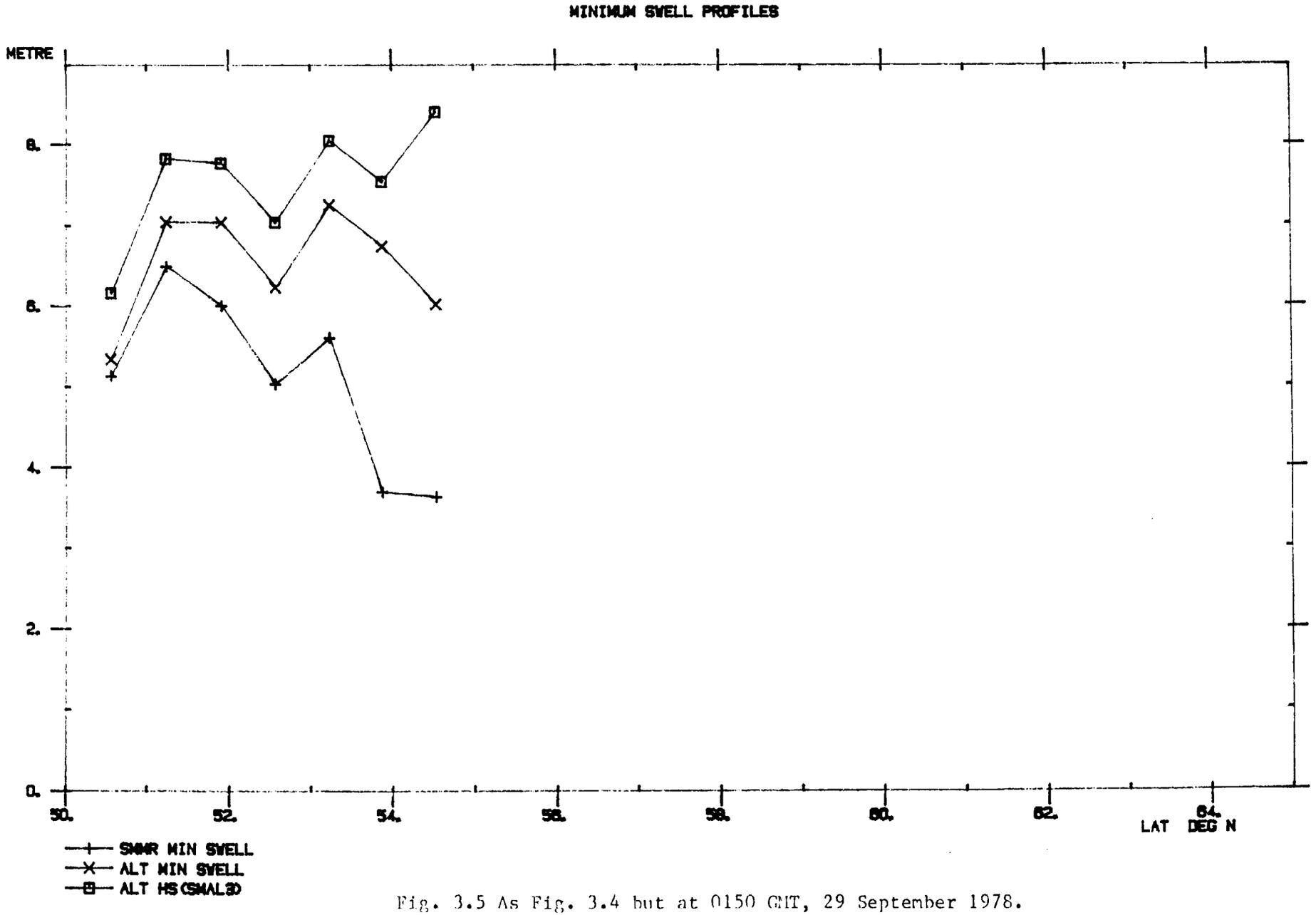

Fig. 3.5 As Fig. 3.4 but at 0150 GMT, 29 September 1978.

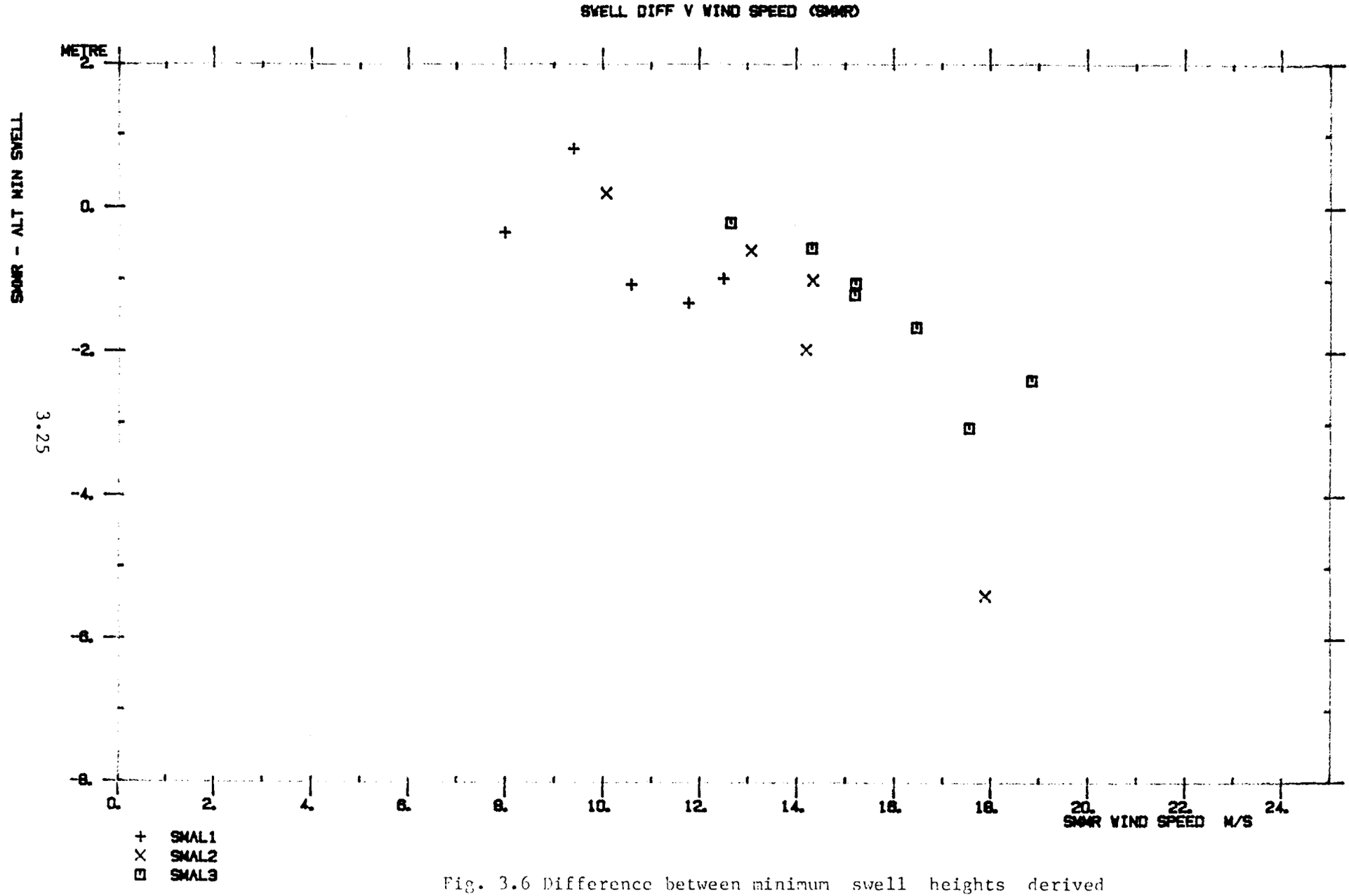

Fig. 3.6 Difference between minimum swell heights derived from altimeter and SMMR winds.

3.2. Wind speed

3.2.1 Physical basis

Pulse-limited altimeters such as those flown on GEOS-3 and Seasat are capable of measuring the intensity of backscattered returns from the surface by means of the Automatic Gain Control. Airborne measurements of the average backscattering cross-section per unit area (σ^o), made during the 1960s and early 1970s (Barrick, 1974) showed that for incidence angles near vertical ($<15^o$) the dependence of σ^o on incidence angle was consistent with a specular point model in which a nearly Gaussian distribution of surface slopes was assumed. However, considerable variance in the magnitudes of σ^o occurred but it was not clear whether this was due to a dependence on geophysical parameters. In 1969/1970 a comprehensive set of aircraft measurements was obtained at 9.0 GHz while flying near a NASA ship recording wind and wave data (Genest, 1970). Ten out of 16 flights were used in the analysis and the radar was calibrated against ground transponders of known signal strength; the overall r.m.s. system error was estimated to be 0.9dB.

$\sigma^o(0^o)$ was found to be related to wind speed but there was little correlation with the height, period or direction of waves. Barrick (1974) developed a specular-point model in order to explain the observed wind speed dependence, which showed a decrease in σ^o for increasing wind speed (in contrast to the larger incidence angles of 20^o-60^o used by scatterometers).

The relationship between σ^o near the vertical and the distribution of specular points is given by

$$\sigma^o = \pi \sec^4\theta p\ (-\tan\theta, 0)|R(0)|^2 \qquad (3.7)$$

where $p\ (\zeta_x, \zeta_y)$ is the joint probability density function of the surface slopes ζ_x $(=\partial\zeta/\partial x)$ and ζ_y $(=\partial\zeta/\partial y)$, ζ is the surface elevation w.r.t. x, y plane and R(0) is the Fresnel reflection coefficient for the surface at normal incidence and which depends on radar frequency. According to the formula the strength of the return is proportional to the probability of the surface having specular points tilted at a slope of $-\tan\theta$ so as to be normal to the incident ray.

If the sea surface slopes are assumed to be Gaussian and isotropic then

$$p\ (\zeta_x, \zeta_y) = \exp[-\tan^2(\theta)/s^2]/\pi s^2$$

(with $s^2 = \langle \zeta_x^2 + \zeta_y^2 \rangle$ i.e. total mean square surface slope).

and

$$\sigma^o = \{|R(0)|^2 \sec^4\theta \exp[-\tan^2(\theta)/s^2]\}/s^2$$

At $\theta = 0^o$

$$\sigma^o(0^o) = |R(0)|^2/s^2$$

(Equivalent to

$$\sigma^o(0^o) = 20\log_{10}|R(0)| - 20\log_{10}s \qquad \text{in dB)}$$

For a given radar frequency, $\sigma^o(0^o)$ just depends on the total mean square slope. Brown (1978) has investigated the spectral domain and distinguishes two scales separated by a wavelength λ_d = 6.6 cm,

which is three times the radar wavelength. According to Brown (1978) Eq. (3.7) holds for all surface features of wavelength greater than λ_d, and shorter scales contribute only a small amount to the backscatter coefficient at near-normal incidence. The problem which remains is to relate the surface slopes to the wind conditions.

3.2.2 Dependence of mean square slope on wind speed.

Using Phillips (1957) relation for the spectrum of surface elevation, multiplying by k^2 (k is the spatial wavenumber) and integrating, Barrick (1974) derives the mean square slope as

$$s^2 = B_g \ln(k_\nu/k_\gamma) \quad \text{for } k_\nu < 380 m^{-1}$$

and

$$s^2 = B_g \ln(380/k_\gamma) + B_e \ln(k_\nu/380) \text{ for } k_\nu > 380 m^{-1} \quad \} (3.8)$$

B_g, B_e are dimensionless constants whose values have been determined empirically as 0.005 and 0.015 respectively, k_ν marks the highest wavenumber for which equilibrium is obtained and k_γ is the peak of the Phillips spectrum.

k_ν can be approximated as $k_\nu = 50U^{1.4} m^{-1}$, with U in ms^{-1}, and $k_\gamma = g/U^2$. Eq. (3.8) can then be used to obtain s^2 as a function of wind speed.

Cox & Munk (1954) measured s^2 using airborne photography of sun-glitter patterns. From their data they deduced a linear variation of s^2 with wind speed. Furthermore the effect of oil slicks on the sea surface was found to reduce the mean square slope by a factor of two or three which indicates that the main contribution is from shorter waves which are in equilibrium with the local wind. Cox and Munk's results agree quite well with Barrick's theoretical result

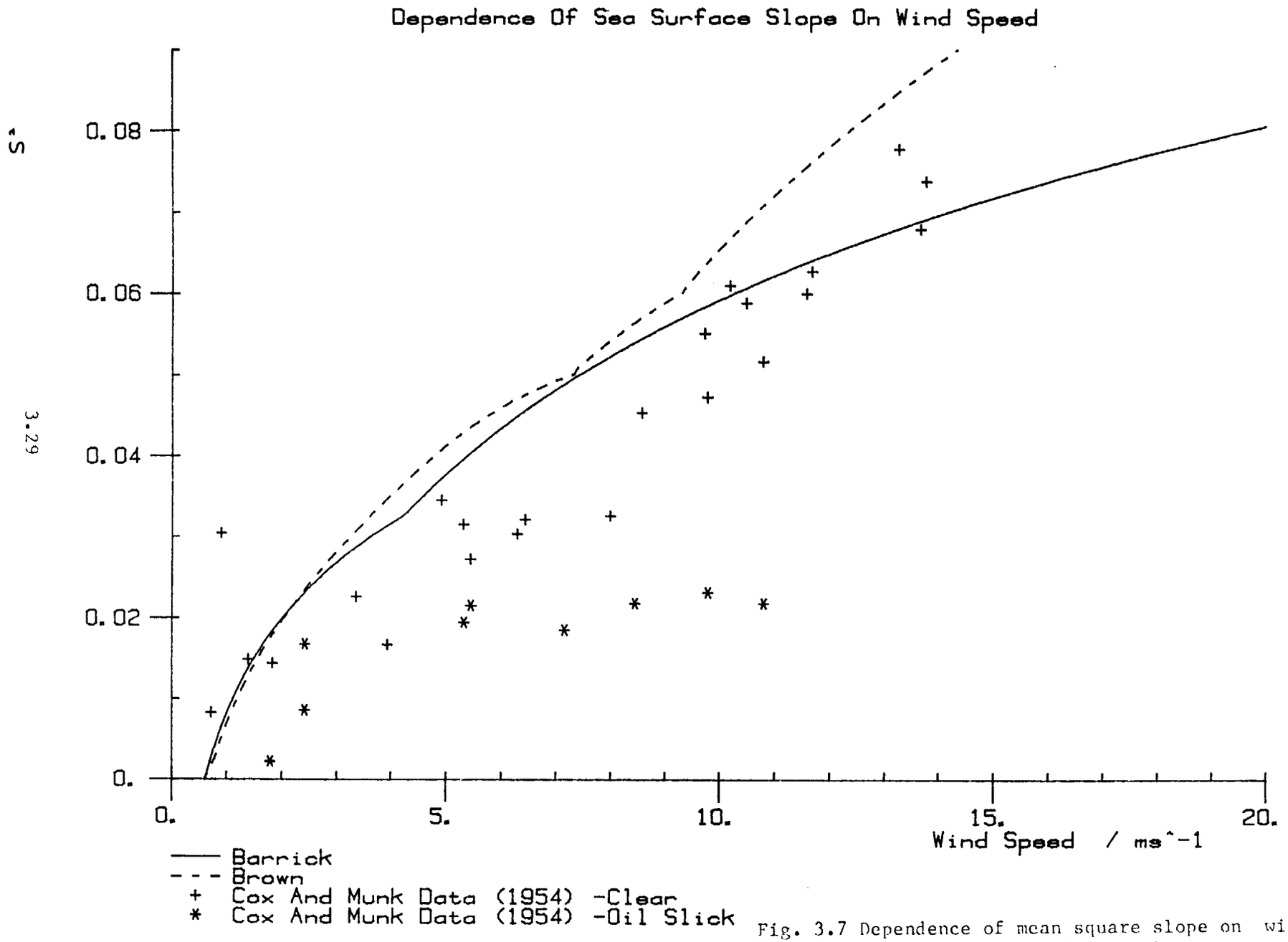

Fig. 3.7 Dependence of mean square slope on wind speed as implied by Brown et al.'s (1981) algorithm compared with Barrick's (1974) curve and the Cox & Munk sun-glitter data.

(Fig. 3.7). Wu (1972) reanalysed the Cox and Munk data and fitted a logarithmic relationship implying that the slope is less sensitive to wind speed at higher winds than lower winds. Wu explained the change in terms of the transition between hydrodynamically smooth and rough regimes.

From Eqs (3.7) and (3.8) Barrick (1974) obtained $\sigma^{o}(0^{o})$ as a function of wind speed. Although the spread of the airborne backscatter measurements about this theoretical curve is large (3-5dB) the broad agreement obtained has encouraged researchers to base the development of algorithms for satellite altimeters (and for the near-nadir cells of scatterometers) on this approach.

3.2.3 The GEOS-3 and Seasat altimeter wind speed algorithms

3.2.3.1 GEOS-3

For GEOS-3 two algorithms have been used. Mognard & Lago (1979) assumed a linear variation of slope with wind speed:

$$s^2 = \alpha + \beta U$$

where α and β are constants to be determined.

Brown (1979a) preferred the logarithmic dependence given by

$$s^2 = a \ln U_{10} + b$$

In this case the coefficients a, b were obtained empirically by a best fit to surface wind estimates from ships, wind hindcasts and buoys. Brown (1979a) used a data base prepared by the Spaceflight Meteorology Group with hindcasts every 390km along the ground track. All SMG wind speeds were binned at 2.6 ms^{-1} intervals. It was found

necessary to correct the σ^o data for mispointing errors because these could lead to biases of 2 dB varying on a pass-to-pass basis. $\sigma^o(0^o)$ was plotted against wind speed separately for swell and no-swell conditions, to try to isolate the effect of larger waves on the slopes. The scatter in the data was reduced if only ship reports were used and a double-branched mean square fit to the latter gave the following values for a and b:

$$a = 0.02098 \quad b = 0.01075 \quad U_{10} \leq 9.2 \text{ ms}^{-1}$$

$$a = 0.08289 \quad b = -0.12664 \quad U_{10} \geq 9.2 \text{ ms}^{-1}$$

Buoy wind speeds (measured when swell was present) appeared to support this relationship but with a slight bias. For the no-swell case intercomparisons were hampered by the lack of data especially from ships. Using the combined SMG hindcasts and ship data, Brown found that the coefficients resulting from a least squares fit were a = 0.03731, and b = -0.01324.

The main differences between the swell and no-swell curves were in the 4 $\text{ms}^{-1} < U_{10} < 12 \text{ ms}^{-1}$ range; lower σ^o values were obtained when swell was absent. However, the accuracy of the data and the difficulty of identifying swell mean that firm conclusions should not be drawn on the effects of swell. The above results were based on a limited data set during the early part of the GEOS-3 mission.

Mognard and Lago (1979) used a linear algorithm

$$\sigma^o(0^o) = |R(0)|^2/(\alpha + \beta U_{12.5})$$

with $\alpha = 0.003$, $\beta = 0.00512$, $R(0)^2 = 0.617$ and with the wind speed in ms^{-1}.

3.2.3.2 Seasat

Following the encouraging results obtained with GEOS-3 Brown, Stanley & Roy (1981) developed a three-branch logarithmic relationship using data from the entire intensive mode of GEOS-3 operations at times when overpasses of buoys occurred. The following values of a, b were obtained, depending on the measured value of σ^o:

$a = 0.01595 \quad b = 0.017215 \qquad \sigma^o \geq 10.9dB$

$a = 0.039893 \quad b = -0.031996 \qquad 10.12 \leq \sigma^o < 10.9dB$

$a = 0.080074 \quad b = -0.124651 \qquad \sigma^o < 10.12dB$

The first stage in processing is to calculate s^2, the mean square slope, from

$$s^2 = 10^{-(\sigma^o + 2.1)/10}$$

An initial estimate of the wind speed is obtained from

$$U_1 = \exp (s^2 - b)/a$$

with a,b as above.

For winds below 16 ms^{-1} the winds are corrected using a polynomial technique

$$U_2 = \sum_{i=1}^{5} a_i (U_1)^i$$

with

$a_1 = 2.087799$

$a_2 = 3.649928 \times 10^{-1}$

$a_3 = 4.062421 \times 10^{-2}$

$a_4 = -1.904952 \times 10^{-3}$

$a_5 = 3.288189 \times 10^{-5}$

The relationship between s^2 and U_{10} is shown in Fig. 3.7. Agreement with Barrick's (1974) results is good for wind speed below

9.5 ms^{-1}, but increasingly diverges at higher speeds giving a much lower value for wind speed for a specified $\sigma^{o}(0^{o})$

Before applying this algorithm to Seasat data it was decided to take advantage of the overlap between the GEOS-3 and Seasat missions and to examine the consistency of σ^{o} measurements at the cross-over points where these occurred with a time difference of less than 1 hour. Seasat σ^{o} was found to be systematically 1.6 $\pm$ 0.37dB higher with no obvious dependence on wind speed. Since the GEOS altimeter had undergone extensive preflight σ^{o} calibration it was decided to reduce all Seasat values by 1.6dB before computing winds. It should be noted that the cross-over comparison only covered wind speeds in the range 2-12 ms^{-1}.

After Seasat altimeter winds were processed it was discovered (Queffeulou, personal communication) that discontinuities were present in the calibration relating σ^{o} to AGC. These have the effect of producing erroneous winds at 6 and 50 ms^{-1}. Data are being reprocessed by the Jet Propulsion Laboratory to remove these (relatively minor) discrepancies.

3.2.4 Validation of the Seasat wind algorithm

Since GEOS-3 data were used to tune the wind speed algorithm they cannot be used in its evaluation. Fedor & Brown (1982) in a comparison of Seasat altimeter winds with 87 overflights of NOAA buoys reported a mean difference of -0.25 ms^{-1}, with a standard deviation of 1.6 ms^{-1} for the range 1-10 ms^{-1}. However, several researchers have recently pointed out that Seasat altimeter wind

speeds tend to be an underestimate when true near-surface winds exceed $10ms^{-1}$. Fig. 3.8 is a comparison between ocean weather ship measurements in the North Atlantic and Seasat (Queffeulou,1984). The ship measurements are averaged over ten minutes and the distances to the satellite tracks are indicated, in nautical miles, at each point. The altimeter measurement is averaged over 5 secs (about 35 km). As well as the underestimate at high speeds there is a suggestion that the altimeter overestimates at low speeds. Similar behaviour at high speeds is observed in Fig. 3.9, which uses in-situ data from a JASIN buoy and OWS Lima when R.A. footprints lay within 50 km. Wentz, Cardone & Fedor (1982) compared the wind speed data deduced from the altimeter, the Scanning Multichannel Microwave Radiometer (SMMR) and the scatterometer at nadir. They concluded that for wind speeds below 10 ms^{-1} the three sensors are in agreement but for higher winds the altimeter speed is an underestimate. Fedor & Brown (1982) did not report such behaviour but the 87 near overflights of NOAA data buoys used in their analysis were limited to a range of 0-12 ms^{-1}. We have extended comparisons to 21 ms^{-1} by using the SMMR winds at nadir during a stormy period in the N.E. Atlantic. SMMR winds have been found to agree well with in-situ data provided a change in bias is allowed for part-way through the mission as reported by Allan & Guymer (1984). This change has been related by Wentz & Peteherych (1984) to a sudden drop in the brightness temperatures of the 18 GHz channels. The passes used in the present study occurred on 28/29 September when SMMR winds exhibited little bias and are among those used by Mognard (1983a) to determine swell conditions near a storm in

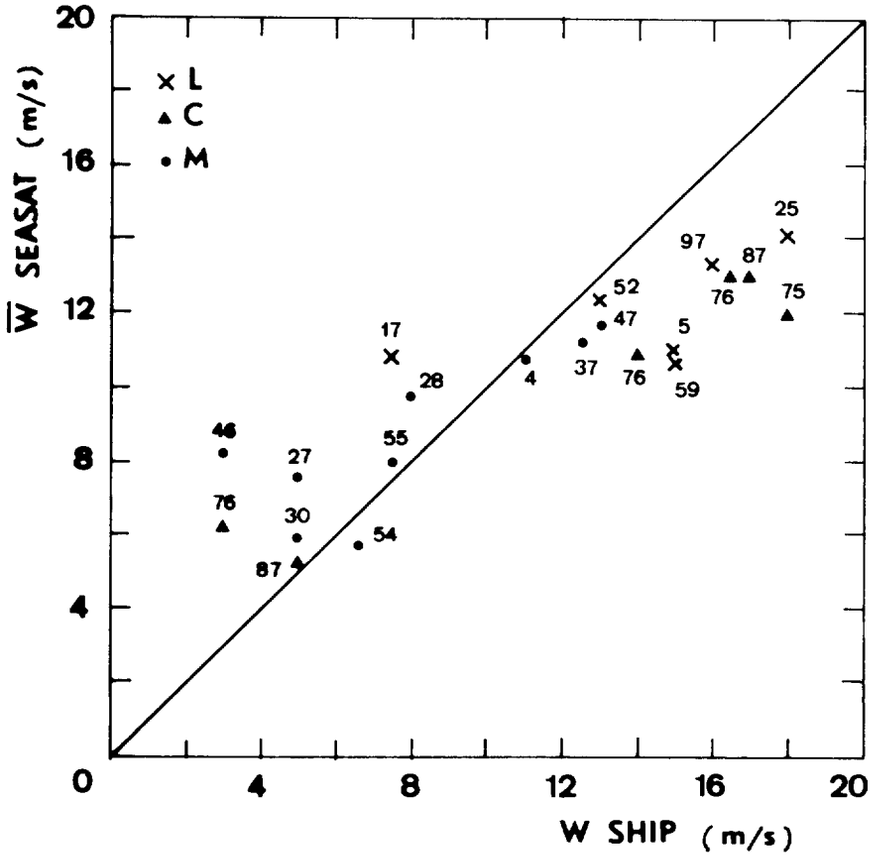

Fig. 3.5 Comparison of Seasat altimeter wind speeds with those obtained from Ocean Weather Stations L, C and M. Numbers indicate distance from ground track in miles.

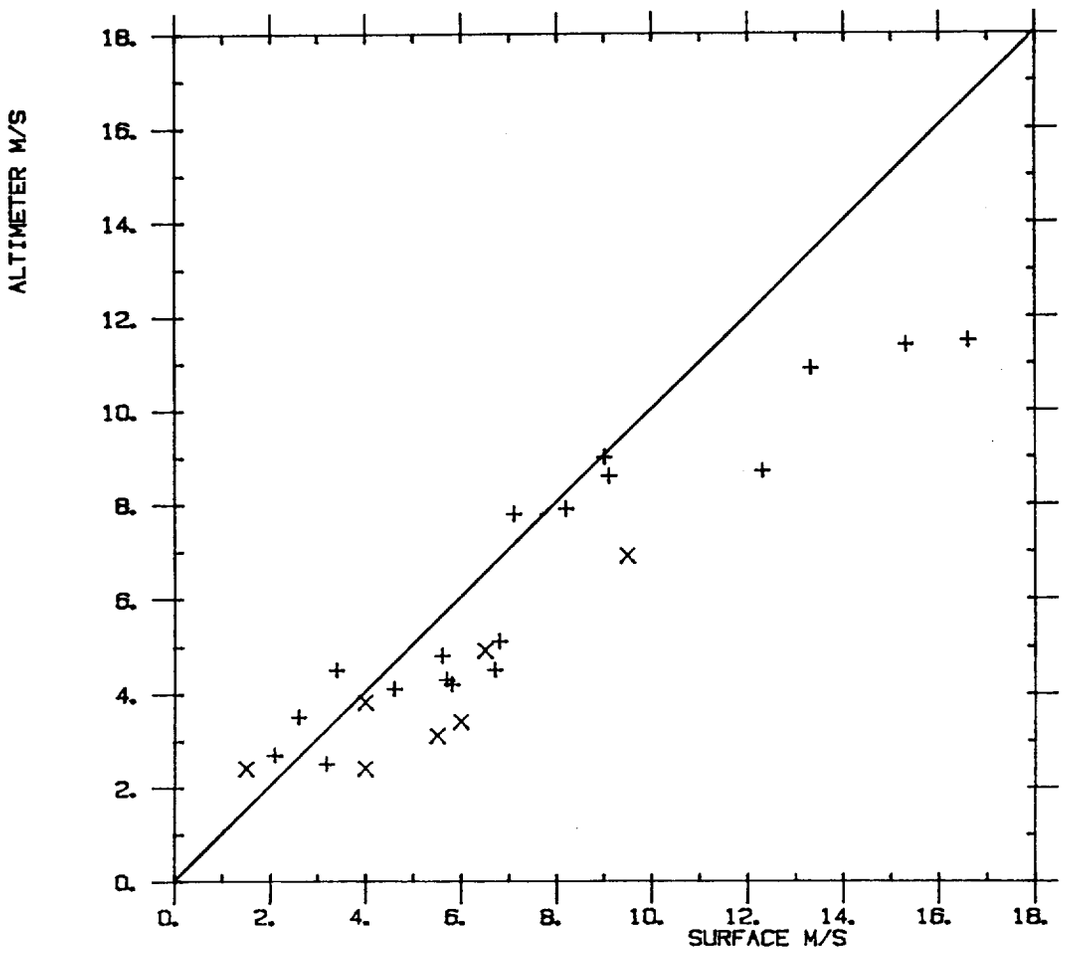

Fig. 3.9 Seasat altimeter wind speed versus in-situ wind speed (+ JASIN buoy W2, X OWS Lima).

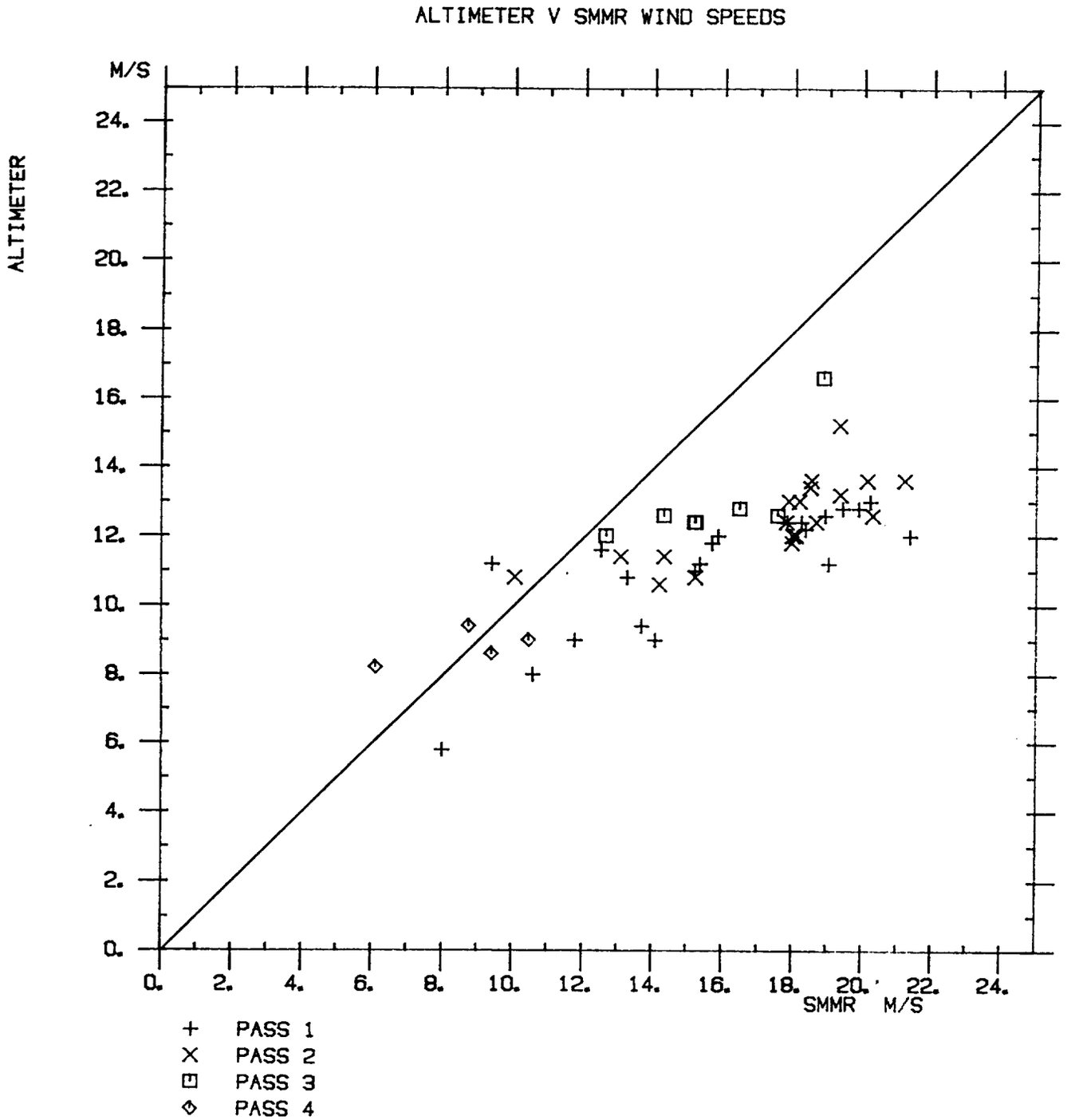

Fig. 3.10 Seasat altimeter versus SMMR near-nadir wind speeds on four passes in N.E. Atlantic (28/29 September 1978).

NE Atlantic. Fig. 3.10 shows the results of the intercomparison; again a marked tendency of the altimeter to underestimate higher wind speeds is seen. At 20 ms^{-1} the error is just over 6 ms^{-1}.

These studies all reveal a problem with the altimeter wind algorithm when applied to Seasat σ^{o}s in wind speeds greater than 10 ms^{-1}. It is of interest to note that this is outside the range of speeds for which the GEOS-3/Seasat $\sigma^{o}(0^{o})$ calibration is valid. Moreover, the discrepancy is in the same sense as the difference between the Brown et al. (1981) and Barrick (1974) curves in Fig. 3.7. It appears that the tuning of the algorithm to GEOS-3 data may have resulted in errors at higher wind speeds, and further investigation is needed.

The above errors have implications for studies using mean wind fields from Seasat sensors. Chelton & O'Brien (1982) in a comparison of scatterometer and altimeter wind fields for the Tropical Pacific for the Seasat period, found that scatterometer winds were 20% higher; Mognard (1983b) showed a similar difference for the World Ocean. Such results are difficult to interpret as far as algorithm validation is concerned because differences may arise from the sampling characteristics of the sensors and it is dangerous to rely on any one of the sensors as being correct unless extensive validation has been carried out against reliable in-situ measurements. Nevertheless, the SASS/ALT comparisons have been used to substantiate the need for a new SASS algorithm. An algorithm which incorporates a sea surface temperature dependence has been developed by P. Woiceshyn at JPL, and Mognard (1983b) shows that a

3-month wind speed map produced using this algorithm agrees better with the equivalent map computed from the altimeter. However, the possibility of serious errors in the altimeter wind seems to have been neglected and without further comparisons against in-situ data it is difficult to evaluate the accuracy of this new algorithm.

Errors in altimeter winds also affect the extraction of swell information from H_s estimates as discussed in 3.1.3.

3.3 Ocean topography

The steps involved in retrieving the precise topography of the sea surface from altimeter data are only briefly outlined here since they have been well covered elsewhere (see below). Attention is drawn to matters that should receive attention for ERS-1. Most of the experience has been gained with Seasat. The main stages can be divided as follows:

(i) Integration of telemetered data received at ground stations to a single master data set and its conversion to earth-located engineering units using the spacecraft attitude history and coarse orbit data.

(ii) Processing with sensor file algorithms. These operate on tracking-loop parameters h, H_s, AGC (not on the raw waveform) and consist of data quality operations and instrument corrections (Hancock et al., 1980).

(iii) Processing with geophysical algorithms to correct the data for propagation effects, reference data to geoid etc. (Lorell et al., 1980).

3.3.1 Sensor file algorithms

The data quality checks are:

- o to flag the data according to the operating mode of the instrument.
- o blunder point analysis. This removes outliers due mainly to lost bits when data are telemetered to ground but also includes cases where data points lie outside the design specifications because of islands,rain etc.
- o time tagging the data to account for internal delays within the system.

After this the following corrections were made:

- o height calibration drift. The Seasat mission was too short for any drift to be detected but this could be more of a problem during the expected 2-3 year life-time of ERS-1.
- o taking account of changes in the distance between the antenna feed and the centre-of-gravity of the spacecraft due to fuel being consumed. This is important for making the precise range measurements from the altimeter comparable with the orbit.
- o bias correction. This has been attributed to sea-state effects (wave skewness and differences in reflective properties of wave troughs and crests) and the non-Gaussian form of the transmitted pulse. The former effect is discussed in 5.1; it is anticipated that ERS-1 will not suffer from the second problem. For Seasat the bias was empirically determined from a sequence of overpasses at the

laser tracking station used as the prime calibration site and amounted to 5±2% of H_s. However, because of uncertainties no correction was applied to Geophysical Data Records.

- o tracker lag. This is significant when the altimeter passes over regions where the height acceleration is large e.g. ocean trenches.
- o pointing angle correction which in extreme conditions (large values of significant waveheight and off-nadir pointing near the specified limit of 0.5^{o} for Seasat) could attain 25 cm The correction was supplied from a look-up table which was also used to correct H_s values (the largest correction for H_s<10 m could be 1 m).
- o data compression from 10 s^{-1} samples (each derived from 100 pulses) to 1 s^{-1}. On ERS-1, data will be reduced from 20 s^{-1} to 1 s^{-1}.

3.3.2 Geophysical Data Record (GDR) Algorithms

A full discussion of all the effects taken into account is given in Foster et al. (1980).

The propagation corrections which affect the travel-time of the pulse and hence the inferred height of the antenna above the surface are:

- o dry tropospheric correction. Only an approximate knowledge of the surface atmospheric pressure field is required.
- o wet tropospheric correction. This is a more variable component and cannot be reliably obtained from surface

humidity measurements alone. It is generally accepted that the required accuracy can only be provided by passive microwave measurements on the satellite itself. Seasat carried the SMMR; ERS-1 will have the ATSR/M.

- ionospheric correction. Lorell et al. (1982) reported that errors in determining this by modelling were 3-5 cm for Seasat. In periods of high solar activity the effect may cause more serious errors. It should be noted that ERS-1 is expected to be in orbit when a solar maximum is approaching. ERS-1 will also carry an experimental tracking system, PRARE (Precise Range And Range-rate Experiment) which eliminates the effect by using two frequencies.

The other computations carried out in GDR processing are:

- referencing the height measurements to the geoid. The Goddard Earth Model (GEM) 10B was used for Seasat.
- solid earth tides.
- ocean tides. For Seasat GDR processing the Schwiderski model was recommended but the Parke-Henderschott model was included (though it should only be used in the deep ocean). Data from the altimeter itself can be used to extract tides but a particular problem for ERS-1 is that it is in a sun-synchronous orbit. Tidal corrections deduced from TOPEX, the U.S. altimetric satellite due to be launched soon after ERS-1, will be invaluable for studies of ocean circulation using ERS-1 data.

- o inverse barometer effect. If the ocean develops a full response a change of 1 mb in surface pressure produces a change in sea surface height of 1 cm. Generally however the ocean takes about two days to respond. Problems are likely to occur near storms and in coastal regions where wind set-ups and Ekman transports may occur which complicate the relationship. Further work should be carried out on this topic for ERS-1. It is possible that surface pressure fields could be deduced from ERS-1 scatterometer winds using the geostrophic assumption. If available winds from the N-ROSS scatterometer would be very valuable because of their greater coverage.
- o Orbit determination. This is of vital concern if mean currents are to be studied from satellite altimeters. Wakker et al (1984) provide a comprehensive study of accuracies to be expected for ERS-1 assuming various configurations of tracking stations. One problem is the shape of ERS-1 which makes it difficult to use models to interpolate the orbit between measurements by tracking stations. However, when studying mesoscale variability it is not necessary to know the satellite orbit with great precision because the errors are primarily on a large space-scale.

3.4 Sea ice parameters

3.4.1. The ice boundary

Relatively few publications describe the use of altimeter data to study sea ice. An exception concerns the use of the GEOS-3 altimeter to determine the location of the sea ice boundary. Dwyer & Godin (1980) describe the development of an operational ice edge detection scheme based on the great contrast in the backscattering properties of sea ice and open water.

Fig. 3.11, taken from Dwyer and Godin's report, illustrates schematically the different characteristics of ocean and ice returns. Also shown are the locations of the GEOS-3 altimeter sampling gates when operated in its global mode, used exclusively for the sea ice study. Note that in the global mode the transmitted pulse length was 200 ns, thus explaining the very much broadened and smoothed return pulse characteristics compared with those of the Seasat altimeter discussed later.

The altimeter range servo operated on the signal levels in the ramp (R) and plateau (P) gates to create an error signal (e =2R-P) to drive the time opening of the ramp gate to the T_o position (see Fig. 3.11). The tracker Automatic Gain Control (AGC) operated on the plateau gate data, and was telemetered to ground as a one second average to be used as a measure of the energy received in the early part of the return. A one second average measure of energy received in the late return (i.e. from angles increasingly off-nadir) was provided by the Average Attitude Specular Gate (AASG).

As the altimeter passed from the ocean to sea ice or vice versa, the change from the normal ocean return to the more intense and peaked return from the ice caused marked differences in the AGC

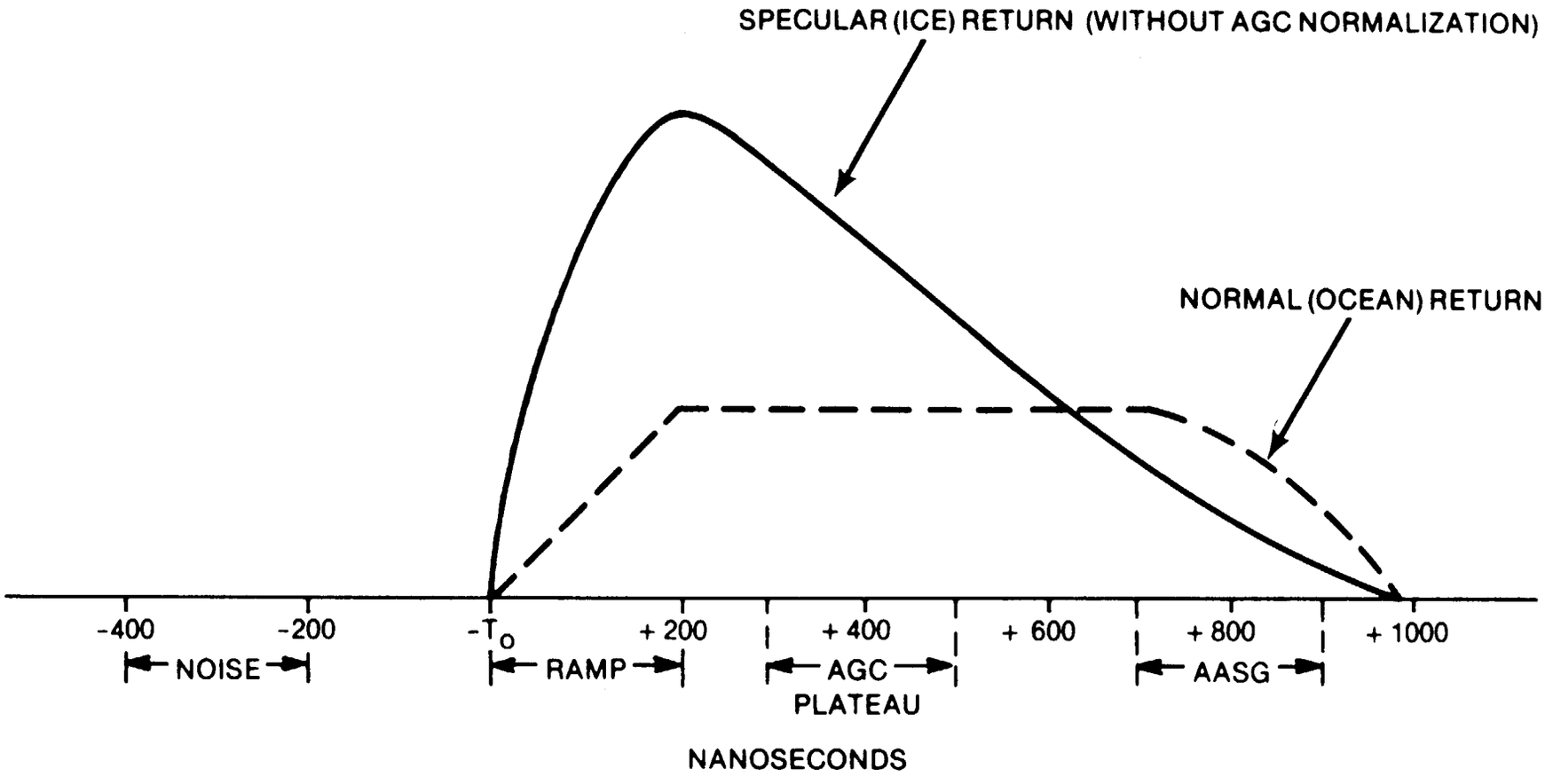

Figure 3.11 Schematic ice and ocean return waveforms as observed by GEOS-3 (from Dwyer and Godin, 1980).

and AASG signal levels. An example of the variation of these parameters during an ice-ocean transition is shown in Fig. 3.12(a). Shown in Fig. 3.12(b) is the variation of an ice index parameter calculated at a 0.5 s^{-1} rate as

$$\text{ICE INDEX} = ((100+\text{AGC})/100(\text{AASG}))) - 10 \qquad (3.9)$$

The AGC value is in dB and the AASG value is in volts. In practice the ice index was only calculated for data points in which the AASG value was less than 0.033 volts (over water the AASG was consistently greater than 0.045 volts) and this accounts for the lack of ice index data to the right of the plot.

Also shown in both figures is the location of the ice boundary, as judged from satellite optical and infrared imagery by the Fleet Weather Facility/Joint Ice Centre. This organisation and the GEOS-3 project team used data from February 1979 to develop and tune the ice index algorithm to give a value of zero at the ice boundary. On the basis of a series of case studies covering Bering Sea data during March 1979, it was established that the signals were repeatable and that the ice index algorithms produced reliable ice boundary locations with an accuracy comparable to the 1-3 km accuracy of the optical and infrared data. From March to 1 July 1979 the data were incorporated in the Ice Centre's daily analysis. A further case study in May 1979 confirmed continued accurate ice boundary location under different seasonal conditions.

A point worth noting is that both the AGC and AASG signals continue to vary for some six seconds following the ice/sea

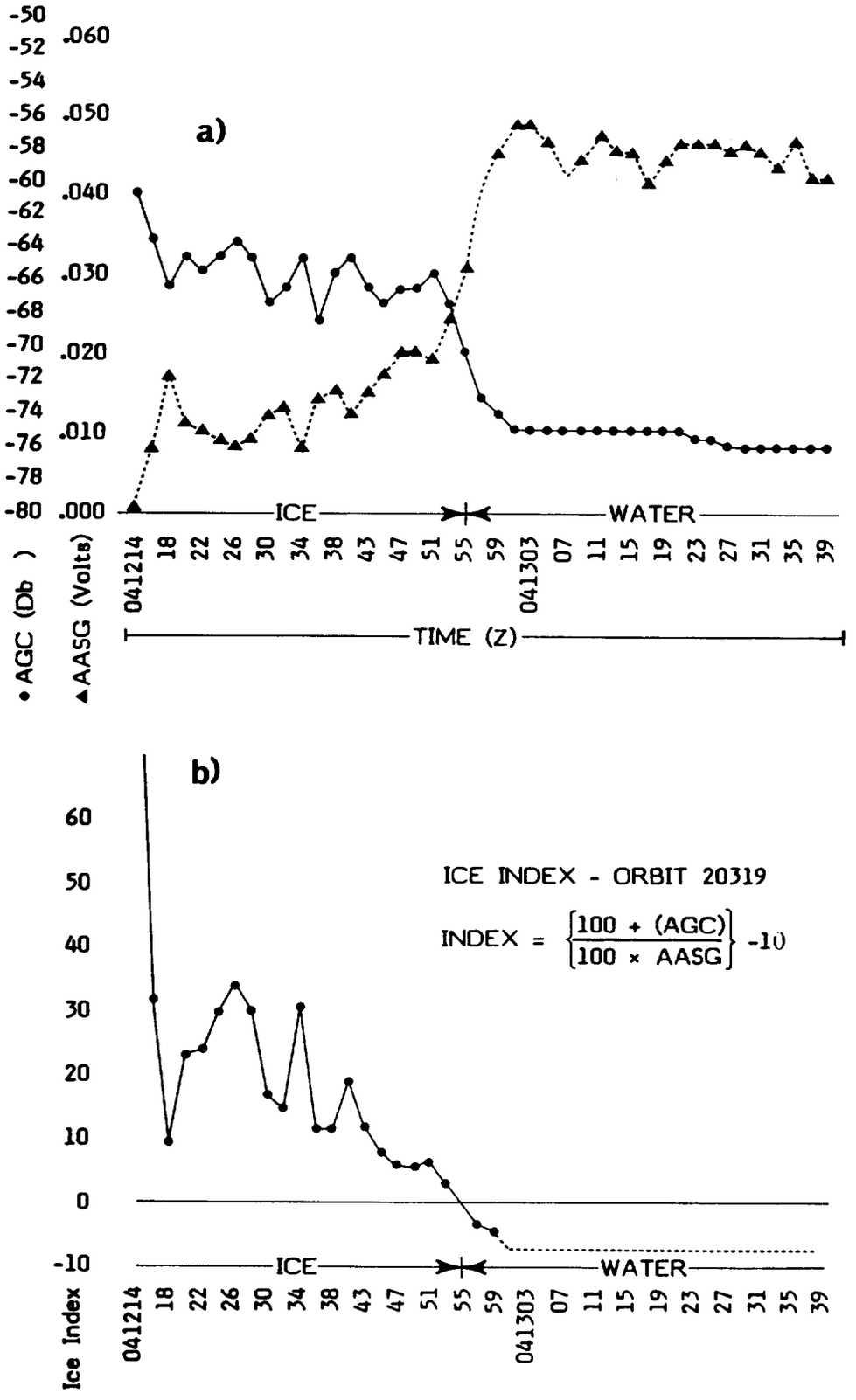

Figure 3.12(a). AGC and AASG vs Time

(b). Ice Index v Time

transition shown in Fig. 3.12(b), corresponding to a ground track distance of ~40 km. This can only be partly accounted for by the broad beamwidth of the GEOS-3 altimeter operated in the global mode (footprint radius ~7km). Thus the altimeter appears to have registered the presence of ice well beyond the 'classical' ice boundary. This latter point is discussed further in Section 7.2.

Two published accounts exist of the use of Seasat altimeter data over sea ice. Marsh & Martin (1982) used global histograms of the on-board computed values of AGC and significant waveheight (H_s), (excluding land data), to develop selection criteria for eliminating ice 'contaminated' data points from their ocean mean surface model. They found that the AGC distribution was strongly peaked and centred on a value of 32 dB but with an extended tail to high values. The H_s distribution consisted of a broad peak centred on ~2 m but with maximum power at zero, a value not obtainable from characteristic ocean returns. Histograms of the high-valued AGC data points and those with zero H_s as a function of latitude showed a strong correlation with the latitudes at which sea ice was expected during the Seasat lifetime. On the basis of their analysis Marsh and Martin rejected data points with H_s values close to zero or AGC value greater than 36 dB in order to achieve an ice-free data set.

Rapley (1984a), in an analysis of the propagation of ocean swells into the ice pack, adopted an AGC threshold of 33 dB to define the Antarctic winter ice boundary. He found it necessary to use a spatial resolution of 67 km (10 s AGC averages) in order to minimise inconsistencies in the ice boundary location resulting from ice

motion between altimeter passes. The disposition of the boundary determined in this way, and its observed spatial variability were consistent with passive microwave data collected in previous years (e.g. Zwally et al., 1984). Work is currently in progress to compare these data with simultaneous optical and infrared images.

3.4.2 Ice characteristics/Ice type

During their generation of ice boundary data described above, Dwyer and Godin noted a qualitative correspondence between their Ice Index parameter and ice type. For example, high values of ice index appeared to correlate with smooth young ice, whereas low positive values were associated with lesser ice concentrations or, alternatively, high concentrations of rough ice. Unfortunately no further work has been published on this topic.

3.4.3 Ocean swell penetration

The penetration of ocean swells within the ice pack controls the size distribution of ice floes and thus affects ice dynamics and the thermodynamics of ice growth and decay. Rapley (1984a) has investigated the use of the on-board computed values of H_s to provide an approximate measure of the degree of penetration of the ice pack by ocean swells. He points out that the characteristic evolution of waveform shape is as shown in Fig. 3.13(a), and that this may be accounted for by a progressive reduction of surface slopes consistent with the damping of waves and swell by interaction with the floes (Fig. 3.13(b)). In spite of a number of difficulties resulting from

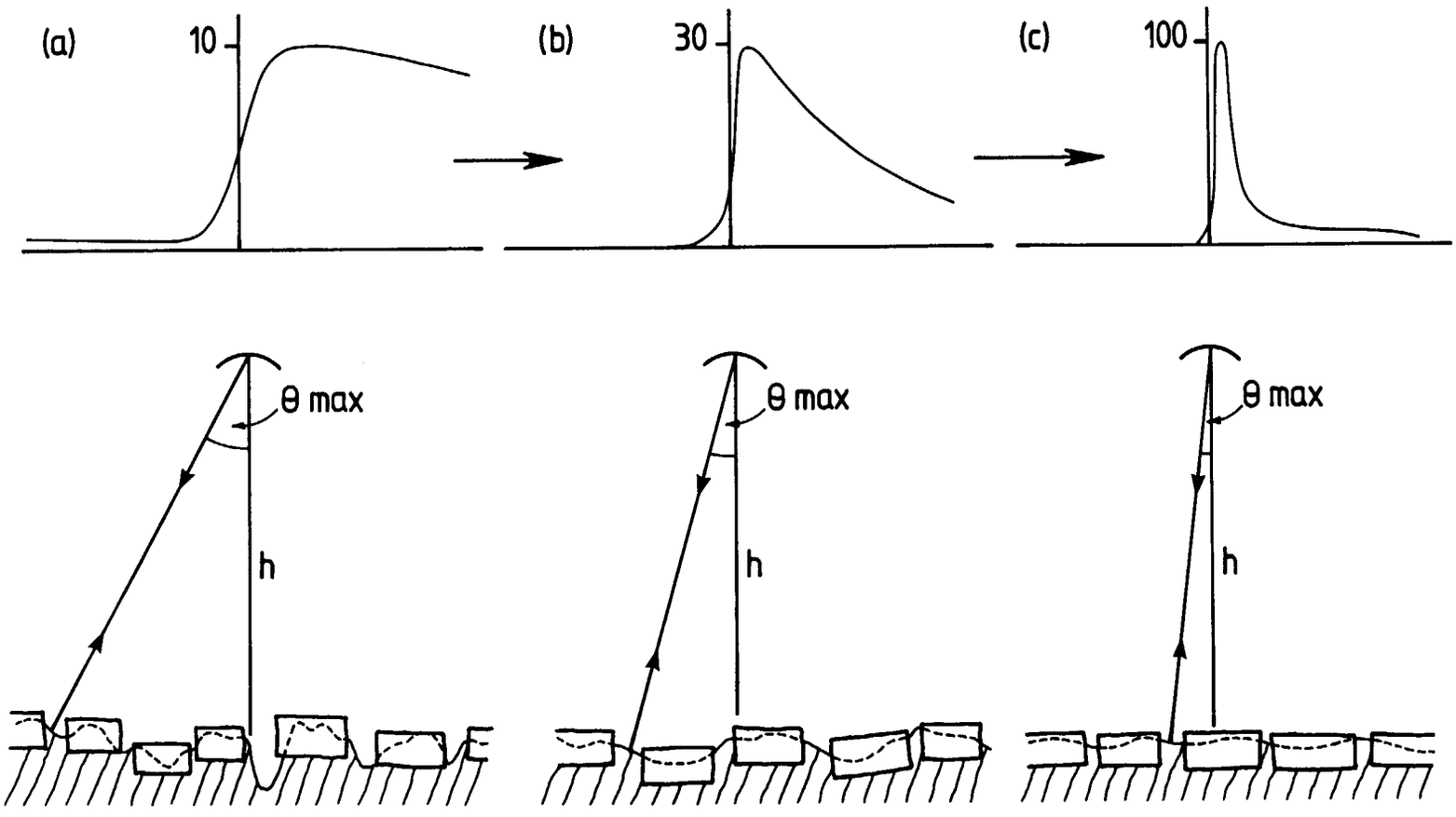

Figure 3.13 The evolution of Seasat sea ice waveform, shape and strength as a function of increasing distance from the ice boundary. Leading edge slopes depend on the height distribution of scatters at nadir just as for ocean returns. Falltimes are determined by the distribution of surface slopes as shown schematically in the lower panels. Pulse strengths are relative to a value unity for standard ocean returns. Pulse shape and strength change as ocean waves and swell are damped out by the action of ice floes within the pack (from Rapley 1984(a)).

improper operation of the altimeter tracker over sea ice, the smoothed H_s data provide a measure of pulse 'peakiness' which is related to the degree of flatness of the reflecting elements of the surface. Altimeter maps of the 'swell penetration' zone and its temporal evolution show a plausible correspondence with nearby ocean swell storms, the latter being derived using the method of Mognard (1983a, 1984). An example is shown in Fig. 3.14.

— FLEWEAFAC ice boundary 14/9/78

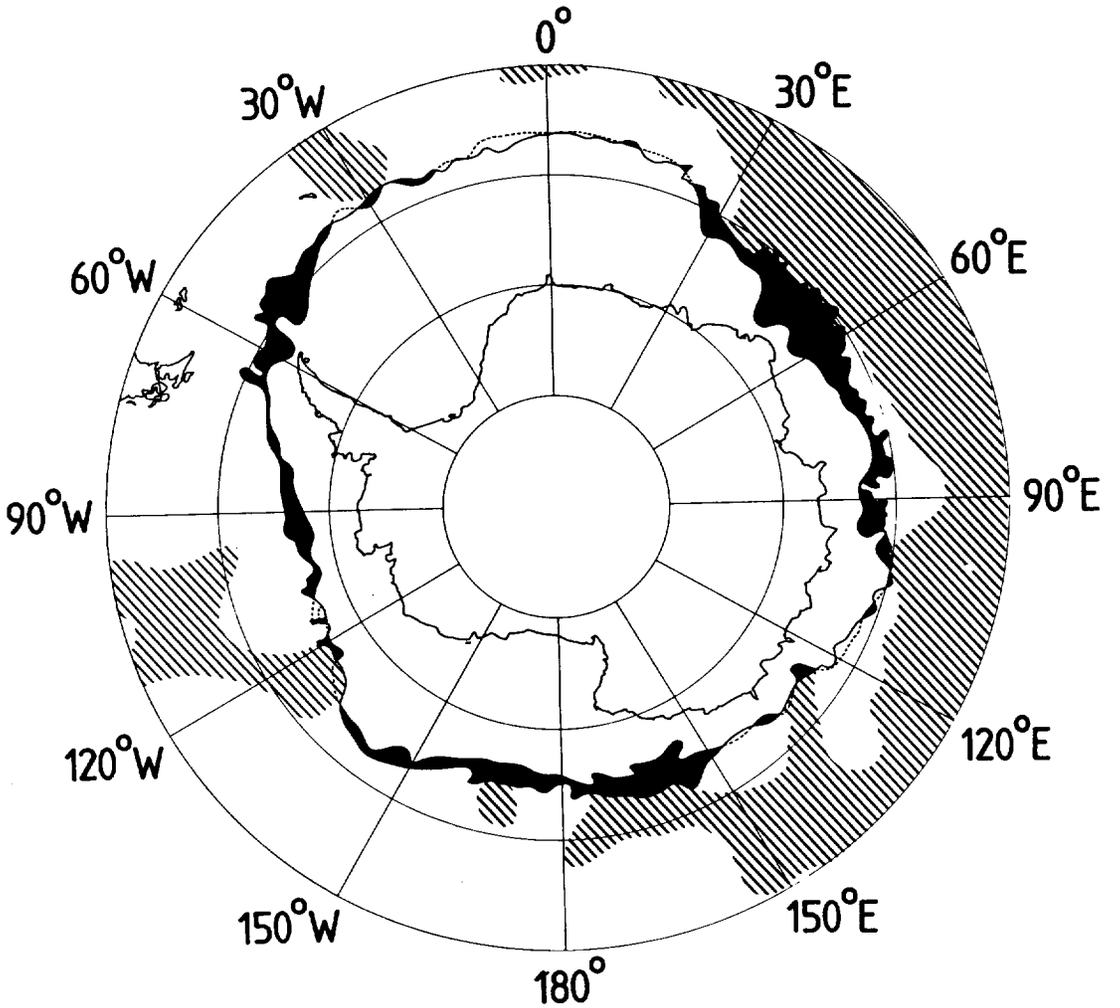

Figure 3.14 The Antarctic ice boundary for 14/9/78 as determined by the US Fleet Weather Facility, Suitland. Also shown are regions of high ocean swell at sea, and the penetration of ocean swell into the pack ice as deduced from the Seasat 'SWH' data, (solid areas).

4. Implications of Selenia design

The ERS-1 radar altimeter is similar in many respects to the Seasat instrument. Table 4.1 lists some of the major similarities and differences. The most significant differences are the use of a lower power transmitter, the provision of an 'ice mode' of operation, and the implementation of the Suboptimal Maximum Likelihood Estimator (SMLE) tracking algorithm.

The ice mode uses a window width expanded by a factor x 4, and a centre-of-gravity tracker. The ice mode will provide improved tracking over the steeper slopes of the ice sheet margins and over land, but it is envisaged that the oceans mode should be used for operation over sea ice and over the flatter central portions of the ice sheets (Griffiths, 1984).

4.1 Pulse compression

The full-deramp pulse compression scheme employed on the ERS-1 altimeter is similar in concept to that of Seasat (MacArthur, 1976). A Surface Acoustic Wave (SAW) dispersive delay line is used to generate a 20μs long chirped (LFM) pulse with 330MHz bandwidth (equivalent to a 1/330MHz = 3.03ns compressed pulse). A receiver local oscillator of identical chirp slope is mixed with the radar return, mapping range differences into the frequency domain, where they are analysed in a set of 63 x 3.03ns contiguous range bins. The frequency-domain formation of the range bins is carried out using an FFT algorithm rather than the digital filterbank of the Seasat altimeter. This has a minor effect upon the shape and sidelobe level of each range bin, but is unlikely to be significant.

Table 4.1 ERS-1/Seasat radar altimeter differences

	ERS-1	Seasat
frequency:		
	13.832-13.432GHz	13.34-13.66GHz
i.e.	13.632GHz centre freq.	13.5GHz
	330MHz bandwidth (=3.03ns)	320MHz (=3.125ns)
PRF:	1.014kHz	1.020kHz
power:	50W peak	2kW
pulse length:		
	20 s (chirp duration)	3.2 s
	3.03ns (compressed)	3.125ns
antenna:		
	1.2m diameter	1m
	>41.5dBi gain	>40dBi
	1.3 degrees beamwidth	1.6 degrees
	<-25dB first sidelobe	<-20dB sidelobes, $\pm 70^{\circ}$
	PLF dia = 1.5km	1.7km
	BLF dia = 18.1km	22.3km
processing:		
Oceans mode:		
	No. of range bins = 63 x 0.45m	60 (+3) x 0.47m
	Range window width = 28.6m	28.1m
	No. of pulses summed = 50	50
	Interpolation method: HDOT from tracker	HDOT from tracker
	Height error algorithm: SMLE	adaptive split gate
	Trackers: separate alpha-beta trackers for height, H_s and AGC	alpha-beta tracker for height, first-order AGC tracker
	H_s measurement spec:	
	<----------range 1m - 20m---------->	
	<----------accuracy 0.5m or 10% (whichever is greater)--------->	
	Altitude measurement spec: range 745-825km	
	<----------precision $\pm$10cm (1 , 1s), 2m absolute---------->	
	Backscatter coefficient measurement spec:	
	<----------$\pm$ 1dB (1) but $\pm$ 0.5 dB at 8 dB for ERS-1---------->	
	Telemetry: data from every 50-pulse average at 50ms rate	data from two 50-pulse averages, averaged (see Rapley et al.,(1983) p2.14 or MacArthur (1978) p101)

Table 4.1 (contd)

Ice mode		
	x4 window width (i.e.individual bins are 1.5m) centre of gravity tracker; estimates range and AGC, but not slope; ice mode switching under ground control	provision for changing tracker time constants, but no ice mode per se.
Acquisition sequence		
	CW phase consisting of 20 s 13.632GHz pulses; spec. <5s at up to ±50m/s, 95% of trials	see MacArthur(1978), p96 et seq.

4.2 Pulse summation

Fig. 4.1 shows the stages of processing carried out on the raw range bin signals, and operation of the Height Tracking Loop (HTL). Firstly, pulse summation takes place, using linear interpolation with the range rate term of the range tracker to obviate the effects of 'blurring' (see Rapley et al., 1983, p68), in a similar manner to the Seasat instrument. When significant range rate lag occurs, blurring will result, though this is unlikely to happen over the open ocean.

4.3 Adaptive gate selection

The processing of the radar return defined by the 50-pulse averaged range bin signals, in order to estimate range, leading edge slope (H_s) and signal strength (σ^o), is carried out by the Suboptimal Maximum Likelihood Estimator algorithm. This attempts to match an idealised linear return to the actual return shape, deriving error signals in respect of each of the three parameters, which are minimised by separate feedback loops termed, respectively, the Height Tracking Loop (HTL), the Slope Tracking Loop (STL), and AGC. Each error signal is filtered by an alpha-beta tracker, resulting in a second-order loop in each case.

The SMLE algorithm (Somma et al., 1982) is a simplified derivative of the Maximum Likelihood Estimator (MLE). The MLE fits the idealised return to the actual return by a form of weighted least-squares fit, where the weights are equal to the reciprocal of the data variances, see section 3.1.2.1. The SMLE replaces this weighting function by a rectangular 'window' in each case (Fig. 4.2).

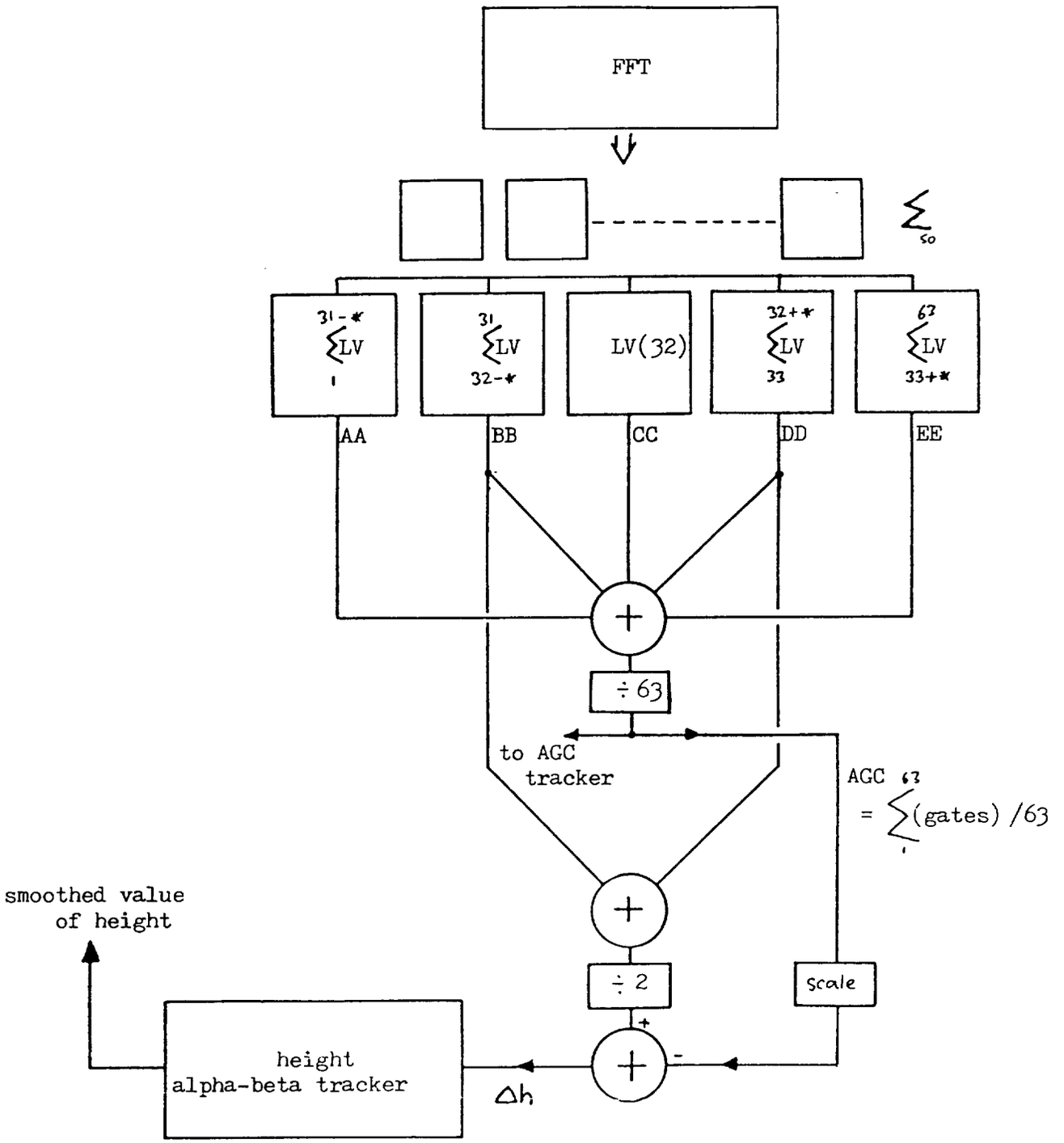

Fig. 4.1 Sub-optimal Maximum Likelihood Estimator (SMLE) height tracker

Fig. 4.2 MLE and SMLE algorithms.

The MLE algorithm seeks values of α_j in each case to satisfy

$$\sum_i \frac{1}{\bar{V}_i^2}\left(V_i - \bar{V}_i\right)\frac{\partial \bar{V}_i}{\partial \alpha_j} = 0$$

where α_j is the parameter to be estimated

$\bar{V}_i$ is the estimate of mean value of V_i from the model

V_i is the actual signal in the i^{th} range bin

The SMLE replaces the weighting function $\frac{\partial \bar{V}_i}{\partial \alpha_j}$ by a rectangular function in each case.

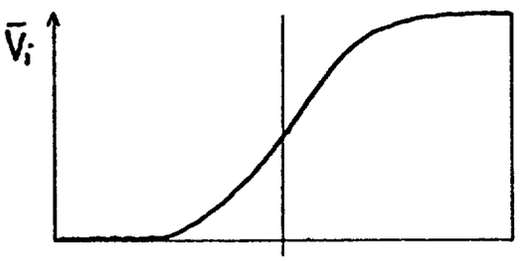

Mean return

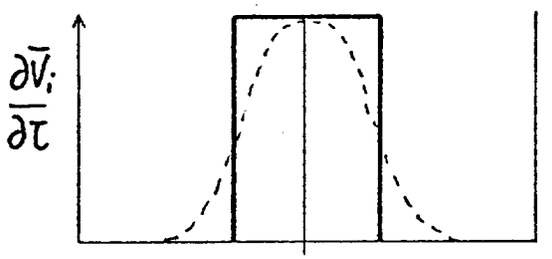

Height estimator. Dotted line is MLE weighting function, solid line is SMLE. Width of SMLE window is adaptively controlled.

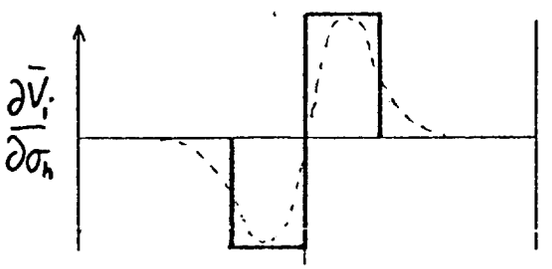

SWH (slope) estimator. Dotted line is MLE weighting function, solid line is SMLE. Width of SMLE window is adaptively controlled.

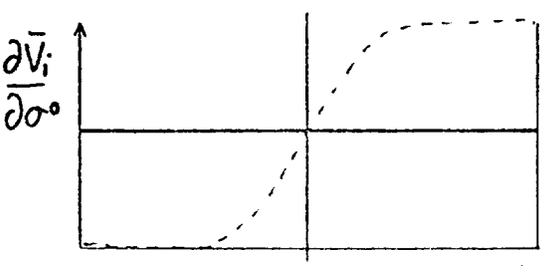

Signal strength (AGC) estimator. Dotted line is MLE weighting function, solid line is SMLE. Width of SMLE weighting function is fixed at entire range window width (63 range bins).

The practical implementation of this algorithm, using the nomenclature of the Selenia altimeter simulation code, is described in section 4.3.2.

The second stage of processing therefore consists of the formation of this central portion of the set of range bins known as the window (and not to be confused with the term 'range window', which refers to the entire set of 63 range bins). The window width, which is adaptively controlled to attempt to match the slope of the leading edge of the return, can be varied in steps of two range bins (i.e. one range bin steps symmetrically either side of the centre) from a minimum value of 3 to a maximum of 35 range bins. The initial value used when emerging from the acquisition sequence, is 35 range bins. The range window is therefore divided into five portions, AA, BB, CC, DD and EE (Fig. 4.3), and (BB+CC+DD) forms the window, though the estimation of leading edge slope is made using fractional parts of range bin signals, and is thus essentially continuous in nature.

A comparison of the ERS-1 and Seasat window width selection schemes is shown in Fig. 4.4. In the Seasat altimeter the central processing gate M_i (equivalent to BB+CC+DD) was selected on the basis of the gate triplet E_i, M_i, L_i for which $\overline{L_i - E_i}$ is closest to $0.665 \times \overline{L_6 - E_6}$, and the value of H_s determined by addressing a lookup table with $\overline{L_i - E_i}$. For the ERS-1 altimeter, the window width selection is made in steps of two range bins. The values of time constants currently used in the simulation program are initial loop bandwidths of 3 Hz (for 5 seconds, to allow the loops to settle after the acquisition sequence) with a track mode bandwidth of 0.3Hz. The

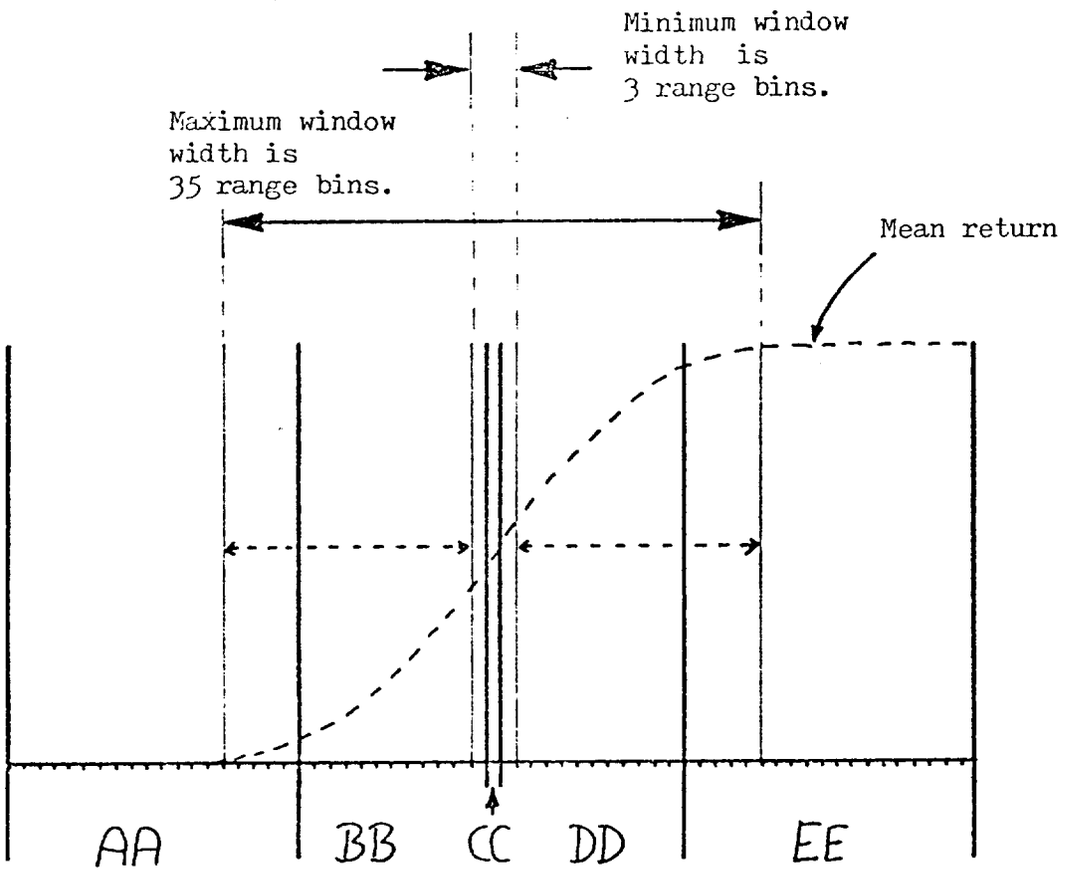

Fig. 4.3 Formation of window to estimate leading edge slope of return pulse. (The width of the window (BB+CC+DD) is adaptively varied, from a minimum of 3 to a maximum of 35 range bins, to match the leading slope.)

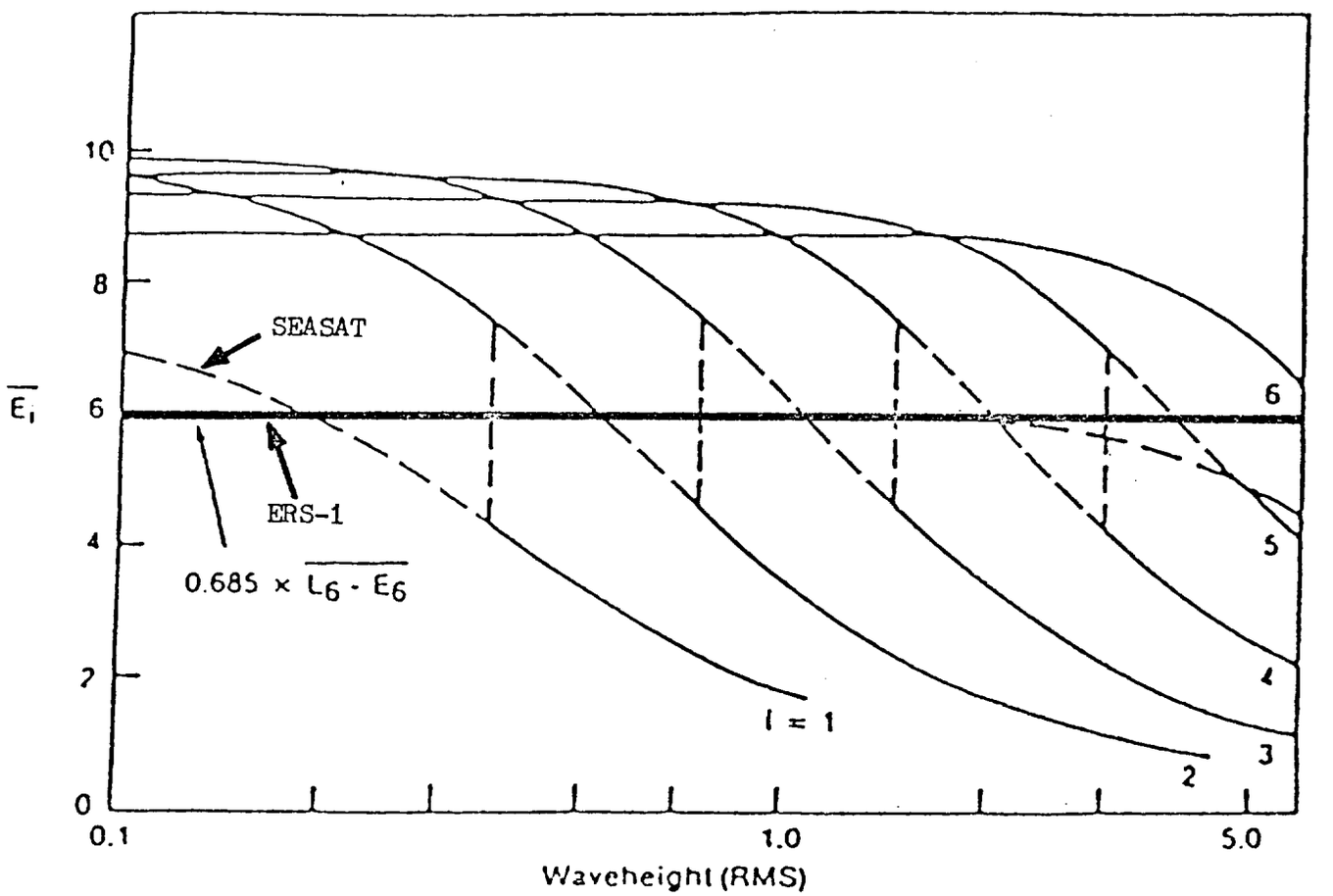

Fig. 4.4 A comparison of Seasat and ERS-1 window width selection schemes (adapted from Townsend, 1980).

loop damping factor in each case is 0.4, i.e. slightly underdamped. This underdamping means that the range rate 'length of memory' (see Rapley et al.,1983,pp77 et seq.) is shorter than for the critically-damped case, which allows a faster response to range rate changes and less likelihood of blurring during pulse summation, though at the expense of overshoot in the transient response.

4.3.1 Implications for ocean and sea ice data product retrieval

(a) The form of the h-vs-offset characteristic. When there is significant range lag, the slope error term tends to $2A_1$ (see section 4.3.2, Fig. 4.6), so the widest value of window is selected (though this will not be instantaneous because of the smoothing effect of the slope tracking loop). With Seasat the characteristic was linear over essentially the widest H_i gate (about 8 range bins - see Fig. 4.4 of Rapley et al., 1983). Since with the ERS-1 altimeter the widest value of (BB+DD) allowed is 35 range bins, the h-vs-offset characteristic will be linear over a much wider region than with Seasat, which has been identified as being crucial.

(b) Behaviour over sea ice. The Seasat tracker exhibited a characteristic 'relaxation oscillator effect'; with specular type returns, the (H_i - AGC) height error term was instantaneously very large, giving a substantial offset from which the tracker recovered over about 14 loop updates, then starting the process again (Rapley et al., 1983, p115 et seq.). We can see that the SMLE height error algorithm will behave similarly, since the height error ((BB+DD) - AGC) will also be anomalously large for a specular return within the

(BB+DD) window. The window width will also oscillate, though to a large extent filtered by its own alpha-beta tracker time constants.

4.3.2 Practical implementation of the SMLE algorithm

This section presents the SMLE height, slope (H_s) and AGC algorithms, using the terminology of the Selenia altimeter simulation code.

First we shall define some of the variables. The 50-pulse-averaged signals in the 63 range bins are denoted by LV(i), i = 1 to 63. This set of range bins is divided into five portions; AA, BB, CC, DD and EE (Fig. 4.5). BB, CC and DD form the window, which the slope tracker attempts to match to the leading edge of the return. The window width can vary from 3 to 35 range bins. The initial value, as used when emerging from the acquisition sequence, is the widest allowed, i.e. 35 range bins.

There are three variables associated with the window width: NE is the width, in range bins, of the window (BB+CC+DD). NE is an integer. R9 is the width, in range bins, of BB or DD. R9 is an integer; thus

NE= 2*R9+1.

The leading edge slope, R30, is estimated with finer resolution than single range bins (i.e. real rather than integer). It is related to R9 by

R9= INT(1./R30)

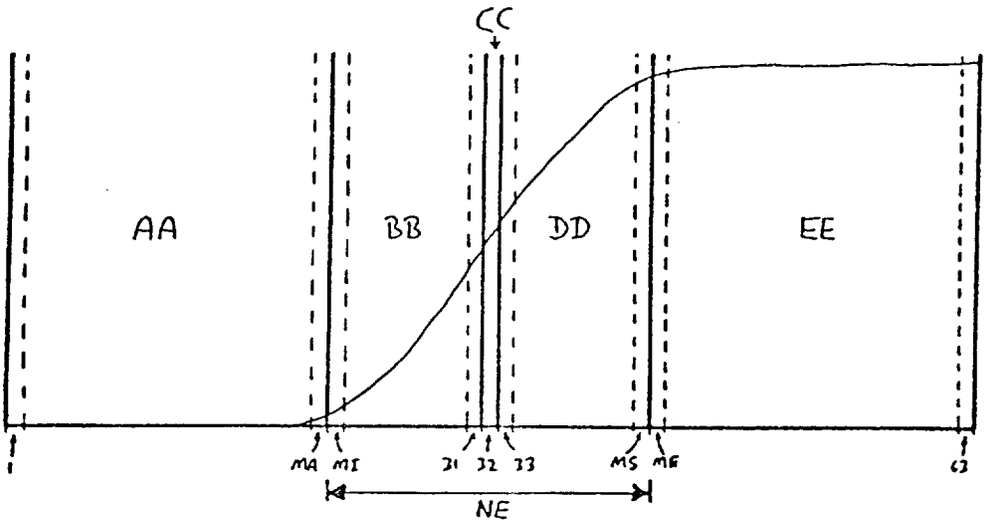

$$MI = 32 - (NE - 1)/2$$

$$MA = MI - 1$$

$$MS = 32 + (NE - 1)/2$$

$$ME = MS + 1$$

$$AA = \sum_{i=1}^{MA} LV(i)$$

$$BB = \sum_{i=MI}^{31} LV(i)$$

$$CC = LV(32)$$

$$DD = \sum_{i=33}^{MS} LV(i)$$

$$EE = \sum_{i=ME}^{63} LV(i)$$

$$R10 = (AA + BB + CC + DD + EE)/63$$

Fig. 4.5 Formation of window width to match leading edge slope.

Also calculated is the AGC term, $R10 = \sum_{i=1}^{63} LV(i)/63$, i.e.

$$R10 = (AA+BB+CC+DD+EE)/63$$

Height error algorithm

The height error Δh is provided by the difference between (BB+DD) and AGC (cf. Seasat (M_i - AGC)). In the code, the height error is designated by R12, and is given by the expression:

$$R12 = (BB+DD)/2 - (NE-1)*R10/2$$

The (NE-1) term weights the AGC value R10 (which is per range bin) according to the window width, and subtracting 1 to account for not using CC. The height error is calculated every 50ms, and the height alpha-beta tracker is updated at a 1ms rate, to control interpolation during pulse summation. The AGC alpha-beta tracker is updated at a 10ms rate.

Slope error algorithm

Fig. 4.6 shows the leading edge of the return, and the straight line that the slope algorithm attempts to match to its slope. It is assumed that the probability distribution of the ocean surface scatterers is symmetric, thus the leading edge is symmetric about its half-power point. The slope algorithm acts so as to equalise the two shaded areas, so the slope error is found from the difference between the two areas. Let the window width, in range bins, be denoted by W (i.e. like NE, only real rather than integer).

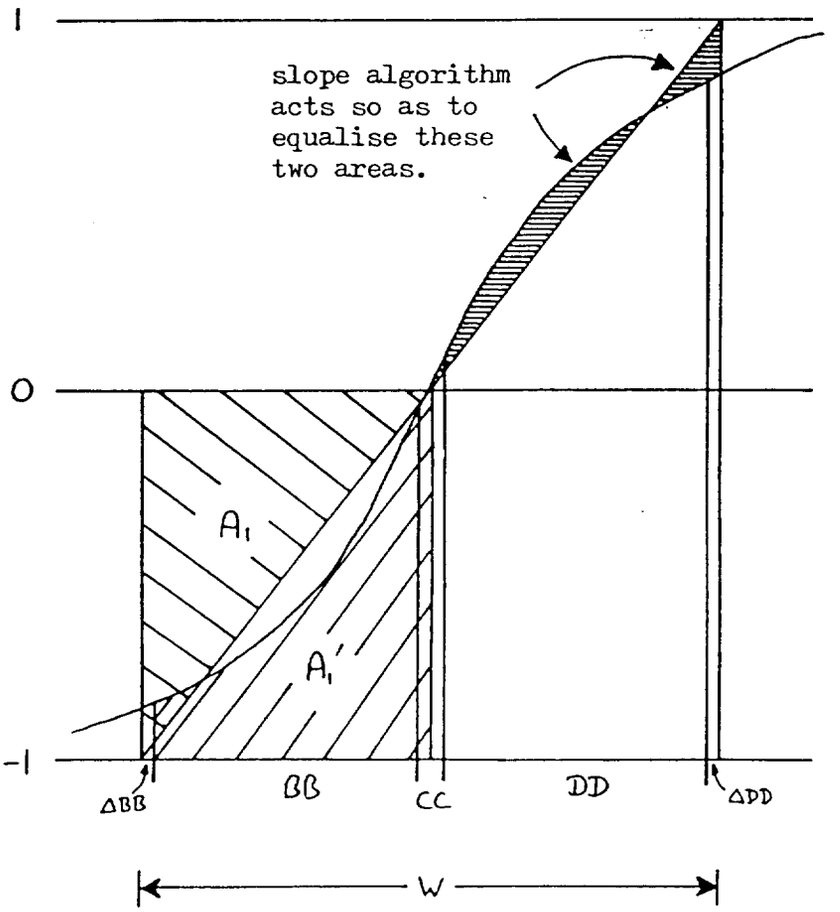

Fig. 4.6 Slope error algorithm .

$$A_1 = (1/2).(W/2).1 \qquad 2A_1 = W/2$$

$$2A_1' = DD - BB + \Delta DD - \Delta BB,$$

Now, DD - BB = (LV(NE)-LV(NA)) * (fractional part of window width) and (fractional part of window width) = 1/R30 - R9, denoted by RSPICC,

(LV(NE)-LV(NA)) is denoted by AVSPIC

so DD - BB = -RSPICC*AVSPIC

The area error signal is given by $2A_1' - 2A_1$

= DD - BB - RSPICC*AVSPIC - W/2

= -(BB - DD + RSPICC*AVSPIC) - W/2

To convert this from area error to slope error, multiply by $(2/W)^2$; (2/W is denoted by FINES)

so slope error is given by the expression:

```
-(BB-DD+RSPICC*AVSPIC)*FINES**2-FINES
```

and the new value of slope is

```
R44=R44-(BB-DD+RSPICC*AVSPIC)*FINES**2-FINES
```

This feeds a separate alpha-beta tracker, which is updated at a 50ms rate, giving a smoothed value of slope, R30. This addresses an algorithm to read out H_s, which is what is telemetered:

```
Hs=((0.306/R30)**2-0.036)
```

which assumes the Brown Model (Brown, 1977) for ocean surface.

The value of R30 also updates NE for the next computation cycle:

```
R9=INT(1./R30)
NE=2*R9+1
```

4.4 The ice mode and sea ice tracking

In order to maintain lock over steeply sloping and undulating ice sheet surfaces, the ERS-1 altimeter is provided with an alternative tracking mode. In this mode the range window width is increased by a factor of 4 and a centre of gravity tracker is substituted for the SMLE algorithm. It should be stressed that the ice mode is not intended for use over sea ice. However, switching between the oceans mode and the ice mode will have some impact on data collection close to the Greenland and Antarctic coastlines, and will therefore affect the completeness of sea ice coverage. The technical details of the switching procedure are not currently available. However, given that the daily prediction of coastal transition times is likely to be limited to an accuracy of ~1 s due to orbit uncertainties, losses of order 10 km can be expected if mode switching is attempted as precisely as possible at the coastline.

In section 2.7 it was pointed out that standard ocean trackers suffer from a number of difficulties when processing strongly peaked and rapidly fluctuating returns from sea ice. At least part of the problem arises from the use of an AGC control signal derived from the mean power of the return. The initial peaks of quasi-specular returns reach high absolute values when processed by a mean power AGC, increasing the gain on the height loop error

signal (Fig. 4.7(a)). For Seasat this resulted in oscillatory behaviour in the height loop, as noted earlier.

A solution to this problem is to use the peak value to control the AGC since this results in a height error signal gain which is independent of pulse 'peakiness' (Fig. 4.7(b)). However the statistical noise on the AGC signal is inevitably increased. The compromise adopted in the US Geosat tracker design is to operate with a bimodal, adaptive algorithm which normally employs a mean-value AGC but which switches to peak value operation when the return pulse peak-to-mean ratio exceeds a fixed value. It is strongly recommended that a similar approach should be adopted for the ERS-1 altimeter.

4.5 Fully automatic data processing

The ERS-1 altimeter design is in so many respects similar to that of Seasat that the degree of fully automatic ground processing of ocean data is also likely to be very similar. Some differences will be as follows:-

(i) The on-board processor includes an 'attitude' loop which detects spacecraft mispointing by its effect on the echo waveform shape. Data from the loop are used to correct the on-board computed geophysical parameters. However, it is not known as yet whether these corrections will be sufficiently accurate to eliminate the need for further attitude corrections based

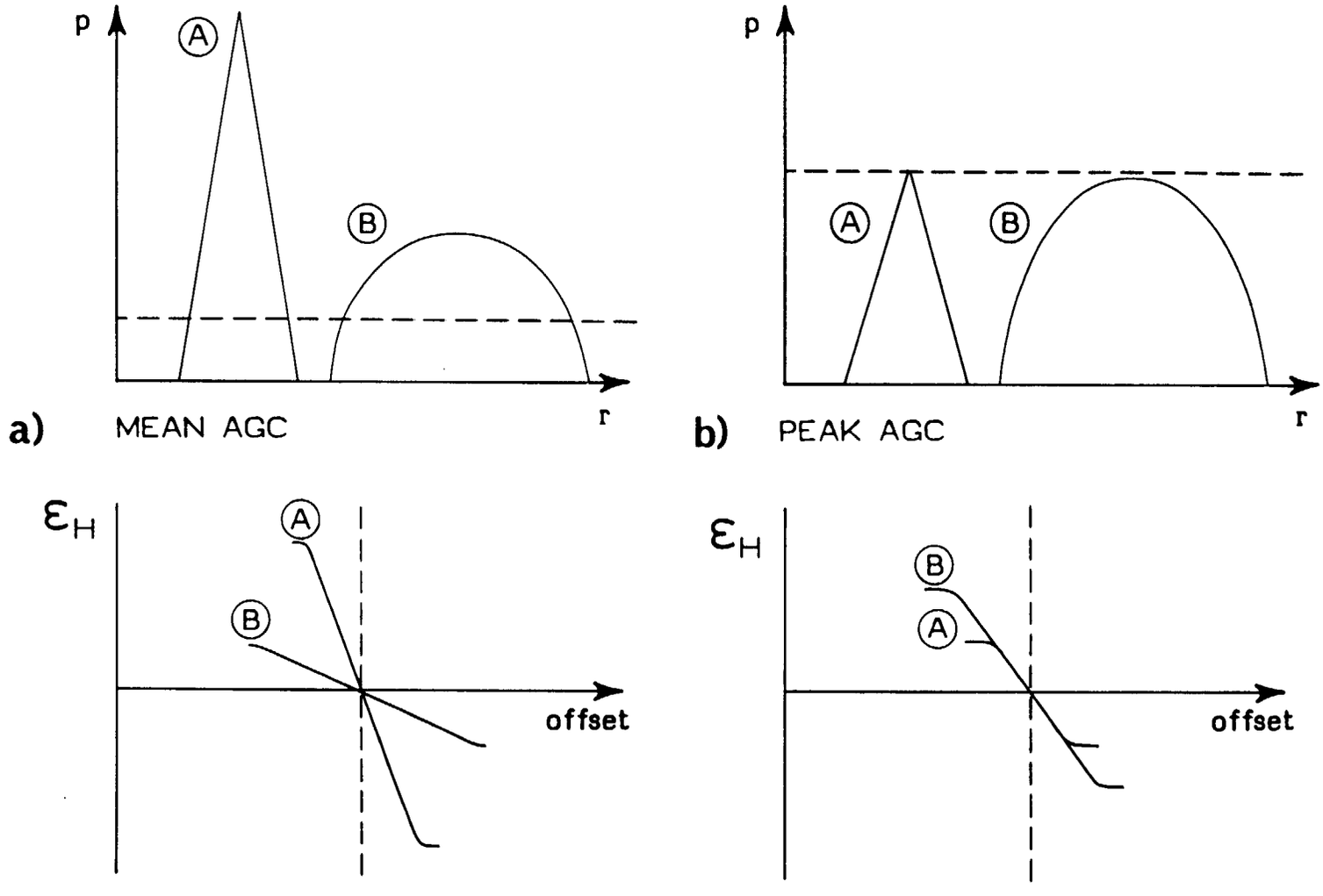

Figure 4. 7 Peak AGC results in improved H loop stability when processing non-standard (peaky) pulses.

on the spacecraft pointing data, and further analysis of the waveform, during ground processing.

(ii) A specific use of the attitude loop output, when combined with the mean power AGC value, will be to provide a pulse 'peakiness' parameter which could be used for ice boundary detection in much the same way as achieved by Dwyer & Godin(1980) for GEOS-3 (see section 3.4.1). Note that an on-board peak-AGC/mean AGC switching algorithm could be used to flag the presence of ice in the altimeter footprint, but would not be tuned for location of the conventional ice edge given by the 15% ice contour.

The ability of the instrument to track more extreme topographic surfaces, and the emphasis placed on analysis of coastal region, sea ice, ice sheet and land data will have a major impact on the ground processing system since these will require retracking and processing of the waveform data. Given that the bit rate associated with the waveform data is some three orders of magnitude greater than that for the on-board computed geophysical parameters, the impact on the processing and archiving facilities required is clearly very large. However, a full discussion of the altimeter ground segment requirements is beyond the scope of this report.

5. Estimation of wave parameters for ERS-1.

5.1 Skewness, sea state bias and wave period.

In this section the possibility of extracting other wave parameters from the radar return (as well as significant wave height) will be examined. In particular, the possibility of obtaining wave period and skewness information will be discussed. The extraction of a period parameter can be carried out on the basis of Gaussian surface statistics, whereas the skewness of the sea surface is a nonlinear wave effect and requires the use of a non-Gaussian model for the sea surface. If nonlinear wave effects are significant they can affect the estimation of the position of the mean sea surface level - an effect known as sea state bias. If the slope of the mean level is to be used to calculate surface current (assuming a geostrophic balance) then the position of the mean level needs to be known accurately and the sea state bias needs to be determined. How this may be done will be discussed below.

5.1.1 Wave period

The starting point for the extraction of a wave period parameter from the radar return is an equation (due to Barrick, 1968, 1972) which relates the backscattering coefficient σ^o to the joint probability density function of surface slopes $p(\xi_x, \xi_y)$. For the purposes of extracting a period parameter from the radar return it is only necessary to consider the back- scatter at zero incidence angle $\sigma^o(0^o)$ for which

$$\sigma^o(0^o) = \pi |R(0)|^2 p(\xi_x = 0, \xi_y = 0)$$

where R(0) is the Fresnel reflection coefficient of the air-sea interface at normal incidence. From both the Gaussian theory (Longuet-Higgins, 1957) and the non-Gaussian theory (section 3.1.1.2)

$$p(\zeta_x = 0, \zeta_y = 0) = \frac{1}{2\pi}(\mu_{020}\mu_{002} - \mu_{011}^2)^{-\frac{1}{2}}$$

where μ_{020}, μ_{002} are the surface slope variances $\langle \zeta_x^2 \rangle$, $\langle \zeta_y^2 \rangle$ and μ_{011} is the covariance between ζ_x and ζ_y given by $\langle \zeta_x \zeta_y \rangle$. If principal axes are chosen then

$$\Delta_2^{\frac{1}{2}} = (\mu_{020}\mu_{002} - \mu_{011}^2)^{\frac{1}{2}} = \sqrt{\mu_{020}\mu_{002}}$$

and this may be interpreted as the geometric mean of the maximum and minimum slope variances.

The value of $\sigma^o(0^o)$ may be estimated from the radar return usually indirectly via the automatic gain control (Brown, 1979a and Mognard & Lago, 1979). So the radar return can give information on the surface slope variances. This has been used by some investigators (see for example Brown, 1979a and Mognard & Lago, 1979) to derive wind speed from the radar return (under the assumption of isotropy and using an empirical relationship between wind speed and r.m.s. slope; see section 3.2). Brown(1979b) has, under the assumption of isotropy, examined the mean square slope of the waves. Here it will be shown how a period parameter may be derived from Δ_2.

If $\underline{\Psi}(k_1, k_2)$ is the wavenumber spectrum then, using principal axes,

$$\Delta_2 = \int_{-\infty}^{\infty}\int_{-\infty}^{\infty} k_1^2 \underline{\Psi}(k_1, k_2)\, dk_1\, dk_2 \times \int_{-\infty}^{\infty}\int_{-\infty}^{\infty} k_1'^2 \underline{\Psi}(k_1', k_2')\, dk_1'\, dk_2'$$

(see Longuet-Higgins, 1957). We now make the following change of variables

$$k^2 = k_1^2 + k_2^2 , \quad \theta = \tan^{-1}(k_2/k_1)$$

such that

$$\Psi(k_1, k_2)\, dk_1\, dk_2 = \psi(k, \theta)\, dk\, d\theta$$

and

$$\Delta_2 = \int_0^\infty \int_0^{2\pi} k^2 \cos^2\theta\, \psi(k,\theta)\, dk\, d\theta \times \int_0^\infty \int_0^{2\pi} k'^2 \sin^2\theta'\, \psi(k',\theta')\, dk'\, d\theta'$$

$$= \frac{1}{g^4} \int_0^\infty \int_0^{2\pi} \omega^4 \cos^2\theta\, E(\omega,\theta)\, d\omega\, d\theta \times \int_0^\infty \int_0^{2\pi} \omega'^4 \sin^2\theta'\, E(\omega',\theta')\, d\omega'\, d\theta'$$

where the dispersion relationship

$$\omega^2 = gk$$

and

$$\psi(k,\theta)\, dk\, d\theta = E(\omega,\theta)\, d\omega\, d\theta$$

have been used. $E(\omega,\theta)$ is the directional wave frequency spectrum.

To make further progress it is necessary to make some assumption about $E(\omega,\theta)$. Here the common assumption that the directional spreading of the waves is independent of frequency will be made, so that

$$E(\omega,\theta) = S(\omega)\, G(\theta)$$

where

$$\int_0^{2\pi} G(\theta)\, d\theta = 1.$$

An alternative simplifying assumption is that of isotropy but this is just a special case of the above ($G(\theta) = 1/2\pi$). Δ_2 is now given by

$$\Delta_2 = \frac{m_4^2}{g^4}\left[1 - \int_0^{2\pi}\cos^2\theta\, G(\theta)\,d\theta\right]\int_0^{2\pi}\cos^2\theta'\, G(\theta')\,d\theta'$$

where

$$m_n = \int_0^{\infty} \omega^n S(\omega)\,d\omega .$$

The above shows how the surface slope information Δ_2 may be related to the fourth frequency spectral moment m_4. If the spreading function $G(\theta)$ is now expressed in the form given by Longuet-Higgins, Cartwright & Smith (1963) as

$$G(\theta) = \frac{(2r)!!}{2\pi\,(2r-1)!!}\cos^{2r}(\theta/2)$$

where

$$(2r)!! = 2.\ 4.\ 6.\ \ldots\ 2(r-1).\ 2r$$

and

$$(2r-1)!! = 1.\ 3.\ 5.\ \ldots\ (2r-3).\ (2r-1)$$

then

$$m_4 = g^2\,\Delta_2^{1/2}\,(r+1)(r+2)\left[(2r+1)(r^2+r+1)\right]^{-1/2} \quad (5.1)$$

Thus from $\sigma^0(0)$ it is possible to obtain, in principle, an estimate of the fourth moment of the frequency spectrum, m_4 (if some value of r is assumed). For the isotropic case r=0 and m_4 is obtained directly. It is now possible to define a new period parameter T_A where

$$T_A = 2\pi\left(\frac{m_0}{m_4}\right)^{1/4}$$

where $m_0 = \mu_{200}$, the variance of the sea surface ($H_s = 4\sqrt{m_0}$). This is related to the more conventional period parameters T_z (zero-upcrossing period) and T_c (crest period) and the bandwidth parameter ε by

$$T_A = \sqrt{T_z\,T_c}$$

$$= (1-\varepsilon^2)^{1/4}\,T_z$$

where

$$T_z = 2\pi \left(\frac{m_0}{m_2}\right)^{1/2} \quad , \quad T_c = 2\pi \left(\frac{m_2}{m_4}\right)^{1/2}$$

and

$$\varepsilon^2 = 1 - m_2^2/(m_0 m_4) .$$

Thus T_A may be regarded as the geometric mean of the zero-upcrossing and crest periods. For a narrow band spectrum $\varepsilon \to 0$ and so $T_A \to T_z$, but in general T_A will differ from T_z, and comparing the two may give a means of estimating ε (see section 5.3.4 below).

In Figs 5.1 and 5.2 the percentage error in calculating m_4 and T_A by assuming isotropy (r = 0) is given. Over a realistic range of values of r (0 to 15) it can be seen that, while the variation of m_4 is of the order of 50%, the variation of T_A is only of the order of 10% (as $T_A \propto m_4^{-1/4}$). Thus T_A is fairly insensitive to any assumption which may be made about the directional spread of the waves (that is, the choice of r).

The implications of this work for wind speed retrieval require further investigation.

5.1.2 Skewness.

As noted above, in order to derive this parameter from the radar return a non-Gaussian model for the sea surface is necessary. Using the results of section 3.1.1.2 the double integral in Eq. 3.1, I(t), will be evaluated to obtain the form of the return from a nonlinear

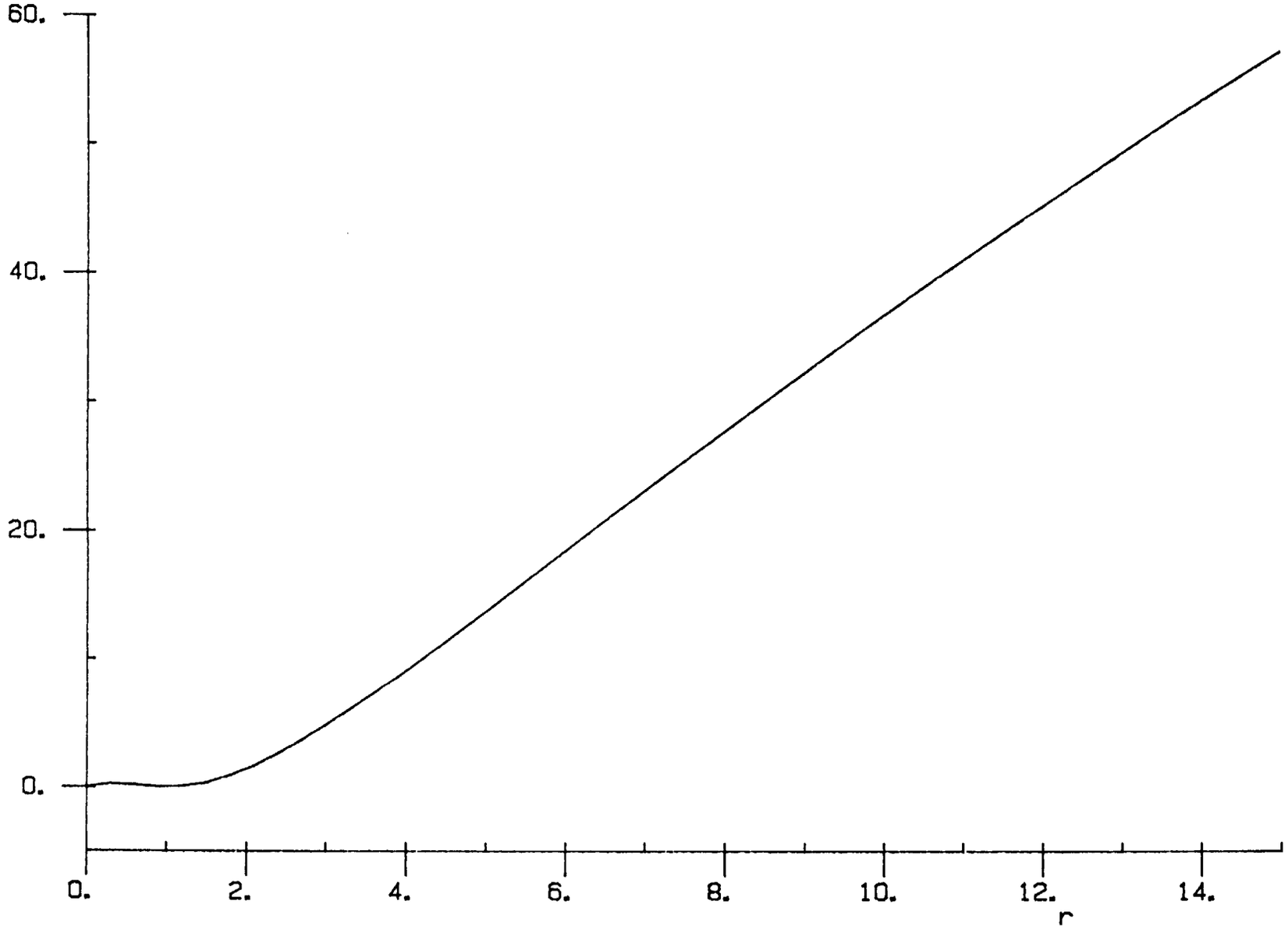

Fig. 5.1 Percentage error in calculating m_4 by assuming isotropy (r=0).

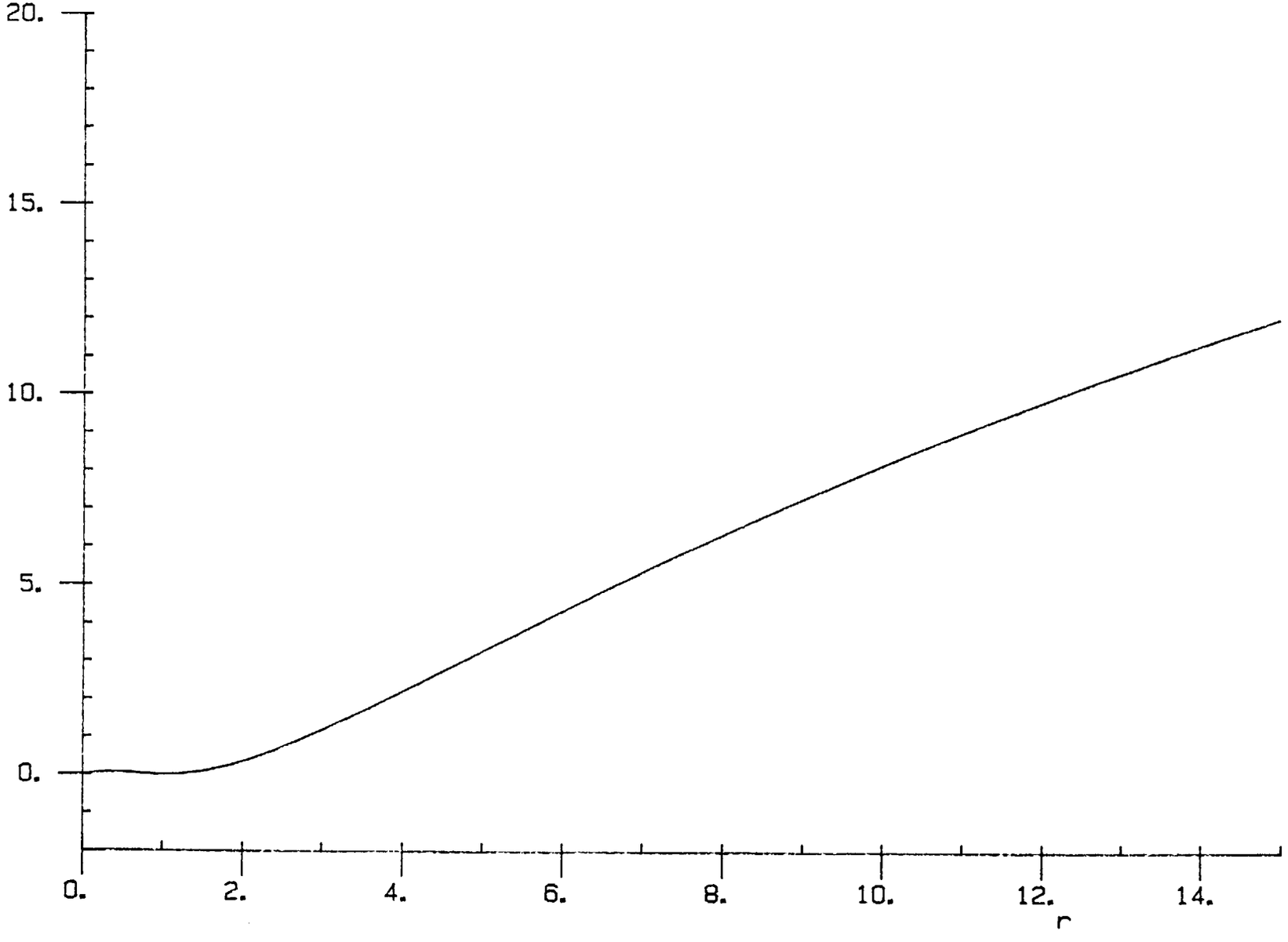

Fig. 5.2 Percentage error in calculating T_A by assuming isotropy (r=0).

sea surface.

$$I(t) = \eta P_T (2\pi\mu_{200})^{-1/2} \left(\frac{c}{2}\right) \int_{-\infty}^{\infty} \int_{0}^{\infty} \exp\left\{ -\frac{c^2(\tau-\hat{\tau})^2}{8\mu_{200}} - \frac{(t-\tau)^2}{2\sigma_\rho^2} \right\} \times \left[1 - \frac{1}{6}\lambda_{300} \frac{c^3(\tau-\hat{\tau})^3}{8\mu_{200}^{3/2}} + \frac{(\lambda_{300}+\delta)}{2} \cdot \frac{c(\tau-\hat{\tau})}{2\mu_{200}^{1/2}} \right] d\hat{\tau}\, d\tau .$$

Make the following change of variables

$$x = \frac{c\tau}{2\mu_{200}^{1/2}} , \quad \hat{x} = \frac{c\hat{\tau}}{2\mu_{200}^{1/2}} , \quad y = \frac{ct}{2\mu_{200}^{1/2}}$$

and let

$$\beta^2 = c^2\sigma_\rho^2 / 4\mu_{200}$$

then

$$I(t) = \eta P_T (2\pi)^{-1/2} \left(\frac{2\mu_{200}^{1/2}}{c}\right) \int_{-\infty}^{\infty} \int_{0}^{\infty} \exp\left\{ -\frac{(x-\hat{x})^2}{2} - \frac{(y-x)^2}{2\beta^2} \right\} \times \left[1 - \frac{1}{6}\lambda_{300}(x-\hat{x})^3 + \frac{(\lambda_{300}+\delta)}{2}(x-\hat{x}) \right] d\hat{x}\, dx .$$

With the further change of variable

$$u = \rho^{1/2}\left(x - \frac{\hat{x}}{\rho} - \frac{y}{\rho\beta^2} \right)$$

where

$$\rho = (1+\beta^2)\beta^{-2}$$

$$I(t) = \frac{\eta P_T}{\sqrt{2\pi}\rho}\left(\frac{2\mu_{200}^{1/2}}{c}\right)\int_0^\infty\int_{-\infty}^\infty e^{-\frac{1}{2}u^2}\left[1 - \frac{1}{6}\lambda_{300}\left(\frac{u}{\rho^{1/2}} - \frac{(\hat{x}-y)}{\rho\beta^2}\right)^3 + \frac{(\lambda_{300}+\delta)}{2}\left(\frac{u}{\rho^{1/2}} - \frac{(\hat{x}-y)}{\rho\beta^2}\right)\right] du$$

$$\exp\left\{-\frac{1}{2}\frac{(\hat{x}-y)^2}{(1+\beta^2)}\right\} d\hat{x}$$

$$= \eta P_T \rho^{-1/2}\left(\frac{2\mu_{200}^{1/2}}{c}\right)\int_0^\infty \exp\left\{-\frac{1}{2}\frac{(\hat{x}-y)^2}{(1+\beta^2}\right\}$$

$$\left[1 - \frac{1}{6}\lambda_{300}\left\{-\frac{3}{\rho^2\beta^2}(\hat{x}-y) - \frac{(\hat{x}-y)^3}{\rho^3\beta^6}\right\}\right.$$

$$\left. - \frac{(\lambda_{300}+\delta)}{2}\frac{(\hat{x}-y)}{\rho\beta^2}\right] d\hat{x}$$

This result may be further simplified by the change of variable

$$v = 2^{-1/2}(1+\beta^2)^{-1/2}(\hat{x}-y)$$

so that

$$I(t) = \eta P_T\left(\frac{2\mu_{200}^{1/2}}{c}\right)\beta\sqrt{2}\int_{\frac{-t}{\sqrt{2}\sigma_c}}^\infty e^{-v^2}\left[1 + Av^3 - Bv\right] dv$$

where

$$\sigma_c^2 = \sigma_\rho^2 + 4\mu_{200}/c^2$$

$$A = \frac{\sqrt{2}}{3}\lambda_{300}\left[1 + \frac{c^2\sigma_\rho^2}{4\mu_{200}}\right]^{-3/2}$$

and

$$B = \frac{(\lambda_{300}+\delta)}{\sqrt{2}}\left[1 + \frac{c^2\sigma_\rho^2}{4\mu_{200}}\right]^{-1/2} - \frac{\lambda_{300}}{\sqrt{2}}\left(\frac{c^2\sigma_\rho^2}{4\mu_{200}}\right)\left[1 + \frac{c^2\sigma_\rho^2}{4\mu_{200}}\right]^{-3/2}.$$

Finally the above may be integrated to obtain

$$I(t) = \left[\eta P_T\sqrt{2\pi}\ \sigma_\rho\right]\frac{1}{2}\left[1 + \operatorname{erf}\left(\frac{t}{\sqrt{2}\sigma_c}\right)\right.$$

$$\left. + \frac{e^{-t^2/2\sigma_c^2}}{\sqrt{\pi}}\left\{A\left(\frac{t^2}{2\sigma_c^2}+1\right) - B\right\}\right].$$

In the Gaussian limit ($\lambda_{300} = \delta = 0$) this reduces to the result due to Brown (1977) given in section 3.1.1.1.

From the above it can be seen that the following wave parameters may be estimated from the radar return

(i) μ_{200} - the sea surface variance (and hence H_s)

(ii) λ_{300} - the skewness of the sea surface

(iii) δ - a skewness coefficient with unknown physical significance (see section 3.1.1.2)

The sea surface skewness λ_{300} provides a measure of the nonlinearity of the wave field as it describes the peakier crests and flatter troughs of nonlinear waves. The skewness coefficient δ does not appear to have any physical significance but it is important for correcting sea state bias . Lipa & Barrick (1981) have made use of a similar theory to that presented above to estimate skewness from the Seasat altimeter. However, as the altimeter pulse shape was not sufficiently close to Gaussian they had to deconvolve the integrals determining the pulse shape numerically. This should not be necessary for ERS-1, and the functional form given above can be fitted to the return pulse directly. Lipa & Barrick (1981) make use of Jackson's (1979) result for $p(\zeta, \zeta_x = 0)$ which is identical functionally to the result used here for $p(\zeta, \zeta_x=0, \zeta_y=0)$. It differs only in that the parameter is replaced by λ_{120} (in our notation). From their results λ_{300} lies in the range 0.1 to 0.29, based on 24 second averages. In the next section it will be shown how these non-zero values of the skewness coefficients can be used to correct sea state bias.

In order to illustrate the effects of wave nonlinearity on the return pulse shape the theoretical return $P_r(t)$ is plotted in Figs 5.3 to 5.7 for various values of λ_{300} and δ with H_s = 4 m and zero pointing angle. $P_r(t)$ is as given in section 3.1.1.1 except that the double integral is now the one evaluated above. The return is normalised, for illustrative purposes only, so that the maximum power is unity. In practice the automatic gain control will normalise the altimeter radar return. It can be seen from the figures that changes in λ_{300} and δ lead to changes in the pulse shape and position.

5.1.3 Sea state bias

In this section we will consider the effect on the mean level estimate of assuming that the sea surface is Gaussian when in fact it is non-Gaussian. Most "on board" altimeter algorithms are based on the Gaussian assumption for the sea surface. If nonlinear wave effects are significant the use of the Gaussian theory leads to an error in the estimate of the position of the mean sea level; an effect known as sea state bias.

Two factors give a bias in the estimate of mean sea level derived from the radar return; one physical and one instrumental. The physical factor has been called, somewhat inappropriately, "electromagnetic bias" (see Jackson, 1979; Lipa & Barrick, 1981). This effect has been incorrectly attributed to the focussing of radar energy by the flatter troughs of nonlinear waves and its scattering by their sharper crests. In fact, as noted above (section 3.1.1.2),

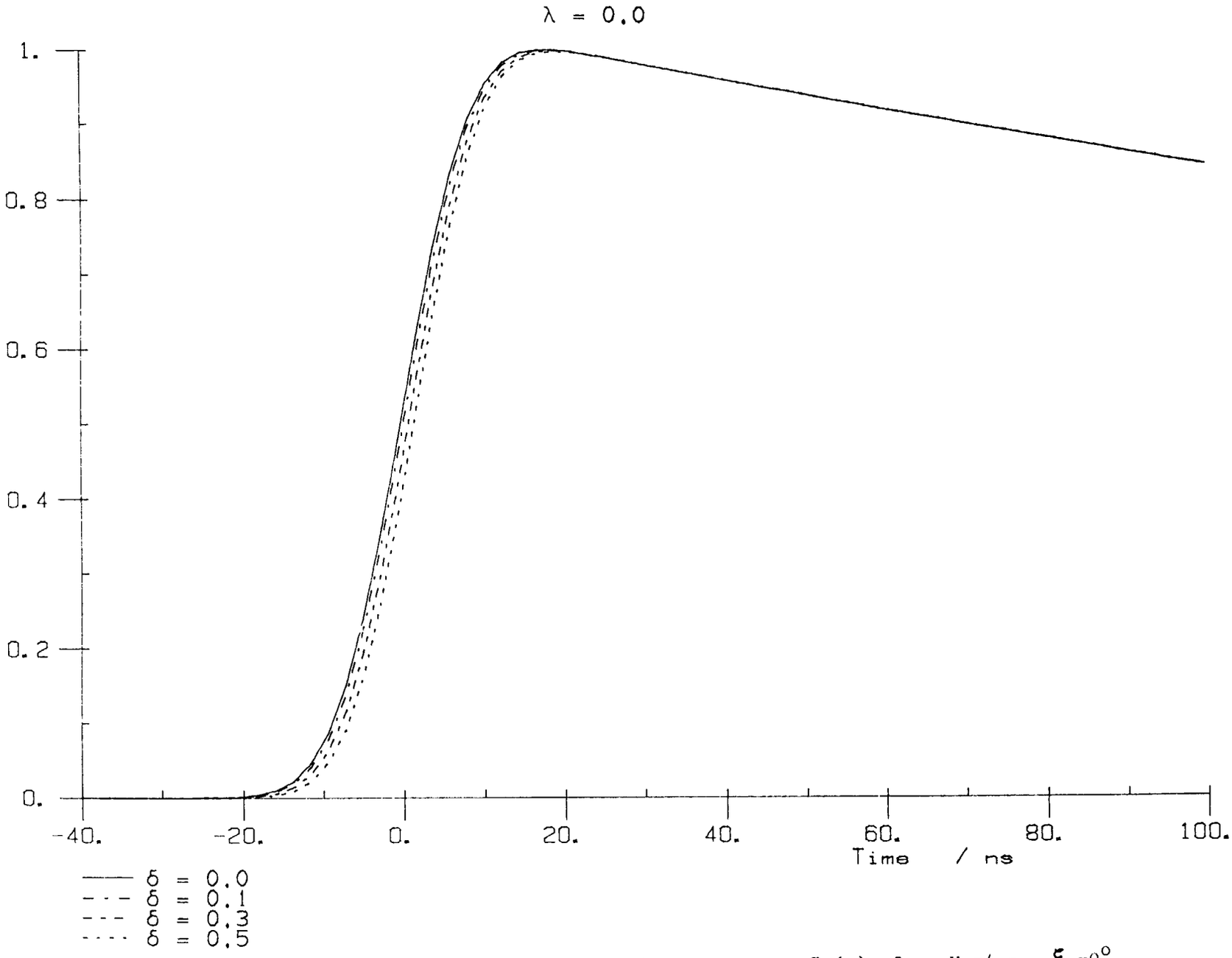

Fig. 5.3 Normalised return power $P_r(t)$ for H_s=4 m, ξ =0°, λ_{300}=0 and δ =0,0.1,0.3,0.5.

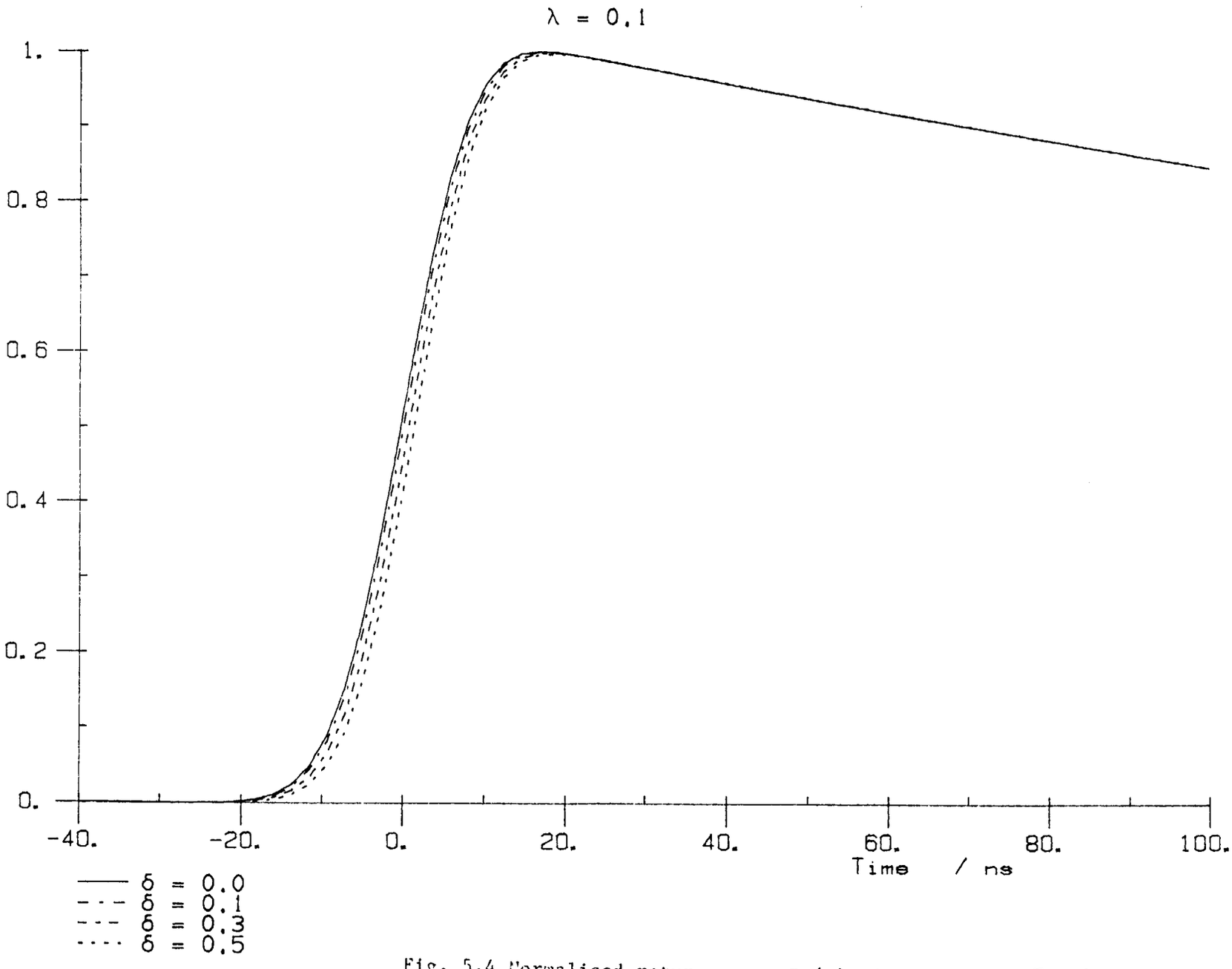

Fig. 5.4 Normalised return power $P_r(t)$ for H_s=4 m, ξ =0°, λ_{300}=0.1 and δ =0,0.1,0.3,0.5.

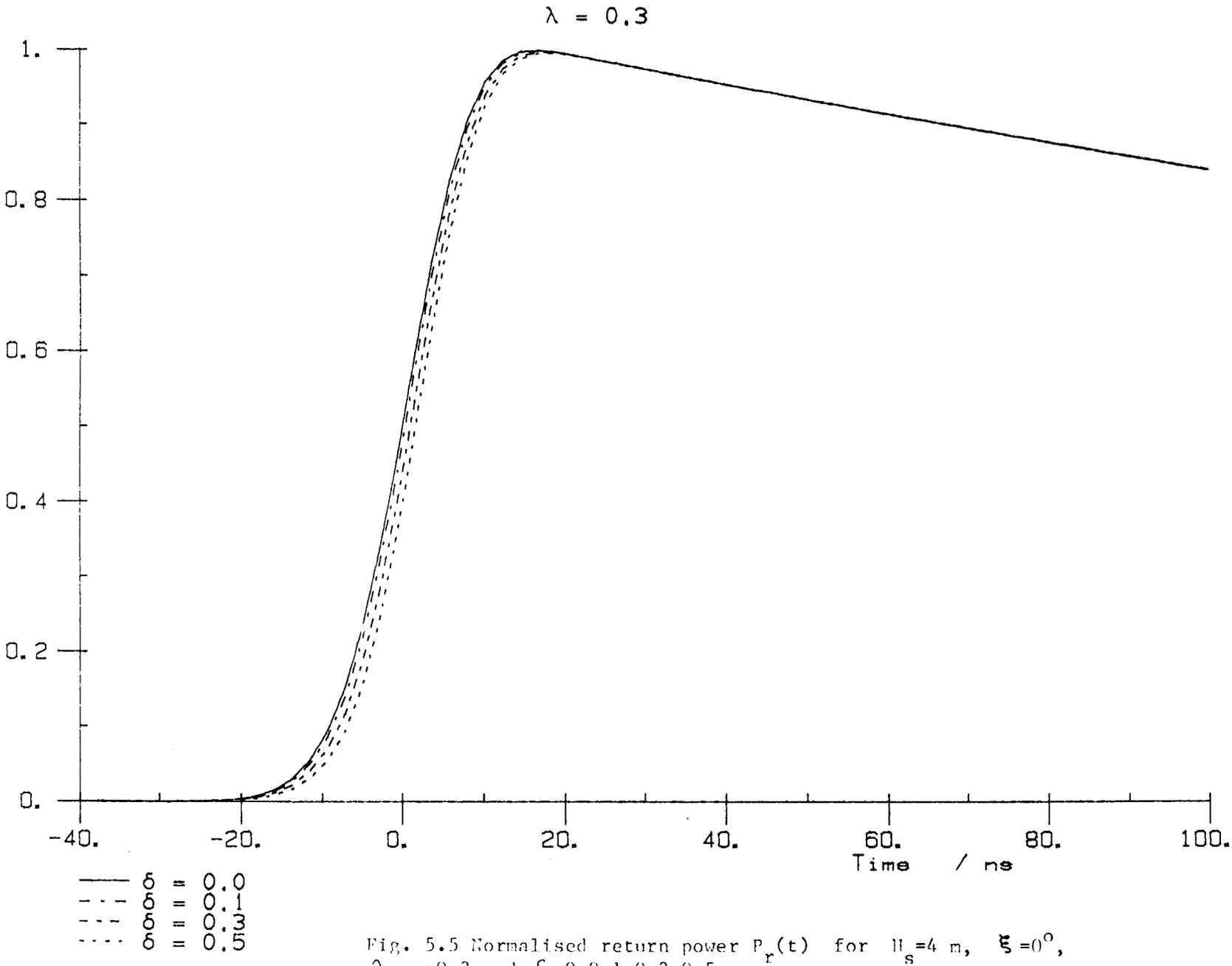

Fig. 5.5 Normalised return power $P_r(t)$ for H_s=4 m, ξ=0°, λ_{300}=0.3 and δ=0,0.1,0.3,0.5.

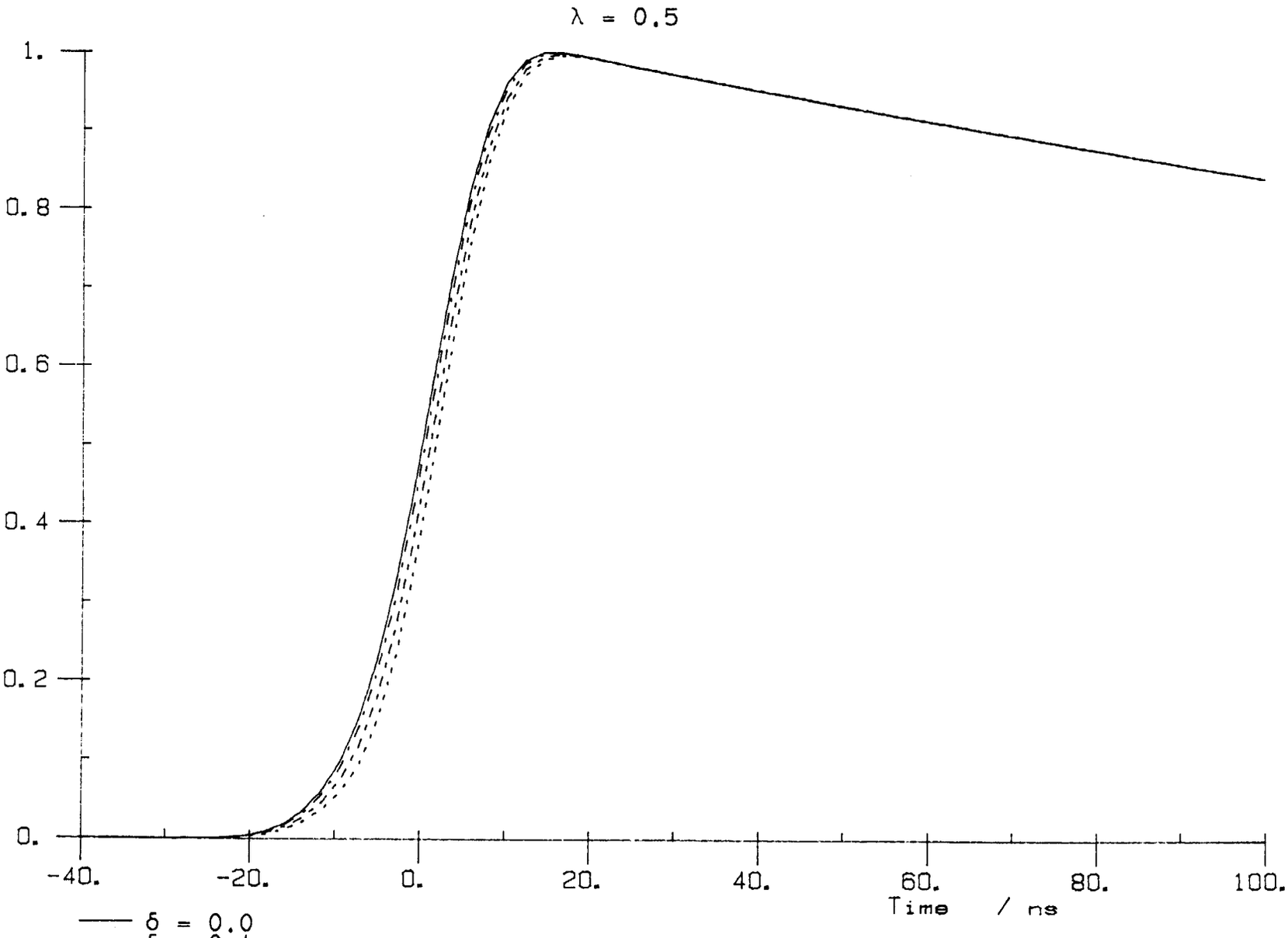

Fig. 5.6 Normalised return power $P_r(t)$ for H_s=4 m, ξ =0°, λ_{300}=0.5 and δ =0,0.1,0.3,0.5.

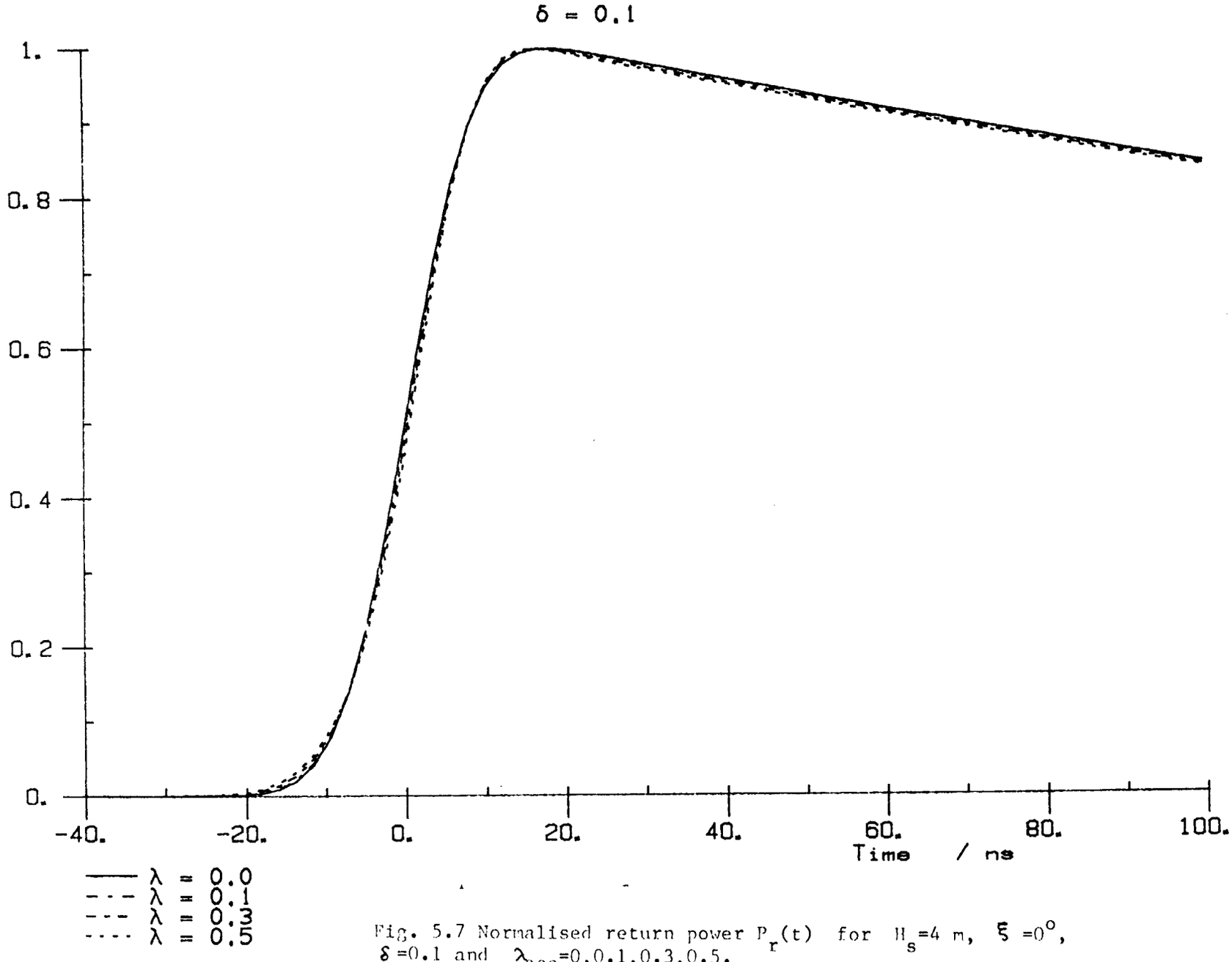

Fig. 5.7 Normalised return power $P_r(t)$ for H_s=4 m, ξ =0°, δ =0.1 and λ_{300}=0,0.1,0.3,0.5.

the altimeter does not sense the sea surface elevation distribution $p(\zeta)$, but senses the distribution of the elevation of points of zero slope $q(\zeta)$ and these differ for the non-Gaussian case. From the results of section 3.1.1.2 it is easy to show that

$$\int_{-\infty}^{\infty} \zeta\, p(\zeta)\, d\zeta = 0$$

while

$$\int_{-\infty}^{\infty} \zeta\, q(\zeta)\, d\zeta = -\frac{\delta}{2}\, \mu_{200}^{1/2} = -\frac{\delta}{8}\, H_s .$$

Thus the mean level sensed by the radar is displaced by an amount $-\frac{1}{2}\delta\mu_{200}^{1/2}$ from the actual mean sea level. The results of Jackson (1979) and Lipa & Barrick (1981) indicate that $\delta > 0$, so the mean level estimate is biased downwards. As δ and μ_{200} can be estimated from the radar return this bias may be corrected.

The instrumental bias is introduced due to the method used to track the mean level. To illustrate this, consider the theoretical leading edge response of the radar return which may be written as

$$I(\tau) = \frac{1}{2}\left[1 + \mathrm{erf}(\tau) + \frac{e^{-\tau^2}}{\sqrt{\pi}}\left\{A(\tau^2+1) - B\right\}\right]$$

where the return has been normalised (as might be done by the automatic gain control of the altimeter) and

$$\tau = t/\sqrt{2}\,\sigma_c$$

(See section 5.1.2 for definitions of σ_c, A and B). For a Gaussian sea surface (A = B = 0) the time $\tau = 0$, which determines the position of the mean level, corresponds to the half-power point of the return I(0) = 1/2. A method used for tracking the mean level ($\tau = 0$) is to locate the half-power point of the return $I(\tau) = 1/2$ and to choose

the time origin $\tau = 0$ to correspond to this point. For a non-Gaussian sea surface

$$I(0) = \frac{1}{2}\left[1 + \frac{1}{\sqrt{\pi}}(A - B)\right]$$

which is not the half-power point. Therefore tracking the half-power point leads to an error in the mean level estimate. If the factor $(c^2\sigma_p^2/4\mu_{200})$ is small, as is the case for pulse-limited satellite altimeters, then A and B are approximately given by

$$A = \sqrt{2}\,\lambda_{300}/3$$

$$B = (\lambda_{300} + \delta)/\sqrt{2}$$

and so

$$I(0) = \frac{1}{2}\left[1 - \frac{1}{\sqrt{2\pi}}\left(\frac{1}{3}\lambda_{300} + \delta\right)\right]$$

For positive λ_{300} and δ this implies that the mean level will again be biased downwards.

From the full results for the radar return (as illustrated in Figs 5.3 to 5.7) the magnitude of this error can be assessed by the displacement in time of the curves for non-zero λ_{300} and δ as compared to that for $\lambda_{300} = \delta = 0$, in the region of t=0. It can be seen that this error is of the order of one nanosecond, which corresponds to an order 15 cm error in the mean level estimate. This is a significant error for many applications.

Another source of instrumental bias might be the method used to determine the half-power point of the return. The Seasat altimeter suffered from such a bias (see Lipa & Barrick, 1981). This can be eliminated by correctly determining the half-power point. Better still, however, is the elimination of these instrumental biases by

fitting the theoretical non-Gaussian return (given in section 5.1.2) to the actual return. In contrast, the bias due to the fact that the altimeter senses the mean level of points of zero slope rather than the actual mean sea level can only be corrected once this fit has been performed and the parameters μ_{200} and δ estimated.

The above shows how it is possible to correct for sea state bias in the mean sea level estimate and this should make available better data for other applications such as surface current determination.

5.1.4 Wave period from skewness

It has been suggested (Huang & Long 1980; Huang, et al. 1981; Walsh 1979) that there may be a single relationship between sea surface skewness and significant slope (defined as the standard deviation of the sea surface elevation divided by the wavelength of waves at the spectral peak). Using such a relationship it should be possible, from altimeter measurements of significant wave height and skewness, to obtain the wavelength of waves at the spectral peak. The application of the dispersion relationship would then allow the corresponding wave period to be estimated.

For such an approach to work it is necessary to know the form of the relationship between skewness and significant slope. Phillips (1961) originally suggested that skewness is proportional to the slope of the waves on theoretical grounds. More recently Huang & Long (1980), on the basis of laboratory measurements and field data, have suggested the following empirical relationship

$$\lambda_{300} = 8\pi s'$$

where λ_{300} is the skewness and the significant slope s′ is given by

$$s' = \mu_{200}^{1/2}/L$$

where μ_{200} is the variance of the sea surface elevation and L the wavelength of waves at the spectral peak. Here this relationship will be investigated using the theory of Longuet-Higgins (1963).

From Longuet-Higgins (1963) it can be shown that

$$\lambda_{300} = \mu_{300}/\mu_{200}^{3/2}$$

and that

$$\mu_{300} = 6\int_0^\infty \left[\int_0^{\omega'} k\, S(\omega)\, d\omega\right] S(\omega')\, d\omega'$$

and

$$\mu_{200} = \int_0^\infty S(\omega)\, d\omega$$

where

$$k = \omega^2/g$$

Here the wave number k and the frequency ω are related through the dispersion relationship. An algebraic error in the theory has been corrected (see Srokosz, 1984a, for details), the results are valid for a uni-directional sea with frequency spectrum $S(\omega)$.

For a given spectrum it is now possible to use the equations to derive the relationship between skewness and significant slope. Consider a generalised Pierson-Moskowitz spectrum

$$S(\omega) = \alpha\, \omega^{-n} \exp\left\{-\left(\beta/\omega\right)^m\right\}$$

where α and β are constants with

$$\beta^m = \frac{n}{m}\,\omega_0^m$$

so that $\omega = \omega_0$ is the spectral peak. For m = 4, n = 5 we obtain the Pierson-Moskowitz spectrum. Substituting into the above equations gives, after some algebra (Srokosz, 1984a), the following relationship between skewness and significant slope

$$\lambda_{300} = 3\pi s' \left[\left(\frac{n}{m}\right)^{2/m} \left(\frac{\pi}{2}\right)^{1/2} \frac{1}{\Gamma^2\left(\frac{n-1}{m}\right)} \right.$$
$$\left. {}_2F_1\left(1, \frac{2(n-2)}{m}, 1+\frac{(n-1)}{m}; \frac{1}{2}\right) \right]$$

where $\Gamma(.)$ is the Gamma function and ${}_2F_1(.)$ a generalised hypergeometric function. For this result to hold we require m>3 and n>4 for convergence of the integrals. It can be seen that skewness is proportional to significant slope but the "constant" of proportionality depends on the assumed spectral form through m and n. Table 5.1 gives results for the ratio $\lambda_{300}/\pi s'$ for various values of m and n, including those for the Pierson-Moskowitz spectrum (m=4, n=5).

Table 5.1 Values of $\lambda_{300}/\pi s'$.

n\m	4	5	6	7
4	3.66	2.16	1.40	0.98
5	6.96	4.33	2.88	2.03
6	10.28	6.95	4.81	3.45
7	12.67	9.51	6.97	5.17

It can be seen that the constant of proportionality varies greatly depending on the spectral shape. In order to see if the variations

in the relationship between skewness and significant slope may be explained in a simple manner in terms of the bandwidth of the spectrum, we have also calculated values of the bandwidth parameter ν given by

$$\nu^2 = \frac{m_0 m_2}{m_1^2} - 1$$

where

$$m_r = \int_0^\infty \omega^r S(\omega)\, d\omega.$$

are the spectral moments. For the generalised Pierson-Moskowitz spectrum

$$\nu^2 = \frac{\Gamma\left(\frac{n-3}{m}\right)\Gamma\left(\frac{n-1}{m}\right)}{\Gamma^2\left(\frac{n-2}{m}\right)} - 1.$$

Values of ν obtained from this result are given in Table 5.2.

Table 5.2 Values of ν.

n \ m	4	5	6	7
4	0.64	0.62	0.61	0.60
5	0.42	0.41	0.39	0.39
6	0.33	0.31	0.30	0.29
7	0.28	0.26	0.25	0.24

By comparing results for $\lambda_{300}/\pi s'$ and ν it can be seen that there is no systematic dependence of the ratio $\lambda_{300}/\pi s'$ on the bandwidth parameter ν. From the above, it can be concluded that no single relationship, such as that of Huang & Long (1980), is adequate to describe all the dependence of skewness on significant slope in all sea states. In order to obtain wavelength or period information from

altimeter skewness measurements it is necessary to have some spectral information. This, if available, would obviate the need to use skewness measurements to obtain wave period.

5.1.5 Verification and Calibration

It is reasonably easy to verify and calibrate satellite measurements of significant waveheight and wind speed, since these parameters are routinely observed at sea. The variables discussed in this section, skewness and the wave period T_A, present different problems. For the reason given in Srokosz (1984a), surface following buoys are not able to measure the skewness of the sea surface correctly. Other instruments should be able to measure this parameter. However, all such instruments have their own drawbacks, for instance pressure recorders suffer from problems of attenuation and wave staffs have to be fixed to a structure which may interfere with the wavefield. Considerably worse problems occur with the period parameter T_A. As shown above this depends upon the fourth moment of the frequency spectrum of surface elevation, m_4, a parameter that it has proved impossible to measure with conventional instruments, due to their high frequency cut-offs. The implication of this is that calibration and verification of T_A can only be done by using other remote sensing techniques, such as stereophotography or sun glitter.

5.1.6 Applications

In this section it has been shown how more information can be obtained from the altimeter radar return than has been done routinely for previous altimeter missions (GEOS-3 and Seasat). The use of this information can give further insight into the physics of the oceans. One example of this would be to map globally, for some suitable time period, both the significant waveheight and the skewness and to compare the maps. It might be expected that wave nonlinearity would be more significant in areas of wave generation, and skewness is a measure of this nonlinearity. Therefore this comparison could allow the determination of those areas where active wave generation is occuring and where the sea is high and steep (large H_s and λ_{300}). Another example of the use of the data would be to compare the altimeter determined period T_A with in-situ measurements of T_z and hence obtain an estimate of the parameter ε (see section 5.1.1) which cannot be measured by standard techniques, but is important in the statistical theory of waves. Other applications of the altimeter data can be found but, as stated in section 5.1.5, all the applications depend on the verification and calibration of the wave parameters obtained from the radar return by in situ measurements. This should be a priority if full use is to be made of the altimeter data.

5.2 Wave parameters for real-time.

At present the only wave parameter it is proposed to produce in real time is significant waveheight. This will be calculated on board the satellite using the SMLE algorithm. This algorithm has already been described in section 4.3. However there are two other wave parameters that could be produced in real, or near-real time. These are the wave period (T_A), described in 5.1, and minimum swell height, described in 3.1.3. Both of these rely upon the σ° value.

Minimum swell has been calculated from Seasat data, Hognard et al. (1983), although not in real-time. As outlined in section 3.1.3 this depends critically upon the measurement of wind speed, via a fourth power. The wind speeds from the Seasat altimeter are an underestimate for high velocities, so the minimum amount of swell present in such conditions is seriously overestimated. It is by no means certain that the wind speed algorithm for ERS-1 will avoid this problem. Until the wind speed algorithms have been thoroughly calibrated and verified it would be unwise to issue minimum swell data in real-time. Regions of low wind speed where swell dominates might be depicted, but these would be immediately evident from the wind speed and waveheight products.

T_A involves a different set of problems. This is a new altimeter parameter and, furthermore, it is not a period normally used. Customers for real-time data would probably have little use for it since their applications would be expressed in terms of T_z. However, it may prove possible to connect T_A and T_z (see section 5.1); in which case a useful estimate of T_z might be disseminated in

real time. Preliminary results using JASIN data imply that $T_z \sim 1.8T_A$. It should be noted that T_A and T_z are measuring different properties of the wave spectrum and are not even approximately equal.

5.3 Wave parameters for research

Because of the extra computing power available on the ground it is possible to produce more wave parameters for research purposes than in real-time from on-board algorithms. In addition to this, data which is not produced in real-time can be issued if necessary with caveats; for example, in the case of minimum swell calculated from high wind speeds. The title of this section 'Wave parameters for research' is somewhat misleading since in addition to research many applications do not require data in real-time. At first sight it appears that more time will be available to do the computations on the ground; however, if the rate of data acquisition is greater than the rate of processing a backlog of unanalysed data will build up causing unacceptable delays in distributing the data. It is particularly important that data collected during the commissioning phase are processed promptly, if calibration and validation are to be carried out rapidly.

There are a number of parameters that can, and should, be available routinely; whether these should be calculated routinely or on request is a different matter. The wave parameter that must be available is, of course, H_s. The other variables that could be provided can be divided into two classes: those that can be calculated from other parameters that would be present at Level 2 and non-linear parameters that have to be calculated from waveform data.

Taking the non-linear parameters first. These consist of the sea surface skewness, λ_{300}, and the cross-skewness parameter, δ. These have been described in section 5.1. Potentially they are very useful, in particular for calculating sea state bias for ocean topography studies. However, these parameters have never both been derived from an altimeter signal and it is not known whether the ERS-1 altimeter is capable of measuring them. (Lipa & Barrick, 1981, have derived λ_{300} from Seasat data.) If it can be shown that both these variables can be derived then they should be included in the list of parameters provided.

The other two variables which can be specified at present are minimum swell and the wave period T_A. These can both be calculated from other altimeter products, minimum swell from H_s and wind speed and T_A from 0°. This means that it is not as vital for these to be available routinely. However, it may be useful. T_A is a new parameter and as such needs to be investigated further. The outcome of such investigations will obviously influence its inclusion or not. Minimum swell on the other hand has been calculated from Seasat data (a review is given in 3.1.3). The algorithm used to derive the minimum swell depends upon wind speed to the fourth power, this means that its accuracy is critically dependent upon the accuracy of the wind speed. The wind speed algorithm for the Seasat altimeter seriously underestimates high wind speeds. Unless this can be corrected for ERS-1 then either minimum swell should not be included in the routinely derived products or the values should be flagged in some way.

The above discussion has, of necessity, only concerned those wave parameters that it is known can be derived from the radar altimeter, at least in theory. This does not mean that other possible wave parameters cannot be obtained; the skewness and period parameters described earlier in this chapter, for instance, have been derived only in the last year. For this reason in any plans concerning non-real time wave parameters allowance must be made for extra variables.

5.4 Summary

A relationship between $\sigma^{o}(0^{o})$ and m_4, the fourth spectral moment of the sea surface, has been derived assuming Gaussian statistics which allows estimates of a new period parameter T_A to be obtained from radar altimeter data using on-board parameters. T_A can be interpreted as the geometric mean of the more familiar zero up-crossing and crest periods.

A non-Gaussian model has been used to obtain the form of the radar return from a non-linear sea surface. The theory shows that, in principle, the waveform data can be analysed to yield (in addition to H_s) the skewness of the sea surface (λ_{300}) and a skewness coefficient (δ) of unknown physical significance. Global maps of T_A and skewness do not exist but would be very useful , for example in identifying areas of wave generation.

These results have also been applied to the problem of determining sea-state bias. The 'physical' bias (due to the non-Gaussian distribution of specular points) is proportional to ($\delta.H_s$).

An additional 'instrument' bias, arising from the method used to track the mean level is found to be a function of both λ_{300} and δ. By fitting the theoretical return to the actual return a more precise correction for sea-state bias can be made. It is further concluded that a unique relation between skewness and significant wave slope does not exist, as suggested by some researchers, and that therefore wavelength or wave period cannot be obtained from skewness measurements alone.

It is not known whether these new parameters can be extracted with sufficient accuracy from the ERS-1 altimeter and simulation studies are required. Moreover the estimates cannot be validated adequately using conventional instruments; stereophotography and analysis of sun-glitter patterns are considered to be the most promising validation techniques available at present.

6. Estimation of wind speed for ERS-1

The review of techniques for extracting wind speed from GEOS-3 and Seasat (see section 3.2) has revealed a number of areas on which attention must be focussed if it is to be demonstrated that ERS-1 wind speeds meet the specification of ± 2 ms^{-1} for $0 < U < 24$ ms^{-1}. These are:

(i) the absolute accuracy of σ^o determinations

(ii) the need for an improved understanding of mean square slope of the sea surface as a function of wind speed

(iii) the variability of winds at sea

(iv) calibration/validation of the altimeter winds and establishing their consistency with the scatterometer.

Subsequent sections cover these topics followed by a discussion of fast delivery winds.

6.1 Accuracy of σ^o

The 1.6 dB difference between GEOS-3 and Seasat (3.2.3.2) is a disturbing and hitherto unexplained feature of satellite altimeter measurements over the sea, particularly when compared with the precision that is required for ERS-1. It implies difficulties in applying an algorithm developed for one satellite altimeter to another instrument. If such differences are constant then simple correction schemes can be devised before processing the winds. However, the comparisons with Seasat (3.2.4) suggest that either the σ^o bias of 1.6 dB changed for winds exceeding 10 ms^{-1} or that the

relationship between σ^o and wind speed differed in some way for the two satellites. Fig. 6.1 shows the variation of σ^o with wind speed according to the Brown et al. (1981) algorithm. The effects of a 1 dB uncertainty in measured σ^o is also shown, the two spikes at 10.1 and 10.9 dB being caused by changes in the σ^o - wind speed slope due to the use of three values for the coefficients a,b and is not really a problem. Vertical lines indicate the 2 ms^{-1} specification. An important fact to notice is that the wind speed accuracy resulting from a 1 dB error is better than 2 ms^{-1} only for speeds less than 10 ms^{-1}. For higher speeds a small σ^o variation produces a large error in speed. A more stringent σ^o accuracy is therefore required at lower values of σ^o. For instance, an accuracy of 0.5 dB at 8 dB and 1 dB at 20 dB with a linear variation in between (as proposed for ERS-1), increases the upper limit at which specifications can be met to ~ 15 ms^{-1} (Fig. 6.2) In order to increase the limit to 24 ms^{-1} σ^o would be required to an accuracy of ~0.2 dB at 7 dB. Every effort should be made to ensure that ERS-1 σ^o measurements on ERS-1 are well-calibrated.

Two factors also likely to affect σ^o accuracy are :

(i) errors in determining the pointing angle,

(ii) atmospheric attenuation.

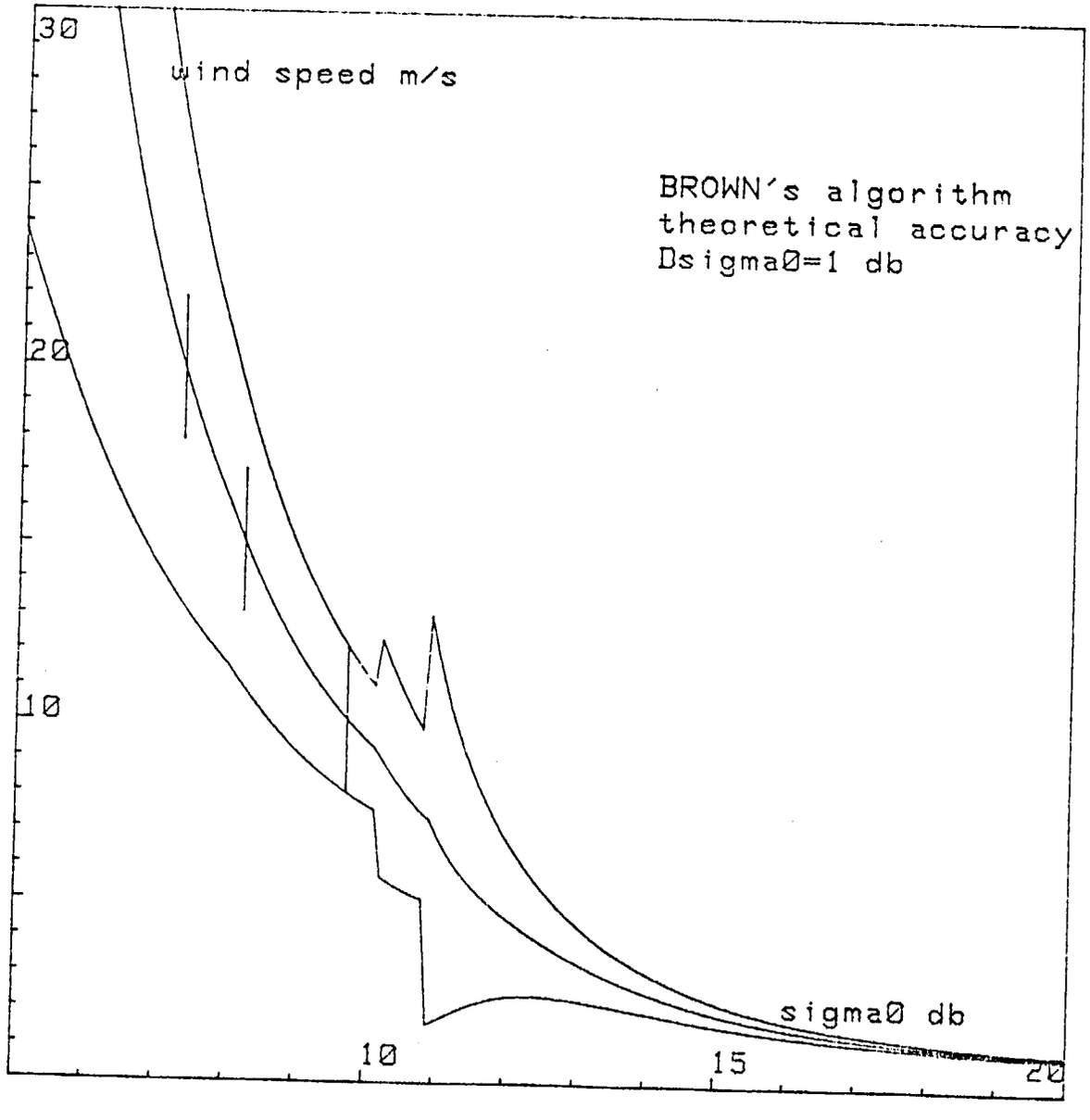

Fig. 6.1 Altimeter wind speed as a function of σ^{o}; 1 dB error shown.

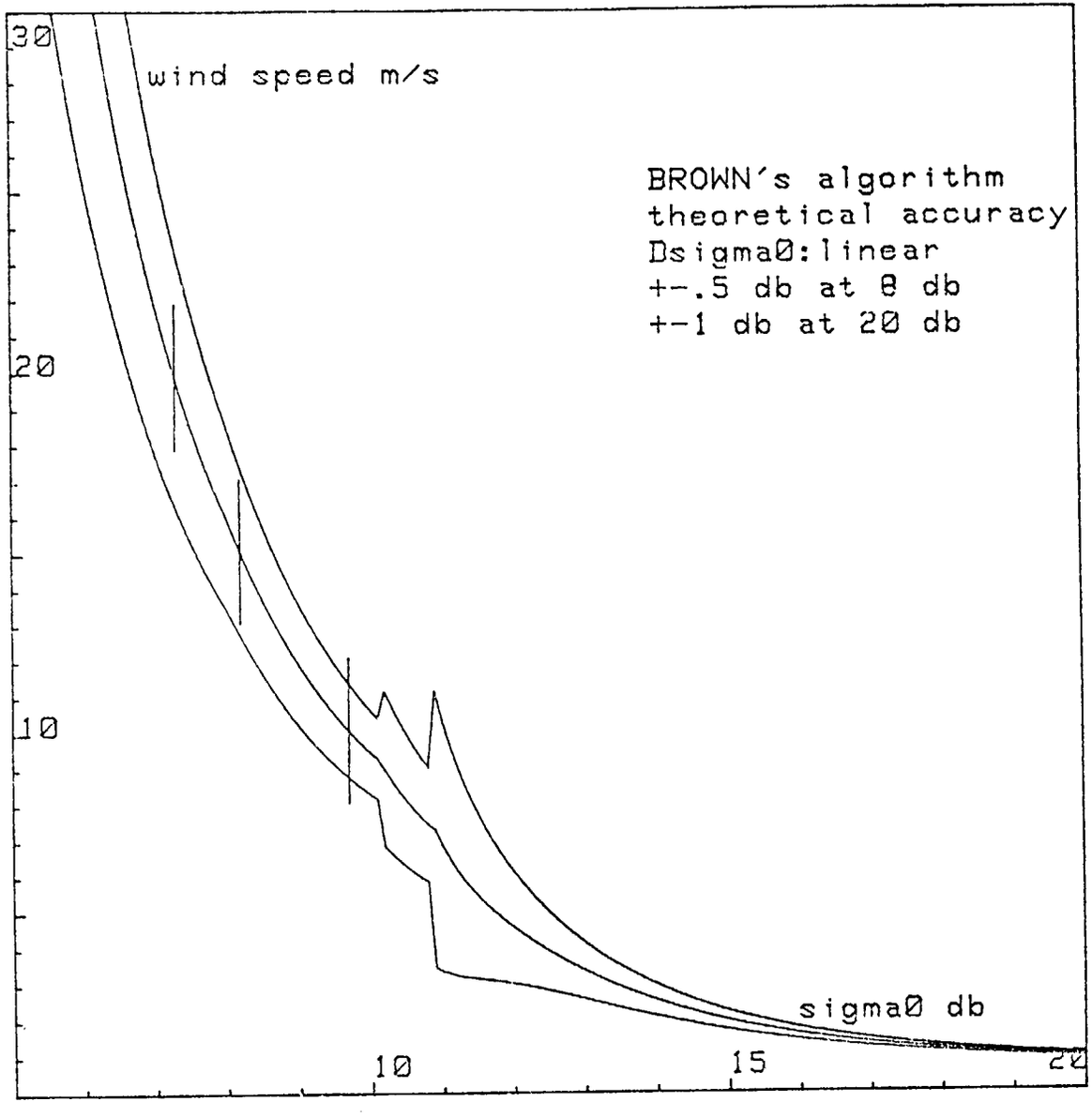

Fig. 6.2 Altimeter wind speed as a function of σ°; linear error shown.

6.1.1 Pointing angle

In deriving $\sigma^o(0^o)$ from AGC measurements account must be taken of the loss in antenna gain due to off-nadir pointing. This correction is sea-state dependent and for Seasat its possible magnitude could reach 6 dB. It is therefore important that the antenna pointing angle, ξ, be precisely measured. On Seasat, using data from the spacecraft attitude control system, ξ could be determined to no better than 0.2^o. For an indicated off-nadir pointing of 0.5^o this uncertainty translates into a σ^o error of +1.5 dB to -2.2 dB (Townsend, 1980) which is several times larger than the ERS-1 σ^o specification. Information from the trailing edge of the waveform can be used to improve the estimation of pointing angle (3.1.1.1). A similar situation will apply to ERS-1 where the pointing accuracy from the spacecraft system is expected to be 0.3^o (Dornier, 1983) but further work is required to quantify the consequences of pointing errors for ERS-1 and to investigate ways in which their effects can be minimised. In particular, steps should be taken to avoid the problems experienced by the attitude control system on Seasat where glint in the field of view of the attitude sensing device caused a change in the spacecraft orientation which on one occasion at least was sufficiently large to cause loss of altimeter lock for several minutes (Townsend, 1980). There were also occasions when the pointing angle derived afterwards from the return pulse shape was quite inconsistent with the spacecraft-derived values.

6.1.2 Atmospheric attenuation

Liquid water in the atmosphere can result in attenuation of a radar beam both on its path to the surface and on its return. Jones et al. (1982) reported that improved Seasat scatterometer winds could be obtained if an attenuation correction, based on SMMR vertically-polarized brightness temperatures at 37 and 18 GHz, was used. For light to moderate rain or high liquid water content the two-way attenuation correction could exceed 0.5 dB. On one pass, however,it appeared that anomalously high backscatter resulted when the SASS overflew a thunderstorm near the area of the JASIN experiment (Guymer et al.,1981). Seasat and ERS-1 altimeters operate at a similar frequency to the SASS so attenuation is likely to have roughly the same effect. However, no correction has been applied to the Seasat altimeter σ^o's, though the SMMR could supply this.

An example of the effect of rain on Seasat altimeter data is given in Fig. 6.3. A decrease in σ^o of over 1 dB can be seen. Monaldo et al. (1984) have investigated the effect of different cloud/rain conditions on the signal strength. For non-precipitating clouds the attenuation coefficient (normalized to cloud liquid water content) is approximately 0.17 (dB/km)/(gm^{-3}) at 13.5 GHz and for deep convective clouds this gives a two-way attenuation of ~0.7 dB/km. Such clouds are often a few kilometres deep.

For precipitating clouds with moderate rain rates of 10 mm/hr (a rate included in the specifications of ERS-1) the attenuation coefficient is 0.4 dB/km. Thus for a 5 km deep rain cell the two-way attenuation is 4.0 dB. Even in light rain (2 mm/hr) falling from a

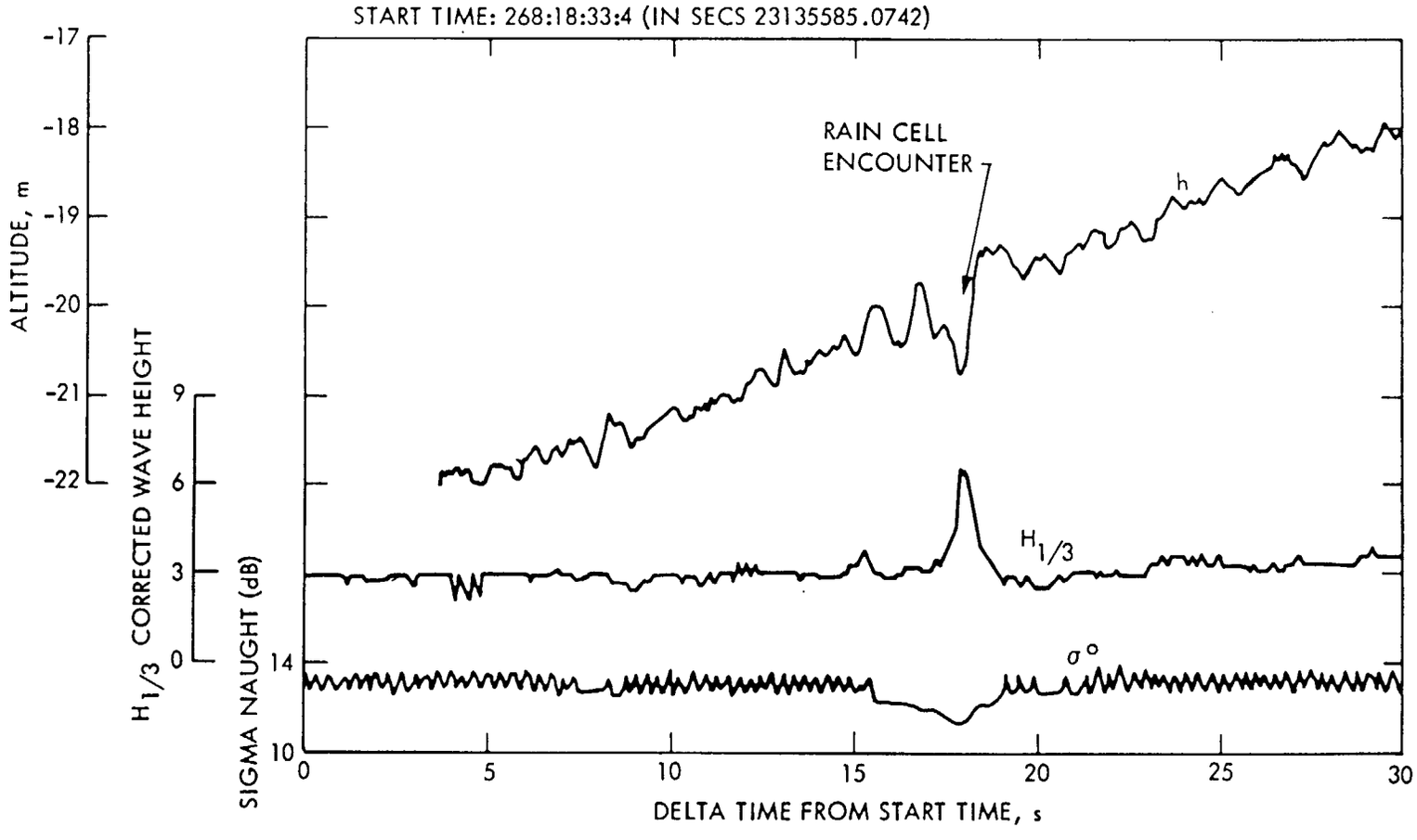

Response of Altimeter h, $H_{1/3}$ and σ^o to Rain Cell

Fig. 6.3 Response of Seasat h, Hs and σ^o to rain cell (from GOASEX Workshop report).

5 km thick layer the attenuation is 0.6 dB which is still significant when trying to retrieve moderate to high wind speeds.

The effect of attenuation therefore cannot be neglected for winds in the 10-24 ms^{-1} range where the algorithm is sensitive to errors in σ^o. ATSR/M estimates of total liquid water may provide the best means of correcting the data - the specification for this quantity is 10%. In moderate to heavy rain it will probably be impossible to correct the σ^o's and the data must then be flagged or edited out. A combination of the ATSR/M and the departure of the altimeter waveform from a standard ocean return could be used to generate this flag. Visible and infra-red imagery and ship reports may also prove useful in cases where ATSR/M values appear doubtful.

Attenuation effects may explain some of the spuriously high winds found in altimeter comparisons but a detailed study of Seasat winds in relation to SMMR liquid water and rain rate estimates is required to test the results of Monaldo et al. (1984).

Further details of the effects of atmospheric attenuation, their likely magnitudes in various conditions and possible correction schemes can be found in Appendix A.

6.2 Improved understanding of the relationship of mean square surface slope to wind

There are two basic criticisms that can be made of the method of deriving wind speed from radar altimeter measurements. The first concerns the assumption of isotropy for the sea surface made in deriving Eq. 3.7. The second is the fact that both empirical

relationships between wind speed and mean square slope are based on a single data set collected 30 years ago (Cox & Munk, 1954). (In fact Barrick (1974) also uses the same data to justify the assumption of isotropy.)

Cox and Munk's data consist of only 29 points which were taken under a limited range of wind and wave conditions. The wind speeds varied from 0-14.5 ms^{-1} (when corrected to a height of 19.5 m above the sea surface) and the values of H_s varied from 0-1.8 m. In addition to the limited range of conditions, the waves are not fully developed at any of the wind speeds. This may well have an effect on the relationship between wave slope and wind speed. At present we do not know . Generally, swell is present in the open ocean. This may modify the slopes to an extent and may be responsible for some of the scatter observed in comparisons with in-situ data.

For ERS-1 it is likely that an empirical algorithm similar to that developed for Seasat will be used. It is therefore very desirable that airborne campaigns should be conducted to extend the data base for the algorithm. Photographs of sun-glitter under a wide range of conditions should be obtained with coincident surface wind and wave measurements. Opportunity should also be taken to overfly the area with an airborne altimeter and preferably a combined altimeter/scatterometer of the type successfully flown by the Rutherford Appleton Laboratory during MIZEX (Powell et al., 1984). It is considered that the most valuable information on surface wave structure at very short wavelengths can be obtained from stereophotography. Though difficult and expensive, consideration

should be given to integrating such measurements into a pre-launch campaign. It would also be advantageous to carry a radiometer similar to the ATSR/M on the same aircraft as the altimeter/scatterometer so as to examine the effects of wind on ATSR/M retrievals as well as atmospheric attenuation effects on the active microwave systems. In this case radiosonde ascents should also be made. It is recommended that the usefulness and practicalities of such an experiment be assessed as a matter of urgency. A suitable location would be the Western Mediterranean during summer months when cloud conditions are favourable.

6.3 Variability of wind at sea

Part of the variance observed when comparing surface data with altimeter data may be explained by differences in spatial and temporal averaging and time and space variability. Some assumptions made by Brown et al. (1981) in determining the algorithm's constants may not be justified, e.g. surface data averaging time and altimeter averaging distance are not specified and the equivalence has to be verified. For instance, with Taylor's hypothesis, for a 15 ms^{-1} mean wind speed a 10 min averaging period is equivalent to a 9 km spatial averaging, which corresponds to ~1.5 s of altimeter data. The assumption of wind uniformity over 110 km also has to be substantiated and, in the same manner, stationarity over a 90 min period may not be justified as shown by the following two examples.

Fig. 6.4 is a wind speed record for 9 and 10 December 1982 from the Pennarc'h coastal watchtower in Brittany. Time increases from

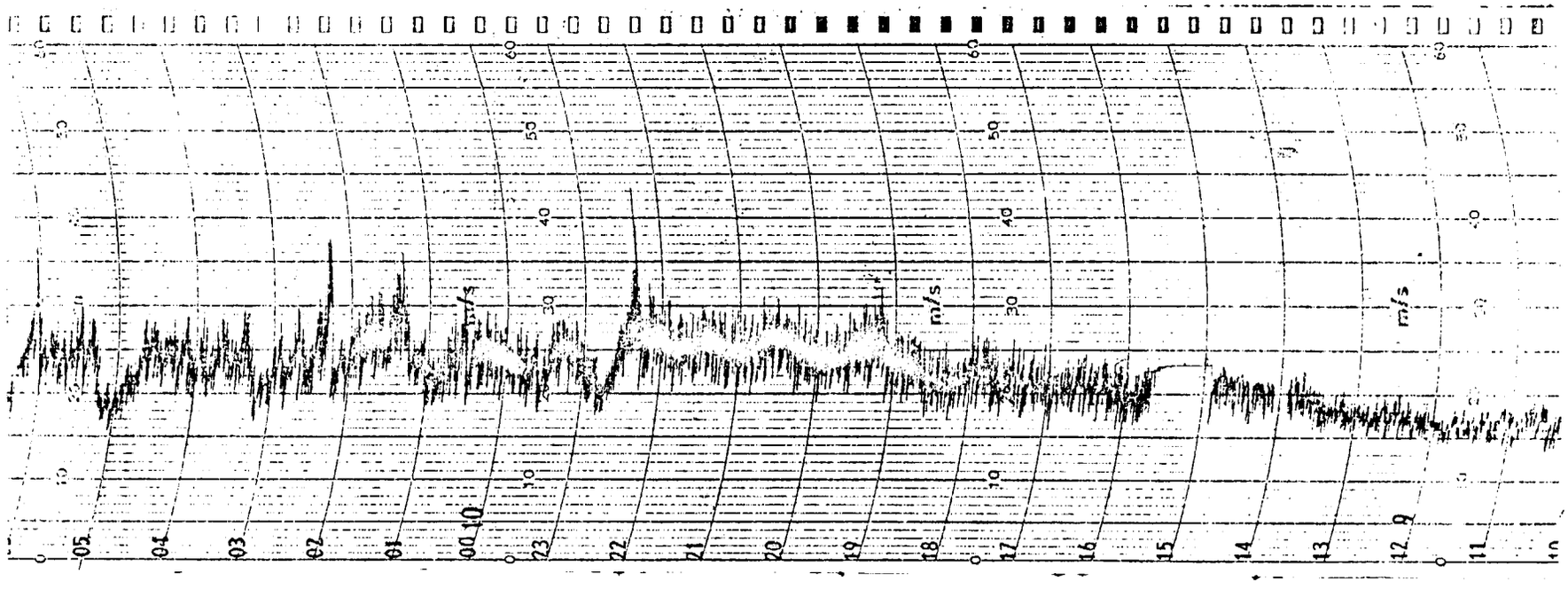

Fig. 6.4 Wind speed record on 9/10 December 1982 at the Penmarc'h coastal tower.

right to left and is indicated in hours at the bottom of the graph; the speed scale is 0 to 60 ms^{-1}. A change in wind conditions was observed on the 9th at 2230 corresponding to a cold front passage, the wind direction (not shown here) veering from SW to NW. Before this time (to the right) the 10 min structure appears relatively smooth but later the values fluctuate between 20 and 30 ms^{-1} with a period of about 1 hr. Fronts can easily be detected either through continuous measurements or using surface meteorological maps. Their influence can then be taken into account.

Fig. 6.5 is an example of wind data, obtained on board the CNEXO oceanographic ship "LE SUROIT", during the PROMESS (Penmarc'h Radar Oceanographic Microwave Experiment on Signature Studies) in February 1984. The sampling frequency of raw wind speed and direction data was 2 s^{-1}. The graph is a plot of the 1 min averaged wind vector for a period of 4 hr 33 min and clearly shows speed fluctuations having a period shorter than 1hr 30min. Note particularly, at the end of the record, the speed increase from 7 to 17 ms^{-1}, the time between the two vertical lines being 10 min.

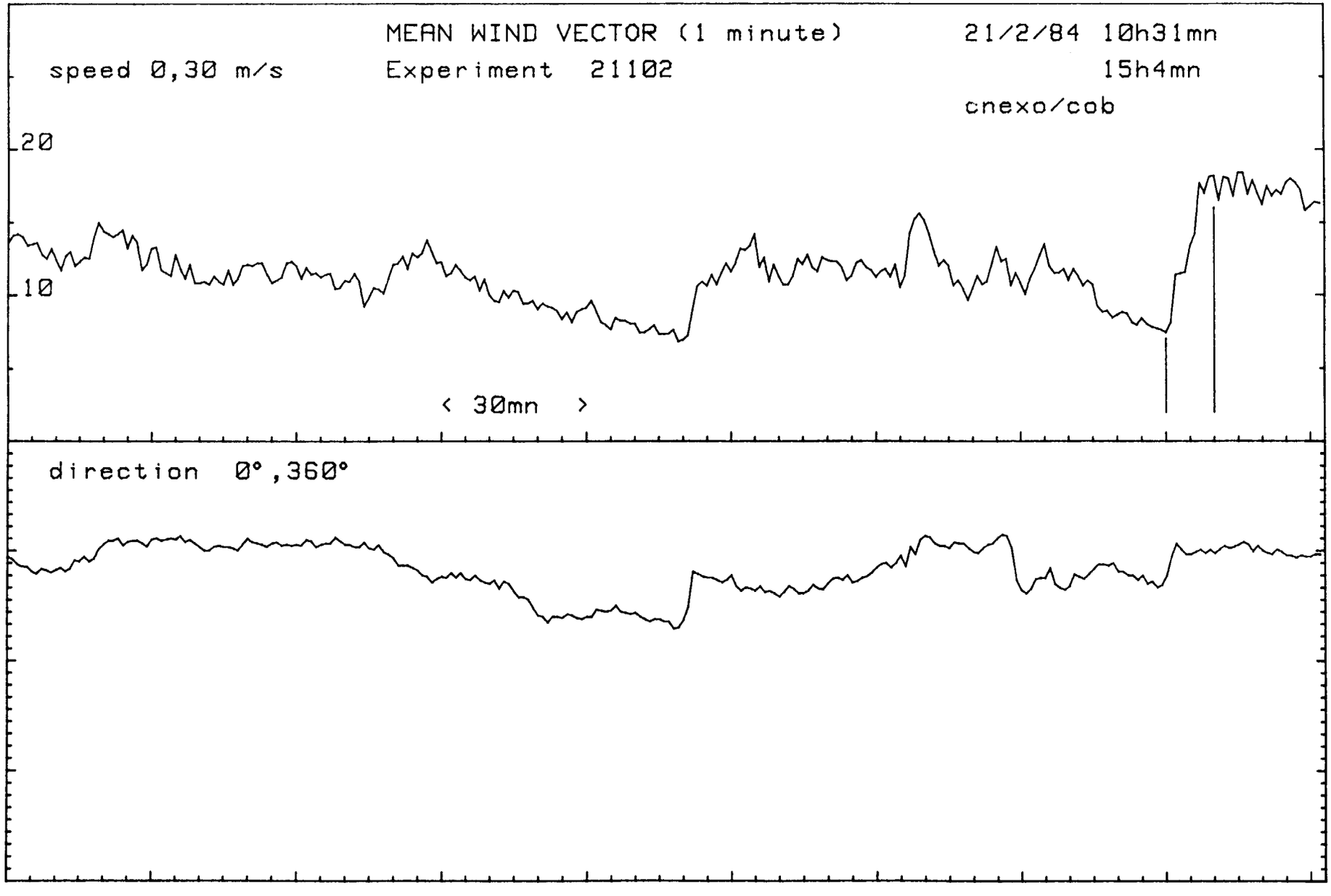

Fig. 6.5 Example of 1-minute speed and direction averages obtained from "LE SUROIT" during the PROMESS campaign.

6.4 Geophysical calibration and validation of the ERS-1 altimeter and scatterometer for sea-state and wind

6.4.1 Introduction

The goal of this section is to give an initial outline of desirable features that should be contained within the geophysical calibration and validation phase for ERS-1 altimeter and scatterometer measurements of wind. It is also relevant to include a discussion of sea-state.

Sea-state and wind calibrations/validations (C/V) of the two sensors should be achieved together (when possible) for the following reasons:

- o for the interpretation of sea-state or wind measurements both parameters must be taken into account e.g. detection of swell, growth stage of the sea)
- o the altimeter measures both waveheight and wind speed
- o the influence of sea-state on the scatterometer (modulation of short waves,effect of existing swell) is negelected in current algorithms but may need to be incorporated.

Surface-based instruments for measuring sea-state and wind may be used at a single location for both altimeter and scatterometer validations , but at different times, if the measurement site is correctly selected in relation to the overlap of ascending and descending swaths. An important point is that data sets used for validation must be independent of those used in calibrating the sensor.

6.4.2 Constraints

The aim of the C/V phase is to obtain accurate surface data covering as broad a range of the parameter under investigation as possible. This has to be carried out during the 6-month commissioning phase which commences shortly after launch. For the reasons given in 8.5 the C/V phase should be completed during the first half of the commissioning phase. So, during this time the satellite should be on a short repeat cycle (three days) in order to overfly the in-situ arrays as often as possible. During this time, the orbit will be arranged to give overpasses at the laser height calibration site(s) at which a monitoring of sea-state and wind will also be required (for sea-state bias).

A larger set of C/V data will be obtained if the surface sites are located in the vicinity of crossing points. Furthermore, at a crossing point, data from two tracks will be more independent if the two tracks are separated sufficiently in time (24 to 48 hr). Fig. 6.6, for instance, shows the ERS-1 ground tracks for a 3-day repeat cycle in the North Atlantic Ocean. The minimum time shifts between the two data sets are approximately 34 hr at point 1, 14 hr at point 2 and 10 hr at point 3.

The broad range of measurement (0-25 ms^{-1} for wind speed and 0-20 m for H_s) requires careful selection of surface sites, according to their climatology and to the satellite launch date.

In winter the north-east part of the Atlantic Ocean is a favourable site for experiencing a broad range of weather conditions. During the summer the northern part of this area would probably be

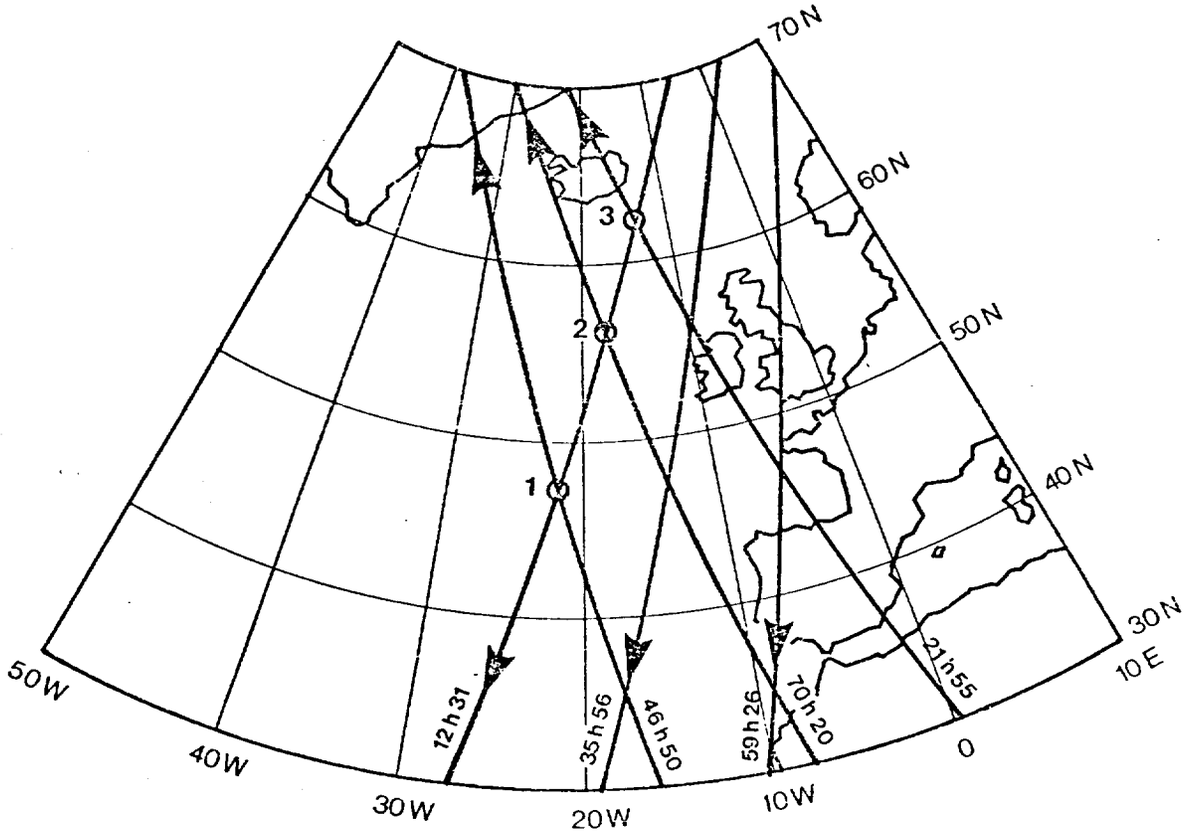

Fig. 6.6 ERS-1 N.E. Atlantic ground tracks for a 3-day repeat cycle.

satisfactory but the statistics need to be examined. A study using Seasat data is suggested. The 3-month data set, which was obtained in the northern hemisphere summer, might be analysed to evaluate the distributions of significant waveheight and wind speed encountered in these areas. GEOS-3 data could also be used.

Although we are concerned with wind and waves the effect of sea surface temperature should also be considered, particularly in the estimation of friction velocity or wind stress. Thus it is also a requirement that surface data are obtained under the satellite track at sites having differing values of sea surface temperature.

The C/V sites also have to be chosen according to the proximity of coasts. They must be sufficiently distant to avoid coastal effects (tidal currents, bottom topography) on the physical behaviour of the measured parameters and on the contamination of the sensor footprint by land or islands. Use of an offshore area makes it easier to model the behaviour of parameters, such as fetch and sea-state, if required. On the other hand the distance should not be unnecessarily large because of the increased costs and difficulties of deploying and maintaining a measurement network at sea and the need to be conveniently situated for aircraft sorties. The locations will therefore involve compromises between science and logistics.

6.4.3 Measured surface parameters

6.4.3.1 Sea-state

Sea-state is described by the spectrum of the free surface displacements from which significant waveheight is deduced. For the scatterometer the directional spectrum may be needed.

To be representative of a given sea-state surface measurements (at fixed locations) have to be taken for a 20 - 40 min period. For instance, a swell with a 10 s period travels 28 km in 30 min. The distance of 28 km is equivalent to about 4 s of altimeter data. Therefore measuring sea-state at the surface for 30 min is compatible with the size of the altimeter footprint and the satellite velocity.

However, Seasat altimeter data have shown that strong variations of H_s may occur over short distances(~60 km) (Queffeulou,1983) and it seems necessary to measure the wave parameters as close as possible to the track.

6.4.3.2 Wind

The size of the nominal scatterometer resolution cell is 50 km x 50 km and this raises the question of spatial and temporal fluctuations of winds at sea (6.3). Can the "synoptic" (in space) scatterometer measurement be compared with a surface measurement at a fixed point? What averaging time should be used? The answers will depend, in part, on the atmospheric stability conditions. For comparison with the satellite the surface measurement has to be expressed in terms of a neutral stability wind at a fixed height or,

better, the friction velocity u_*. This means that, in addition to wind speed and direction at one or more points in the resolution cell it will be necessary to estimate the stability conditions, preferably from in-situ measurements. It is therefore suggested that surface platforms for wind calibration/validation should include (at least) speed, direction, dry and wet air temperatures, surface pressure, sea surface temperature. Note that the stability correction for friction velocity increases with the measurement height; as a consequence near-surface buoy measurements do not necessarily need temperature measurements.

In order to investigate the influence of sea-state on scatterometer measurements the directional spectrum of waves will be needed from one measurement site at least.

In a similar way sea-state and stability conditions must be taken into account for the altimeter.

6.4.4 Outline of possible technique

For the selection of C/V sites we can take advantage of the crossing points. Three methods have been identified. The first consists of selecting an area in the vicinity of one particular crossing point. In the second, the crossing points are used systematically. The third method is an intermediate between the first two methods.

6.4.4.1 Use of a single crossing point

As an example Fig. 6.7 shows a descending pass (DA), an ascending one (AC) and the corresponding scatterometer swath on the right of track. The ten resolution cells, from 225 km to 500 km from the track, are represented. The greatest time difference between these two passes is about 30 hr for a 3-day repeat cycle.

The following plan may be envisaged:

- o at crossing point A a wave measuring device provides two validation data sets every three days
- o within B, the area defined by the overlap of ascending and descending scatterometer swaths, the use of 5 surface meteorological packages provides 10 data sets every three days (one for each of the ten incidence angles). This can be achieved by deploying the devices in the locations indicated either by the stars or the crosses in Fig 6.7. The configuration defined by the stars is more interesting for two reasons. First, the measurement points are separated from each other by a larger distance. Second, the orientation of the stars is roughly north-south and, in the North Atlantic, meteorological disturbances propagate in general from west to east, so a north-south distribution of measurement devices is more likely to cover a large range of values.
- o points C and D are of interest because one wave and wind measuring device provides a calibration point for both the altimeter and the scatterometer. The positions of these points along the tracks will have to be defined according to

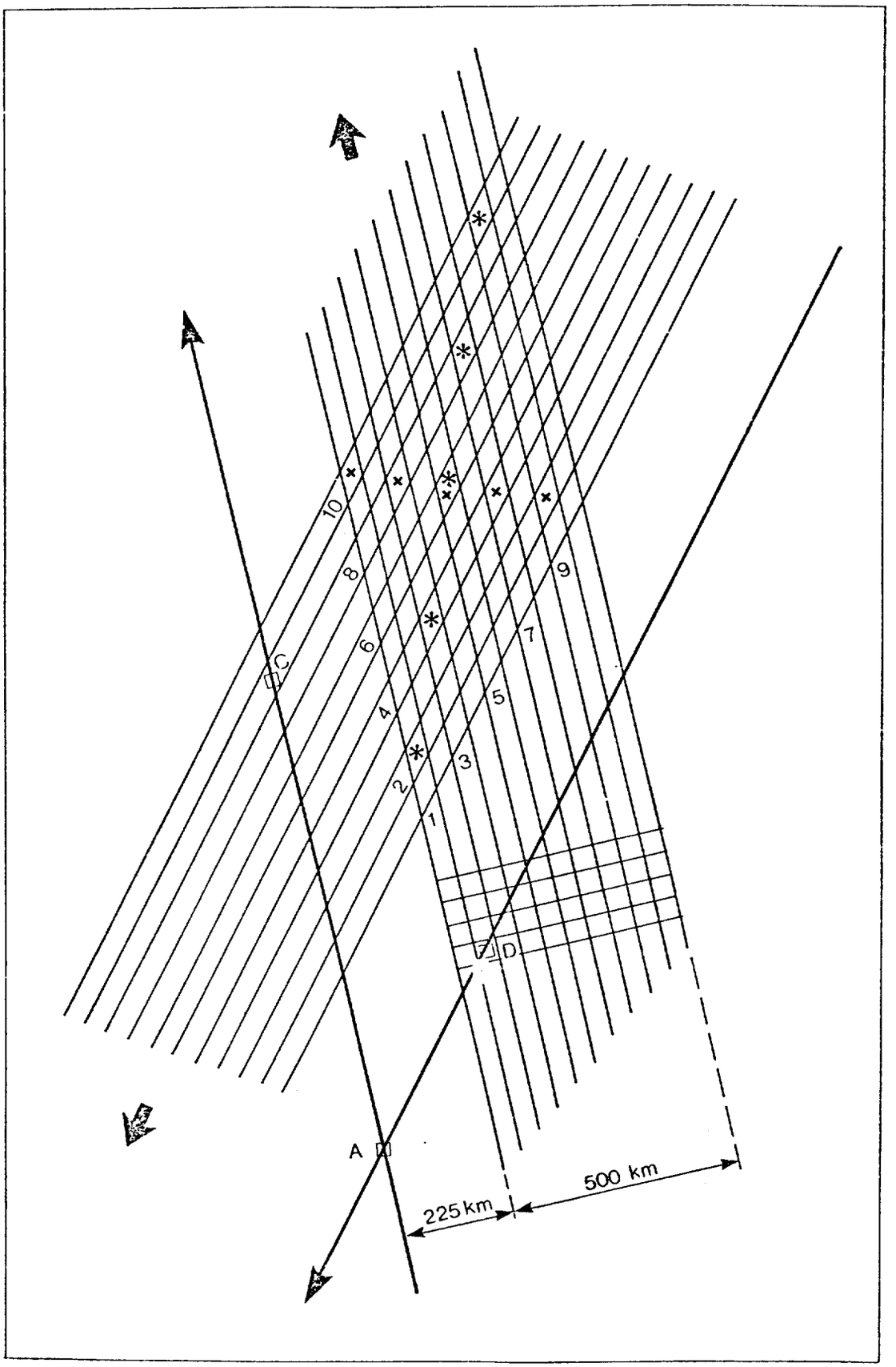

Fig. 6.7 Geographical distribution of sea-state and wind devices for altimeter and scatterometer calibration and validation (example 1).

the incidence angles to be investigated (extreme angles for example).

6.4.4.2 Use of all crossing points in an area

Fig. 6.8 shows the tracks (for a 3-day period) in the NE Atlantic Ocean and the crossing points, numbered from 1 to 6. The use of one sea-state and one wind device at each of these points for the three days provides:

- o 12 sea-state and altimeter wind data points
- o 10 wind scatterometer C/V data points, distributed as follows:

  5 on Day 2 from points 1,2,4,5 (Fig. 6.9)

  5 on Day 3 from points 1,3,5,6 (Fig. 6.10)

We note that there is no scatterometer data in this area on Day 1. Some advantages and disadvantages of this method are:

- o a larger data set
- o measurement points are far away from each other and therefore the data will be statistically more independent and a larger range of geophysical parameters will be obtained. The main difficulty lies in setting up and maintaining such a wide network.
- o for the scatterometer it needs to be ascertained whether this plan would give a uniform distribution of incidence angles.

This network may be reduced. For instance, using points 1,2,3 and 5 for 3 days the following are obtained:

- o 8 sea-state and altimeter wind speed data sets

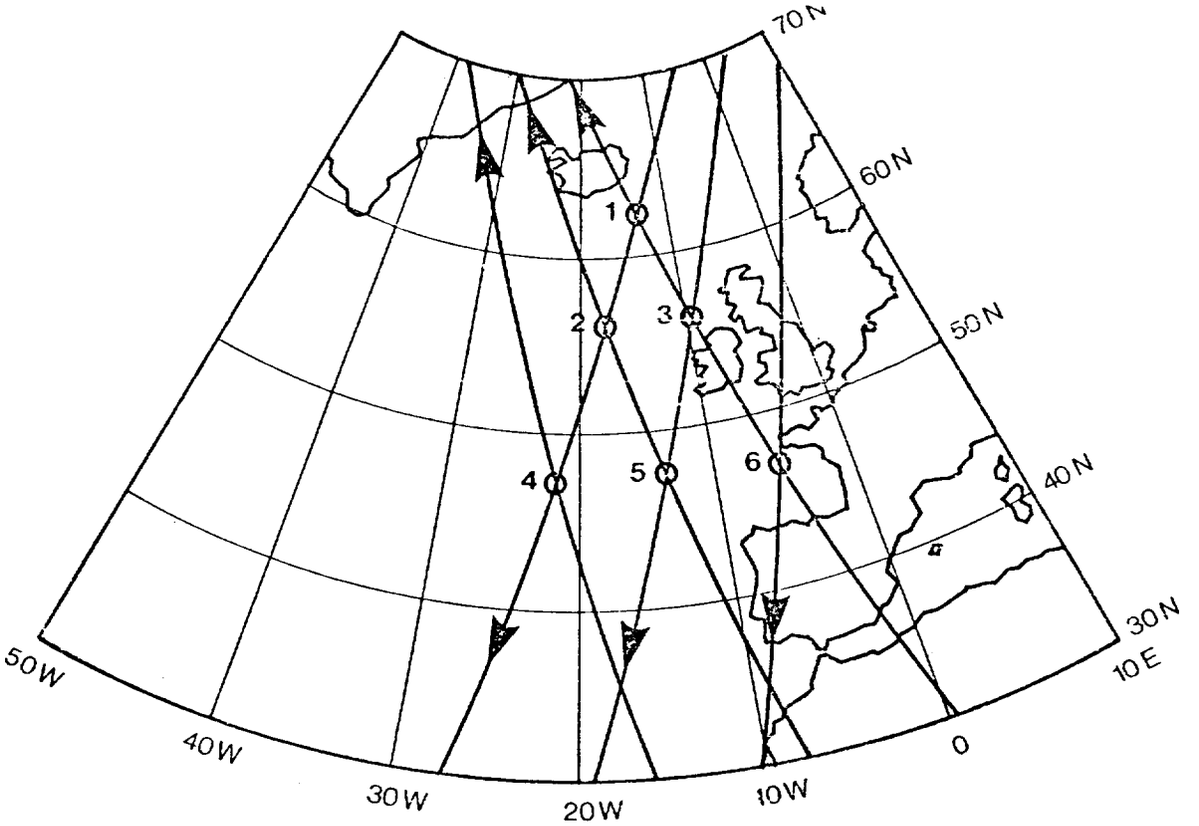

Fig. 6.8 Crossing points of ERS-1 ground tracks in N.E. Atlantic for a 3-day repeat cycle.

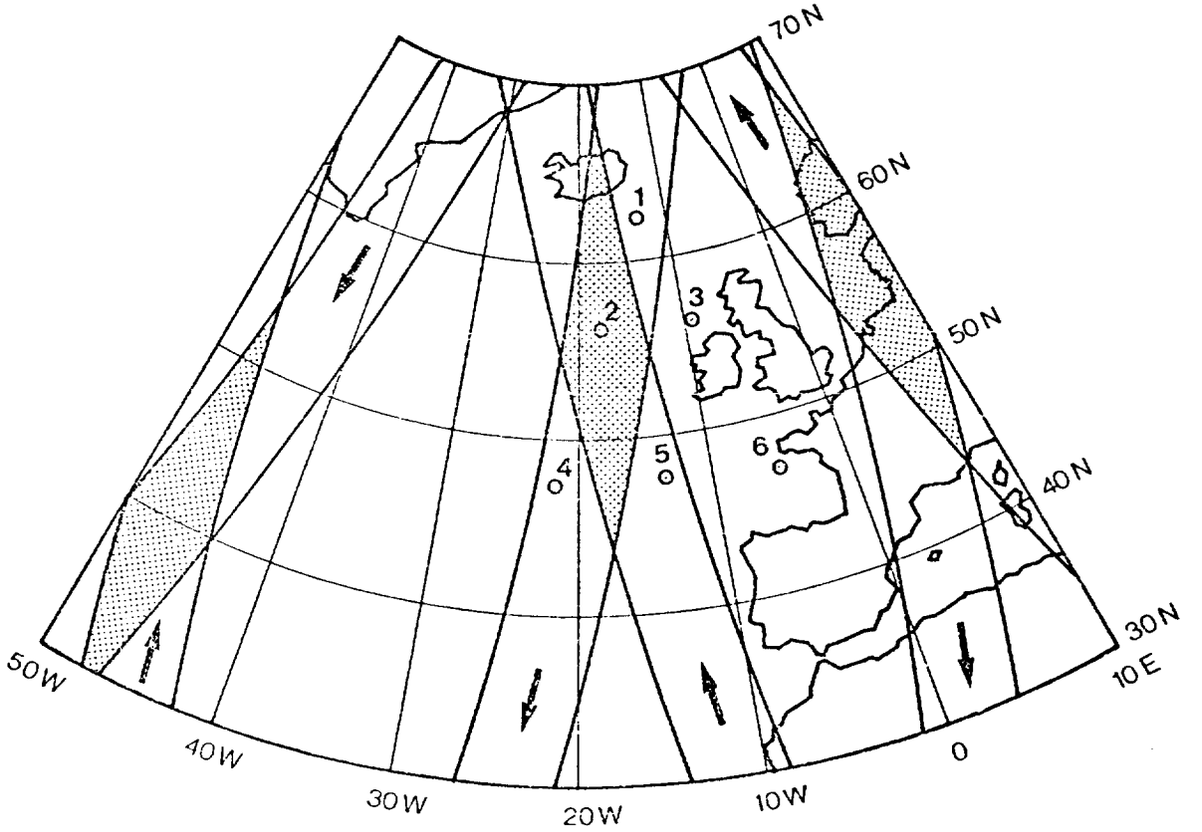

Fig. 6.9 Scatterometer swath for Day 2 (example 1).

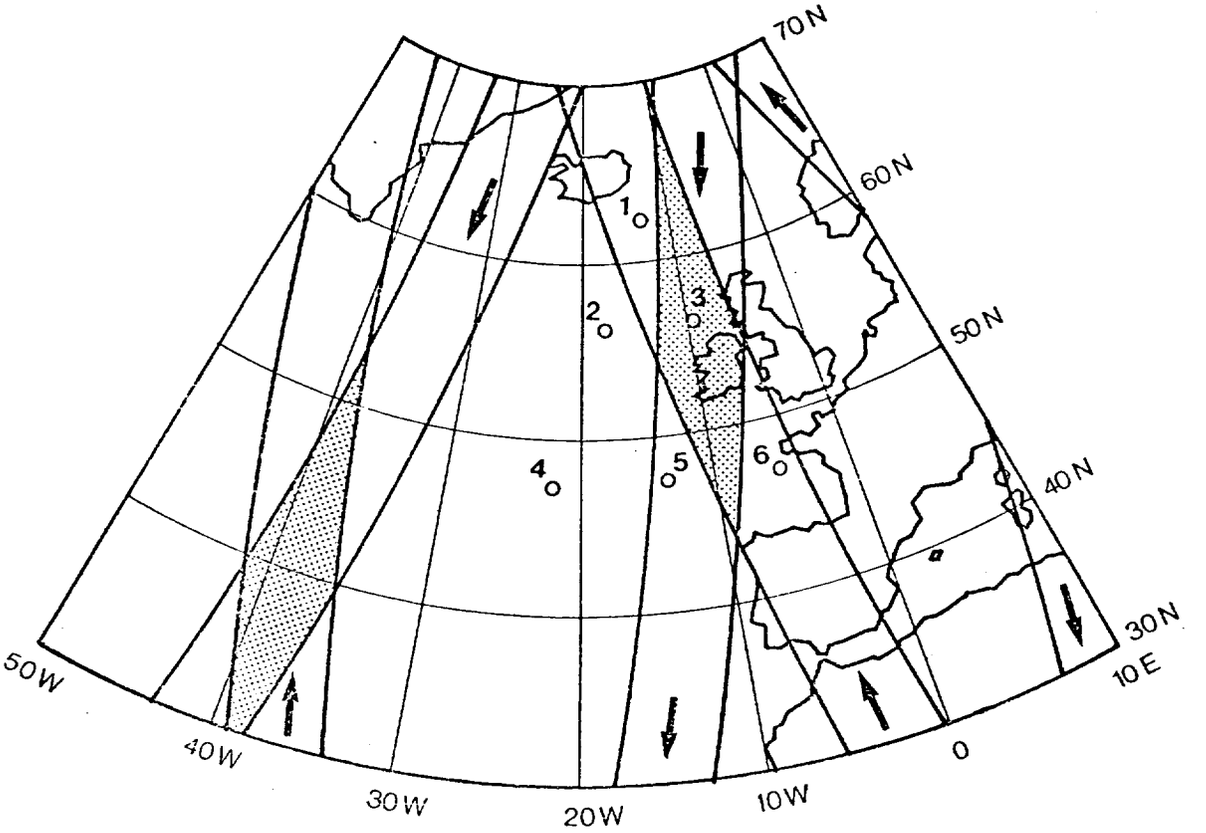

Fig. 6.10 Scatterometer swath for Day 3 (example 1).

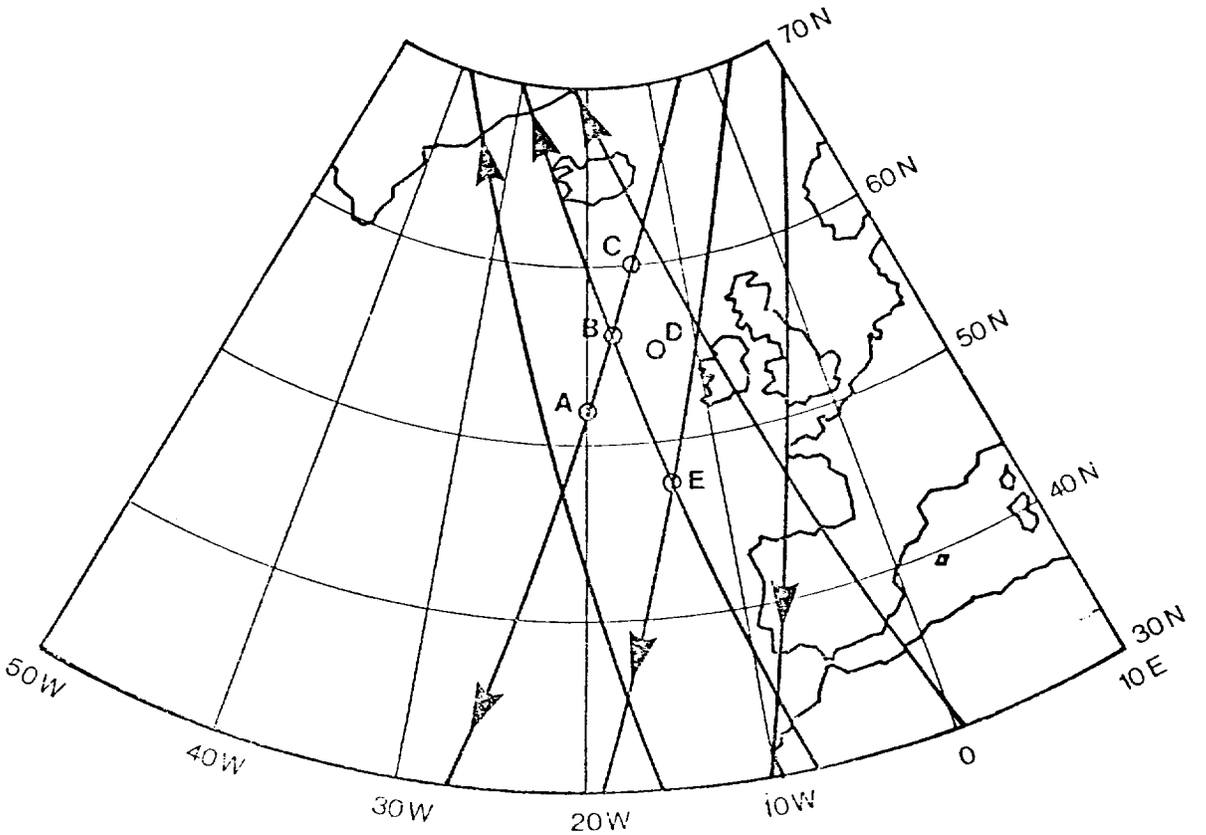

Fig. 6.11 Geographical distribution of surface instruments (example 2).

- o 8 wind scatterometer data sets.

6.4.4.3 Intermediate method

A configuration using both crossing points and overlapping areas may provide an interesting data set. As an example the 5 points of Fig. 6.11 give 3-day totals of:

- o 6 H_s and 6 altimeter wind data sets
- o 13 scatterometer data sets distributed as follows:

  9 points (two of which are at extreme incidence angles) for Day 2 (Fig. 6.12)

  4 points (three at extreme incidence angles) for Day 3 (Fig. 6.13).

Another configuration, like that of Fig. 6.14 would give:

- o 8 H_s and altimeter wind points
- o 11 scatterometer points (four of which are for extreme angles).

Table 6.1 summarizes the number of measurement devices and number of calibrations obtained for several examples using the three different methods.

The above is intended to provide only a possible framework for planning C/V activities. Further work is needed in the following areas:

- o identification of satellite and surface parameters to be calibrated and validated. This may include wave parameters other than H_s.
- o selection of ground measurement sites and time period

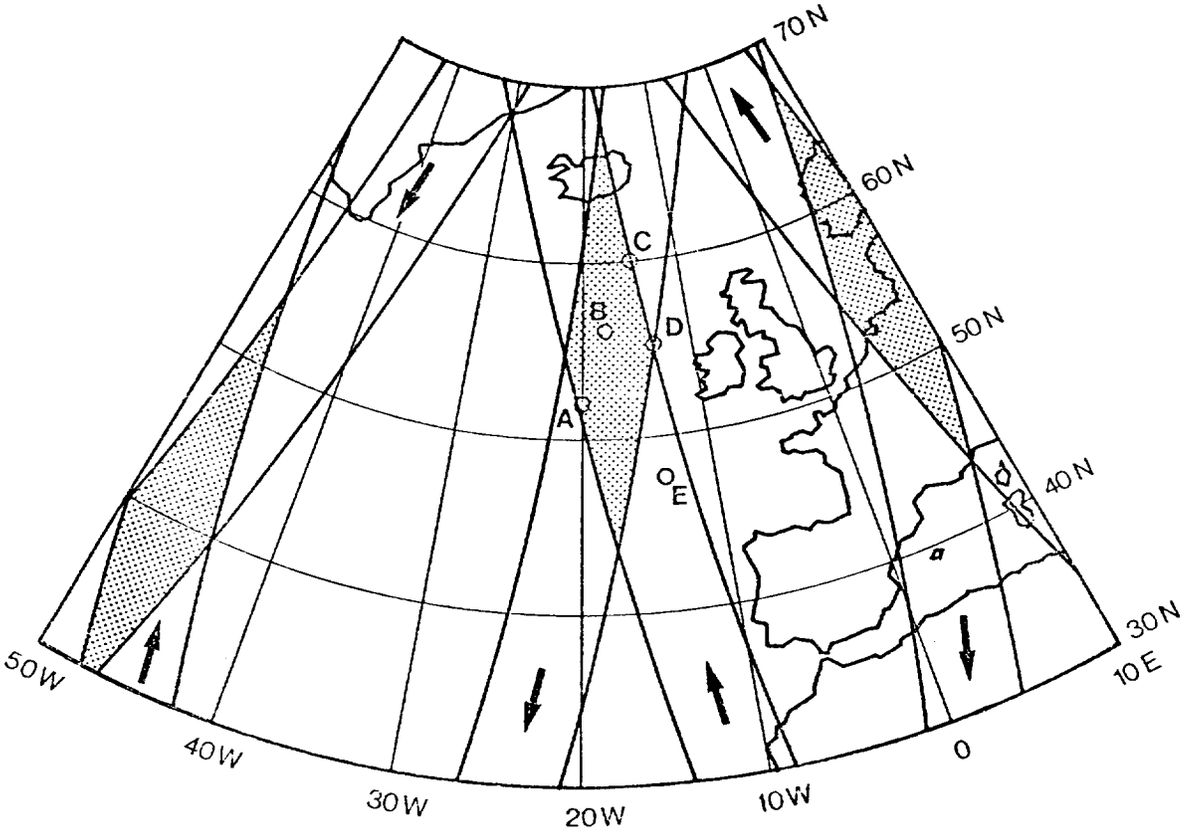

Fig. 6.12 Scatterometer swath for Day 2 (example 2).

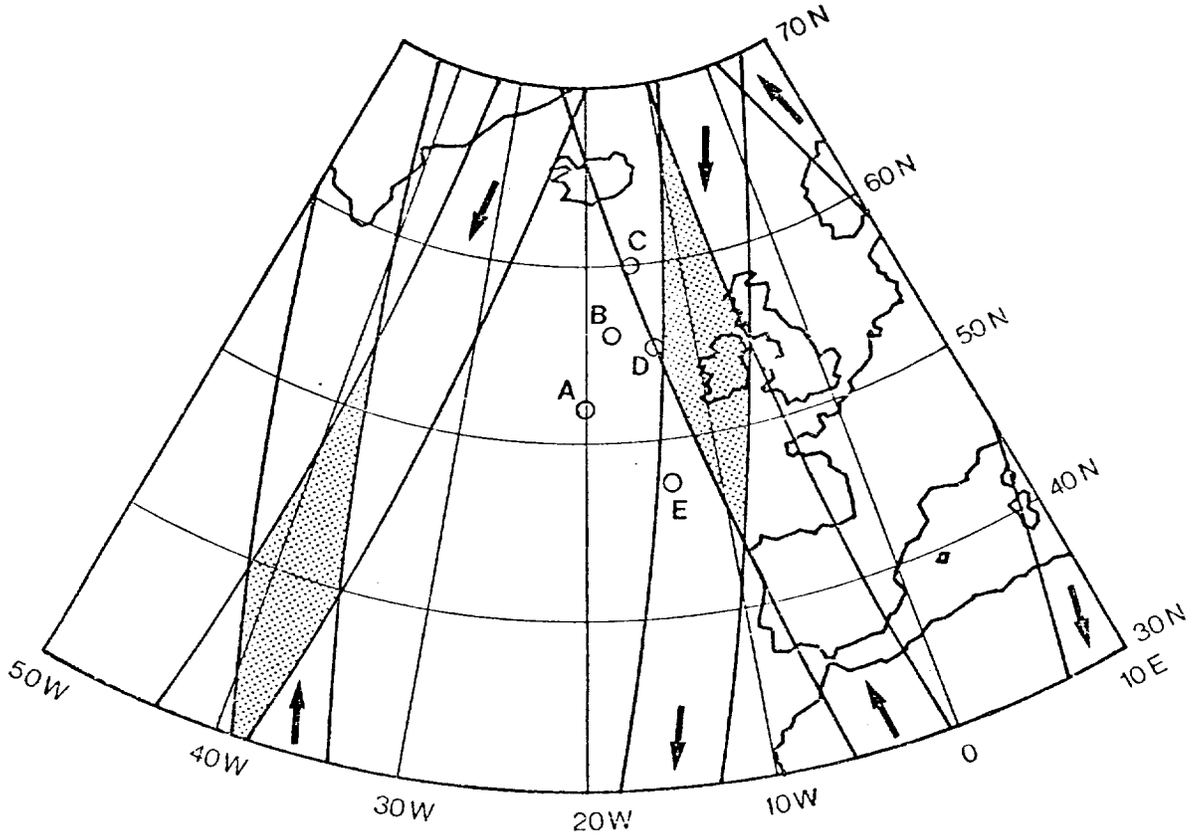

Fig. 6.13 Scatterometer swath for Day 3 (example 2).

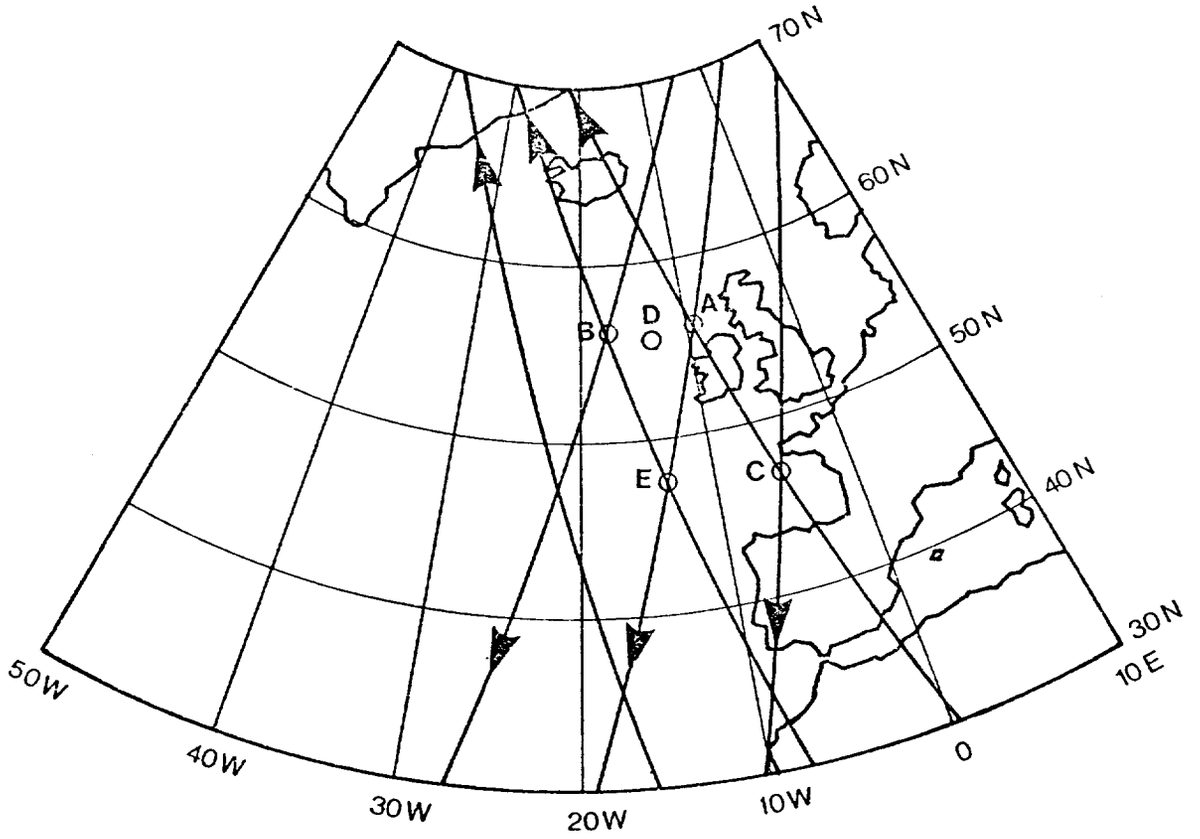

Fig. 6.14 Geographical distribution of surface instruments (example 3).

Table 6.1 Summary of number of different calibrations achieved using the three methods outlined in the text.

METHOD	NUMBER OF MEASUREMENT DEVICES		NUMBER OF COMPARISONS			
	SEASTATE	WIND	H_s	$U_{alt.}$	$U_{scatt.}$	
AREA AROUND ONE CROSSING POINT	3	7	4 40	4 40	12 120	(3 days) (1 month)
ONLY CROSSING POINTS 1 to 6 →	6	6	12 120	12 120	10 100	(3 days) (1 month)
1, 2, 3 and 5 →	4	4	8 80	8 80	8 80	(3 days) (1 month)
INTERMEDIATE METHOD ex : figure 6.11 →	5	5	6 60	6 60	13 130	(3 days)
figure 6.14 →	5	5	8 80	8 80	11 11	(3 days)

- o determination of the number and distribution of surface measurements
- o identification of surface sensors and supporting data required
- o study of relationships with C/V activities of other ERS-1 sensors (ATSR/M,SAR wave mode) and with other satellites (TOPEX,N-ROSS)
- o collection of surface data from campaigns not specifically set up for ERS-1 ,e.g. internationally-coordinated experiments within the WCRP
- o availability of satellite and surface calibration/validation data sets within the PAF and a strategy for processing (see also 8.7).

6.5 Implications for fast delivery winds

Present evidence indicates that it is unlikely that ERS-1 Radar Altimeter wind speeds can be retrieved in real-time to meet specification if the Seasat algorithm is used as it stands. This is particularly true of the upper half of the wind speed range, 12-24 ms^{-1} where the pointing angle and attenuation corrections discussed in 6.1.1 and 6.1.2 require substantial additional processing to achieve the desired accuracy. However, since much of the difference between Seasat and in-situ/SMMR data appears to be systematic it may be possible to construct an ERS-1 algorithm having a similar form but with coefficients specifically tuned to in-situ data obtained during the commissioning phase. These winds must also be validated during the initial phase before winds can be released

with confidence (see 6.4). Unlike Seasat there will be no overlap on ERS-1 with other wind sensors that could be used in algorithm development.

Despite the problems that have been discussed in this report the ERS-1 altimeter still maintains a considerable advantage over the wind scatterometer as far as wind speed determination is concerned in that similar altimeters have flown before. Indeed, it is precisely because of this that we have been able to criticize its performance. The scatterometer will be the first to give backscatter data at C-band from a spacecraft and, given the relatively poor data base of airborne measurements at this frequency is best regarded as a proof-of-concept rather than a pre-operational instrument whose performance is subject to considerable uncertainty.

7. Estimation of sea-ice parameters

7.1 Characteristics of return signal and implications

The operation of radar altimeters over flat, horizontal and statistically homogeneous surfaces, such as the open ocean, is well understood. Sea ice, which is typically rough and is not statistically homogeneous, represents a very different reflecting surface, resulting in significant effects on the operation of a pulse-limited radar altimeter such as will be flown on ERS-1. Sea ice return signals can be highly specular in nature if the roughness of the surface is small compared to the radio wavelength (about 2.2 cm for ERS-1). It is thought that this may occur where grease ice damps out wind-induced capillary waves on a normal ocean surface or where ice floes contain sufficiently flat surfaces. The surface thus acts as a mirror with radiation only very close to the nadir point (the first Fresnel zone) being reflected to the altimeter. The result is a strongly peaked return with a duration almost equal to that of the transmitted pulse.

The surface roughness of sea ice may be significantly different from that of the ocean. This may be due to the suppression of swell by floes with increasing distance inside the ice pack (see sections 3.4.3 and 7.3) and to irregular surfaces typically associated with multi-year ice. Scattering of the transmitted pulse occurs first from surface crests and later from the troughs; the leading edge of the return waveform thus becomes the integral of the

height distribution of point scatterers. In cases where the vertical distribution of roughness is neither symmetrical about the mean level nor uniform over the pulse-limited footprint, interpretation will be complex but the leading edge will contain statistical information on roughness.

Return pulses from sea ice may also demonstrate 'glistening' if horizontal facets of the rough surface are smooth over dimensions which are large compared to the radio wavelength. The pulse may contain as much power as the specular case to within a factor of $1/\sqrt{2}$ (Robin et al., 1983).

The combined effects of returns from specular, glistening and rough surfaces, as is characteristic of sea ice, will cause significant departures of pulse shapes from typical ocean returns. Specifically, signal strength will be significantly higher in terms of both magnitude and variability as the altimeter passes over areas of sea ice as opposed to open ocean. Work in progress on the peak amplitudes of Seasat pulses during a traverse across the pack of the eastern Weddell Sea shows increases of two orders of magnitude within 50 km of the ice edge. Robin et al. (1983) estimated that an increase of up to 5 orders of magnitude is possible. Inhomogeneity of the surface will result in very rapid changes in the rate of returned power (up to an order of magnitude between consecutive returned waveforms, that is 0.1s). This may be due to specular reflectors with very narrow polar diagrams passing through the range window footprint.

Pulse shape shows considerable variability but generally evolves from the standard ocean shape near the ice edge becoming increasingly peaked deeper into the pack. Rapley (1984a) has suggested that this results from a reduction in the magnitude of the angular distribution of surface slopes as ocean waves are attenuated by the ice.

Once within the ice pack the passage of strongly reflecting features through the footprint causes features to migrate from the rear of the echo waveform towards the leading edge and to subsequently recede as described in section 2.7. Similar effects are observed when passing on to the ice from regions of open water or vice versa.

Although sea ice pulses are typically strongly peaked, low-level leading edge distortions or 'precursor' features are often observed. As yet the possibility of these resulting, at least in part, from instrument effects has not been ruled out. Certainly some of the features observed can be attributed to large scale surface roughness and ridges. Occasional examples of increased power throughout the region of the range window prior to the pulse leading edge, are suggestive of passage over icebergs of height greater than the 14 m range window coverage.

The implications of these characteristics of sea ice returns have been discussed elsewhere in this report. They may be summarised as follows:-

(i) The strongly peaked and highly variable sea ice return waveforms introduce coupled errors into the on-board computed geophysical parameters, necessitating re-tracking of the

waveforms on the ground. Any automatic re-tracking algorithm must be sufficiently sophisticated to recognise the leading edge of the nadir return when strong off-axis returns are also present.

(ii) By noting the range, strength, shape and degree of variability of the retracked returns there is good reason to believe that a number of the ice parameters, identified in Table 2.9, may be deduced from the altimeter data. This prospect is discussed in more detail in subsequent sections.

7.2 Determination of the ice boundary

The conventional definition of the ice boundary is given variously as the contour within which the ice concentration exceeds either 10% or 15%. Either way, the presence of ice banding and the general variability of ice concentration values often make it difficult to define the boundary on a regional scale much more precisely than 10-15 km.

Detailed examination of Seasat waveforms in the vicinity of the summer ice edge in Baffin Bay and the winter ice edge in the Southern Ocean, reveals the presence of distortions of waveform shape attributable to the presence of ice some tens of kilometres before a major increase in the signal strength occurs (Fig. 7.1). This is consistent with the variations in GEOS-3 AGC and AASG, noted in section 3.4.1 to extend beyond the ice boundary determined from satellite optical and infrared imaging data.

We define a pulse 'peakiness' parameter (PP) such that:-

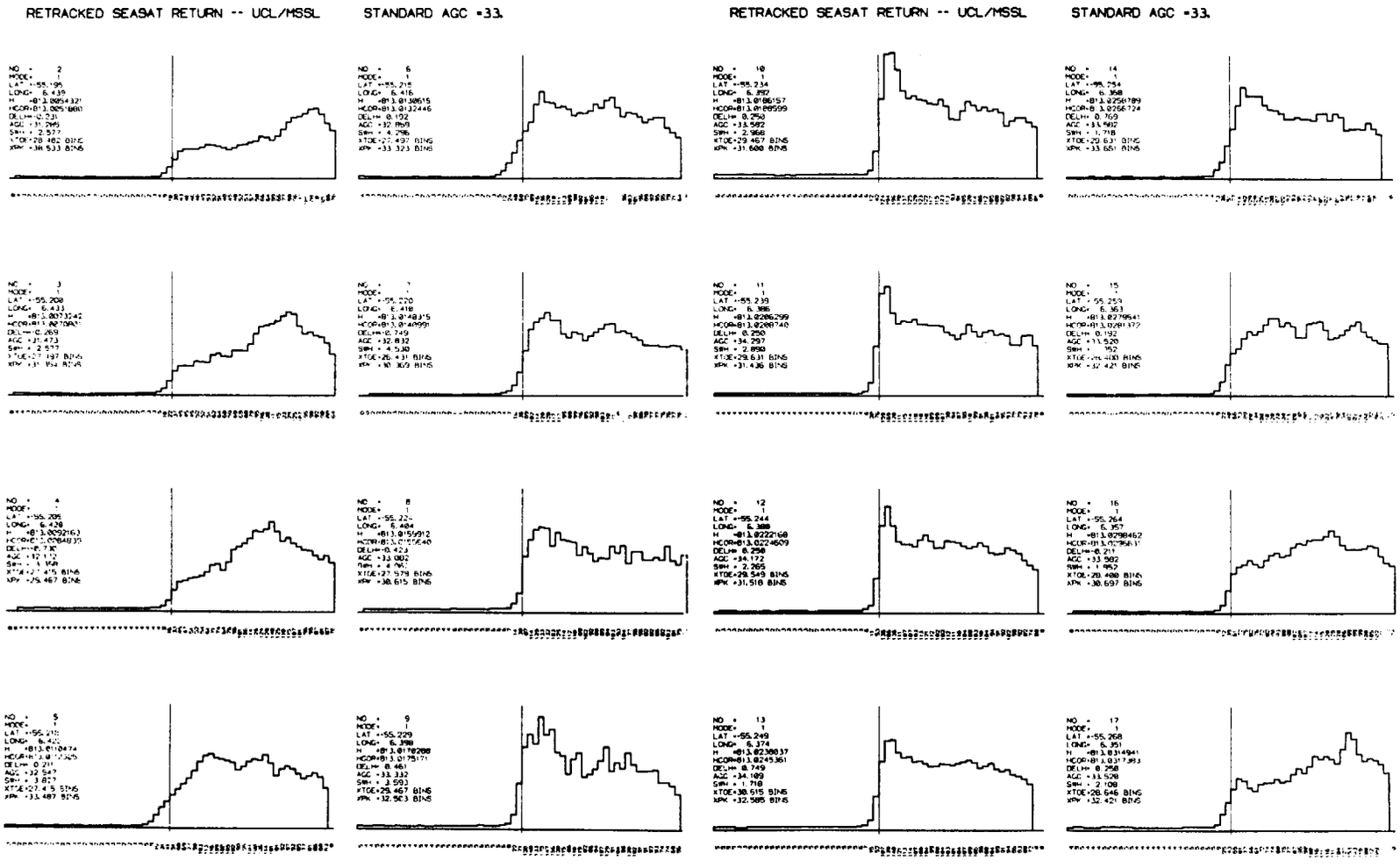

Figure 7. 1 Seasat waveforms immediately prior to the dramatic rise in signal strength corresponding to the AGC-derived ice boundary. Even here the effects of ice patches on the waveforms can be observed.

$$PP = 30\ P/I \qquad 7.1$$

where I is the integral energy within a waveform, P is the energy in the peak channel and the calculations are carried out after retracking and correcting for the altimeter antenna response. Over the ocean, histograms of P, I and PP are stable, well behaved and strongly peaked as shown in Fig. 7.2(a). In the vicinity of the ice boundary all three distributions show some broadening, in response to the pulse distortions noted above (Fig. 7.2(b)). Once beyond the ice boundary all three distributions strongly register the presence of ice (Fig. 7.2(c)).

Although the 'peakiness' parameter PP is defined differently from the ice index of Dwyer and Godin (see section 3.4.1), it is similar in concept and in its behaviour, and shows promise for tuning as a discriminator of the conventional ice boundary.

Tests of the peakiness parameter over ocean tracks suggest that it provides an extremely sensitive and reliable measure of the ocean-like or non-ocean-like nature of return waveforms. Used alone or in conjunction with an AGC value threshold it offers a far more reliable method of ice detection than the use of a simple AGC threshold. Nevertheless, even the latter appears to provide a sensitive means of registering the presence of ice, at least under winter conditions (work in progress using data from the Bering and Chukchi Seas indicates that the AGC signal is less effective at registering the presence of sea ice under summer conditions). Fig. 7.3 shows a comparison of the Antarctic ice boundary determined using a Seasat AGC threshold

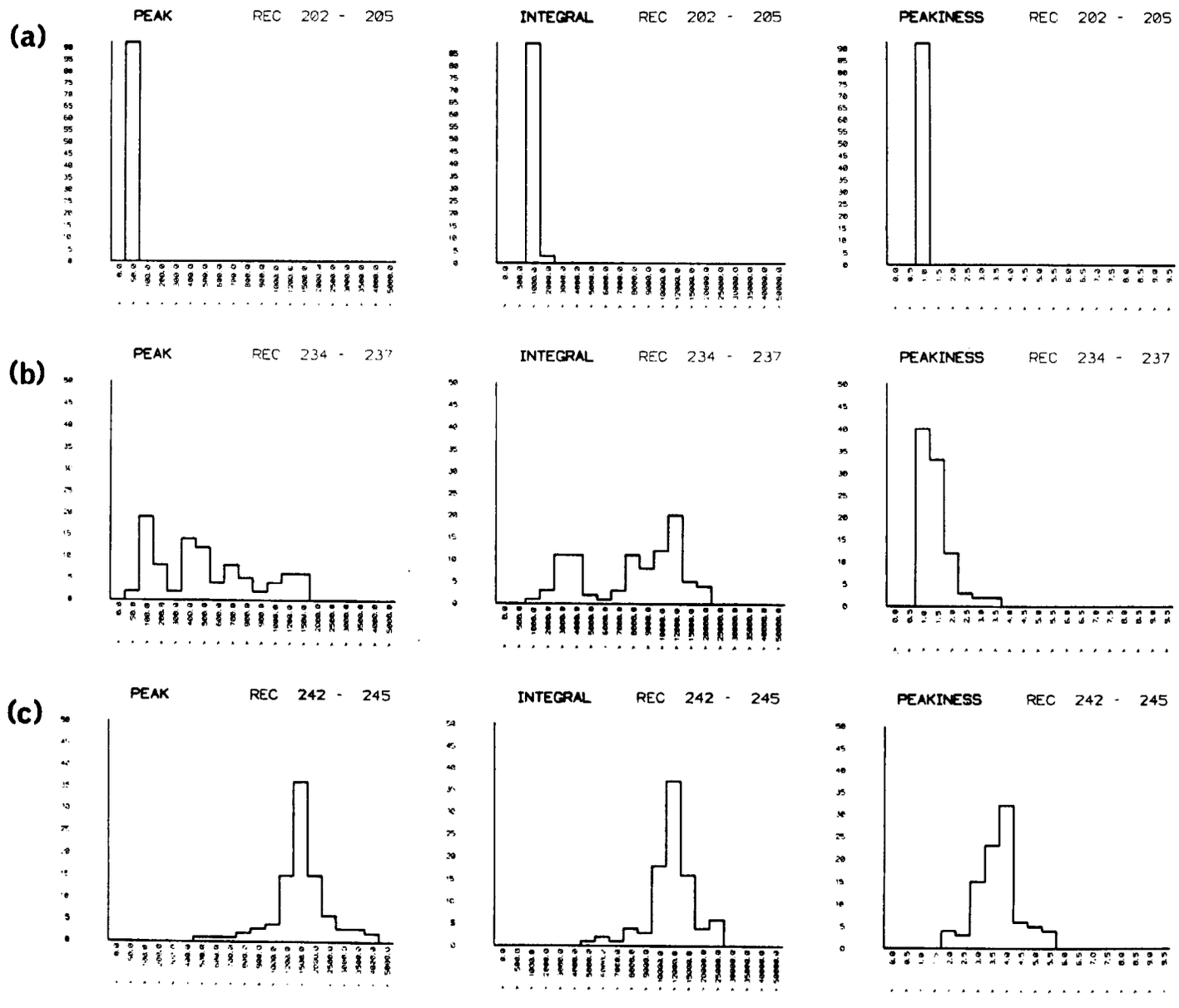

Figure 7.2 Histograms of waveform peak value, integral and 'peakiness' (PP = $\frac{P}{I}$ x 30) for (a) open ocean, (b) immediately pre-AGC ice boundary, (c) immediately post AGC ice boundary.

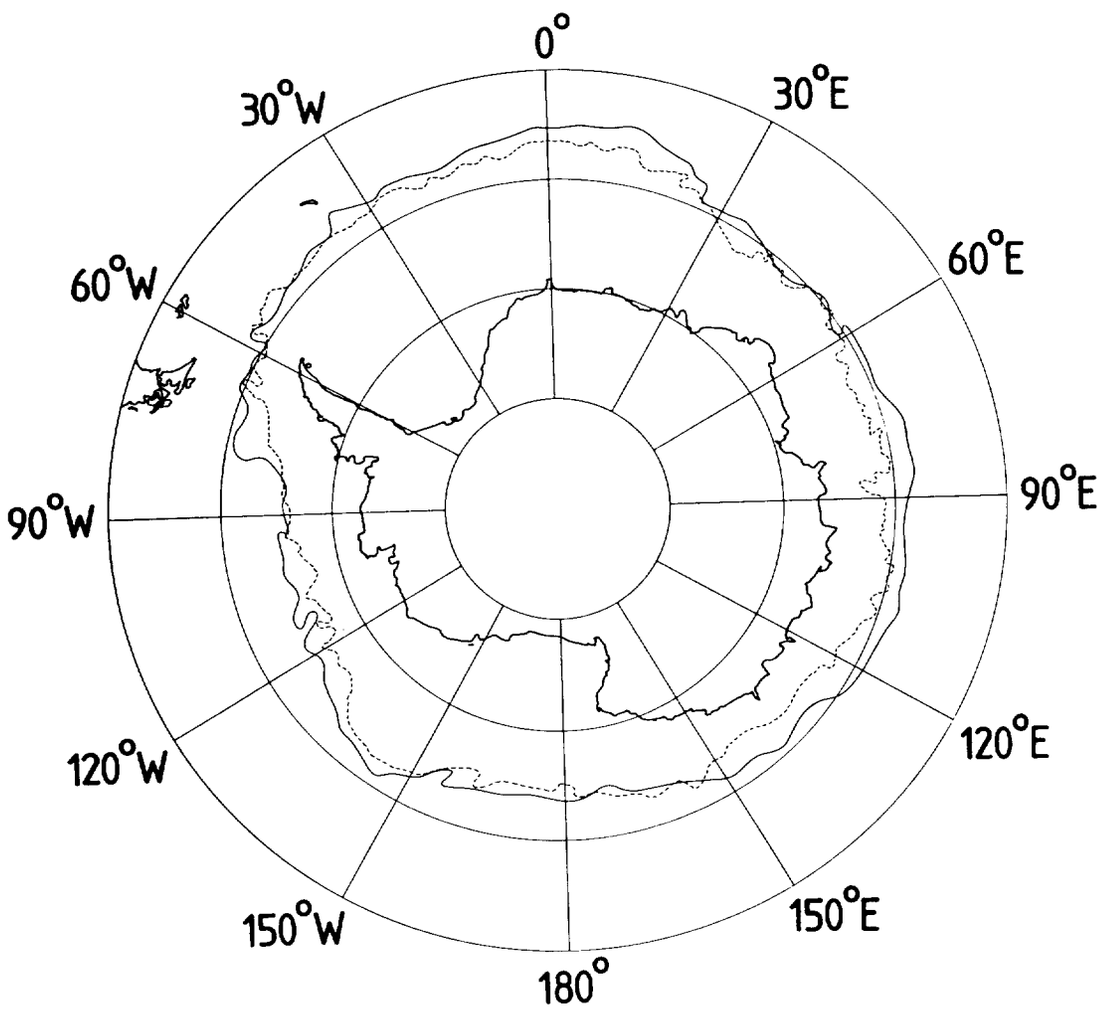

Figure 7.3 A comparison of the Seasat AGC-deduced ice boundary (continuous) and the ice boundary for the same period published by the US Fleet Weather Facility. Generally the AGC-deduced boundary lies outside the conventional 15% concentration contour based on optical and infra-red imagery.

of 33 dB compared with data from the Fleet Weather Facility. The altimeter-determined ice zone generally extends beyond the conventional ice boundary, emphasising the extreme sensitivity of the altimeter to the presence of ice. It is apparent that the altimeter could prove to be of great value in identifying regions of new ice growth.

In addition to the effects described above, the presence of sea ice in the altimeter footprint manifests itself in the on-board computed data streams as a greater degree of height and AGC variability. Fig. 7.4 shows the variation of the standard deviation of the height value as Seasat passed from open sea onto the Antarctic sea ice. Generally, over the oceans, the variance of the 10 s^{-1} values of absolute height about the mean is <10 cm. Over sea ice the variance is much greater - in the example shown it is increased to ~1 m. The variance of H_s also increases substantially in going from open water to ice. Preliminary results indicate that a value of 40 cm may mark the transition. The ability to use on-board computed parameters to register the presence of ice is of particular value for the generation of a quick-look ice product.

In conclusion, there exist a number of promising methods for establishing the presence of ice and thus determining the location of the ice boundary, either using on-board computed data or the echo waveforms. The validation of these techniques is an important part of future work, especially the comparison with in-situ data. Certainly there exists a danger in relying on comparisons with visible and infra-red imagery which in some

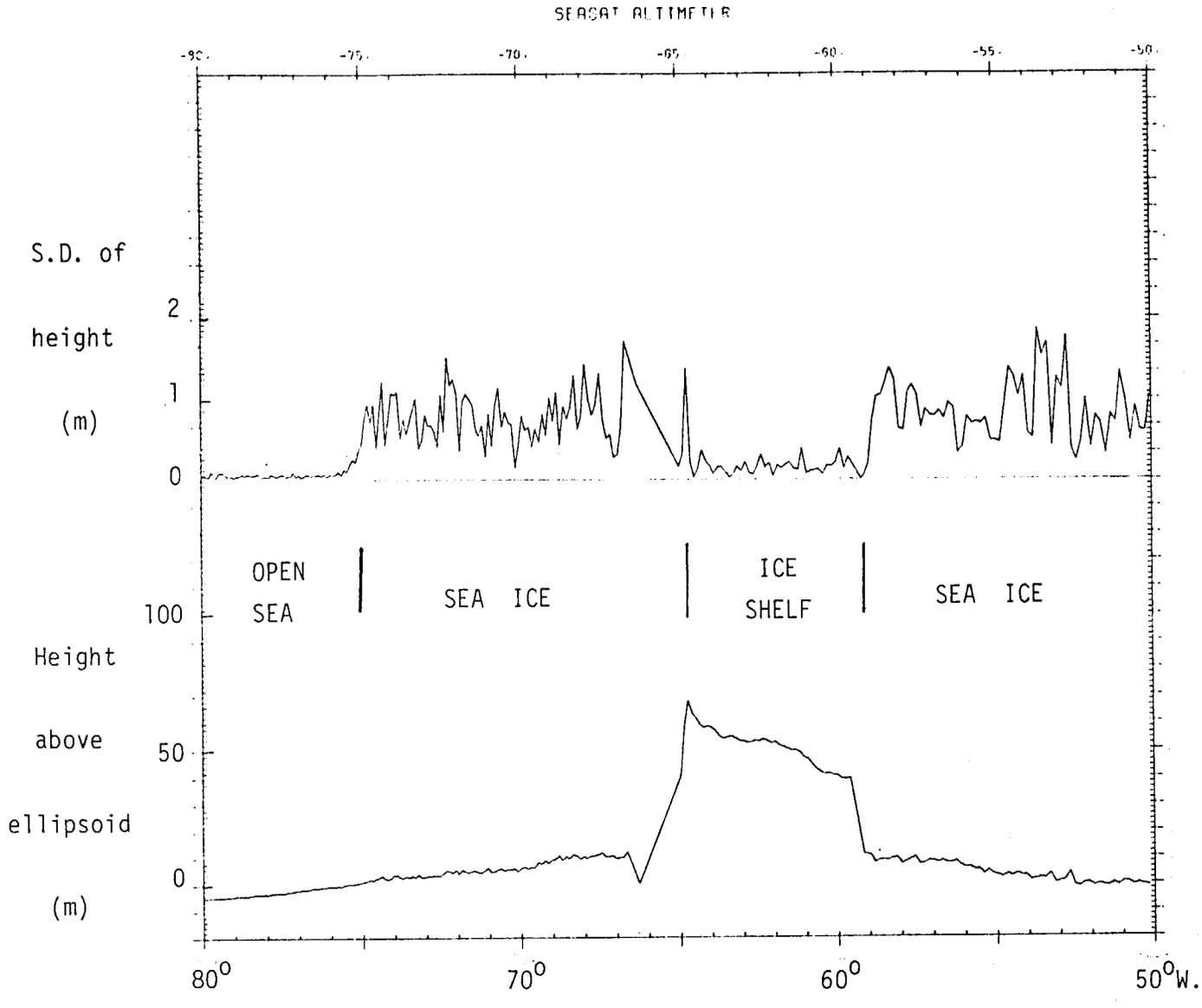

Fig. 7.4 Plot of height of surface above Reference ellipsoid, and the variance of height, For a pass across the Antarctic Peninsula (Rev. 207, 11 July 1978).

cases may give erroneous ice-edge positions owing to difficulties with cloud cover or in the recognition of different ice types. Nevertheless the combination of ERS-1 altimeter data with the greater coverage of the ATSR/M could prove a most useful source of information on the location and nature of the ice boundary.

7.3 Propagation of swell into sea ice

The Southern Ocean is a region of intense storms and large swells which are free to propagate over very large distances. These waves are attenuated by the sea ice which, apart from other considerations, will prevent momentum from being continually transferred from the lower layers of the atmosphere. In-situ data have shown that the amplitude of a given swell component declines exponentially with distance from the ice edge, the attenuation coefficient being a strong function of wave frequency and ice thickness (e.g. Squire & Moore, 1980).

As described in section 3.4.2, the evolution of return echo shape, in particular the degree of pulse peakiness, has been suggested to characterise the decline of ocean swell amplitudes and increasing surface flatness in the interior of the pack. The method should prove particularly powerful if the most strongly reflecting elements of the ice surface correspond to grease ice between floes, or very smooth small floes (<10 m), since the slope probability distribution function of the reflectors will then correspond to that of the underlying ocean surface. Work is currently in progress to study and analyse waveform shapes in

order to assess the ability of the altimeter to provide quantitative measurements of swell propagation. In-situ data, urgently required for validation purposes, are not available for comparison with Seasat data, but have been obtained during the MIZEX aircraft campaigns in which a pulse limited Ku band altimeter was deployed for ice studies. Further development of the technique will almost certainly rely heavily on analysis of the MIZEX data.

7.4 Other ice products

Experience with Seasat waveforms suggests that the extraction of several additional sea ice products may be possible. For example, examination of the parameters P, I and PP described in section 7.2 reveals distinct zones within the pack ice which are reflected in their magnitude, variability and frequency distribution. The height distribution of reflectors may also show correlations. At the time of writing no in-situ or alternative data are available to determine the nature of the ice to which the zones correspond, but Seasat passive microwave data are being obtained to continue the investigation. Appropriate visible and infra red images are also being sought. MIZEX data, including simultaneous altimetry, visible imagery, microwave radiometry and surface measurements and observations, should prove very useful in this context.

Another possibility is the identification of leads and polynyas within the ice pack. This may be achieved using the inverse

of the method for ice detection which combined thresholds in PP and AGC to label ocean-like returns. Patterns of change and rates of change in P and I may also enable deductions to be made as to the nature of ice within the zones observed. The specularity of return waveforms may indicate the presence of flat, highly reflective ice surfaces. Similarly, the migration of specular reflectors through the range window, related to "snagging" as discussed in section 2.7, may suggest characteristics of the surface's reflectivity at different slant angles, itself a function of surface roughness.

The detection of icebergs, should also be possible given that the reflecting surface, unless entirely specular, should follow a characteristic path of decreasing and then increasing slant range as it passes through the range window. Their presence may also be indicated by unexpected losses of lock. This product is partly restricted, however, by the coarse spatial sampling which will result from ERS-1's relatively small footprint and well spaced ground track spacing at latitudes of between 60 to 75^{o}S.

7.5 Calibration and validation

Campaigns and research programmes designed to calibrate and validate altimeter data are already underway using an airborne instrument designed and built by the Rutherford Appleton Laboratory to operate at 13.6 GHz. This work began in 1983. In February of that year the RAL instrument was flown over the marginal ice zone of the Bering Sea in a NASA Convair 990 aircraft. Supporting datasets from radiometry and high- and low-level photography were also collected, and provide information on concentration and floe size distribution. Furthermore, the surface observations taken from ships within the pack ice give details of ice type, ice thickness, microwave reflectivity and backscatter, and microwave absorption. In June 1984 a second campaign was mounted in the Greenland Sea during MIZEX-East '84. Again similar, but more extensive, supporting data were obtained including laser profilometry which will give accurate surface roughness measurements of Greenland Sea multi- and first-year sea ice.

From Seasat records we may say that a spaceborne altimeter will detect the transition from open water to ice and whether the ice cover is continuous or pack ice (see Section 7.2). The lack of precise correlation between the edge as detected by the altimeter and that seen in visible and IR NOAA satellite imagery is likely to be due to the relatively low resolution of the NOAA imagery (1.1 km). Further studies using high resolution image data derived from, e.g. Landsat, should improve the position. Passive microwave sensors such as the ESMR (Electrically Scanning Microwave Radiometer) and SMMR

have also been shown to yield ice edge position, but at a much coarser spatial resolution than is, in principle, achievable by means of the altimeter. It is important that the algorithms used to detect the ice edge, both from the altimetric standpoint and from that of the radiometer , are validated against one another.

Concentration estimates are also available at low resolution from passive microwave instruments, once again assuming that the algorithm (whether the official NASA version or the University of Bergen version) is reliable. These sensors offer an exciting possibility, especially after the launch of the DMSP satellite which will carry a Special Sensor Microwave Imager (SSM/I), viz. to calibrate/validate any altimetric algorithm with those of the passive microwave instruments. Floe size distribution and ice type might be considered in similar manner but would also neccessitate some in-situ surface measurements. That the satellite altimeter is capable of monitoring seas and swell penetration of pack ice could only be verified by means of surface wave buoy measurements, preferably in the Southern Ocean alongside any open ocean wave programme.

The knowledge gained over the next two years in analysing the supporting data (especially from MIZEX) in conjunction with altimeter data sets will allow deficiencies to be flagged. Prior to the launch of ERS-1 it is desirable that further calibration/validation campaigns be carried out in the light of the experience gained. To date the major problem has been in achieving truly coincident datasets (both in time and space). This has been due in large part to the fact that both the Bering Sea and Greenland Sea campaigns were

mounted within the context of a much more extensive research scenario. This situation inevitably results in compromise between agencies and scientific disciplines, and leads to flight-planning problems due to conflicts of interest. It would be of great value if a short, but dedicated, data gathering programme were designed such that all surface validation and supporting airborne measurements, e.g. laser profilometry, were simultaneous in time and site specific.

In 1986 the German polar research vessel Polarstern will conduct an Antarctic winter experiment which will include scientists from the Scott Polar Research Institute. Helicopter support is provided for and as the vessel will operate in isolation there should be no conflicting demands in terms of cooperative work with other ships or overflying aircraft. An icebreaker in the Antarctic costs many tens of thousands of Accounting Units per day to operate and visits such regions infrequently. Since the U.S. altimetric satellite GEOSAT is also expected to be operational during the period some effort should be made to coordinate ground-based measurements which may assist in the ineterpretation of the satellite data. Of particular relevance are the plans of SPRI to fly an impulse radar for determining ice thickness in the Weddell Sea and to make wave measurements well into the ice pack. Although the experiment is still being defined it is highly likely that several airborne remote sensing systems (including scatterometers and radiometers) will be flown.

8. Implications for overall organisation and formats

8.1 The problem

ERS-1 is a pre-operational satellite which is designed to demonstrate how microwave remote sensing data can be used on a routine basis across a wide spectrum of disciplines. In this respect it goes a stage further than the proof-of-concept Seasat system. It is therefore of the utmost importance if the ERS-1 mission is to be a success, that not only should the space hardware meet its specifications and operate reliably for the nominal 2-year mission but that the ground segment be designed in such a way as to enable useful products to be generated in a form that will appeal to the different types of customers.

Some lessons can be learnt from the Seasat mission, though it should be noted that this experience has been gained mainly by the remote sensing scientific community which has been prepared to expend considerable effort in processing the data. It is salutary to note that such resources would probably not have been committed to improving data availability and quality had Seasat not failed prematurely. The two main products from Seasat are the Sensor Data Records and Geophysical Data Records and it is the latter for which most requests have been made. A user who obtains the global altimeter GDR is confronted with fourteen 1600 bpi tapes written in binary integers. His first task is to unpack the data, the method for which varies from computer to computer. Scaling factors and offsets used to keep numbers small have to be removed.

The next problem is to organise the data in a way more suited to the studies he is conducting. For example he is probably interested in specific geographical regions and may only require a limited number of the geophysical variables in each data cycle. Since the data are stored chronologically without latitude/longitude pointers in the headers it is necessary to read every data record on all the tapes to complete the task and this can be time-consuming. Even after this the user may find that the effort has not been justified because the data coverage is poor and/or the variations in geophysical parameters uninteresting. The above problems have been well-recognised by NASA who have developed the Pilot Ocean Data System at JPL (Brown & Klose, 1984). This allows accredited users to examine data sub-sets on-line and to process to higher levels in digital and graphical form for rapid examination of data quality etc. Desired data sets can then be ordered via different media.

For ERS-1 there are additional problems. A fundamental constraint, imposed by the delegates of the participating nations, is that the ERS-1 project is committed only to the generation and dissemination of Fast Delivery Products. Off-line activities will utilise national facilities but under the coordination of ESA and various proposals are at present under consideration. As can be seen from sections 2.2 -2.5 most of the interest in altimeter data lies in off-line products and requires the synthesis of many different data streams. Given the above organisational structure the definition of a concensus ground segment plan by the user community is a matter of some urgency. A further difficulty is that of data volume. Given

that ERS-1 is expected to operate for three years and that there is a requirement for archiving a basic 20 s^{-1} waveform product (2.4.2) it has been estimated that the data volume will be ~10^4 times greater than that of the Seasat GDRs (Rapley , 1984b)

Given the requirements implied by the definition of useful data products in Section 2.2.3 and the matters raised earlier in this section a number of themes emerge which are expanded in following sections. Many of these are also discussed in Rapley(1984b)

(i) Requirement for global data

(ii) Easy accessibility to desired products

(iii) Algorithm development and strategy for reprocessing of data

(iv) Requirements for archive facilities

(v) Cbncept of an Altimeter Foundation Product

8.2 Requirement for global data

One of the great contributions that satellites have been able to make is that of providing global, synoptic measurements of the Earth. In meteorology this has complemented the existing World Weather Watch of routine atmospheric measurements but in the oceans no conventional synoptic observations are made on a global scale. More and more emphasis is being placed on considering the ocean-atmosphere-cryosphere system as a coupled system which interacts globally and for many applications purposes data are required all over the world rather than in specific geographical locations. Building up a global data base may place Europe in a strong position for the future

exploitation of such information. Indeed, an attraction of satellite remote sensing is that the coverage inevitably extends over regions which might not have a high priority for study by conventional techniques. In this way interesting phenomena can be identified and monitored for relatively little extra effort.

In sections 2.2-2.5 specific requirements have emerged for global data to meet different objectives in the study of waves, sea-ice, wind and ocean topography. There is a need, in support of the WCRP, to provide sea surface elevation and winds across all the world's oceans taking advantage of ERS-1's high inclination orbit. Although sea-ice is not global in extent it is most important that as much of it as possible is monitored so as to be able to accurately estimate the seasonal and interannual variations in ice-cover. Waves in the open ocean can travel great distances and the building up of a global wave climatology (as opposed to a limited number of continental shelf sites) is regarded as one of the main tasks which ERS-1 can contribute which will affect ship routing and longer-term planning for possible oil exploration.

These requirements affect two areas of the mission:-

(i) duty cycle of the altimeter

(ii) acquisition of data and its subsequent archival

8.2.1 Duty cycle

The requirements mean that the altimeter would be required to operate continuously during the mission for the periods when it is viewing ocean or sea-ice surfaces, i.e. ~70% of the time. There are

additional requirements (not covered in this volume) for coverage over continental ice which is a part of the nominal mission and indeed there are some grounds for maintaining a continuous operation of the instrument (this may prolong its useful life, and there is interest in data over land, see Rapley et al., 1984b). However, ERS-1 is power-limited and it is recognised that user requirements for the different sensors may necessitate a trade-off to meet available supply. In this case strong consideration should be given to preserving a global ocean and ice mission for the altimeter for the following reasons:

(i) In terms of energy consumption the altimeter compares favourably with the other main sensors (~40% of the wind scatterometer and about the same as the SAR imaging mode, assuming a 10% duty cycle of the latter). Moreover it provides simultaneously three essentially different variables, height, reflectivity and statistical properties of the elevation of the surface. Therefore in order to save significant energy, a considerable amount of potentially useful information has to be thrown away.

(ii) Some of the objectives , such as determination of tidal constituents and mapping of mesoscale variability, rely on long, uniform series of measurements. Assuming that these will already have been affected by planned changes to the ERS-1 orbit during the mission it is vital that these data sets are otherwise as unbroken as possible.

Global coverage of the regions of interest can be obtained without continuous operation, e.g. having the altimeter working on alternate days only similar to the NIMBUS-7 SMMR. Studies of the effect of such a duty cycle are needed. Given that for most wind, wave and sea-ice uses the altimeter in a continuously operating mode will probably sample less frequently than required it would seem that such an option will prove unsatisfactory.

8.2.2 Acquisition and archival

To meet the requirements, it is not sufficient that the altimeter should always be active over oceans and ice; the arrangements for onboard storage and subsequent telemetry to ground stations has to be such that all data gathered over oceans and ice are received at the ground stations and delivered to the ERS-1 PAF in a standardised format for archiving. In addition some of these data (H_s and wind speed) are required to be disseminated within three hours of acquisition by the satellite which places additional demands on the acquisition - record/playback - telemetry to ground station - dissemination chain. Fig. 8 of Francis (1984) raises doubts as to whether this global requirement for Fast Delivery products can be met. However, recent changes to the SAR wave mode imply that there is increased capacity on the spacecraft tape-recorder so this problem may be alleviated.

More than one ground station is required to obtain global data since Kiruna will only be able to receive data from 9 passes. For

off-line purposes the archived data sets need to be combined at some stage to produce a unified, internally consistent data set of low level data.

8.3 Accessibility of data products

As stated by Haskell (1984) and reiterated in Rapley (1984b) the question of easy, timely access by end users to accurate, understandable ERS-1 data products is a key issue for the success of the mission. As pointed out earlier the altimeter user community so far identified consists mainly of a section of the research community whose viewpoint (with the exception of requirements of specialist data centres) may not be representative of the users we expect to be customers in 5-10 years time. Even their experience suggests that acquiring and being able to use remote sensing data is generally unsatisfactory. If other sections of the scientific and commercial community with less experience and a greater reluctance to undertake extra processing are to be widely attracted to ERS-1 products considerable effort must be placed on making the desired products available more easily than hitherto. The following points are important:

(i) well-thought out catalogues and data summaries

(ii) flexibility to access data from a number of selected viewpoints

(iii) full visibility of algorithms, calibration, validation, documentation, ordering procedure, costs

(iv) role of specialist data centres

(v) policy regarding routine processing

(vi) standardisation of formats.

8.3.1 Catalogues

Before obtaining data sets users will wish to see what is available. The catalogue should be comprehensive and up to date including not only a list of times and orbit numbers during the period but be broken down by geographical area and should summarise environmental conditions as recorded by the altimeter. It could contain (for each product):

a) plots of the satellite tracks through geographical areas (ocean basins or lat/long squares) (as in Fig. 2.5).

b) tables or maps indicating number of data points and passes recorded in each 10^{o} square

c) tables or maps showing mean, maximum and minimum geophysical parameters e.g. waveheight, sea-ice index.

A convenient way of generating these data summaries would be during the preparation of geophysical subsets (i.e. processing from Level 2 to 3). It is anticipated that such products would be circulated on a monthly basis. A separate catalogue should be produced when Level 0 data is processed to levels 1, 1.5 and 2 since this will be purely chronological.

By examining the catalogue a user should be able to rapidly assess whether the quantity of data, its time and location, range of conditions and quality are adequate for further progress to be made

(either direct access to an on-line data bank or ordering of data sets).

8.3.2 Access from selected viewpoints

Users will come from a wide variety of scientific disciplines and applications and will wish to examine the data in various ways. The higher level data sets should be flexible enough to facilitate such investigations so that, for example, wind/wave statistics along a given ocean route could be obtained. This will probably mean that a number of requests for high level data will be generated on demand because the requirements are fairly specific to each application. However, an important activity prior to launch will be the identification of standard types of high level data products. Workshops attended by potential users with on-line access to GEOS-3 and Seasat data sets would be one way of developing user awareness and of assessing the usefulness of different ways of presenting and storing data.

8.3.3 Full visibility

Users must be able to obtain full information on the calibration and validation procedures that have been carried out, together with the Calibration/Validation data, documentation on algorithms, data products and the methods used to generate them, and an easy-to-understand procedure for ordering data, including a clear breakdown of costs involved before the product has to be ordered. Users should be informed of the amount of data they have requested, e.g. pages of

lineprinter output, number of computer compatible tapes. If on-line facilities are made available for this then adequate safeguards should be incorporated to prevent accidental ordering of data. (This is especially likely to occur when new users try out the system).

8.3.4 Role of specialist data centres

Rapley (1984b) recommended that the PAF should provide access to all ERS-1 altimeter data at least up to the level of instrument and environment-corrected geophysical variables, i.e. up to Level 2. Beyond a certain agreed level which may vary according to product, devolution to centres specialising in specific applications may occur. As an example a wave data product similar to that in Table 2.3 may be handed over to MIAS (as the RNODC for Waves) who would then be responsible for disseminating high-level products in response to enquiries. Such a division of responsibility is implied in an ESA summary of proposals received for the off-line ground segment facility (ESA, 1984). It would have the advantage of using existing links to potential customers and would also prove valuable in gaining access to sources of in-situ data for validation purposes.

8.3.5 Routine processing policy

It seems to have been widely assumed within the scientific community that ERS-1 data will be processed at least to Level 2 as a matter of routine. Strong views were expressed at the Radar Altimeter workshop that certain products must be systematically processed but it was not clear that this would be true. It is

possible that in order to meet financial and physical constraints imposed by the sheer volume and complexity of the data only a basic data product will be archived (see 8.5) and processing to other levels will only be carried out on demand, according to variables and geographical zone, etc. It is argued that technological advances will be such that, to the user, the two schemes appear identical. Although it is realised that there are problems in archiving global satellite data for long periods, at different levels, when the mission may last several years, the user community is concerned that the alternative will lead to product inaccessibility and non-uniformity which might be disastrous for ERS-1 as a pre-operational satellite. A study of the implications should be carried out based on GEOS-3 and Seasat altimeter data obtained at the raw waveform level.

8.3.6 Standardisation of formats

Much time and effort could be saved if a standard tape format could be devised for radar altimeter data. This would reduce duplication of effort at the software development stage both when a new instrument is launched and when software is prepared at individual institutes for a given instrument. Since ERS-1 is likely to be one of several altimeters flying at about the same time considerable advantages would be gained if formats were to be agreed in advance between the agencies involved. Scott & Huckle (1984) considered this topic and have presented a preliminary layout for a possible standard format based on the Seasat Sensor Data Record with

features incorporated from the EXOSAT project final observer tapes. Thought must be given to the encoding of data to ensure maximum portability across different computer systems. Judicious use of file marks in the data stream can assist data handling when tapes are used. Also the use of direct access record pointer techniques can facilitate access to data from specific geographical areas.

8.4 Algorithm development and strategy for data reprocessing

It will be clear from previous chapters, in which the procedures for retrieval of geophysical parameters are discussed in detail, that algorithm development is likely to continue through the whole of Phase C/D until well after launch. Experience gained from GEOS-3, Seasat and NIMBUS-7 shows that major efforts have been required to tune algorithms using comparisons of spacecraft and in-situ data. This is partly due to the empirical nature of the algorithms themselves (a reflection of the incompleteness of our understanding of microwave emission and scattering from the surface of the Earth) and also because calibration problems with sensors have occurred. This is particularly true of the NIMBUS-7 SMMR.

For Seasat the reprocessing of data using new algorithms is a major but manageable task because the data sets are relatively small and limited. In the case of ERS-1 data are expected to flow continuously for a period of 2-3 years or longer. If, during this time, it proves necessary to change the algorithms this will cause large problems because of the need to reprocess data already received and archived by the PAF before the change, whilst maintaining the

processing schedule for new data. It is therefore very important that substantial efforts should be made in the initial 6-month commissioning phase to arrive at algorithms which will serve satisfactorily for the duration of the mission. This implies that calibration/validation activities should be held during the first part of the commissioning phase so that the algorithms can be ready for routine processing by its end. This would also enable problem areas such as a lack of high wind speed validations to be identified and action taken (e.g.conduct extra aircraft campaigns) during the second 3 months. The advantage of this scheme is that reprocessing of the commissioning phase data using the updated algorithms would be accepted as having a low priority and would be carried out in "slack" periods during the rest of the mission.

Should subsequent changes be necessary, say one year after launch, the volume of data might be so large that reprocessing would have to await the end of the mission or alternatively be delegated to facilities outside the PAF.

8.5 Altimeter Foundation Product

During the ERS-1 Radar Altimeter Data Products Workshop an attempt was made to define a fundamental data set which would form the basic archive in the ground segment. It was named the Altimeter Foundation Product (AFP) and would act as the starting point from which all subsequent data products could be derived. In order to avoid archiving all the telemetered data the AFP should be reversible. It would also serve as the fundamental scientific data product containing relevant data in a near raw form so that the study

of fundamental processes would not be obscured by irreversible data processing. Hence the AFP would have to have a form suitable for distribution on various media, particularly magnetic tape. If the concept were implemented the format of the AFP could be standardized (8.3.6).

Fig. 8.1 shows how the AFP could fit into a scheme for processing ERS-1 altimeter data. The major advantage of this approach was seen to be the reduction of storage requirements for the low level data. A full study needs to be undertaken of the feasability of the AFP and its advantages/disadvantages in relation to user accessability and financial implications.

8.6 Dissemination of fast delivery products

As discussed in Chapter 2 certain wind, wave and sea-ice products are amenable to dissemination via radio-facsimile charts. A convenient way of distributing numerical information would be to encode the information into groups of 5 digits and to load the data on to the Global Telecommunications System (GTS) in the same way as meteorological reports are handled. For the altimeter values derived from each sample would appear as separate entries. In order to minimize the volume for most purposes a value every 10 s (70 km along track) would suffice. Variables to appear in the coded report should include:

- o satellite and sensor identifiers
- o latitude/longitude of the footprint centre

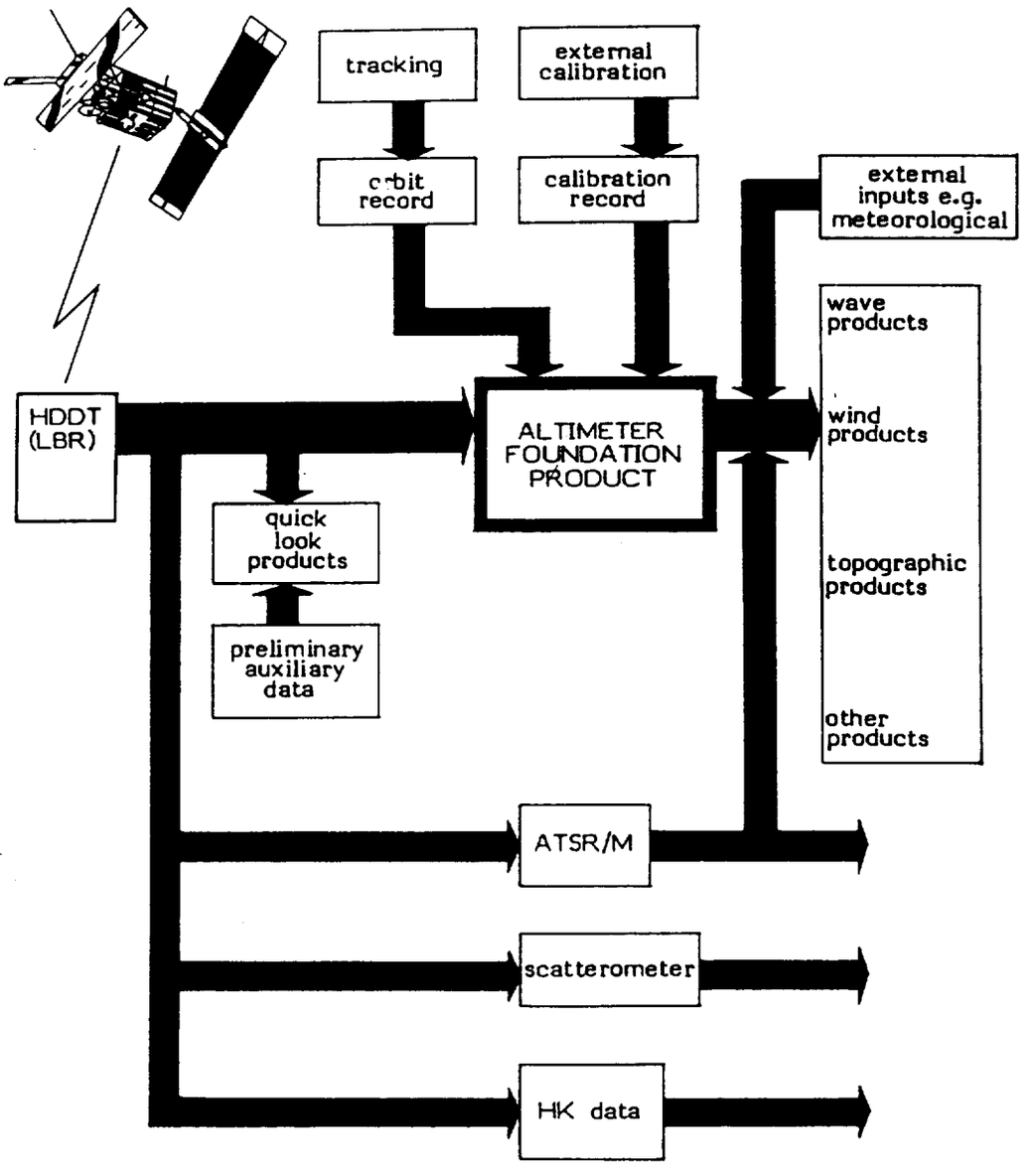

Figure 8.1 A possible scheme for handling ERS-1 altimeter data based on the generation of an Altimeter Foundation Product (AFP)

o date and approximate time

o significant waveheight, wind speed, coarse height, sea-ice indicator, plain language storm warning.

8.7 Data products for calibration/validation

As emphasised in 8.4 the calibration/validation activity must be carried out as speedily as possible after the launch of ERS-1. It is important, therefore that altimeter data for the calibration zones (laser station, in-situ measurement campaigns) be easily accessible. One of the first steps in the proceesing of data after it arrives at the PAF should be to isolate data falling within the calibration zones and to store it separately ready for merging with in-situ data. Obtaining rapid and easy access to in-situ data may be more of a problem. At present delays of several weeks often occur before data obtained at sea are returned to land for processing and formats of data vary considerably. Some data are already transmitted in near real-time (for example SST data sent to NOAA and selected ships' meteorological reports on the World Weather Watch) and it is anticipated that more data will be handled this way in the future. The Ocean Observing Systems Programme of the World Climate Research Programme is concerned with this general area and it is suggested that the appropriate channels are used to ensure maximum availability of the required in-situ data bearing in mind the heavy demands that are already placed on GTS.

9. Conclusions and recommendations

1. A number of possible ocean and sea-ice data products have been identified at various levels. Some of the details are likely to change in the period before ERS-1 is launched but this preliminary work should help in the sizing of processing and archival facilities. (2.2-2.5)

Recommendation

ESA should use the material in this report as a basis for discussion with potential users as to the products they require. This may involve consultation with specialist data centres, where appropriate. ESA should ensure that the PAF is designed with sufficient flexibility and spare capacity to allow for growth.

2. Easy and timely access to global ocean and sea-ice data from ERS-1 at Level 2 (for ice Level 1.5) and above is essential if the requirements of users are to be met. (Chapter 8)

Recommendation

The ERS-1 altimeter should operate continuously over oceans and sea-ice throughout its life-time and the entire R.A. data set should be archived at Level 2 (for ice Level 1.5) in the PAF.

3. Additional information, which could be included in the fast delivery product, may be useful for supporting campaign operations. Parameters we have identified (see Table 9.1) are sea-ice boundary, wave period, uncorrected range (as an aid to detection of large icebergs and western boundary currents, if the local geoid can be taken out at Kiruna). (Chapter 2)

Recommendation

ESA should examine the possibilities of incorporating these parameters into the dissemination scheme at Kiruna.

4. There is considerable interest in non-real-time wave parameters for research and for deriving wave climate statistics for off-shore operations. (2.2)

Recommendation

ESA should ensure that sufficient emphasis is given to wave parameters in the design of the PAF.

5. The real-time usefulness of wind and wave data should not be limited to model input. (2.2.2)

Table 9.1 Additional parameters to be considered for inclusion in the ERS-1 Fast Delivery Product

Parameter	Suggested expression*	Comments
Wave period T_A	$T_A = 1.07 H_s^{\frac{1}{2}} \sigma^{0\,\frac{1}{4}}$	Based on Eq. 5.1 with r = 8, a reasonable value for the ocean
Pulse peakiness PP	PP = 30 P/I	
Uncorrected range R	$R = c\Delta t/2$	Δt may include some instrument corrections

H_s = significant waveheight

σ^0 = normalised radar cross-section (not in dB)

P = energy in peak range gate

I = integral energy within a waveform

c = speed of light

Δt = 2-way uncorrected time delay

* These formulae are based on preliminary findings and are likely to be modified prior to launch.

Recommendation

Modifications should be made to the Global Reference Mission (supplied to the industrial contractors for sizing purposes) to reflect the general interest in real-time wind and wave data from the altimeter.

6. The Seasat wind algorithm does not meet specifications at wind speeds greater than ~12ms^{-1}. A number of discrepancies in the extraction of wind speed have been identified. (3.2.4)

Recommendation

A separate study should be made of differences between GEOS-3, Seasat, in-situ and SMMR winds to investigate the nature of the discrepancies in relation to theory. Consideration should be given to making aircraft altimeter measurements of σ^{o} over the ocean, close to surface wind and wave measuring devices, and to obtaining a comprehensive set of sun glitter data. Stereophotography of the sea surface should be combined with these measurements. A new wind speed algorithm should be developed for ERS-1 by an algorithm development team.

7. Pointing angle errors and atmospheric attenuation due to rain will be significant for wind speed retrieval by ERS-1, particularly for higher wind speeds. (6.1)

Recommendation

Methods for correcting ERS-1 altimeter data for pointing angle errors and atmospheric attenuation should be examined, the latter study including the role of ATSR/M data.

8. At present it cannot be demonstrated that swell can be retrieved from radar altimeter data, except in conditions of low wind speed when the energy of the sea component of the waves is small. (3.1.3)

Recommendation

Further research is required to determine whether minimum swell calculated using accurate wind speeds is a useful quantity for ERS-1. Use should be made of simultaneous wind velocity and wave spectra information such as are obtained at U.K. Data Buoys supplemented by comparisons of Seasat minimum swell (using a revised wind algorithm) with in-situ data.

9. In principle, more wave information can be derived from a satellite altimeter than was obtained from Seasat - skewness, a skewness coefficient, wave period and the generalised variance of slopes. As well as being useful in their own right, these should enable better corrections for sea-state bias to be made. (Chapter 5)

Recommendation

Further work is needed, using simulation studies of the altimeter return, to assess the accuracy with which the above wave parameters can be extracted from the ERS-1 altimeter. It is also necessary to investigate the spatial variability of the wave field. The latter can be achieved through the use of stereophotography (see Recommendation 6).

10. A number of promising methods exist for establishing the presence of sea-ice from altimeter data, using either on-board computed data or echo waveforms. (7.3)

Recommendation

Future work should include the validation of methods for identifying sea-ice using satellite and aircraft altimeter data and comparisons with in-situ observations. The combined use of the ATSR/M and R.A. for ice boundary monitoring should be considered.

11. There is some suggestion that the waveform over sea-ice may be parameterised to reveal distinct zones within the pack ice, which correspond to changes in the surface characteristics of the ice. (7.4)

Recommendation

Studies using Seasat and GEOS-3 data should be continued and extended to other cases, in order to establish repeatability and consistency with independent data. MIZEX aircraft data should also be analysed from this perspective.

12. Calibration and validation is an important part of the ERS-1 altimeter mission, especially during the first 3 months of the commissioning phase. For winds this should be combined with that for the scatterometer to ensure consistency between sensors. (6.4)

Recommendation

Detailed planning of the calibration/validation of the altimeter should begin as soon as possible and, where appropriate, should be linked with the planning of field experiments, such as WOCE and TOGA. For winds and waves there should be close co-operation between ESA's R.A. and Active Microwave Instrument Teams.

13. The ERS-1 altimeter will be an improvement on Seasat's. The SMLE algorithm will give better on-board estimates of H_s, the Δh versus offset characteristic curve will be linear over a much broader region and the switch to the ice mode will improve tracking over rough ice topography. (Chapter 4)

Recommendation

The effect of ice-mode switching on sea-ice data in coastal margins should be investigated.

14. The documentation of H_s algorithms in the literature is inadequate. (3.1.2.2)

Recommendation

ESA should ensure that the users have full visibility of algorithms and that it is clear which algorithms have been used in generating different data sets.

10. References

Allan T.D. (ed.) 1984 Report of Working Group 6 (Ocean Topography). European Association of Remote Sensing Laboratories, April.

Allan T.D. & Guymer T.H. 1984 Seasat measurements of wind and waves on selected passes over JASIN. Int. J. Remote Sensing, 5, 379-408

Barrick D.E. 1968 Rough surface scattering based on the specular point theory. I.E.E.E. Trans. Antennas & Propagation, AP-16, 449-454

Barrick D.E. 1972 Remote sensing of sea-state by radar. In Remote sensing of the troposphere, ed. V.E. Derr, ch. 12, U.S. Government Printing Office, Washington, D.C.

Barrick D.E. 1974 Wind dependence of quasi-specular microwave sea scatter. I.E.E.E. Trans. Antennas and Propagation, AP-22 ,135-136.

Bouws E., Komen G. & Nooren G. 1984 Satellite measurements and model forecasts of wind waves and swell. ERS-1 Radar Altimeter Data Products Workshop Report, ESA SP-221, 113-116.

Brown G.S. 1977 The average impulse response of a rough surface and its applications. I.E.E.E. J. of Oceanic Eng., OE-2 ,67-74

Brown G.S. 1978 Backscattering from a Gaussian-distributed perfectly conducting rough surface. I.E.E.E. Trans. Ant. and Propag., AP-26 ,472-482. erratum: in IEEE Trans. Ant. and Propag., AP-28 , 943-946 (1980).

Brown G.S. 1979a Estimation of surface wind speeds using satellite-borne radar measurements at normal incidence. J. Geophys. Res., 84, 3974-3978.

Brown, G.S. 1979b Surface roughness slope density estimates for low sea-state conditions. J. Geophys. Res., 84, 3987-3989.

Brown G.S. 1982 A theory for near-normal incidence microwave scattering from first year sea ice. Radio Science, 17, 233.

Brown G.S., Stanley H.R. & Roy N.A. 1981 The wind speed measurement capability of spaceborne radar altimeters. IEEE J. Oceanic Eng., OE-6 , 59-63.

Brown J.W. & Klose J.C. 1984 The NASA/JPL Pilot Ocean Data System. ERS-1 Radar Altimeter Data Products Workshop Report, ESA SP-221, 85-90.

Carter D.J.T. & Challenor P.G. 1981 Estimating return values of wave height. IOS Report No. 116

Carter D.J.T. & Challenor P.G. 1984 The impact of Satellite Altimeter Data on Wave Research. ERS-1 Radar Altimeter Data Products Workshop Report, ESA SP-221, 47-50.

Chelton D.B. & OBrien J.J. 1982 Satellite microwave measurements of surface wind speed in the tropical Pacific. Tropical ocean-atmosphere newsletter, 11 , 3-4.

Cox C.S. & Munk W.H. 1954 Statistics of the sea surface derived from sun glitter. J. Mar. Res., 13 , 198-227.

Donelan M.A. & Pierson W.J. 1984 Does the scatterometer see wind speed or friction velocity? Proc of URSI Commission F Symposium on Frontiers of Remote Sensing of the Oceans and Troposphere from Air and Space Platforms, Shoresh, Israel, 14-23 May 1984, NASA Conf. Pub. 2303, 75-87.

Dornier 1983 ERS-1 Phase B Final Review Documentation, Doc. No. ER-HO-DSF-SY-0003.

Draper L. 1983 Catalogue of wave prediction models. MIAS Ref. Publication No. 5

Draper L. and Bownass T.M. 1983 Wave devastation behind Chesil Beach. Weather, 38 ,(11) 346-352.

Drewry D.J. (ed.) 1984 Report of Panel 2 (Topography). in ERS-1 Radar Altimeter Data Products Workshop Report, ESA SP-221, 237-247.

Dwyer R.E. & Godin R.H. 1980 Determining sea-ice boundaries and ice roughness using GEOS-3 altimeter data. NASA CR-156862.

ESA 1984 The ERS-1 Off-line Ground Segment Programme: Summary of national proposals to ESA and possible harmonisation. Information Note, ESA/PB-RS(84)15.

Ewing J.A. 1983 Wind waves: a review of research during the last twenty-five years. Geophys. J.R. Astr. Soc., 74, 313-329.

Farrow J.B. 1975 The influence of the atmosphere on remote sensing at microwave and radio wavelengths, prepared for ESRO under ESTEC Contract No. 1838/72 ESA.

Fedor L.S. & Barrick D.E. 1978 Measurements of ocean wave heights with a satellite radar altimeter. EOS Trans. AGU, 59 ,(9) 843-847

Fedor L.S. & Brown G.S. 1982 Waveheight and wind speed measurements from the Seasat radar altimeter. Journal of Geophysical Research, 87 ,(C5) 3254-3260.

Fedor L.S., Godbey T.W., Gower J.F.R., Guptill R., Hayne G.S., Rufenach C.L. & Walsh E.J. 1979 Satellite altimeter measurements of sea state: an algorithm comparison. Journal of Geophysical Research, 84 ,(B8), 3991-4001.

Foster J.E., Thomas L., Guymer T.H., Crease J. & 11 other authors 1980 Study on satellite radar altimetry in climatological and oceanographic research. ESA Contract Report, SP/153/06/01/FR(80).

Francis C.R. 1984 The ERS-1 altimeter: an overview ERS-1 Radar Altimeter Data Products Workshop Report, ESA SP-221, 9-16.

Frassetto R., Guymer T., Zecchetto S., Brossier C., Ciraolo L. & Rapley C. 1984 The altimeter as a support to the scatterometer in coastal waters and enclosed seas. ERS-1 Radar Altimeter Data Products Workshop Report, ESA SP-221, 193-198.

Genest E. 1970 Space Geodesy Aircraft Experiment Final Report, NASA Contract NASW 1932.

Goldhirsh J. & Rowland J.R. 1982 A tutorial assessment of atmospheric height uncertainties for high-precision satellite altimeter missions to monitor ocean currents. IEEE Transactions on Geoscience and Remote Sensing, GE-20 ,(4) 418-434.

Gower J.F.R. 1979. The computation of ocean wave heights from GEOS-3 satellite radar altimeter data. Remote sensing of the Environment, 8, 97-114.

Griffiths H.D. 1984 Special difficulties of retrieving surface elevation over continental ice. ERS-1 Altimeter Data Products Workshop, ESA SP-221, 61-66.

Guillaume A. 1984 The use of altimeter data in sea-state forecasting. ERS-1 Radar Altimeter Data Products Workshop Report, ESA SP-221, 43-46.

Guymer T.H. (ed.) 1984 Report of Panel 1 (Wind, Waves and Sea Ice), in ERS-1 Radar Altimeter Data Products Workshop Report, ESA SP-221, 227-236.

Guymer T.H., Businger J.A., Jones W.L. & Stewart R.H. 1981 Anomalous wind estimates from the Seasat scatterometer. Nature, 294 , 735-737.

Guymer T.H., Drewry D.J. & Rapley C.G. (eds.) 1984 ERS-1 Radar Altimeter Data Products Workshop Report, ESA SP-221, 259pp.

Hancock D.W., Forsythe R.G. & Lorell J. 1980 Seasat altimeter sensor file algorithms. I.E.E.E. J. Oceanic Eng., OE-5 , 93-99.

Haskell A. 1984 Factors affecting the archiving, processing and dissemination of ERS-1 altimeter data. ERS-1 Radar Altimeter Data Products Workshop Report, ESA SP-221, 99-102.

Hasselmann, K., Ross D.B. , Muller P. and Sell W. 1976 A parametric wave prediction model. J. Physical Oceanography, 6 , 200-228.

Hobbs P.V. 1978 Organization and structure of clouds and precipitation on the mesoscale and microscale in cyclonic storms. Rev. Geophys. Space Phys., 16, 741-755.

Hobbs P.V. & Biswas K.B. 1979 The cellular structure of narrow cold-frontal rainbands. Quart. J. R. Met. Soc., 105, 723-727.

Houze R.A. Jr. & Hobbs P.V. 1982 Organization and structure of precipitating cloud systems. Advances in Geophysics, 24, 225-315.

Huang N.E. & Long S.R. 1980 An experimental study of the surface elevation probability distribution and statistics of wind-generated waves. J. Fluid Mech., 101, 179-200.

Huang N.E., Long S.R., Tung C.C., Yuen Y. & Bliven L.F. 1981 A unified two-parameter wave spectral model for a general sea state. J. Fluid Mech., 112, 203-224.

Jackson F.C. 1979 The reflection of impulses from a nonlinear random sea. J. Geophy. Res., 84, 4939-4943.

James P.K. & Browning K.A. 1979 Mesoscale structure of line convection of surface cold fronts. Quart. J. R. Met. Soc., 105, 371-382.

Jones W.L., Schroeder L.C., Boggs D.H., Bracalente E.M., Brown R.A., Dome G.J., Pierson W.J. & Wentz F.J. 1982 The Seasat-A Satellite Scatterometer. The Geophysical Evaluation of Remotely Sensed Wind Vector over the ocean, J. Geophys. Res., 87 ,(C5) 3297-3317.

Kitaigorodskii S.A. 1961 Application of the theory of similarity to the analysis of wind generated wave motion as a stochastic process. Izv. Akad. Nauk. SSSR, Ser. Geofiz 1 , 105-1A (Eng. trans. 1 , 73-80).

Kjelaas A. & Guddal J. 1984 Comparisons between GEOS-3/Seasat wave data and wave model data. ERS-1 Radar Altimeter Data Products Workshop Report, ESA SP-221, 117-120.

Large W.G. & Pond S. 1981 Open ocean momentum flux measurements in moderate to strong winds, J. Physical Oceanography, 11 , 324-336.

Le Borgne P. 1982 Radiometrie hyperfrequence spatiale, application a la teledetection des zones de precipitation au dessus de l'ocean. These, Universite de Rennes I.

Lipa B.J. & Barrick D.E. 1981 Ocean surface height-slope probability density function from SEASAT altimeter echo. J. Geophys. Res., 86, 10921-10930.

Longuet-Higgins M.S. 1957 The statistical analysis of a random, moving surface. Phil. Trans. Roy. Soc. Lond., A249 , 321-387.

Longuet-Higgins M.S. 1963 The effect of non-linearities on statistical distributions in the theory of sea waves. J. Fluid Mech., 17 , 459-480.

Longuet-Higgins M.S., Cartwright D.E. & Smith N.D. 1963 Observations of the directional spectrum of sea waves using the motions of a floating buoy. Ocean Wave Spectra, Prentice Hall, 111-136.

Lorell J., Colquitt E. & Anderle R.J. 1982 Ionospheric correction for Seasat altimeter height measurement. J. Geophys. Res., 87 , (C5) 3207-3212.

Lorell J., Parke M.E. & Scott J.F. 1980 Seasat Geophysical Data Record (GDR) Users Handbook. JPL Intern. Rep. 622-97, revision A, Jet. Propulsion Lab.

MacArthur J.L. 1978 Seasat-A radar altimeter design description. Johns Hopkins APL, SDO 5232.

Marsh J.G. & Martin T.V. 1982 The Seasat altimeter mean sea surface model. J. Geophys. Res., 87 , 3269-3280.

Millet J.M. 1984 Determination du contenu en eau de l'atmosphere par radiometrie hyperfrequence spatiale. These Universite Paris VII.

Mognard N.M. 1983a Swell propagation in the North Atlantic Ocean using Seasat altimeter. In Satellite Microwave Remote Sensing, T.D. Allan (ed.), Ellis Horwood Ltd, 425-437.

Mognard N.M. 1983b Comparison of sea surface wind speed estimates derived from Seasat SASS, ALT and SMMR: initial study, ESA Contract Report, October 1983.

Mognard N.M. 1983c Apport de l'altimetrie - radar sur satellite a la determination de letat de la mer. Ph.D. Thesis, L-Universite Paul Sabatier de Toulouse (Sciences).

Mognard N.M. 1984 Ocean wave parameters extraction using satellite short-pulse radar altimeters. Proc. ERS-1 Altimeter Data Products Workshop, ESA SP-221, 37-42.

Mognard N.M. & Lago B. 1979 The computation of wind speed and wave heights from GEOS-3 data. J. Geophys. Res., 84 , 3979-3986.

Mognard N.M., Campbell W.J., Cheney R.E., Marsh J.G. & Ross D.B. 1981 Southern ocean waves and winds derived from SEASAT altimeter measurements. Proc. Conf. Wave dynamics and radio probing of the ocean surface, Miami Florida (in press).

Mognard N.M., Campbell W.J., Cheney R.E. & Marsh J.G. 1983 Southern Ocean mean monthly waves and surface winds for Winter 1978 by Seasat radar altimeter. J. Geophys. Res., 88 , 1736-1744.

Monaldo F.M., Goldhirsh J. & Walsh E.J. 1984 Altimeter height measurement errors introduced by the presence of variable cloud and rain attenuation. Proc. of URSI Commission F Symposium on Frontiers of Remote Sensing of the Oceans and Troposphere from Air and Space Platforms, Shoresh, Israel, 14-23 May 1984, NASA Conf. Pub. 2303, 287-296.

Moore R.K., Birrer I.J., Bracalente E.M., Dome G.J., & Wentz F.J. 1982 Evaluation of atmospheric attenuation from SMMR brightness temperatures for the Seasat satellite scatterometer. J. Geophys. Res., 87 ,(C5) 3337-3354.

Moskowitz L. 1964 Estimates of the power spectrums for fully developed seas for wind speeds of 20 to 40 knots. J. Geophy. Res., 69 ,(24) 5161-5179.

NOAA 1980 NOAA/NOSS Oceanic Data System Ocean Products list (Prepared by NOSS Technical Working Group), NTIS, 47C

NERC/SERC 1983 A study of ocean and ice topography from space. A joint Natural Environment Research Council/ Science & Engineering Research Council proposal for the development of satellite altimetry, September 1983.

Parsons C.L. 1979 On the remote detection of swell by satellite radar altimeter. Monthly Weather Review, 107, 1210-1218.

Peckham G. 1982 Altimeter : signal statistics. (unpublished note).

Phillips O.M. 1957 On the generation of waves by turbulent wind, J. Fluid Mech., 2 , 417-445.

Phillips O.M. 1961 On the dynamics of unsteady gravity waves of finite amplitude Part 2. J. Fluid Mech., 11 , 143-155.

Pierson W.J. 1977 Comments on a parametric wave model. J. Physical Oceanography, 7 , 127-134.

Pierson W.J. & Moskowitz L. 1964 A proposed spectral form for fully developed seas based on the similarity theory of S.A. Kitaigorodskii. J. Geophy. Res. 19 (24), 5181-5190.

Powell R.J., Birks A.R., Wrench C.L., Bradford W.J. & Maddison B.F. 1984 Radar altimetry over sea ice. ERS-1 Radar Altimeter Data Products Workshop Report, ESA SP-221, 129-134.

Queffeulou P. 1983 Seasat waveheight measurements: a comparison with sea-truth data and a wave forecasting model - application to the geographical distribution of strong sea states in storms. J. Geophys. Res., 88, (C3) 1779-1788.

Queffeulou P. 1984 A review of wind speed determination from radar altimeters. ERS-1 Radar Altimeter Data Products Workshop Report, ESA SP-221, 31-36.

Rapley C.G. 1984a First observations of the interaction of ocean swell with sea ice using satellite radar altimeter data. Nature, 307 , 150-152.

Rapley C.G. (ed.) 1984b Report of Panel 3 (Overall definition of the altimeter off-line ground segment) in ERS-1 Radar Altimeter Data Products Workshop Report, ESA SP-221, 249-256.

Rapley C.G. 1984c Observations of sea ice and icebergs from satellite radar altimeters. NASA Conf. Pub. 2307, Frontiers of remote sensing of the oceans and troposphere from air and space platforms, 527-536.

Rapley C.G., Griffiths H.D., Squire V.A., LeFebvre M., Birks A.R., Brenner A.C., Brossier C., Clifford L.D., Cooper A.P.R., Cowan A.M., Drewry D.J., Gorman M.R., Huckle H.E., Lamb P.A., Martin T.V., McIntyre N.F., Milne K., Novotny E., Peckham G.E., Scott R.F., Thomas R.H., & Vesecky J.F. 1983 A study of satellite radar altimeter operation over ice-covered surfaces. ESA CR-5182/82/F/CG (SC).

Rapley C.G., Feldman U., Griffiths H.D., LaViolette P., Piacsek S., Thomas R. & Vesecky J. 1984 Report of the working group on sea ice. Proc. URSI Symp. on the frontiers of remote sensing of the oceans and troposphere from air and space platforms. Israel 14-23 May 1984.

Rapley C.G., Griffiths H.D., Squire V.A., Olliver J.G., Birks A.R., Cooper A.P.R., Cowan A.M., Drewry D.J., Gorman M.R., Guzkowska M., Laxon S., Mason I.M., McIntyre N.F., Novotny E., Paterson R., Scott R.F. & Street-Perrot F.A. 1985 Applications and scientific uses of ERS-1 radar altimeter data, ESA report 5684/83/NL/BI.

Robin G. de Q., Drewry D.J. & Squire V.A. 1983 Satellite observations of polar ice fields. Phil Trans. Roy. Soc. Lond., A309 , 447-461.

Rufenach C.L. & Alpers W.R. 1978 Measurement of ocean wave heights using the GEOS-3 altimeter. Journal Geophysical Research, 83 ,(C10) 5011-5018.

Scott R.F. & Huckle H.E. 1984 Standardisation of data formats for radar altimeter data. ERS-1 Radar Altimeter Data Products Workshop ESA SP-221, 205-208.

Somma R. et al 1982 Radar altimeter technical description. Selenia Spazio Report ER-TN-SEL-RA-0018.

Squire V.A. & Moore S.C. 1980 Direct measurement of the attenuation of ocean waves by pack ice. Nature, 283, 365-368.

Squire V.A., Drewry D.J., Cowan A.M. & McIntyre N.F. 1984 Cryospheric data products available through satellite altimetry. ERS-1 Radar Altimeter Data Products Workshop Report, ESA SP-221, 51-57.

Srokosz M.A. 1984a On the skewness of the sea surface. (submitted for publication).

Srokosz M.A. 1984b On the joint distribution of surface elevation and slopes for a nonlinear random sea; with an application to radar altimetry. (submitted for publication).

TOPEX 1981 Satellite Altimetric Measurement of the Ocean. TOPEX Science Working Group Report, Jet Propulsion Laboratory, Tech. Rep. Nr. 400-111.

Townsend W.F. 1980 An initial assessment of the performance achieved by the Seasat-1 radar altimeter. I.E.E.E. J. Oceanic Eng., OE-5 , 80-92.

Wakker K.F., Ambrosius B.A.C. & Aardoom L. 1983 Precise Orbit Determination for ERS-1. European Space Agency Contract Report, ESOC Contract No. 5227/82/D/IM(SC).

Walsh E.J. 1979 Extraction of ocean wave height and dominant wavelength from GEOS-3 altimeter data. J. Geophys. Res., 84 , 4003-4009.

Walsh E.J., Uliana E.A. & Yaplee B.S. 1978 Ocean wave heights measured by a high resolution pulse-limited radar altimeter. Boundary Layer Meteorology, 13, 263-276.

Wang P.Y. & Hobbs P.V. 1983 The mesoscale and microscale structure and organization of clouds and precipitation in mid-latitude cyclones. X: wavelike rainbands in an occlusion. J. Atmos. Sci., 40 , 1950-1964.

Wang P.Y., Parsons D.B. & Hobbs P.V. 1983 The mesoscale and microscale structure and organization of clouds and precipitation in mid-latitude cyclones. VI: wavelike

rainbands associated with a cold-frontal zone. J. Atmos. Sci., 40, 543-558.

WCP 1984 Report of the Workshop on Interim Ocean Surface Wind Data Sets. World Climate Programme Publication No. 68,

WCRP 1983 Large-scale oceanographic experiments in the World Climate Research Programme. WCRP Publication No. 1, Vol I.

Wentz F.J., Cardone V.J. & Fedor L.S. 1982 Intercomparison of wind speeds inferred by the SASS, Altimeter and SMMR. J. Geophys. Res., 87 , (C5) 3378-3384.

Wentz F.T. & Peteherych S. 1984 New algorithms for microwave measurements of ocean winds. Proc. of URSI Commission F Symposium on Frontiers of Remote Sensing of the Oceans and Troposphere from Air and Space Platforms, Shoresh, Israel, 14-23 May 1984, NASA Conf. Pub. 2303, 105-114.

Woiceshyn P.M., Wurtele M.G., Boggs D.H., McGoldrick L.F. & Peteherych S. 1984 A new parameterization of an empirical model for wind/ocean scatterometry. Proc. of URSI Commission F Symposium on Frontiers of Remote Sensing of the Oceans and Troposphere from Air and Space Platforms, Shoresh, Israel, 14-23 May 1984. NASA Conf. Pub. 2303, 57-74.

Wu J. 1972 Sea surface slope and equilibrium wind-wave spectra. Phys. of Fluids, 15 , No. 5.

Zwally H.J., Comiso J.C., Parkinson C.L., Campbell W.J., Carsey F.D., & Gloersen P. 1983 Antarctic sea ice, 1973-1976 : Satellite passive microwave observations. NASA SP-459.

Appendix A. Atmospheric attenuation

The influence of the atmosphere on the altimeter measurement may be separated into ionospheric and tropospheric effects. The first results in a range perturbation; the second involves a range increase resulting from the refractive index of the air, and also an attenuation of the signal strength, with which we are concerned in this chapter.

Near the frequency of 14 GHz signal attenuation is essentially produced by rain. This effect is very serious for altimeter wind speed determination, particularly because heavy rain occurs often occurs with strong winds (meteorological fronts, hurricane etc.). As seen in 6.1, according to the shape of the σ^o versus wind speed curve, at high winds small variations in σ^o produce large fluctuations in the estimates of wind speed. For instance at 12 ms^{-1} a 1 dB attenuation results in a wind speed increase of ~3 ms^{-1}.

In the atmospheric attenuation problem three points may be identified:

(i) the theoretical signal attenuation for a rain pattern homogeneously distributed over the altimeter footprint and for a given rain rate.

(ii) typical rain rates and rain pattern sizes encountered at sea.

(iii) methods for the detection of rain cells in the footprint and possible correction of the attenuation.

A.1 Theoretical signal attenuation by rain at 14 GHz

The most severe attenuation at microwave frequencies is caused by rain. This appears at 3 GHz and becomes serious for all frequencies above 10 GHz. The mechanism of attenuation by atmospheric liquid water involves absorption and scattering by individual cloud droplets. The rain intensity is characterized by the rain rate, generally expressed in mm hr^{-1}. The classifications may differ between authors. For example, in Farrow (1975) and Millet (1984) the following two classifications are found:

Table A.1. Rain-rate classifications

Rate (mm hr^{-1})	Description	Rate (mm hr-1)	Description
0-1	drizzle	0-3.8	light
1-3	light	3.8-20	moderate
3-10	moderate	20-40	heavy
10-30	heavy	40-75	very heavy
> 30	excessive	> 152	extreme

The first one is comparable with the U.S. Weather Bureau classification of light (0-2.5 mm hr^{-1}), moderate (2.5-7.6) and heavy (> 7.6).

The theoretical attenuation may be calculated from rain-rate and the distribution of drop sizes. Figs A.1 and A.2 (from Farrow, 1975) show the one-way attenuation in dB km^{-1} as a function of radar frequency and rain-rate. From Fig. A.1, with λ=2 cm (f=15 GHz), the

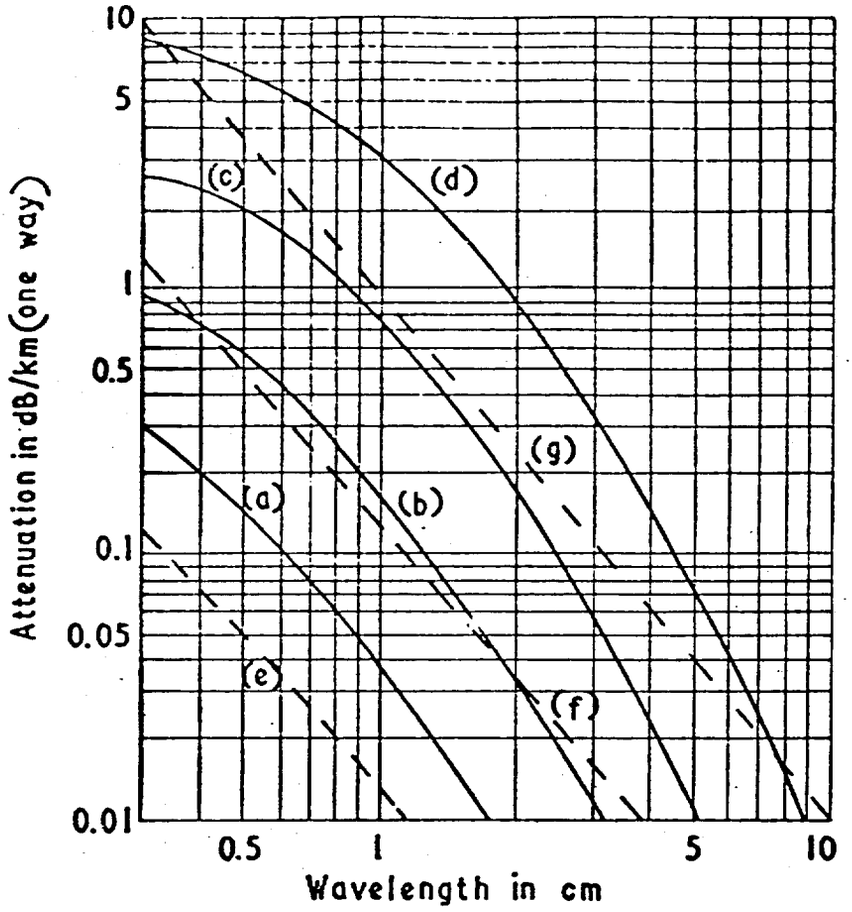

Solid curves show attenuation in rain of intensity. (a), 0.25mm/hr (drizzle); (b), 1mm/hr (light rain); (c), 4mm /hr (moderate rain); (d), 16mm/hr (heavy rain). Dashed curves show attenuation in fog or cloud. (e), 0.032 g/m^3 (visibility about 600m); (f), 0.32g/m^3 (visibility about 130m); (g), 2.3 g/m^3 (visibility about 30m).

Fig. A1 Theoretical values of microwave attenuation by rain and fog (Farrow, 1975)

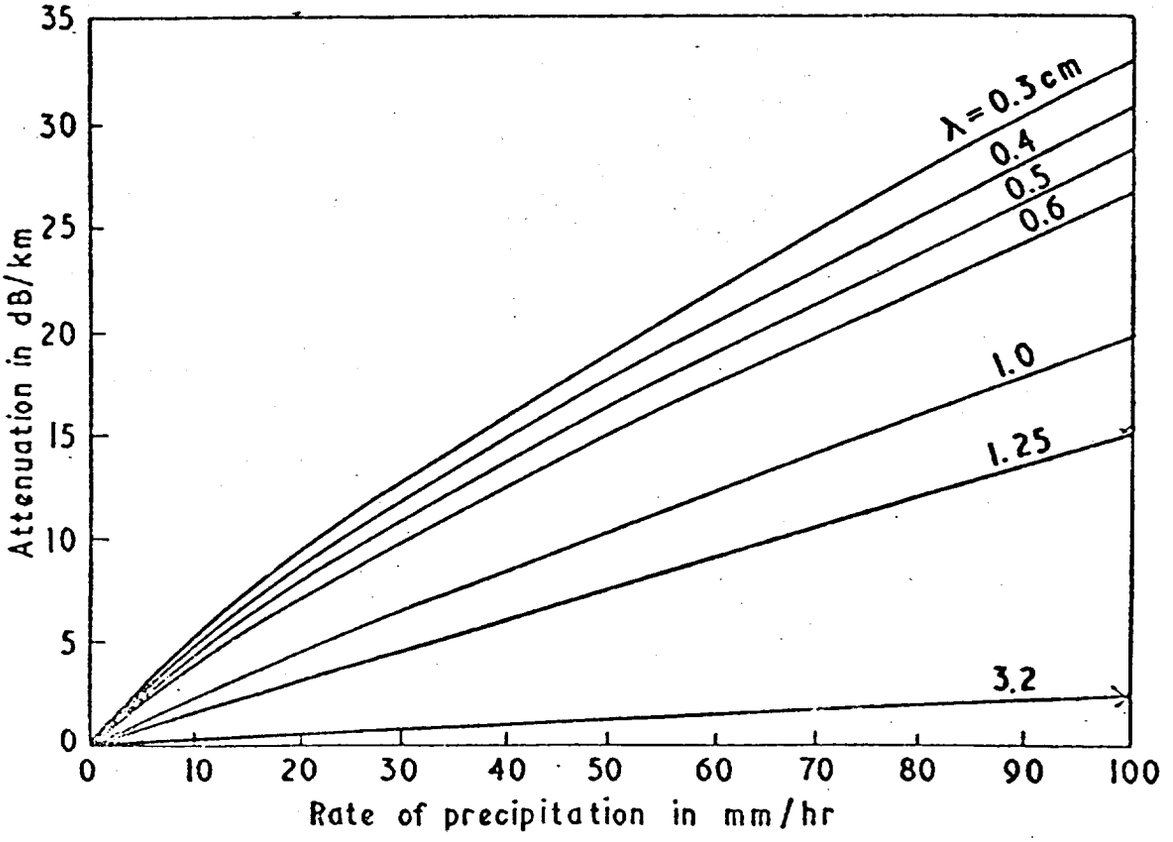

Fig. A2 Microwave attenuation by rain as a function of precipitation rate, based on Laws and Parsons' raindrop size distribution (Farrow, 1975).

theoretical two-way attenuation is about 1.8 dB km^{-1} for heavy rain (16 mm hr^{-1}) and 0.4 dB km^{-1} for moderate rain (4 mm hr^{-1}). Note that to obtain the total attenuation along the path the above values must be multiplied by the rain depth. From the data of Fig. A.1 we also note that the attenuation through thick (non-precipitating) cloud is not negligible.

A quantitative estimate of the attenuation is given by the empirical relation of Olsen et al., cited in Goldhirsh & Rowland (1982):

$$k=aR^b$$

where k is the two-way attenuation coefficient (dB km^{-1}) at frequency f; a,b are dependent on the frequency and drop-size distribution; and R is the rain-rate. At 13.5 GHz for $r < 25$ mm hr^{-1} a=0.0346, b=1.109 while for $25 < r < 50$ mm hr^{-1} a=0.0248, b=1.205

The total two-way attenuation at 13.5 GHz, for a 5 km rain depth and various rain-rates, is given below:

Table A.2. Two-way attenuation at 13.5 Ghz

R (mm hr^{-1})	10	20	30	40
total atten. (dB)	4	10	15	21

A.2 Rain at sea

The most important error in the signal attenuation correction comes essentially from the ignorance of the variability of rain-rate along horizontal and vertical paths. Indeed the measurement of

precipitation is a very difficult task; most measurements give the precipitation rate in discrete intervals of time at one location, when the actual requirement is for instantaneous measurements over the actual sensor-target path.

In general, precipitation occurs in cells of limited size and, from the literature it appears that the best way to measure it is through airborne and ground-based radars, using reflectivity and doppler effects, with high resolution in space and in signal intensity. This, combined with a network of ground stations providing high resolution rain-rate measurements, allows a fast description of the precipitation structures. When coastal sites are used possible orographic and thermal effects have to be taken into account. The use of radars alone provides detailed structure but not absolute rain-rates.

A review of precipitating cloud systems (Houze & Hobbs, 1982) indicates that the regions of heaviest precipitation are often organized on the mesoscale in the form of rainbands. The structure of extratropical cyclone rainbands has been investigated (Houze & Hobbs, 1982, Hobbs, 1978 and Hobbs & Biswas, 1979) and six types of mesoscale rainbands have been identified, as shown on Fig. A.3 (from Hobbs, 1978). The first three types are about 50 km wide, the second type often occurring in series, with the younger, more vigorous, rainbands preceding. The heaviest precipitation is found in the narrow cold frontal band, about 5 km wide, and organized on the small mesoscale into ellipsoidal areas, 50-100 km^2 in area. They are oriented at angles of 30-35^o to the cold front and are called

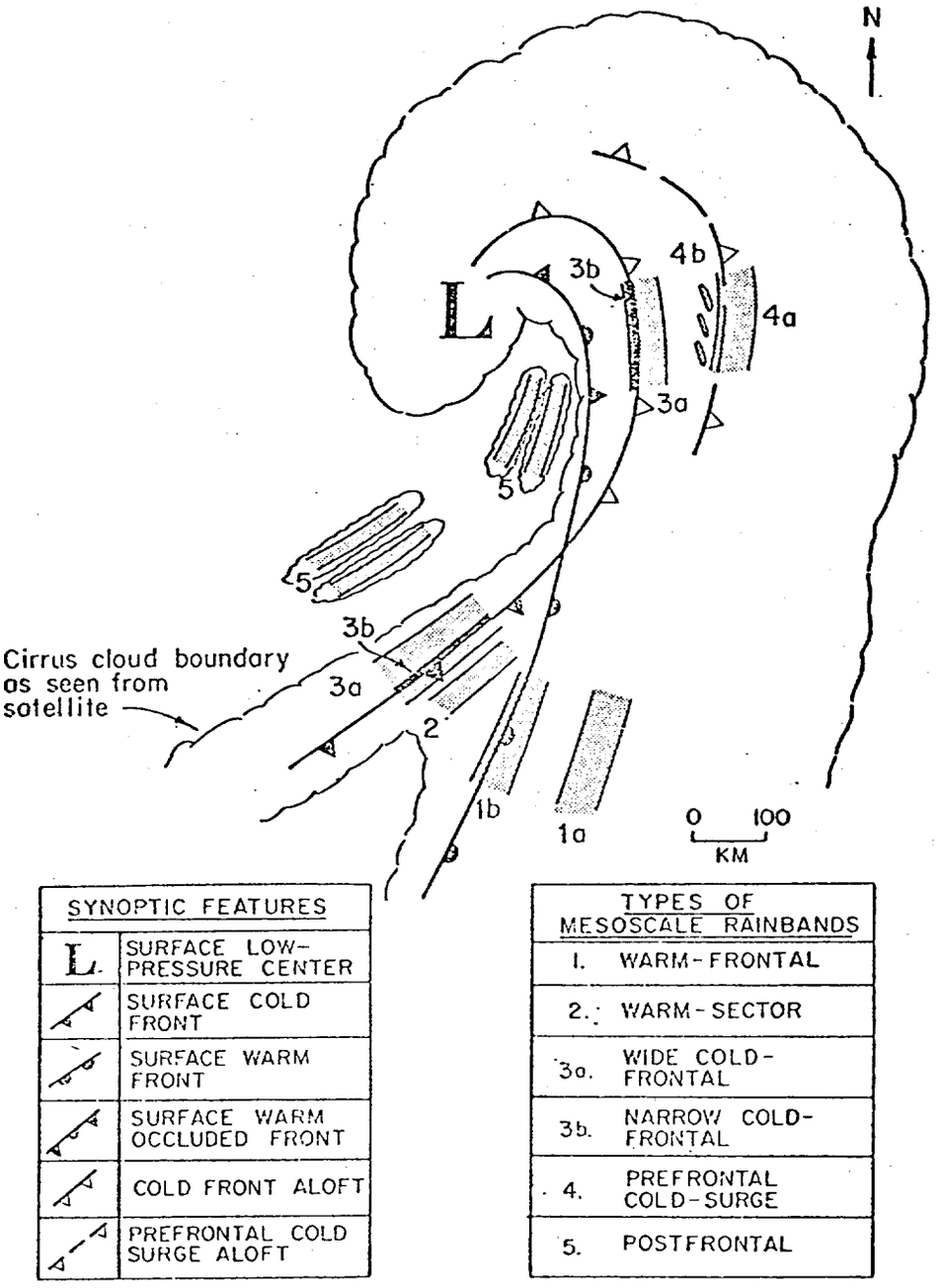

SYNOPTIC FEATURES	
L	SURFACE LOW-PRESSURE CENTER
	SURFACE COLD FRONT
	SURFACE WARM FRONT
	SURFACE WARM OCCLUDED FRONT
	COLD FRONT ALOFT
	PREFRONTAL COLD SURGE ALOFT

TYPES OF MESOSCALE RAINBANDS	
1.	WARM-FRONTAL
2.	WARM-SECTOR
3a.	WIDE COLD-FRONTAL
3b.	NARROW COLD-FRONTAL
4.	PREFRONTAL COLD-SURGE
5.	POSTFRONTAL

Fig. A3 Schematic representation of the types of rainbands observed in cyclonic storms (Hobbs, 1978).

'precipitation core areas' (Hobbs & Biswas, 1979). These areas have been observed (Hobbs & Biswas, 1979 and James & Browning, 1979) to be about 5 km wide, 20 km long and with a 5 km spacing along the cold front. Precipitation is generally confined below the 3 km level.

Superimposed on these structures 'wavelike rainbands' are often observed (Wang, Parsons & Hobbs, 1983 and Wang & Hobbs 1983). For instance in a cold-frontal zone wavelike bands occur on a scale of 3-6 km whereas in the vicinity of a warm occlusion rainbands up to 80 km long and 3-5 km wide and separated by 5-10 km may be encountered. The contribution of these rainbands to the overall rain-rate is important, as shown in Figs. A.4 and A.5 (from Hobbs, 1978 and Wang, Parsons & Hobbs, 1983).

In midlatitude convective systems heavy rain occurs on a small horizontal space scale of order 5 km. Such systems are often organized into multicell storms. In the tropics clouds occur in a spectrum of sizes ranging from small isolated cumulus to large 'cloud clusters', where continuous rain areas cover up to 5×10^4 km^2. Isolated cumulus and cumulonimbus greatly outnumber cloud clusters.

In the case of tropical hurricanes heavy precipitation is generally concentrated in a mesoscale 'eyewall rainband' around the eye of the storm, with several outer rainbands and regions of lighter rainfall in between. The hurricane cloud patterns may be symmetric or assymmetric.

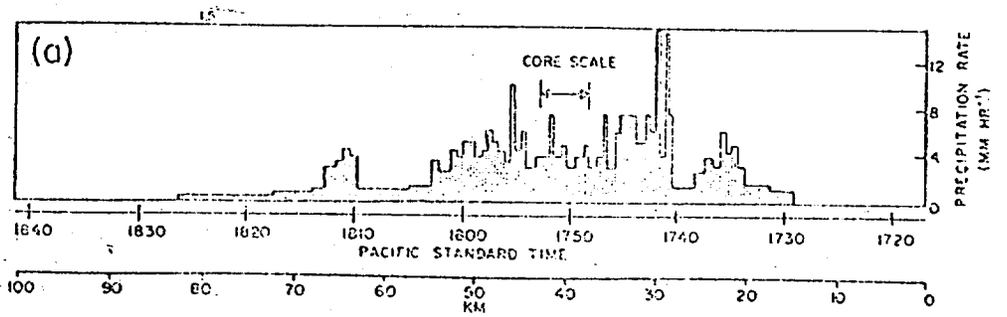

Fig. A4 Mesoscale variation of rain-rate in a mid-latitude cyclonic storm (Hobbs, 1978).

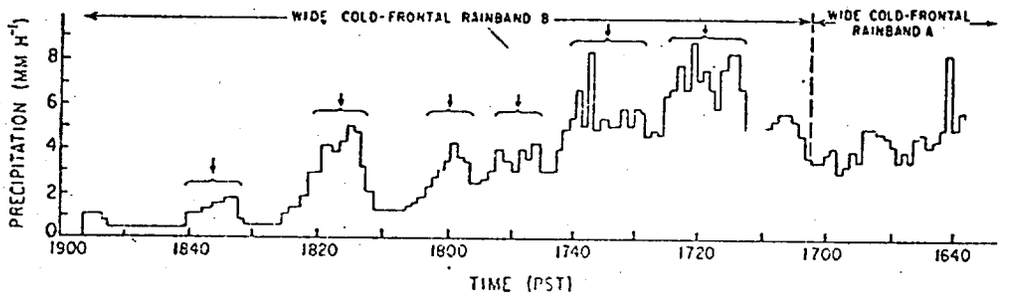

Fig. A5 Contribution from wavelike rainbands to precipitation in a cold-frontal zone (Wang, Parsons & Hobbs, 1983).

A.3 The effect of rain on the ERS-1 radar altimeter

Here we are concerned with the altimeter signal strength attenuation and its consequences for wind speed retrieval, not with the altimeter height bias produced by atmospheric effects. However, it should be noticed that the tracker may lose lock as a result of strong rain attenuation. For example, at 13.5 GHz, a 30 mm hr^{-1} rain-rate over a depth of 5 km results in a 14 dB two-way attenuation if it covers the entire footprint. Fortunately this is a very extreme case and usually a characteristic of rainfall intensity is its variability over distances comparable with the diameter of the altimeter's footprint. For ERS-1 we need to know how to detect rain cells in the altimeter footprint and whether it is possible to correct the data for rain attenuation.

Detection and measurement of rain at sea, on an operational and global basis, will only be possible from space because there are very few direct measurements of precipitation in the open ocean. The three main parameters to be measured are the rain-rate, and the vertical and horizontal extent of rain. The use of Scanning Multichannel Microwave Radiometer (SMMR) data for this purpose has been studied (Le Borgne 1983) and applied to correct Seasat scatterometer estimates of winds (Moore et al., 1982). Some success has been achieved. The choice of frequencies (18 GHz and 37 Ghz) results from a trade-off between sensitivity and resolution on the ground. At 37 GHz the resolution is better (25 km compared with 55 km at 18 GHz) but this channel saturates more rapidly with rain-rate. A second problem is caused by the ambiguity between the rain-rate and

the vertical extent of rain (defined in this case by the altitude of the freezing level). The use of several channels to measure these two parameters by linear equations is not really so effective because degradation of spatial resolution, non-linear variation of the brightness temperature with rain-rate (Millet 1984) and the influence of sea surface temperature on the coefficients used in the equations (Moore et al., 1982). Furthermore the accuracy of such algorithms is very difficult to estimate (from 50% to 100% according to various authors).

The use of infra-red and visible data from satellites may be helpful in determining the horizontal extent of rain cells because of better spatial resolution than at microwave frequencies (Le Borgne 1983, Moore et al., 1982). Two methods can be envisaged in which simultaneous VIS and IR are combined: (i) a visual classification of cloud types from which rain rates are deduced via a parameterization scheme, (ii) automatic analysis of digitized images from geostationary satellites.

So at present the use of measurements from space might allow the flagging of rain areas but on a scale larger than the size of the altimeter footprint. For the altimeter itself it would be of interest to simulate the effects on σ^o of heavy isolated rain cells passing through the footprint.